A New Method for Harmonic Penetration Study in Power Networks with Renewable Generation

Thesis presented for the degree of

Doctor of Philosophy

at the University of Strathclyde

by

JIANFENG LU

(Hons, 2nd class upper)

Supervisor: Professor K.L.Lo

Power System Research Group

Institute of Energy and Environment

Department of Electronic and Electrical Engineering

University of Strathclyde

2014

Declaration

This thesis is the result of the author's original research. It has been completed by the author and has not been previously submitted for examination which has led to the award of a degree.

Acknowledgements

I would like to express my sincere appreciate to my supervisor, Professor K.L.Lo, Head of the Power System Research Group (PSRG), for his supervision and support throughout my research work. The completion of this thesis would not have been possible without his constant encouragement and patient guidance.

I also wish to extend my gratitude to my colleagues, Shuai Shi and Xinyi Gu, for their help and support at various stages of this research work.

Most importantly, I wish to express my sincere gratitude to my parents for their financial support and love during my PhD study.

Abstract

Nowadays, many power electronic equipments are used in industry in seeking higher system reliability and efficiency, and more electronic or microprocessor controllers are used in power system to control AC/DC transmission lines or loads. Moreover, the importance of green energy such as wind and solar is continually growing in our societies not only due to environmental concerns but also to resolve the problem of access to electricity in rural areas. As a result, it creates power quality issues especially harmonics. In electrical power system, harmonics have a number of undesirable effects on power system equipment as well as on its operation. In order to understand the effects of these harmonics it is first necessary to analyse the penetration of these harmonics from their various sources into the network. This process of analysis is commonly known as harmonic power flow or harmonic penetration evaluation.

In the thesis a review is conducted on existing harmonic power flow methods. The previous approaches require long computing time and encounter convergence problem because of poor initial value. They are only applied to small or medium power systems with a single harmonic source. A new fast hybrid method (FHM) is developed in the thesis. It is a frequency domain method which can be used to evaluate the steady state harmonic penetration with discrete harmonic frequency. It is able to solve the convergence problem, simplify the calculation procedure and achieve accurate results. In addition, the proposed method has been applied to single phase balanced large power systems (e.g. Polish 2383-bus power system) to evaluate the harmonic penetration with integrating renewable generations. The investigation also includes the effects of harmonic penetration by changing the power capacities of renewable generations. Harmonic penetration

variation during a 24 hour period is also investigated by tracking the daily generation and load demand curves. The harmonic sources considered in the thesis consist of wind turbine generator (WT), photovoltaic generator (PG), electric vehicle charger (EVC) and traditional six-pulse converters.

Contents

List of Figures

LIST OF FIGURES

List of Tables

LIST OF TABLES

Nomenclature

α	voltage phase angle
β	Current phase angle
$\Delta\alpha$	Voltage phase angle mismatch
$\Delta\beta$	Current phase angle mismatch
$\Delta\bar{I}$	Current mismatch vector
$\Delta\overline{V}$	Voltage mismatch vector
λ	Downhill factor
ω	Angular frequency
$\overline{J}$	Jacobian matrix
$\overline{Y}_{bus}$	Power system admittance matrix
θ	Phase angle
$B_{(i,j)}$	Imaginary part of power system admittance
D	Distortion power
f	Fundamental frequency
$G_{(i,j)}$	Real part of power system admittance
$g_{i,n}^{(h)}$	h^{th} harmonic order reactive non-linear load current at bus n

LIST OF TABLES

$g_{r,n}^{(h)}$ h^{th} harmonic order real non-linear load current at bus n

h It represents harmonic order in the thesis. $h = 1,2,3,\ldots$

I Current

I_{DC} DC component current

$I_{i,n}^{(h)}$ h^{th} harmonic order reactive line current at bus n

$I_{r,n}^{(h)}$ h^{th} harmonic order real line current at bus n

k Ratio of transformer

P Active power

$p.u.$ Per unit

pf Total power factor

Q Reactive power

R Resistance

R_f Fundamental resistance

S Apparent power

T Time period

t_{ij} Line admittance between bus i and bus j

THD_i Total harmonic current distortion

THD_p Total harmonic active power distortion

THD_v Total harmonic voltage distortion

V Voltage

V_{DC} DC component voltage

$X_d^{''}$ d axis sub-transient reactance of synchronous machine

X_f Fundamental negative sequence reactance

$X_q^{''}$ q axis sub-transient reactance of synchronous machine

y_{ci} Shunt capacitor admittance at bus i

z Impedance

AC Alternating current

ASD Adjustable-speed drive

CW Continuous wave

DC Direct current

DFIG Doubly fed induction generator

DM Decoupled method

ESD Electrostatic discharge phenomena

EV Electric vehicle

EVC Electric vehicle charger

FHM Fast hybrid harmonic power flow calculation method

HPF Harmonic power flow

HS Harmonic source

HV High voltage

IEC International electrotechnical commission

IEEE Institute of electrical and electronics engineers

IGBT Insulated-gate bipolar transistor

LV Low voltage

MOSFET Metal-oxide-semiconductor field-effect transistor

MPPT Maximum power point tracker

NEMP Nuclear electromagnetic pulse

NRM Newton-Raphson method

PCC Point of common coupling

PCU Power conditioning unit

PG Photovoltaic generator

PMSG Permanent magnetic synchronous generator

PQ bus Liner load bus

PS bus Non-linear load bus

PV bus Voltage control bus

rms Root-mean-square

SCR Silicon-controlled rectifier

WRIG Wound rotor induction generator

WRSG Wound rotor synchronous generator

WT Wind turbine

WTG Wind turbine generator

Chapter 1

Introduction

1.1 Brief Introduction to Power Quality

1.1.1 Definition of Power Quality

Electric power quality covers all aspects of transmission and distribution level analysis and customer satisfaction. Hence, it plays an important role in power systems with direct impacts on efficiency, security and reliability, and attracts the attention of many researchers and industries [1, 2].

The electric power quality is generally used to express the quality of voltage and/or the quality of current. Therefore, the author in reference [1] defined it as the measure, analysis and improvement of the bus voltage to maintain a sinusoidal waveform at rated voltage and frequency. This definition includes all momentary and steady-state phenomena.

1.1.2 Classification of Power Quality Problems [3–13]

According to specific properties of power quality problems, they are categorized into several different classifications. Some regulations categorizes the power quality problems using the frequency range of the event, e.g. IEC 61000-2-5, shown in Table 1.1 below [1, 3].

Table 1.1: Main phenomena causing electromagnetic and power quality disturbances [1, 3]

Conducted low-frequency phenomena	Harmonics, inter-harmonics Signaling voltage Voltage fluctuations Voltage dips Voltage imbalance Power frequency variations Induced low-frequency voltages DC components in AC networks
Radiated low-frequency phenomena	Magnetic fields Electric fields
Conducted high-frequency phenomena	Induced continuous wave (CW) voltages or currents Unidirectional transients Oscillatory transients
Radiated high-frequency phenomena	Magnetic fields Electric fields Electromagnetic field Steady-state waves Transients
Electrostatic discharge phenomena (ESD)	
Nuclear electromagnetic pulse (NEMP)	

It divides the power quality problems into low frequency ($< 9kHz$), high frequency ($> 9kHz$), electrostatic discharge phenomena and nuclear electromagnetic pulse. In addition, low frequency and high frequency consist of radiated disturbance and conducted disturbance respectively.

In other regulations the most important factor is the magnitude and duration of events. The author in reference [6] gives an example as shown in Figure 1.1.

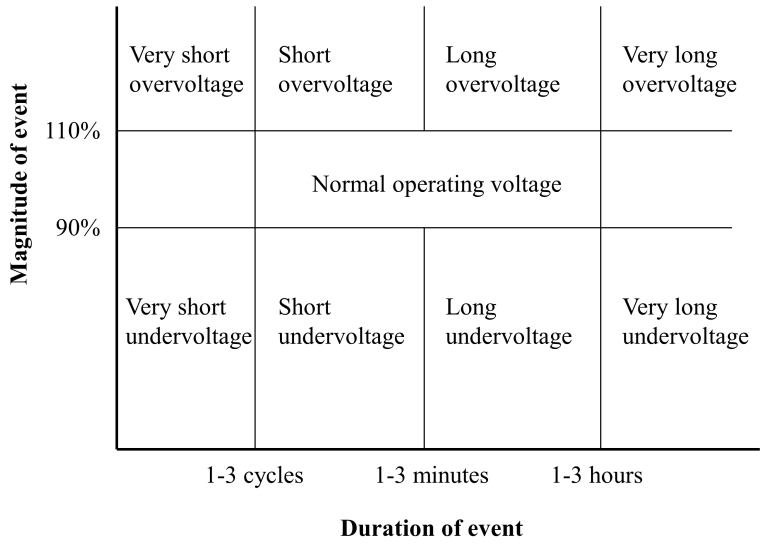

Figure 1.1: Magnitude-duration plot for classification of power quality events [6]

In total, there are nine different sections in the above figure. The horizontal axis represents the duration of event, and is split into four regions: very short, short, long and very long. The vertical axis represents the magnitude of event, that is divided into three regions:

- interruption: voltage magnitude equals zero,
- undervoltage: voltage magnitude is under its nominal value, and
- overvoltage: voltage magnitude is over its nominal value.

Other guidelines such as IEEE standards use the wave shape of each event to classify power quality problems. Table 1.2 indicates the informations about categories and characteristics of electromagnetic phenomena defined by IEEE 1159-2009, that use several additional terms compared with IEC terminology [13].

Table 1.2: Categories and typical characteristics of power system electromagnetic phenomena [13]

Categories	**Typical spectral content**	**Typical duration**	**Typical voltage magnitude**
1. Transients			
1.1 Impulsive			
1.1.1 Nanosecond	$5ns$ rise	$< 50ns$	
1.1.2 Microsecond	$1\mu s$ rise	$50ns - 1ms$	
1.1.3 Millisecond	$0.1ms$ rise	$> 1ms$	
1.2 Oscillatory			
1.2.1 Low frequency	$< 5kHz$	$0.3 - 50ms$	$0 - 4p.u.$[1]
1.2.2 Medium frequency	$5 - 500kHz$	$20\mu s$	$0 - 8p.u.$
1.2.3 High frequency	$0.5 - 5MHz$	$5\mu s$	$0 - 4p.u.$
2. Short-duration rms [2] variations			
2.1 Instantaneous			
2.1.1 Sag		0.5 – 30 cycles	$0.1 - 0.9p.u.$
2.1.2 Swell		0.5 – 30 cycles	$1.1 - 1.8p.u.$
2.2 Momentary			
2.2.1 Interruption		0.5 cycles - $3s$	$< 0.1p.u.$
2.2.2 Sag		30 cycles - $3s$	$0.1 - 0.9p.u.$
2.2.3 Swell		30 cycles - $3s$	$1.1 - 1.4p.u.$
2.3 Temporary			
2.3.1 Interruption		$> 3s - 1min$	$< 0.1p.u.$
2.3.2 Sag		$> 3s - 1min$	$0.1 - 0.9p.u.$
2.3.3 Swell		$> 3s - 1min$	$1.1 - 1.2p.u.$
3. Long-duration rms variations			
3.1 Interruption, sustained		$> 1min$	$0.0p.u.$

Continued on next page

[1] $p.u.$ refers to per unit, which is dimensionless. The quantity $1.0p.u.$ corresponds to 100%. The nominal condition is often considered to be $1.0p.u.$. In this table, the nominal peak value is used as the base for transients and the nominal rms value is used as the base for rms variations.

[2] root-mean-square

Table 1.2- *Continued from previous page*

Categories	**Typical spectral content**	**Typical duration**	**Typical voltage magnitude**
3.2 Undervoltages		$> 1min$	$0.8 - 0.9p.u.$
3.3 Overvoltages		$> 1min$	$1.1 - 1.2p.u.$
3.4 Current overload		$> 1min$	
4. Imbalance			
4.1 Voltage		steady state	$0.5 - 2\%$
4.2 Current		steady state	$1.0 - 30\%$
5. Waveform distortion			
5.1 DC offset		steady state	$0 - 0.1\%$
5.2 Harmonics	$0 - 9kHz$	steady state	$0 - 20\%$
5.3 Interharmonics	$0 - 9kHz$	steady state	$0 - 2\%$
5.4 Notching		steady state	
5.5 Noise	broadband	steady state	$0 - 1\%$
6. Voltage fluctuations	$< 25Hz$	intermittent	$0.1 - 7\%$
7. Power frequency variations		$< 10s$	$\pm 0.1Hz$

1.2 Motivation

Nowadays, many power electronic equipments are used in modern industry for seeking higher system reliability and efficiency, and more electronics or microprocessor controllers are used for the power system control in AC/DC transmission lines or loads. In addition, more and more renewable energy generators such as wind turbines (WTs) and photovoltaic generators (PGs) and modern equipment, e.g. electric vehicle chargers (EVCs), are integrated into the power systems. Some of these new equipments generate harmonic injection into the system. As a result, the actual voltage and current waveforms in the power system are distorted and are a combination of many sine waves of different frequencies, that are integer or non-integer multiples of the fundamental frequency (50 Hz or 60 Hz). These periodical waveforms are regarded as harmonics or inter-harmonics. Hence, the harmonics (include inter-harmonics in this thesis) de-

scribed in Table 1.2 are an important aspect of electric power quality in power systems recently.

The harmonics have great influence on the power system equipment as well as on its operation. They can lead to operation failure of electrical and electronic components, failure of power factor correction capacitors, loss in power generation and transmission, and interference with protection, control and communication networks as well as customer loads. High levels of harmonic distortion can also increase transformer, capacitor, motor or generator heating. Therefore, many standards such as IEC 61000 series standard, IEEE 519 standard and Engineering Recommendation G5/4 are published to limit the harmonics in power systems. However, an efficient, reliable and accurate algorithm that is used to evaluate the steady state network voltages at harmonic frequencies is a fundamental requirement. This process is defined as harmonic power flow evaluation in reference [14] with considering all the harmonic couplings. Arrillaga et al. in reference [5] indicates that if the harmonics generated by the non-linear components are independent, the above process is called harmonic penetration evaluation, that using a decoupled direct (nodal) solution. In this thesis, the process of evaluating the steady state network voltages at harmonic frequencies is defined as harmonic power flow evaluation as well as harmonic penetration evaluation.

Many researchers have devoted themselves to solve the harmonic power flow problems. Therefore, many different approaches have been proposed and implemented until now. According to the modelling techniques of power system components and non-linear loads, they can be classified into three categories: time domain methods, frequency domain methods and hybrid time-frequency domain methods. Despite the time domain methods have high result accuracy, they usually require long computing times especially for a large power system containing many non-linear loads with strong harmonic couplings. Hybrid time-frequency domain methods can achieve the benefits of the accuracy of the time domain and the simplicity of the frequency domain. However, the frequency domain methods are widely used. They represent static load flow with discrete frequencies. Also, they require shorter computing time compared to both time domain and hybrid time-frequency domain methods and indicate the frequency response of the power systems through the calculation.

Newton-Raphson based approach, that is implemented in the frequency domain, is mostly used to the calculations because of its accurate results. However, it requires much computing time, and even leads to convergence problems for especially a large power system with many non-linear loads and strong harmonic couplings. Hence, several methods such as decoupled and fast decoupled harmonic power flow calculation methods are designed to solve the problems. However, these methods still encounter two problems: one is that the iterative initial value must be close to the expected value. Otherwise, the calculations may fail to converge. The other is that the Jacobian matrix should be calculated in each iteration, which may require longer computing time and make the calculation more complicated. Hence, how to solve these two problems and achieve accurate results attracts the author.

In addition, the existing harmonic power flow calculation methods involve a single traditional harmonic source (e.g. six-pulse line-commutated converters and arc furnaces) or single type of traditional harmonic sources that includes only integer-harmonics in small or medium single-phase power systems. However, with increasing use of renewable energy generations (e.g. WTs and PGs) and modern electric devices (e.g. EVCs), the power system contains several types of harmonic sources with a large frequency range, i.e. integer-harmonics, inter-harmonics and sub-harmonics. Therefore, a harmonic penetration evaluation method which can be applied to large power systems with multiple types of harmonic sources is required. It is also worthy to investigate the effects of integrating renewable energy generations and modern electric devices to the harmonic penetration by changing their power capacities as well as tracking their daily generation and load demand curves. This project is contributed to achieve these aims.

1.3 Thesis Objectives and Scope

The aim of this research is to develop a fast computer simulation method to evaluate the harmonic penetration by integrating renewable energy generations and modern electric devices in a large power system. The objective of this thesis includes:

1. Developing a fast harmonic power flow calculation method to solve the convergence problem, simplify the calculation process and achieve accurate results. Moreover, the proposed method should be applied to large power systems with multiple types of harmonic sources and large harmonic frequency range, i.e. integer-harmonics, inter-harmonics and sub-harmonics.

2. Applying the proposed method to a large power system to investigate the effects of integrating renewable energy generations and modern electric devices to harmonic penetration by changing their power capacities. Also it investigates the harmonic penetration variation over a 24 hour period by tracking their daily generation and load demand curves.

In order to achieve the aim of this thesis, the research approach involves several key steps:

1. Review the present harmonic power flow calculation methods, and explore in detail their advantages and disadvantages.

2. Model each component of power system, and develop a fast harmonic power flow calculation method that is implemented in frequency domain.

3. Apply the proposed method, the Newton-Raphson based method and the decoupled method to several power systems to achieve the harmonic voltages and powers. Compare the result obtained by each method to investigate whether the proposed method improves the calculation.

4. Apply the proposed method to a Polish 2383-bus single-phase large power system to evaluate the harmonic penetration, and investigate the effects of integrating renewable energy generations and modern devices in both momentary and long time duration.

1.4 Original Contributions of the Thesis

The original contributions that are used to achieve the objectives in this thesis are summarized below:

- A review of present harmonic power flow calculation methods that are implemented in frequency domain are studied in detail. Moreover, their advantages and disadvantages are explored.

- A fast hybrid harmonic power flow calculation method (FHM) is proposed. It combines three methods: the secant method, the Newton-Downhill method and the decoupled method. The secant method is applied to establish the initial value in order to solve the convergence problem. The Newton-Downhill and decoupled method are used to make the iterative process monotonic decrease. Therefore it can reduce the calculation procedure of Jacobian matrix in order to accelerate the calculation speed and converge successfully.

- The proposed method is tested whether it can solve the convergence problem, calculate quickly and achieve accurate results. The aim is verified through comparing the results obtained from the proposed method to those obtained from the Newton-Raphson method and the decoupled method respectively. The Newton-Raphson and the decoupled methods already exists in MATLAB tool package. Hence their results are used as reference values for comparison purpose.

- The proposed method is applied to a Polish 2383-bus single-phase power system to investigate the effects of harmonic penetration by integrating renewable energy generations. They include wind turbines (WTs) and photovoltaic generators (PGs) and modern electric devices such as electric vehicle chargers (EVCs). The investigation has two aspects: changing their power capacities and tracking their daily generation and load demand curves.

1.5 Thesis Structure

This thesis is organized in eight chapters and reflects on the methodological steps and the contributions of this work. Chapter 1 provides an introduction to the whole thesis. It gives a brief introduction to power quality and the motivation of this research. Furthermore, it presents the research objectives, the research scopes and the original contributions of this thesis.

Chapter 2 studies the harmonic basic theory. It gives the definitions of integer, inter, sub and triplen harmonics. The harmonic expressions such as Fourier series, harmonic sequences and several important formulations and measures for harmonic calculations and analysis are also presented. With increasing use of renewable energy generations and modern electric devices in power systems, the wind turbines (WTs), photovoltaic generators (PGs) and electric vehicle chargers (EVCs) are described as harmonic sources. Finally, it introduces the harmonic effects and the harmonic distortion limited standards.

Chapter 3 reviews in detail the existing harmonic power flow calculation methods. They are classified into the Newton-Raphson based harmonic power flow method, the decoupled harmonic power flow method, the fast decoupled harmonic power flow method, the fast harmonic power flow method, the fuzzy harmonic power flow method, the probabilistic harmonic power flow method and the modular harmonic power flow method, based on several criteria. Moreover, their advantages and disadvantages are investigated. Finally, the Newton-Raphson based method and the decoupled method are applied to a simple 5-bus power system with a six-pulse line-commutated converter to calculate the harmonic power flow.

Chapter 4 proposes a fast hybrid harmonic power flow calculation method (FHM) to evaluate the harmonic penetration in the power systems. It applies the secant method to establish the iterative initial value to solve the convergence problem caused by the poor initial value, and combines both the Newton-Raphson method and the decoupled method together to calculate the harmonic power flow in the power systems in order to reduce the computing time and make the calculation converge successfully.

In chapter 5, the proposed fast hybrid method is applied to 14-bus, 39-bus, 57-bus and 118-bus power systems to evaluate the harmonic penetration. The results contain the computing time, the iterations, the root mean square (rms) values of the bus voltage magnitudes, the total harmonic voltage distortion (THDv), the total active and reactive powers at both sending and receiving ends and the total power losses on each branch. Then, these results are compared to those achieved by the Newton-Raphson based method and the decoupled method to investigate whether the proposed method can solve the convergence problem and accomplish the calculation quickly and accurately.

In chapter 6, the proposed method is applied to a Polish 2383-bus single-phase power system to calculate the harmonic voltages and powers, and investigate the effects of integrating renewable energy generations and modern devices to the harmonic penetration with changing their power capacities. The wind turbines (WTs), photovoltaic generators (PGs) and electric vehicle chargers (EVCs) are regarded as harmonic sources.

Chapter 7 applies the fast hybrid method to evaluate the harmonic penetration during 24 hours in Polish 2383-bus single-phase power system. It has the same harmonic sources as in chapter 6. Their number and position are constant: 82 WTs, 86 PGs, 329 EVCs and 222 six-pulse converters are connected to the power network. The output generation powers and load consumption powers of renewable power generators and all loads are changed per 15 minutes, following their hourly generation and load models respectively. Two different models are used: one is in summer, the other is in winter.

Chapter 8 will summarise the thesis and discuss the contributions of this work. Future work for the development of this research is proposed.

1.6 Associated Publications

Based on the results of the research work reported in this thesis, the following papers have been published:

- **Jianfeng Lu**, Gengyin Li, Ming Zhou and K.L.Lo, "*A methodology to evaluate harmonic penetration in power networks,*" in 11th International Conference on Electrical Power Quality and Utilisation (EPQU), Lisbon, Portugal, 2011.

- **Jianfeng Lu** and Professor K L Lo, " *A fast hybrid methodology to evaluate harmonic penetration in a large power network* ", under preparation.

- **Jianfeng Lu** and Professor K L Lo, " *Harmonic penetration effects of integrating variable power capacities of renewable generations to a large power network* ", under preparation.

References

[1] E. Fuchs and M. Masoum, *Power quality in power systems and electrical machines, 2008*. Academic Press. xix, 1, 2

[2] H. Siahkali, "Power quality indexes for continue and discrete disturbances in a distribution area," in *Power and Energy Conference, 2008. PECon 2008. IEEE 2nd International*, 2008, pp. 678–683. 1

[3] J. Arrillaga, N. R. Watson, and S. Chen, *Power system quality assessment*. John Wiley & Sons New York, NY, 2000. v, xix, 1, 2

[4] J. Arrillaga, B. C. Smith, N. R. Watson, and A. R. Wood, *Power system harmonic analysis*. Wiley, 1997.

[5] J. Arrillaga and N. R. Watson, *Power system harmonics*. Wiley. com, 2004. 6

[6] M. H. J. Bollen, *Understanding power quality problems: voltage sags and interruptions*. Wiley-IEEE Press, 2000. xi, 2, 3

[7] M. Caserza Magro, A. Mariscotti, and P. Pinceti, "Definition of power quality indices for dc low voltage distribution networks," in *Instrumentation and Measurement Technology Conference, 2006. IMTC 2006. Proceedings of the IEEE*. IEEE, 2006, pp. 1885–1888.

[8] S. Chattopadhyay, M. Mitra, and S. Sengupta, *Electric power quality*. Springer, 2011.

[9] R. Dugan, M. F. McGranaghan, and H. W. Beaty, *Electric power systems quality*. McGraw-Hill, 2002.

[10] T. Ise, Y. Hayashi, and K. Tsuji, "Definitions of power quality levels and the simplest approach for unbundled power quality services," in *Harmonics and Quality of Power, 2000. Proceedings. Ninth International Conference on*, vol. 2. IEEE, 2000, pp. 385–390.

[11] V. Yuvaraj, E. Pratheep Raj, A. Mowlidharan, and L. Thirugnanamoorthy, "Power quality improvement for grid connected wind energy system using facts device,"

in *Nonlinear Dynamics and Synchronization (INDS) & 16th Int'l Symposium on Theoretical Electrical Engineering (ISTET), 2011 Joint 3rd Int'l Workshop on*. IEEE, 2011, pp. 1–7.

[12] D. Zejun, Z. Yongqiang, and C. Caihong, "Comprehensive evaluation of power quality based on meaningful classification," in *Critical Infrastructure (CRIS), 2010 5th International Conference on*. IEEE, 2010, pp. 1–4.

[13] "Ieee recommended practice for monitoring electric power quality," *IEEE Std 1159-2009 (Revision of IEEE Std 1159-1995)*, pp. c1–81, 2009. v, xix, 1, 3, 4

[14] D. Xia and G. T. Heydt, "Harmonic power flow studies part i-formulation and solution," *Power Apparatus and Systems, IEEE Transactions on*, no. 6, pp. 1257–1265, 1982. 6

Chapter 2

Harmonics

2.1 Introduction

Power systems are expected to supply pure sinusoidal alternating current and voltage waveforms of single frequency (50 Hz or 60 Hz). However, the actual current and voltage waveforms are distorted and are a combination of many sine waves of different frequencies. Normally they are regarded as non-sinusoidal waveforms. If the frequencies of a periodic non-sinusoidal waveform are integer or non-integer multiples of the fundamental frequency (50 Hz or 60 Hz), we define the spectral components of this non-sinusoidal waveform as harmonics or inter harmonics [1].

Actually, the presence of power system harmonics is not a new phenomenon. The author in reference [1] mentioned that in 1894 the word "harmonic" was first time used in the paper written by Houston and Kennelly. This paper popularized the concept of harmonics and explained that a superposition of a series of harmonics upon a plain sinusoidal fundamental wave would produce such a non-sinusoidal waveform. Then, reference [2] indicated that Steinmetz published a book to devote considerable attention to the study of harmonics in three-phase power systems in 1916. His main concern was third harmonic current caused by saturated iron core in transformers and machines. Later, with rural electrification and the use of telephone service, power and telephone circuits were often placed on common rights-of-way. Harmonic currents produced by transformer magnetizing currents caused inductive interference

with open-wire telephone systems which resulted in the interference of voice communication. Today, the most common harmonic sources are power electronic loads such as adjustable-speed drives (ASDs) and switch-mode power supplies. These loads use diodes, silicon-controlled rectifiers (SCRs), power transistors, and other electronic switches to cut waveforms to control power or to convert AC to DC or DC to AC. The renewable energy generators such as wind turbine generators and photovoltaic generators are mainly studied as harmonic sources due to their employment of these power electronic equipments.

According to references [1–4] electrical power system harmonic problems are mainly due to the substantial increase of power electronic equipments and the electronics or microprocessor controllers in modern industry. They are used for seeking higher system reliability and efficiency. Also they can be used for the power system control in AC/DC transmission lines or loads. Moreover, the electric utility's increased use of capacitor banks that attempting an improved power factor is another reason of power system harmonics generation. The effects of the power system harmonics are operation failure of electrical and electronic components, overheating of neutral wires and transformer, failure of power factor correction capacitors, loss in power generation and transmission, and interference with protection, control and communication networks as well as customer loads.

This chapter gives the definitions of integer, inter, sub and triplen harmonics in section 2.2. The harmonic expressions such as Fourier series, and several important formulations and measures for harmonic calculations and analysis are studied in section 2.3 and 2.4, respectively. Section 2.5 indicates the harmonic sequences. The principles of harmonic current emissions generated by electric vehicle chargers (EVCs), wind turbine (WTs) and photovoltaic generators (PGs) are denoted in section 2.6. The harmonic effects and harmonic distortion limit standards are described in section 2.7 and 2.8, respectively. Finally, a conclusion of this chapter is given in section 2.9. Eighty-three references [1–83] are reviewed and classified in these nine sections.

2.2 Definition of Harmonics

2.2.1 Integer Harmonics

The definition of integer harmonics in power network is sinusoidal periodical waves having frequencies that are integral multiple of fundamental frequency. The power network fundamental frequency is usually 50 Hz or 60 Hz. Integer harmonics can be expressed by the following equation:

$$f^{(h)}(t) = A^{(h)} * \sin(2\pi hft + \alpha^{(h)}) \tag{2.1}$$

where $A^{(h)}$ is the h^{th} harmonic order amplitude. h is an integer, $h = 1,2,3,\ldots$. f is fundamental frequency. And $\alpha^{(h)}$ is the h^{th} harmonic order phase angle.

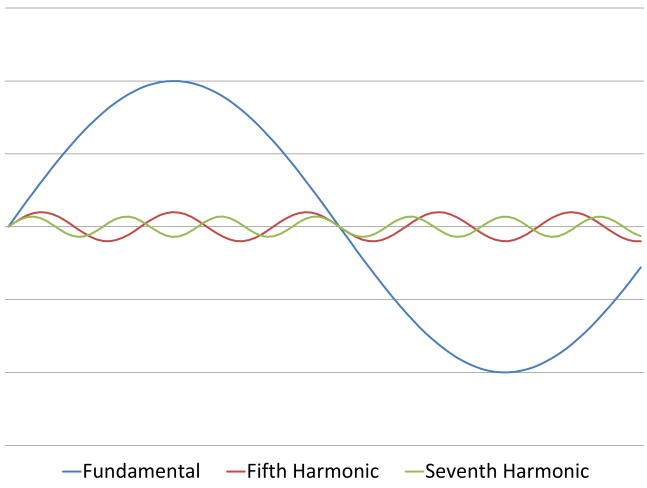

Figure 2.1: First, fifth and seventh harmonic wave forms

Figure 2.1 illustrates the first, fifth and seventh integer harmonic wave forms.

Even Harmonics Even harmonics are the even components of integer harmonics, where $h = 2,4,6,\ldots,2n$.

Odd Harmonics Odd harmonics are the odd components of integer harmonics, where $h = 1,3,5,\ldots,2n \pm 1$.

2.2.2 Inter Harmonics

Inter harmonics are sinusoidal periodical waves with frequencies that are non-integer multiple of power network fundamental frequency. The inter harmonics can be expressed by equation 2.1 as well. But h is non-integer, and should be larger than integer one (e.g. $h = 1.5, 1.8, 2.6, \ldots$).

2.2.3 Sub Harmonics

Sub harmonics are sinusoidal periodical waves with frequencies that are below fundamental frequency. h of equation 2.1 is less than integer one (i.e. $0 < h < 1$).

2.2.4 Triplen Harmonics

The triplen harmonics are defined as the sinusoidal periodical waves that have frequencies which are odd multiples of the third harmonic frequency (e.g. $3^{rd}, 9^{th}, 15^{th}, \ldots$). Triplen harmonics are of particular concern because they are zero sequence harmonics (explained in section 2.5). The consequence of this fact is that the magnitude of these currents on a three-phase w-y-e connection configuration are additive in neutral. This can lead to very large currents circulating in neutral. This phenomenon can be explained through the example below.

For a balanced three-phase w-y-e connection configuration, the phase currents on the 3^{rd} harmonic order are:

$$I_{an}^{(3)} = \mid I^{(3)} \mid \cos 3(\omega t + 0^\circ) = \mid I^{(3)} \mid \cos(3\omega t + 0^\circ) = \mid I^{(3)} \mid \cos(3\omega t) \tag{2.2}$$

$$I_{bn}^{(3)} = \mid I^{(3)} \mid \cos 3(\omega t - 120^\circ) = \mid I^{(3)} \mid \cos(3\omega t - 360^\circ) = \mid I^{(3)} \mid \cos(3\omega t) \tag{2.3}$$

$$I_{cn}^{(3)} = \mid I^{(3)} \mid \cos 3(\omega t + 120^\circ) = \mid I^{(3)} \mid \cos(3\omega t + 360^\circ) = \mid I^{(3)} \mid \cos(3\omega t) \tag{2.4}$$

Hence

$$I_{an}^{(3)} + I_{bn}^{(3)} + I_{cn}^{(3)} = 3 \mid I^{(3)} \mid \cos(3\omega t) \tag{2.5}$$

And

$$I_{an}^{(1)} + I_{bn}^{(1)} + I_{cn}^{(1)} = 0 \tag{2.6}$$

It is assumed that the neutral current, I_N, contains only the fundamental and 3^{rd} harmonic order frequencies. Therefore, it can be expressed by:

$$I_N = I_{an}^{(1)} + I_{an}^{(3)} + I_{bn}^{(1)} + I_{bn}^{(3)} + I_{cn}^{(1)} + I_{cn}^{(3)} = 3 \mid I^{(3)} \mid \cos(3\omega t) \tag{2.7}$$

As a result, such neutral current can lead to a fire hazard, also cause significant overheating in the transformer. Single-phase power supplies for equipment such as electronic ballasts and PCs are the most significant source of triplen harmonics.

2.3 Harmonic Expression

When more and more nonlinear equipment such as transformers, rotating electric machines, rectifiers, converters, PCs, arc furnaces, AC/DC drivers, renewable energy generators (e.g. wind turbine generator, photovoltaic system), and electric vehicle chargers are integrated in the power system, non-sinusoidal periodical voltage and current waveforms occur. See Figure 2.2.

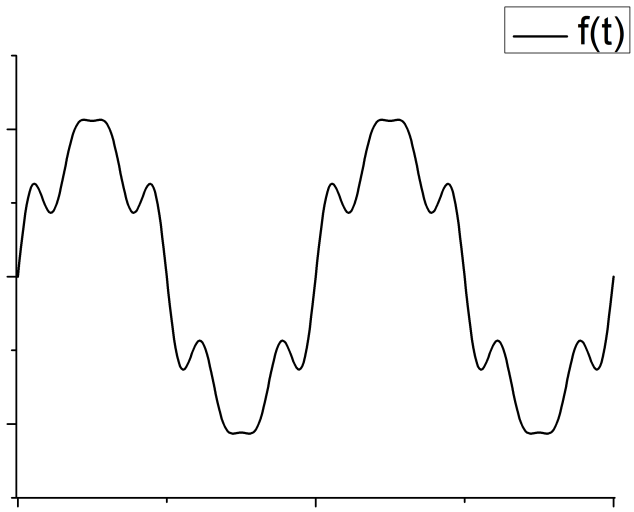

Figure 2.2: A non-sinusoidal periodical voltage waveform

Therefore, Fourier series is involved to reformulate this kind of non-sinusoidal waveform for convenient and better analysis.

Fourier series is an effective approach for harmonic research. It decomposes the non-sinusoidal periodical signal waveform into the sum of a set of sinusoidal components with different frequencies [28, 79]. Each term of Fourier series is called harmonic component of the original non-sinusoidal waveform.

Generally speaking, each non-sinusoidal periodical signal waveform that is over $[0, 2\pi]$ can be expanded by the following equation:

$$f(t) = A^{(o)} + \sum_{h=1}^{\infty} [A^{(h)} \cos(h\omega_o t) + B^{(h)} \sin(h\omega_o)t] \tag{2.8a}$$

$$= A^{(o)} + \sum_{h=1}^{\infty} C^{(h)} \sin(h\omega_o t + \varphi^{(h)}) \tag{2.8b}$$

where $f(t)$ is a non-sinusoidal periodical waveform; h is harmonic frequency; ω_o is fundamental angular frequency; $\varphi^{(h)}$ is the h^{th} harmonic phase angle; $A^{(o)}$ is DC Fourier coefficient; $A^{(h)}$, $B^{(h)}$, and $C^{(h)}$ are harmonic Fourier coefficients.

$$\omega_o = \frac{2\pi}{T} \quad (T \text{ is period}) \tag{2.9}$$

$$A^{(o)} = \frac{1}{T}\int_0^T f(t)\mathrm{d}t = \frac{1}{2\pi}\int_0^{2\pi} f(t)\mathrm{d}x \quad (x = \omega_o t) \tag{2.10}$$

$$A^{(h)} = \frac{2}{T}\int_0^T f(t)\cos(h\omega_o t)\mathrm{d}t = \frac{1}{\pi}\int_0^{2\pi} f(t)\cos(hx)\mathrm{d}x \tag{2.11}$$

$$B^{(h)} = \frac{2}{T}\int_0^T f(t)\sin(h\omega_o t)\mathrm{d}t = \frac{1}{\pi}\int_0^{2\pi} f(t)\sin(hx)\mathrm{d}x \tag{2.12}$$

$$C^{(h)} = \sqrt{\left(A^{(h)}\right)^2 + \left(B^{(h)}\right)^2} \tag{2.13}$$

$$\varphi^{(h)} = \arctan\left(\frac{A^{(h)}}{B^{(h)}}\right) \tag{2.14}$$

Hence, the non-sinusoidal waveform, $f(t)$, shown in Figure 2.2 can be expressed

by sum of the three harmonic components using the Fourier series. They are shown in Figure 2.3 below.

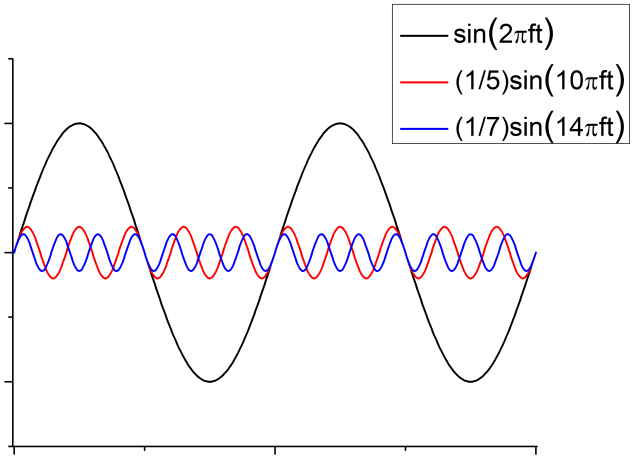

Figure 2.3: The components of the non-sinusoidal waveform

2.4 Harmonic Formulations and Measures [1, 17, 24, 28, 45]

This section will present several typical formulations and measures of harmonics. They are commonly used in harmonic analysis, harmonic calculation and harmonic power flow penetration evaluation.

2.4.1 Harmonic Voltage and Current

The harmonic voltage and current can be expressed by Fourier series expansion in general. Their mathematical equations are:

$$v(t) = V_{DC} + \sum_{h=1}^{n} V^{(h)} \cos(h\omega_o t + \alpha^{(h)}) \tag{2.15}$$

$$i(t) = I_{DC} + \sum_{h=1}^{n} I^{(h)} \cos(h\omega_o t + \beta^{(h)}) \tag{2.16}$$

V_{DC} - DC component voltage
I_{DC} - DC component current
h - harmonic order ($h = 1, 2, 3, \ldots, n$)
$V^{(h)}$ - h^{th} maximum value of harmonic voltage
$I^{(h)}$ - h^{th} maximum value of harmonic current
ω_o - fundamental angular frequency
$\alpha^{(h)}$ - h^{th} harmonic voltage phase angle
$\beta^{(h)}$ - h^{th} harmonic current phase angle

2.4.2 Root Mean Square (rms) Value of Voltage and Current

rms value of non-sinusoidal voltage can be expressed by:

$$\begin{aligned} V_{rms} &= \sqrt{\left(V_{DC}\right)^2 + \sum_{h=1}^{n}\left(v_{rms}^{(h)}\right)^2} \\ &= \sqrt{\left(V_{DC}\right)^2 + \left(v_{rms}^{(1)}\right)^2 + \left(v_{rms}^{(2)}\right)^2 + \ldots + \left(v_{rms}^{(n)}\right)^2} \\ &(V_{DC} = 0 \qquad \text{if non-sinusoidal voltage do not have DC part}) \end{aligned} \tag{2.17}$$

The mathematical equation of rms value of non-sinusoidal current is:

$$\begin{aligned} I_{rms} &= \sqrt{\left(I_{DC}\right)^2 + \sum_{h=1}^{n}\left(i_{rms}^{(h)}\right)^2} \\ &= \sqrt{\left(I_{DC}\right)^2 + \left(i_{rms}^{(1)}\right)^2 + \left(i_{rms}^{(2)}\right)^2 + \ldots + \left(i_{rms}^{(n)}\right)^2} \\ &(I_{DC} = 0 \qquad \text{if non-sinusoidal current do not have DC part}) \end{aligned} \tag{2.18}$$

where $v_{rms}^{(h)}$ and $i_{rms}^{(h)}$ represent h^{th} harmonic rms values of voltage and current, respectively.

2.4.3 Apparent Power

According to the rms value of non-sinusoidal voltage and current shown in equation 2.17 and 2.18, apparent power S can be expressed by:

$$\begin{aligned} S &= V_{rms} I_{rms} \\ &= \sqrt{\left(V_{DC}\right)^2 + \sum_{h=1}^{n} \left(v_{rms}^{(h)}\right)^2} \sqrt{\left(I_{DC}\right)^2 + \sum_{h=1}^{n} \left(i_{rms}^{(h)}\right)^2} \end{aligned} \tag{2.19}$$

2.4.4 Active Power and Reactive Power

The mathematical equation of total active power is:

$$P = V_{DC} I_{DC} + \sum_{h=1}^{n} v_{rms}^{(h)} i_{rms}^{(h)} \cos(\alpha^{(h)} - \beta^{(h)}) \tag{2.20}$$

The mathematical equation of total reactive power is:

$$Q = \sum_{h=1}^{n} v_{rms}^{(h)} i_{rms}^{(h)} \sin(\alpha^{(h)} - \beta^{(h)}) \tag{2.21}$$

2.4.5 Distortion Power

Under sinusoidal condition, power balance can be presented by

$$\left(S^{(1)}\right)^2 = \left(P^{(1)}\right)^2 + \left(Q^{(1)}\right)^2 \tag{2.22}$$

as illustrated by Figure 2.4(a).

However, if voltage and current are non-sinusoidal waveforms, equation 2.22 does not hold. We need to include a parameter D that is named distortion power to preserve the power balance. The new power balance equation is represented mathematically by

$$S^2 = P^2 + Q^2 + D^2 \tag{2.23}$$

Therefore, the distortion power D can be calculated by

$$\begin{aligned} D &= \sqrt{S^2 - P^2 - Q^2} \\ &= \sqrt{S^2 - \left(\sum_{h=1}^{\infty} P^{(h)}\right)^2 - \left(\sum_{h=1}^{\infty} Q^{(h)}\right)^2} \end{aligned} \tag{2.24}$$

Figure 2.4(b) indicates the new power balance in phase diagram.

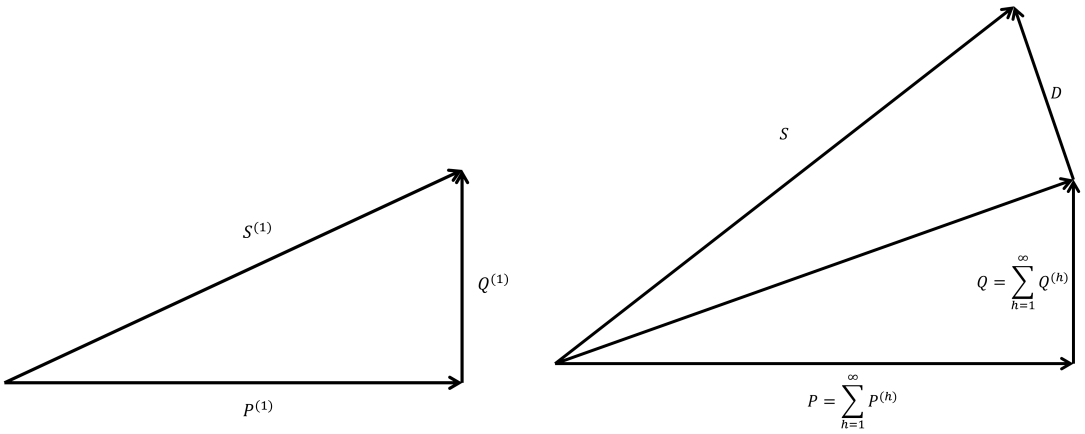

(a) Sinusoidal condition (b) Non-sinusoidal condition

Figure 2.4: Power balance phasor diagram under both sinusoidal condition and non-sinusoidal condition

2.4.6 Total Harmonic Distortion (THD)

Total harmonic distortion (THD) is commonly used to indicate harmonic content of a distorted non-sinusoidal waveform with a single number. It is commonly defined as a ratio of the sum of active powers of harmonic components to the active power at fundamental frequency in percentage. It is also can be considered as a ratio of root mean square (rms) value of harmonic components of a certain non-sinusoidal voltage or current waveform to the rms value of the fundamental component in percentage. Their expressions are shown below.

Total active power harmonic distortion

$$THD_p = \frac{\sum_{h=2}^{\infty} P^{(h)}}{P^{(1)}} \tag{2.25}$$

Total harmonic voltage distortion

$$THD_v = \frac{\sqrt{\sum_{h=2}^{\infty} \left(v^{(h)} \right)^2}}{v^{(1)}} \tag{2.26}$$

Total harmonic current distortion

$$THD_i = \frac{\sqrt{\sum_{h=2}^{\infty} \left(i^{(h)} \right)^2}}{i^{(1)}} \tag{2.27}$$

2.4.7 Total Power Factor

The mathematical equation of total power factor of a non-sinusoidal waveform is

$$pf = \frac{P}{\sqrt{P^2 + Q^2 + D^2}} \tag{2.28}$$

2.5 Harmonic Sequences

For a balanced three-phase power system, harmonic components that are decomposed by Fourier series of a non-sinusoidal waveform (voltage is used to be an example here) can be expressed by

$$\begin{aligned} v_{an}^{(h)}(t) &= V_{an}^{(h)} \cos h(\omega_o t) \\ v_{bn}^{(h)}(t) &= V_{bn}^{(h)} \cos h(\omega_o t - 120^\circ) \\ v_{cn}^{(h)}(t) &= V_{cn}^{(h)} \cos h(\omega_o t - 240^\circ) \end{aligned} \tag{2.29}$$

where $h = 1, 2, 3, \ldots, n$.

Hence, for the fundamental voltages, we obtain

$$\begin{aligned} v_{an}^{(1)}(t) &= V_{an}^{(1)}\cos(\omega_o t) \\ v_{bn}^{(1)}(t) &= V_{bn}^{(1)}\cos(\omega_o t - 120^\circ) \\ v_{cn}^{(1)}(t) &= V_{cn}^{(1)}\cos(\omega_o t - 240^\circ) \end{aligned} \tag{2.30}$$

The phase shift of this balanced three-phase non-sinusoidal fundamental voltage is illustrated by Figure 2.5(a). The negative phase angle displacements indicate that the fundamental voltage phase angles rotate clockwise. Hence, it is regarded as positive sequence harmonics.

The expressions of fifth harmonic voltages are shown below

$$\begin{aligned} v_{an}^{(5)}(t) &= V_{an}^{(5)}\cos 5(\omega_o t) = V_{an}^{(5)}\cos(5\omega_o t) \\ v_{bn}^{(5)}(t) &= V_{bn}^{(5)}\cos 5(\omega_o t - 120^\circ) = V_{bn}^{(5)}\cos(5\omega_o t - 600^\circ) \\ &= V_{bn}^{(5)}\cos(5\omega_o t + 120^\circ) \\ v_{cn}^{(5)}(t) &= V_{cn}^{(5)}\cos 5(\omega_o t - 240^\circ) = V_{cn}^{(5)}\cos(5\omega_o t - 1200^\circ) \\ &= V_{cn}^{(5)}\cos(5\omega_o t + 240^\circ) \end{aligned} \tag{2.31}$$

The positive phase angle displacements represent that the fifth harmonic voltage phase angles rotate anticlockwise and opposite to that of the fundamental voltage as shown in Figure 2.5(b). Therefore, the fifth harmonic voltage is known as negative sequence harmonics.

For third harmonic frequency, the voltages are defined as

$$\begin{aligned} v_{an}^{(3)}(t) &= V_{an}^{(3)}\cos 3(\omega_o t) = V_{an}^{(3)}\cos(3\omega_o t) \\ v_{bn}^{(3)}(t) &= V_{bn}^{(3)}\cos 3(\omega_o t - 120^\circ) = V_{bn}^{(3)}\cos(3\omega_o t - 360^\circ) \\ &= V_{bn}^{(3)}\cos(3\omega_o t) \\ v_{cn}^{(3)}(t) &= V_{cn}^{(3)}\cos 3(\omega_o t - 240^\circ) = V_{cn}^{(3)}\cos(3\omega_o t - 720^\circ) \\ &= V_{cn}^{(3)}\cos(3\omega_o t) \end{aligned} \tag{2.32}$$

Figure2.5(c) expresses the third harmonic voltages in diagram. It is shown that there is no phase angle displacement between each phase of third harmonic voltages. Hence, we define third harmonic voltages as zero sequence harmonics.

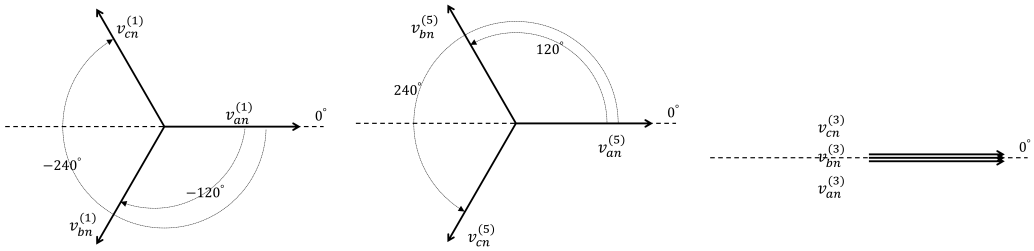

(a) Clockwise (b) Anticlockwise (c) None

Figure 2.5: Phase angle displacements diagrams of fundamental, fifth harmonic and third harmonic voltage respectively

The similar relationships exist for other harmonic orders. Table 2.1 categorizes harmonic sequences in term of their respective harmonic orders. '+', '−' and '0' represent positive, negative and zero sequence respectively.

Table 2.1: Harmonic sequences in balanced three-phase power system

Harmonic order	1	2	3	4	5	6	7	8	9	10	11	12	13
Harmonic sequence	+	-	0	+	-	0	+	-	0	+	-	0	+
Harmonic order	14	15	16	17	18	19	20	21	22	23	24	25	26
Harmonic sequence	-	0	+	-	0	+	-	0	+	-	0	+	-
Harmonic order	27	28	29	30	31	32	33	34	35	36	37	38	39
Harmonic sequence	0	+	-	0	+	-	0	+	-	0	+	-	0

2.6 Harmonic Sources

Non-linear equipment or components integrated in the power system causes harmonic distortion of voltage and current. Many documents were published to categorize them. Fuchs and Masoum in reference [28] classified harmonic sources into two groups. One is industrial non-linear loads such as rectifiers, inverters, arc furnaces, welding machines, or lighting; the other is residential loads with switch- mode power supplies such as television sets or computers. In reference [59], harmonic sources are

categorized into current source non-linear load and voltage source non-linear load. According to their properties, twenty-two configurations of power filters for harmonic compensation are presented as well. However, reference [1] and [45] divided those non-linear equipment or components causing harmonic distortion in the power system into three aspects: saturated devices such as transformers, motors and generators; arcing equipment including arc furnaces, fluorescent as well as mercury lights; and power electronic equipment such as inverters, rectifiers, and switched mode power supplies. References [17, 43] give the details about magnetization non-linearities of transformer,rotating machines, arcing devices, semiconductor based power supply system, inverter fed A.C. drives, thyristor controlled reactors, phase controllers and A.C. regulators. Traditionally, rectifiers and converters are regarded as main harmonic sources [10, 59, 74].

Recently, with technology development more and more renewable energy generators (such as wind generator and photovoltaic generator) and equipment (e.g. electric vehicle charger) are integrated into the power system to supply energy. However, these generators and equipment inject more harmonics into the power system. Hence, they are regarded as harmonic sources as well. This section will describe wind generator, photovoltaic generator, and electric vehicle charger respectively.

2.6.1 Wind Generator

Wind generators are classified into two types according to the wind turbine speed control topologies. One is fixed speed turbine; the other is variable speed turbines. In the early 1990s, the fixed speed wind turbines with induction generators were commonly used. It is simple, robust, cheap, and reliable. The disadvantages are uncontrollable wind speed, uncontrollable reactive power consumption, and limited power quality control. Hence, this type of wind turbines cannot utilize the wind power efficiently. Variable speed wind turbines overcome the disadvantages of fixed speed wind turbines, and become the dominant wind turbines until now. It improves the power quality and reduces mechanical stress. However, it increases the cost of equipment for more complicated electrical and control systems. More harmonics and losses are generated by the power converters connected between the machines and the power network [41].

Figure 2.5 illustrates four different types of wind turbine generators that include fixed speed and variable speed wind turbines. Figure 2.6(a) shows a fixed speed wind turbine that an induction generator is connected to wind turbine generator (WTG) step-up transformer directly through a soft starter. Figure 2.6(b) represents a wound rotor induction generator (WRIG) is connected to WTG step-up transformer directly similar to type A. The generator speed is controllable by a variable rotor resistance. The stator of a doubly fed induction generator (DFIG) is connected to the WTG step-up transformer directly in Figure 2.6(c). But the rotor is connected to the transformer through a power converter. This is a variable speed wind turbine. While the Figure 2.6(d) indicates a variable speed wind turbine that permanent magnetic synchronous generator (PMSG) or wound rotor synchronous generator (WRSG) or WRIG is connected to the step-up transformer through a full scale power converter as well [18, 41, 53].

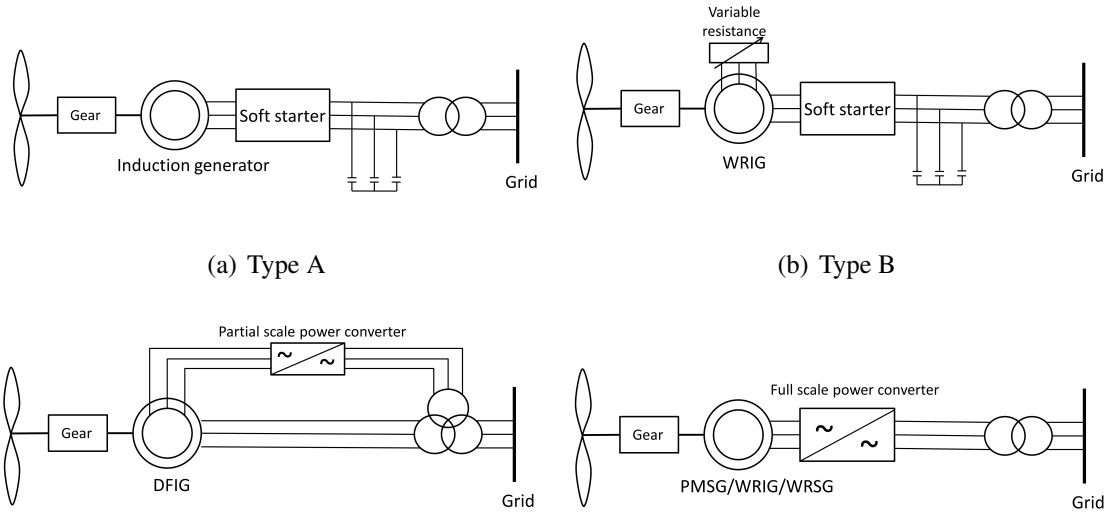

(a) Type A

(b) Type B

(c) Type C

(d) Type D

Figure 2.6: Configuration of four types of wind turbine generators

The harmonic emissions of wind turbines are considered under the following three aspects:

- Harmonics are generated by the grid-side power electrical converters. [5, 37, 38, 54, 75]

- Resonance problems may occur due to the significant amount of capacitance in wind power plant. This can lead to unacceptable levels of harmonic current distortion. [41]

- A long high voltage transmission cable in a typical wind farm generates harmonic currents. The earth capacitance of the cable forms a small impedance for grid-specific voltage harmonics [61, 62].

However, power electrical converters are regarded as the main source for harmonic emissions of wind turbines.

Wind turbine harmonic emissions measurement are published in many articles [25, 38, 39, 42, 47, 49, 54, 55, 63, 75, 76]. Due to IEC 61000-3-6 the aggregated harmonic currents from individual wind turbines of a grid-connected wind farm are established by

$$I_{total}^{(h)} = \sqrt[\beta]{\sum_{i=1}^{N_{wt}} \left(\frac{I_{h,i}}{n_i} \right)^{\beta}} \tag{2.33}$$

where N_{wt} is total number of wind turbines connected to the point of common coupling (PCC); $I_{total}^{(h)}$ represents the total $h^{(th)}$ order harmonic current at PCC; n_i is the ratio of the transformer between the wind turbine and PCC at the i^{th} wind turbine; $I_{h,i}$ is the $h^{(th)}$ order harmonic current at i^{th} wind turbine; and β is defined as

$$\beta = \begin{cases} 1.0 & \text{if } h < 5 \\ 1.4 & \text{if } 5 \leqslant h \leqslant 10 \\ 2.0 & \text{if } h > 10 \end{cases} \tag{2.34}$$

The harmonic emissions spectra of wind farm with a total of 54 permanent magnet synchronous generators (PMSG) [49] and the wind farm consisted by 72 SWT-2.3-93 wind turbines that produced by Siemens [54] are presented in Table 2.2 and Table 2.3 respectively. These data are regarded as harmonic sources in next several sections.

Table 2.2: Harmonic currents generated by the wind farm with 54 PMSGs [49]

Harmonic order'h'	$I^{(h)}/I^{(1)}$ (%)	Harmonic order'h'	$I^{(h)}/I^{(1)}$ (%)	Harmonic order'h'	$I^{(h)}/I^{(1)}$ (%)
1	100	11	1.40	21	0.04
2	1.12	12	0.09	22	0.03
3	0.65	13	0.60	23	0.09
4	0.52	14	0.06	24	0.03
5	1.83	15	0.06	25	0.09
6	0.27	16	0.05	26	0.04
7	0.60	17	0.09	27	0.03
8	0.17	18	0.03	28	0.04
9	0.14	19	0.09	29	0.07
10	0.12	20	0.03		

Table 2.3: Harmonic currents generated by the wind farm with 72 SWT-2.3-93 wind turbines [54]

Harmonic order'h'	$I^{(h)}/I^{(1)}$ (%)	Harmonic order'h'	$I^{(h)}/I^{(1)}$ (%)
1	100	16	0.37
2	0.34	17	0.76
4	0.20	19	0.42
5	0.44	20	0.32
7	0.47	22	0.33
8	0.40	23	0.37
10	0.55	25	0.24
11	1.46	26	0.20
13	1.85	28	0.13
14	0.48	29	0.27

2.6.2 Electric Vehicle Chargers

Electric vehicles (EVs) are becoming an attractive alternative transport to gasoline driven cars. For EVs could offer about 60 % greater mileage from the same amount of petroleum energy and at the same time reduce the CO2 emissions. However, the growing presence of EV battery chargers in residential installations could increase the harmonic levels in the power network. For this reason, some studies tried to model the EV battery chargers and investigate an appropriate approach to estimate the har-

monic emissions of EV chargers and clusters of these loads in the power network [9, 27, 44, 56, 66, 71, 80]. Some published articles [7, 13, 31] predict the impacts of these EV battery chargers on the power network. Others focus on the mitigation of harmonic emissions of EV battery chargers [8, 12, 65].

Single-phase battery chargers and three-phase battery chargers are commonly used in practice [65, 66]. These two types of EV battery chargers are all based on full-wave rectification using diodes. The typical equivalent circuits of them are illustrated in Figure 2.7(a) and Figure 2.7(b) respectively. Figure 2.7(a) shows that the single-phase EV battery charger consists of a single-phase diode bridge with an AC inductor L and its associated resistance R, the resistance R_c and the inductance L_c of the charger circuit and the voltage E of the battery under charge with its internal resistance R_E. The only difference between single-phase EV battery charger and three-phase EV battery charger is the latter one consists of a three-phase diode bridge with three AC inductors L and its associated resistance R in Figure 2.7(b). The inductance L_c is commonly lower than the inductance L.

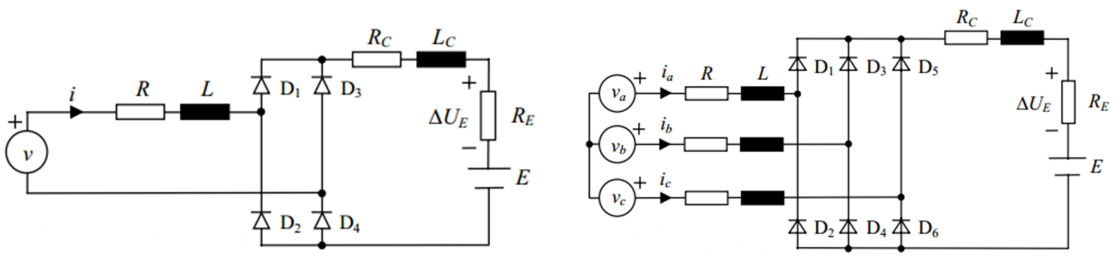

(a) Single-phase EV battery charger

(b) three-phase EV battery charger

Figure 2.7: Typical equivalent circuits of EV battery chargers

The authors [44, 71, 80] defined $X_h(P)$ and $Y_h(P)$ to be the real and imaginary EV battery charger harmonic emission currents of order h in Amperes for an individual charger operating at power P. Then, they plotted each real and imaginary harmonic current versus active power, and interpolated their graphs by polynomial curves with a sufficient number of points. Finally, they obtained a continuous approximation of the

harmonic current injections for each power level, which could be expressed by

$$X_h(P) = a^h_{x_3}P^3 + a^h_{x_2}P^2 + a^h_{x_1}P + a^h_{x_0} \tag{2.35}$$

$$Y_h(P) = a^h_{y_3}P^3 + a^h_{y_2}P^2 + a^h_{y_1}P + a^h_{y_0} \tag{2.36}$$

where $a^h_{x_3}$, $a^h_{x_2}$, $a^h_{x_1}$, and $a^h_{x_0}$ represent the real part coefficients of the approximating polynomials in the h^{th} harmonic order; $a^h_{y_3}$, $a^h_{y_2}$, $a^h_{y_1}$, and $a^h_{y_0}$ are the imaginary part coefficients of the approximating polynomials in the h^{th} harmonic order.

However, each EV battery charger installation point have several EV battery chargers connected in parallel in practice, as shown in Figure 2.8.

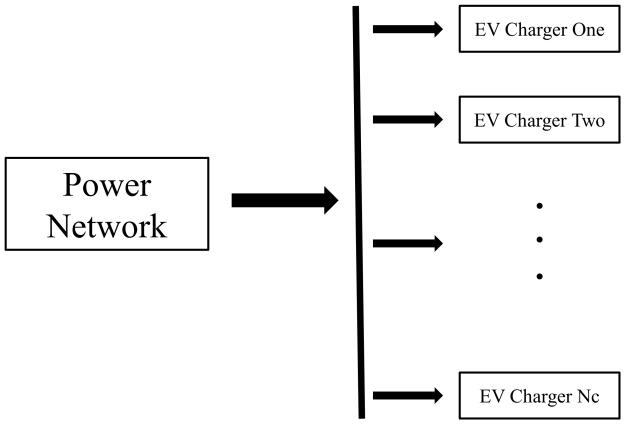

Figure 2.8: EV battery chargers in parallel

Hence, it is important to evaluate the net harmonic currents ejected by N_c EV battery chargers. P. T. Staats, et al. [71], pointed out two random variables that can effect the net harmonic currents calculation. One is the EV battery charger starting time; the other is the initial battery state-of-charge (SOC). For all EVs in the concentration will not begin charging simultaneously, and each charger will not begin operation on a fully discharged battery.

It assumes that the chargers in Figure 2.8 operate independently but in the same fashion and using the same type of charging technology. Therefore, a probability

density function of real and imaginary part is established to predict the net harmonic currents generated by a cluster of EV battery chargers at time j. The mathematical expression is [27, 71]:

$$f_{xhyh}(x,y,j) = \frac{exp\left(\frac{-\eta}{2(1-\gamma^2)}\right)}{2\pi\sigma_{xh}(j)\sigma_{yh}(j)\sqrt{1-\gamma^2}} \tag{2.37}$$

where $\sigma_{xh}(j)$ and $\sigma_{yh}(j)$ represent the standard variance of real and imaginary part of h order harmonic current at time j respectively. γ and η represent the correlation coefficients. Their details and explanations are indicated in references [27, 71].

The author [27] gave the net harmonic emission currents of a cluster of EV battery chargers by applying the above methodology as shown in Table 2.4. Harmonics above the 15th multiple are small in magnitude and are ignored in his study.

Table 2.4: Net harmonic emission current of a cluster of 10 EV battery chargers

Harmonic order'h'	$I^{(h)}/I^{(1)}$ (%)	Phase Angle(°)	Harmonic order'h'	$I^{(h)}/I^{(1)}$ (%)	Phase Angle(°)
1	100	-24	9	14.3	-70
3	31.9	-60	11	9.5	-75
5	24.7	-100	13	4.5	-55
7	17.4	-50	15	3.3	-70

The specifications of the EV battery charger studied are designed:

- For leaded acid battery pack of 20 kWh (@ 5-hour rate), which is equivalent to a battery pack of about 160 Ahr @ 5 hour rate.
- Nominal overall voltage of battery: 120 Vdc.
- Input voltage: 220 Vac, 50 Hz.
- Input current at initial charging: about 36 A.
- Charging time about 6 hours.

2.6.3 Photovoltaic Generators

The photovoltaic (PG) energy is on the way to becoming an attractive renewable energy source in the coming decades due to their relative small size, noiseless operation, simple installation and the possibility to put it close to the user [6]. Hence, the installations of grid-connected PV generators have been supported by government in many countries. However, a large number of grid-connected PG generators connected to a distribution network are potentially able to account for harmonic problems.

The grid-connected PG systems are composed of series arrays of PG modules and a power conditioning unit (PCU) as shown in Figure 2.9 [32]. The PCU includes the maximum power point tracker (MPPT), the DC/AC inverter, the grid interface and the control systems needed for efficient system operation performing. The MPPT is used to track the maximum power point of the current or voltage characteristic with highest possible accuracy to optimise the performance of the PG modules. The direct current (DC) output power generated by PG arrays should be converted into the alternating current (AC) power. Under this condition, an inverter to convert DC power to AC power is required [4, 68, 72].

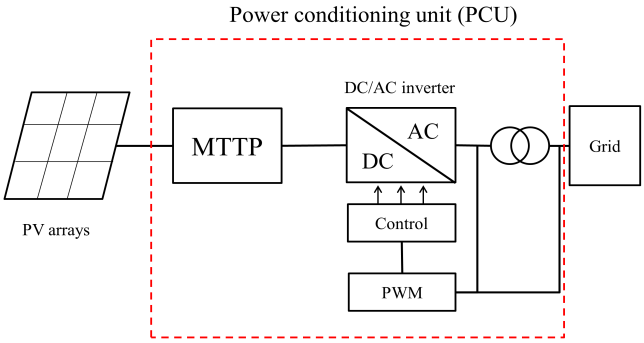

Figure 2.9: The structure of grid-connected PG system

The author in reference [67] denoted that the harmonic current emissions of grid-connected PG systems depended on the type of technology used, on the control strategy of the DC/AC inverter, on the existence of high or low frequency coupling transformer and on the harmonic voltages prevailing in the AC power system. Nevertheless, the

DC/AC inverter is regarded as primary device that ejects harmonic currents to the power network. A dominant role on the harmonic current emission is also given by the performance of the DC/AC inverter under partial generating conditions.

There are various types of inverters that could be used to convert DC power to AC power. The classification of these inverter types are demonstrated in Figure 2.10. A line-commutated inverter uses a switching device like a commutating thyristor that can control the timing of turn-on. But, this switching device cannot control the timing of turn-off. The line-commutated inverter usually uses a supplemental circuit or a source to help to achieve the turn-off timing control. Conversely, a self-commutated inverter can freely control both the ON-state and the OFF-state by using a switching device such as an insulated-gate bipolar transistor (IGBT) or a metal-oxide-semiconductor field-effect transistor (MOSFET). It can freely control the current and voltage waveform at the AC side, adjust the power factor, and suppress the harmonic current. Therefore, it is widely employed to equip the PG systems due to its advantages [4, 6].

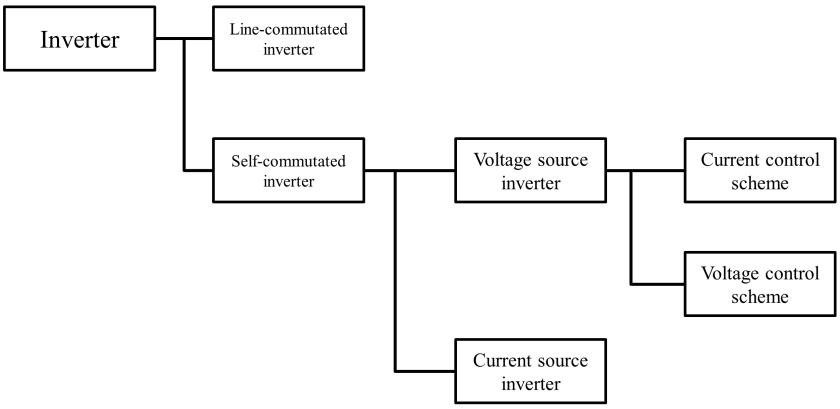

Figure 2.10: The classification of inverter types [4]

The author [19] gave several possible technologies for the DC/AC conversion. One is a centralised inverter for the whole array of PG modules; another is a string inverter that one inverter for each string of PG modules connected in series; and the other is module integrated inverters that a single inverter for each PG module. Module integrated inverters requires installing one inverter for each module. Also the installation

has to withstand different climatic conditions. However it leads to minimise the losses due to mismatching of the current or voltage characteristics, and improves the system modularity and availability.

The inverter requires effective MPP-tracking, high efficiency both for high and low solar irradiance (or radiance), high power factor and low total harmonic distortion (THD) of the currents. Hence, an efficient control scheme is needed. Authors in [15] and [14] indicated control schemes for single- and three-phase grid connected PG inverters respectively. The harmonic emission currents of single- and three-phase PG inverters in frequency domain are also achieved in terms of Laplace transfer functions.

The diagram of a single-phase grid-connected PG inverter and its standard control configuration is shown in Figures 2.11 and 2.12. Note that V_i is input voltage, V_g is grid voltage; L_i and r_i are inverter side inductance and parasitic resistance; L_o and r_o are grid side inductance and parasitic resistance. A long continuous load output filter is used to attenuate the high frequency harmonics injected by the inverter. C is the filter capacitor, and r_c is the relative resistance. i_i and i_o represent inverter current and grid current respectively. i_{ref}, e_i and d denote reference current, error current, and duty cycle or control action disturbance respectively. V_c is the total output of the tracking regulator and the harmonic compensator.

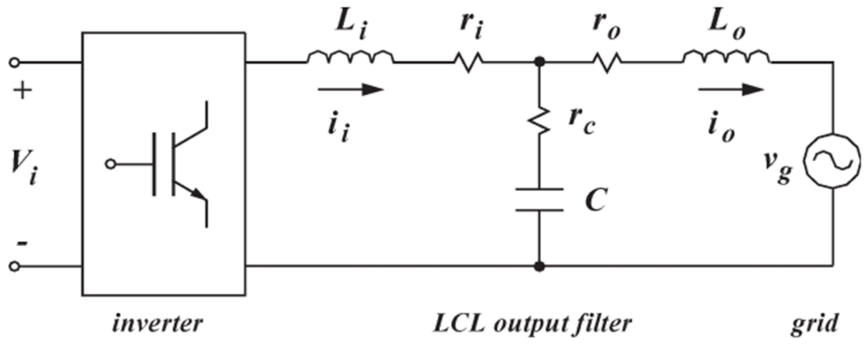

Figure 2.11: Single-phase PG inverter equivalent diagram

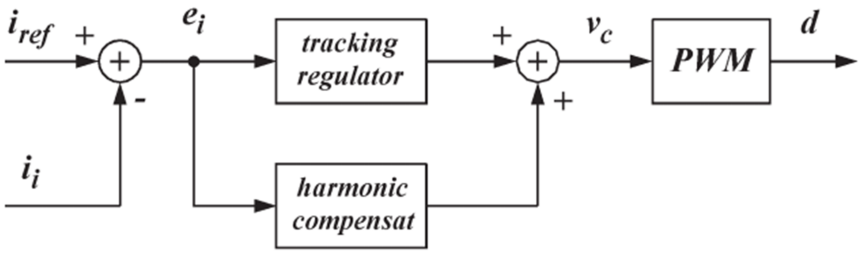

Figure 2.12: Single-phase PG inverter control configuration

In the Laplace domain, the dynamic model of the grid current can be expressed in a general closed-loop form as [84]:

$$i_o(s) = G_7(s)V_i(s) + G_8(s)V_g(s) + G_9(s)i_{ref}(s) \tag{2.38}$$

where $G_7(s)$ is the input voltage to grid current transfer function, $G_8(s)$ represents the grid voltage to grid current transfer function, and $G_9(s)$ denotes the reference signal to grid current transfer function. Their details and explanations are indicated in reference [84].

Figure 2.13 shows the diagram of the three-phase grid-connected PG inverter [14]. The parameters in the three-phase diagram are almost the same with those in the single-phase PG inverter diagram (Figure 2.11). The only difference is that the three-phase PG inverter diagram has a dc-link capacitor (C_{dc}) in the input voltage side. For convenience, it considers the frequency-domain dynamic model of closed-loop harmonic current based on the α - β stationary coordinate system. The equivalent α - β stationary coordinate diagram of three-phase PG inverter and its relative control scheme are illustrated in Figure 2.14(a) and 2.14(b), respectively. $Z_i(s) = L_i s + r_i$, $Z_o(s) = L_o s + r_o$, $Z_c(s) = 1/(C_s) + R_c$. i^*_α and i^*_β represent the reference current in α - β stationary coordinate. d_α and d_β denote the control inputs in α - β stationary coordinate.

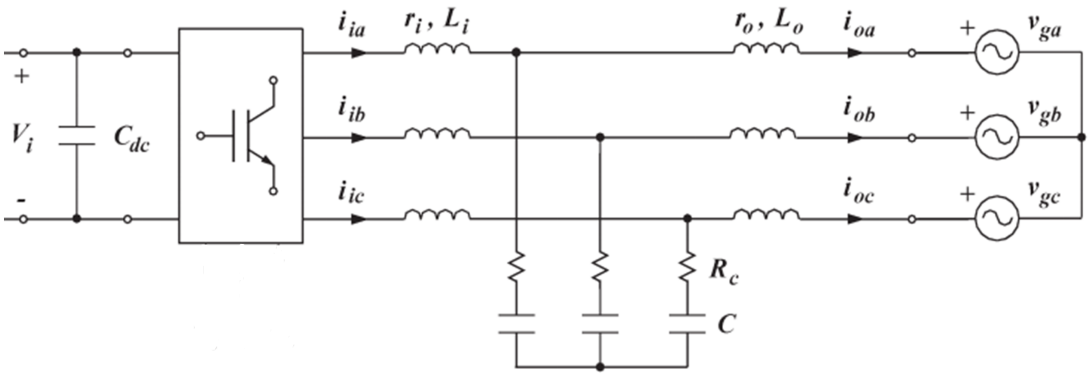

Figure 2.13: Three-phase PG inverter equivalent diagram

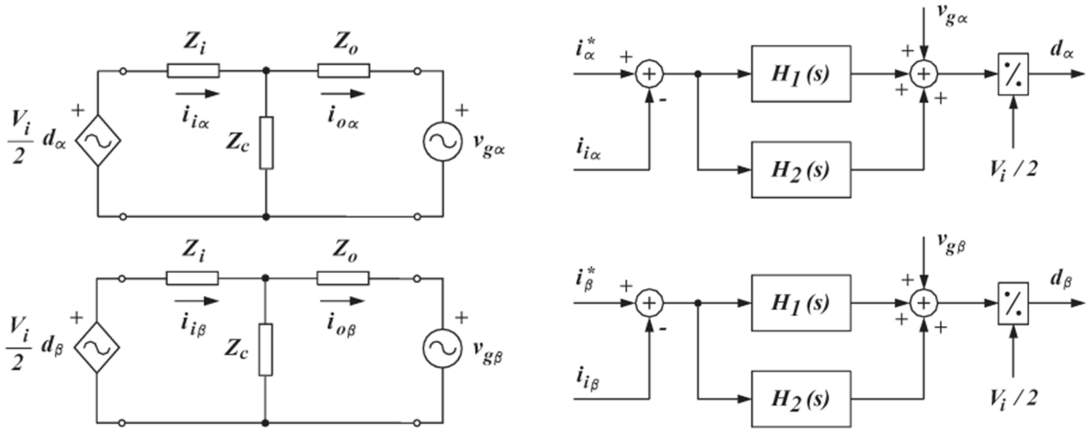

(a) The equivalent α - β stationary coordinate diagram of three-phase PG inverter

(b) Three-phase PG inverter control confituration in α - β stationary coordinate frame

Figure 2.14: Three-phase grid-connected PG inverter

Then it achieves the expression of the dynamic model of harmonic current emission in α - β stationary coordinate:

$$i_{o\alpha}(s) = G_r(s)i_\alpha^*(s) + G_g(s)v_{g\alpha}(s) \tag{2.39}$$

$$i_{o\beta}(s) = G_r(s)i_\beta^*(s) + G_g(s)v_{g\beta}(s) \tag{2.40}$$

where $G_r(s)$ represents the reference signal to grid current transfer function, and $G_g(s)$ represents the grid voltage to grid current transfer function. Their details and explanations are described in reference [14].

Reference [4] gave measured harmonic current emissions spectrum of a 2 kW grid-connected PG inverter in Table 2.5. This data will be used as harmonic injection current source in the next several chapters.

Table 2.5: Harmonic current emissions spectrum of a 2 kW PG inverter

Harmonic order'h'	$I^{(h)}/I^{(1)}$ (%)	$I^{(h)}$ (Amps)	Harmonic order'h'	$I^{(h)}/I^{(1)}$ (%)	$I^{(h)}$ (Amps)
1	100	9	9	0.4	0.036
3	1.5	0.135	11	0.21	0.019
5	0.6	0.054	13	0.2	0.018
7	0.3	0.027			

2.7 Harmonic Effects

In electrical power system, harmonics have a number of undesirable effects on power system equipment as well as on its operation. Harmonics can create series or parallel resonance in power network. Damping property may change due to the presence of harmonics. High levels of harmonic distortion can increase transformer, capacitor, motor or generator heating. The presence of harmonics can also account for the misoperation of electronic equipment that relies on voltage zero crossing detection or is sensitive to waveform, incorrect readings on meters, misoperation of protective relays, interference with telephone circuits, and so on. The detailed studies are provided in references [1–3, 17, 21, 23, 24, 46, 78]. The effects of harmonics can be categorized as follow:

Resonance The presence of harmonics can create series and parallel resonances in the power network. Resonance occurs when the frequency at which the capacitive and inductive reactance of the circuit impedance are equal. Harmonic resonances create problems in operation of power factor correction capacitors and even produce damage to the capacitors due to excessive high current.

Damping Harmonics make variable speed drive motors or a switched mode power supply to introduce small negative impedance or resistance. This will reduce the

damping of the system. The operating performance of electrical devices could be changed by undesirable variation of the degree of damping.

Generator Harmonics produce pulsating or oscillating torques which involve torsional oscillations of rotor elements and rotor heating.

Motor Stator and rotor copper losses increase due to harmonic current flow. The leakage flux created by harmonic currents causes additional stator and rotor losses. Harmonic voltages increase core losses. The positive sequence harmonics develop shaft torques that aid shaft rotations whereas negative sequence harmonics oppose it.

Transformer Stray losses increase due to harmonic current flow. And the presence of high frequency harmonics resonance between winding inductance and line capacitance increase the hysteresis losses.

Relaying The incorrect tripping produced by the presence of harmonic affects the time delay characteristics.

Capacitor Harmonic voltage increases the dielectric loss in capacitors, and the stress on capacitor. The series and parallel resonances between the capacitors and the rest of the system created by harmonics result in overheating and can even reduce the capacitor life. Change of harmonic contents sometimes increases reactive power over permissible manufacturer tolerances.

Cables Harmonics increase the skin effect and proximity effect at a high frequency. As a result the AC resistance increases accordingly. Additional harmonic current also increases copper loss. The increasing of cable dielectric stress caused by harmonic voltage accounts for shortening of the useful life of the cable. However it increases the cost of repairs due to the increasing probability of the number of faults.

Consumer equipment Harmonic changes television (TV) picture size and brightness. Moreover, it creates problems in computer monitor and CPU operation. The fluorescent and mercury arc lighting generated by harmonics result in excessive heating and failure in operation (e.g. Audible noise is produced by harmonic

voltage distortion). The life and efficiency of consumer equipment reduce drastically.

2.8 Harmonic Distortion Limited Standards

Harmonic distortion limited standards play a very important role in harmonic analysis. After the harmonic power flow calculation, the harmonic voltages on PCCs (point of common coupling), the harmonic line currents between two busbars and total harmonic distortions of voltages and currents are established. Then, the harmonic distortion limited standards are regarded as a criterion to consider whether the harmonic distortions are acceptable. Moreover, if a certain electronic equipment can be connected to the power system is determined by these standards as well.

In this section, IEEE (Institute of Electrical and Electronics Engineers) 519 standard, IEC (International Electrotechnical Commission) 61000 series standard and engineering recommendation G5/4 are demonstrated.

2.8.1 IEC 61000 series Standard

The IEC 61000 (or EN 61000) series is one of the most commonly used comprehensive and complete set of standards for power quality in Europe. It totally contains six parts. Among these parts, some aspects of part two (environment) and part three (limits) include harmonic voltage distortion compatibility levels and harmonic current emission limits. The details are listed below [28, 35, 79]:

- IEC 61000-2-2 - Harmonic voltage distortion compatibility levels for public LV (low voltage) power systems. See Table 2.6.
- IEC 61000-2-4 - Harmonic voltage distortion compatibility levels for industrial plants.
- IEC 61000-2-12 - Harmonic voltage distortion compatibility levels for public MV (medium voltage) power systems.

- IEC 61000-3-2 - Harmonic current emission limits for equipment connected at LV power systems with current that is less than 16A per phase. See Table 2.7.
- IEC 61000-3-12 - Harmonic current emission limits for equipment connected at LV power systems with current that is more than 16A but less than 75A per phase.
- IEC 61000-3-6 - The assessment of emission limits for distortion loads in MV and HV (high voltage) power systems.

Table 2.6: IEC 61000-2-2 Harmonic voltage distortion compatibility levels for public LV power systems

Odd harmonics (Non-multiple of three)		**Odd harmonics (Multiple of three)**		**Even harmonics**	
Harmonic order'h'	Harmonic voltage(%)	Harmonic order'h'	Harmonic voltage(%)	Harmonic order'h'	Harmonic voltage(%)
5	6	3	5	2	2
7	5	9	1.5	4	1
11	3.5	15	0.3	6	0.5
13	3	≥ 21	0.2	8	0.5
17	2			10	0.5
19	1.5			≥ 12	0.2
23	1.5				
25	1.5				
≥ 29	x				
The total harmonic voltage distortion level is $THD_v \leq 8\%$ $x = 0.2 + 12.5/h$. For $h = 29,31,35,37$, $V^{(h)} = 0.63\%, 0.6\%, 0.56\%, 0.54\%$.					

Table 2.7: IEC 61000-3-2 Harmonic current emission limits for equipment connected at LV power systems ($< 16A$)

Odd harmonics	**Max harmonic current(A)**	**Odd harmonics**	**Max harmonic current(A)**
3	2.3	2	1.08
5	1.14	4	0.43
7	0.77	6	0.30
9	0.40	$8 \leq h \leq 40$	$0.23 * 8/h$
11	0.33		
13	0.21		
$15 \ldots 39$	$0.15 * 15/h$		

2.8.2 IEEE 519 Standard

According to references [28, 83] IEEE standard is worldwide used reference documents, even outside of the United States. Because it is more practical and provides theoretical background on the phenomena of electricity. IEEE 519 standard is the IEEE recommended practices and requirements for harmonic control in electric power systems. It contains thirteen sections (e.g. application of the standards, converter theory and harmonic generation, harmonic measurements, recommended harmonic limits on the system, effect of harmonics and so on) and is more comprehensive than IEC 61000-3-2. The first official version of this standard was published in 1981.

IEEE 519 standard provides the limits on the voltage and current harmonics distortion at the PCC. It evaluates the harmonic distortion at the PCC by two crucial criteria. One is the limitation of the harmonic current emission that a connected equipment can inject or transmit into the power system; the other is the limitation of the voltage distortion at the PCC. These two criteria are indicated by Table 2.8 and Table 2.9 respectively.

Table 2.8: IEEE-519 Harmonic current limits for non-linear loads at PCC with voltages of 2.4 to 69 kV [28]

I_{sc}/I_L	Maximum harmonic current distortion at PCC (% of fundamental)					THD_i
	Harmonic order (odd harmonics)					
	$h < 11$	$11 \leq h \leq 17$	$17 \leq h \leq 23$	$23 \leq h \leq 35$	$h \geq 35$	
< 20	4.0	2.0	1.5	0.6	0.3	5.0
20 50	7.0	3.5	2.5	1.0	0.5	8.0
50 100	10.0	4.5	4.0	1.5	0.7	12.0
100 1000	12.0	5.5	5.0	2.0	1.0	15.0
> 1000	15.0	7.0	6.0	2.5	1.4	20.0
Even harmonics are limited to 25% of the odd harmonic limits above. I_{sc} represents maximum short circuit current at PCC. I_L represents maximum fundamental frequency load current at PCC. For PCCs from 69 to 138 kV, the limits are 50% of the limits above. A case-by-case evaluation is required for PCCs of 138 kV.						

Table 2.9: IEEE-519 Harmonic voltage limits for public power systems

Voltage at PCC	**Harmonic voltage(%)**	THD_v**(%)**
$V < 69kV$	3.0	5.0
$69 \leq V < 138kV$	1.5	2.5
$V \geq 138kV$	1.0	1.5

2.8.3 Engineering Recommendation G5/4

According to references [34, 35, 81, 82] Engineering recommendation G5/4 was generated on first March 2001 instead of the previous engineering recommendation G5/3. This recommendation sets the planning levels for harmonic voltage distortion to be used in the process for the connection of non-linear equipment. It considers the following three parts of emission phenomena:

- continuous harmonic, sub-harmonic and inter-harmonic voltage distortions within the range of 0 to 2500 Hz,
- short bursts of harmonic voltage distortion, and
- voltage notching.

Moreover, G5/4 gives an assessment procedure for the connection of non-linear equipment.

Planning Levels for Harmonic voltage Distortion This recommendation evaluates the planning levels for harmonic voltage distortion by four different supply voltage levels. First is for 400V distribution systems; second is for 6.6, 11, and 20 kV distribution systems; the third level is from 20 kV to 145 kV primary distribution and sub-transmission systems; the last one is for 275 and 400 kV transmission systems. The planning levels for these four different voltage levels are illustrated from Table 2.12 to Table 2.15 in detail. Table 2.10 indicates a summary of total harmonic voltage distortion levels. And the sub-harmonic and inter-harmonic voltage distortion is represented in Table 2.11.

Assessment Procedure for The Connection of Non-linear Equipment This assessment procedure is generally applicable to any non-linear equipment that injects harmonic current into the electricity power system. And there is no differentiation between loads and generation as far as this procedure is concerned.
This assessment procedure in engineering recommendation G5/4 follows three stages that is the same as it in engineering recommendation G5/3. This three stage approach simplify the estimation of LV equipment that connected to the power system and insure the harmonic voltages are under the planning levels.

- Stage one applies to all 230/400V individual non-linear equipment that is intended for connection to LV networks. See Table 2.16.
- Stage two facilitates the connection of equipment including LV equipment that is too large for consideration under stage one or cannot meet the emission limits of stage one to all systems less than 33 kV. The assessment procedure and limits are given in Table 2.17.
- Stage three is applicable to the connection of all non-linear equipment to the power systems having PCCs at 33 kV or above. The calculation in [82] have provided a summation harmonic voltage V_{hp} and relevant total harmonic distortion THD. Both of these values should not exceed the individual and the THD harmonic voltage planning levels for the relevant power system voltage contained in Table 2.12 to Table 2.15.

Table 2.10: Summary of THD_v planning levels

Voltage at PCC	THD_v**(%)**
400V	5.0
6.6, 11 and 20 kV	4.0
22 kV and 400 kV	3.0

Table 2.11: Sub-harmonic and inter-harmonic harmonic voltage distortion limits

Frequency (HZ)	< 80	80	90	> 90 and < 500
Voltage distortion (% of the fundamental)	0.2	0.2	0.5	0.5

Table 2.12: Planning levels for harmonic voltages in 400V systems

Odd harmonics (Non-multiple of three)		**Odd harmonics (Multiple of three)**		**Even harmonics**	
Harmonic order'h'	**Harmonic voltage(%)**	**Harmonic order'h'**	**Harmonic voltage(%)**	**Harmonic order'h'**	**Harmonic voltage(%)**
5	4.0	3	4.0	2	1.6
7	4.0	9	1.2	4	1.0
11	3.0	15	0.3	6	0.5
13	2.5	21	0.2	8	0.4
17	1.6	> 21	0.2	10	0.4
19	1.2			12	0.2
23	1.2			> 12	0.2
25	0.7				
> 25	$0.2 + 0.5(25/h)$				
The total harmonic distortion (THD) level is 5%.					

Table 2.13: Planning levels for harmonic voltages in 6.6kV, 11kV, and 20kV systems

Odd harmonics (Non-multiple of three)		**Odd harmonics (Multiple of three)**		**Even harmonics**	
Harmonic order'h'	**Harmonic voltage(%)**	**Harmonic order'h'**	**Harmonic voltage(%)**	**Harmonic order'h'**	**Harmonic voltage(%)**
5	3.0	3	3.0	2	1.5
7	3.0	9	1.2	4	1.0
11	2.0	15	0.3	6	0.5
13	2.0	21	0.2	8	0.4
17	1.6	> 21	0.2	10	0.4
19	1.2			12	0.2
23	1.2			> 12	0.2
25	0.7				
> 25	$0.2 + 0.5(25/h)$				
The total harmonic distortion (THD) level is 4%.					

Table 2.14: Planning levels for harmonic voltages in systems $>$ 20kV and $<$ 145kV

Odd harmonics (Non-multiple of three)		**Odd harmonics (Multiple of three)**		**Even harmonics**	
Harmonic order'h'	**Harmonic voltage(%)**	**Harmonic order'h'**	**Harmonic voltage(%)**	**Harmonic order'h'**	**Harmonic voltage(%)**
5	2.0	3	2.0	2	1.0
7	2.0	9	1.0	4	0.8
11	1.5	15	0.3	6	0.5
13	1.5	21	0.2	8	0.4
17	1.0	> 21	0.2	10	0.4
19	1.0			12	0.2
23	0.7			> 12	0.2
25	0.7				
> 25	$0.2 + 0.5(25/h)$				
The total harmonic distortion (THD) level is 3%.					

Table 2.15: Planning levels for harmonic voltages in 275kV and 400kV systems

Odd harmonics (Non-multiple of three)		**Odd harmonics (Multiple of three)**		**Even harmonics**	
Harmonic order'h'	**Harmonic voltage(%)**	**Harmonic order'h'**	**Harmonic voltage(%)**	**Harmonic order'h'**	**Harmonic voltage(%)**
5	2.0	3	1.5	2	1.0
7	1.5	9	0.5	4	0.8
11	1.0	15	0.3	6	0.5
13	1.0	21	0.2	8	0.4
17	0.5	> 21	0.2	10	0.4
19	0.5			12	0.2
23	0.5			> 12	0.2
25	0.5				
> 25	$0.2 + 0.3(25/h)$				
The total harmonic distortion (THD) level is 3%.					

Table 2.16: Maximum permissible harmonic current emissions in amperes (equipment rated $>$ 16A per phase)

Harmonic order'h'	**Emission current$I^{(h)}$**	**Harmonic order'h'**	**Harmonic current$I^{(h)}$**	**Harmonic order'h'**	**Harmonic current$I^{(h)}$**
2	28.9	15	1.4	28	1.0
3	48.1	16	1.8	29	3.1
4	9.0	17	13.6	30	0.5
5	28.9	18	0.8	31	2.8
6	3.0	19	9.1	32	0.9
7	41.2	20	1.4	33	0.4
8	7.2	21	0.7	34	0.8
9	9.6	22	1.3	35	2.3
10	5.8	23	7.5	36	0.4
11	39.4	24	0.6	37	2.1
12	1.2	25	4.0	38	0.8
13	27.8	26	1.1	39	0.4
14	2.1	27	0.5	40	0.7

Table 2.17: Maximum permissible harmonic current emissions in amperes per customer

'h'	PCC on 6.6, 11 or 20kV systems	PCC on 22kV systems	'h'	PCC on 6.6, 11 or 20kV systems	PCC on 22kV systems	'h'	PCC on 6.6, 11 or 20kV systems	PCC on 22kV systems
2	4.9	3.3	15	0.3	0.3	28	0.2	0.2
3	6.6	4.4	16	0.4	0.4	29	0.8	0.8
4	1.6	1.3	17	3.3	2.0	30	0.1	0.1
5	3.9	2.6	18	0.2	0.3	31	0.7	0.7
6	0.6	0.6	19	2.2	1.8	32	0.2	0.2
7	7.4	5.0	20	0.3	0.3	33	0.1	0.1
8	0.9	0.9	21	0.1	0.1	34	0.2	0.2
9	1.8	1.5	22	0.3	0.3	35	0.6	0.6
10	1.4	1.4	23	1.8	1.1	36	0.1	0.1
11	6.3	4.7	24	0.1	0.1	37	0.5	0.5
12	0.2	0.2	25	1.0	1.0	38	0.2	0.2
13	5.3	4.0	26	0.3	0.3	39	0.1	0.1
14	0.5	0.5	27	0.1	0.1	40	0.2	0.2

2.9 Conclusion

This chapter presented the basic theory of harmonics. It focused on the definition of harmonics, harmonic expression, relative harmonic measures, harmonic sequences, harmonic sources, harmonic effects and harmonic distortion limited standards. Harmonics can be defined as the sinusoidal periodical waves having frequencies that are integral multiple of fundamental frequency. The mathematical definitions of integer harmonics, inter harmonics, sub harmonics and triplen harmonics are shown in Table 2.18 on next page.

Fourier series is widely used to decompose a periodic non-sinusoidal waveform into several harmonic components. Due to the rotating direction of phase shift of a balanced three-phase non-sinusoidal voltage with different harmonic orders, it considers the positive, negative, and zero harmonic sequences.

This chapter mainly denoted the harmonic current emissions of wind turbine generators, electric vehicle battery chargers, and photovoltaic generators, respectively. Har-

Table 2.18: Mathematical definitions of integer harmonics, inter harmonics, sub harmonics and triplen harmonics

Terms	Definition
Integer harmonics	$f^{(n)}(t) = A^{(n)} * \sin(2\pi nft + \alpha^{(n)})$, where f is fundamental frequency, $n = 1, 2, 3, \ldots$
Inter harmonics	$f^{(n)}(t) = A^{(n)} * \sin(2\pi nft + \alpha^{(n)})$, where f is fundamental frequency, $n > 0$, n is decimal.
Sub harmonics	$f^{(n)}(t) = A^{(n)} * \sin(2\pi nft + \alpha^{(n)})$, where f is fundamental frequency, $0 < n < 1$.
Triplen harmonics	$f^{(n)}(t) = A^{(n)} * \sin(2\pi nf^{(3)}t + \alpha^{(n)})$, where $f^{(3)}$ is third harmonic frequency, n is odd integer.

monics generated by wind turbine generators are commonly caused by the grid-side power electrical converters. A long high voltage transmission cable in a typical wind farm generates harmonic currents as well. The full-wave rectification using diodes accounts for the harmonic emissions of electric vehicle battery chargers. Meanwhile, grid-connected photovoltaic (PG) generator creates harmonics through the PG inverters. Some of the main adverse harmonic effects include the resonances, increased of stator and rotor copper and core losses, overheating, dielectric loss in capacitors, malfunction and failure of power system components, life reduced of power electronic equipments and undesired torques in generators.

Documents for control of power system harmonics come in three levels of applicability and validity: guidelines, recommendations, and limited standards. IEC 61000 series (or EN 61000 series) standard and IEEE 519 standard are most commonly used for harmonics in the United States (US) and Europe, respectively. The engineering recommendation G5/4 is specially used in United Kingdom (UK).

References

[1] G. K. Singh, "Power system harmonics research: a survey," *European Transactions on Electrical Power*, vol. 19, pp. 151–172, 2009. vi, 15, 16, 21, 28, 40

[2] W. M. Grady and S. Santoso, "Understanding power system harmonics," *IEEE Power Engineering Review*, vol. 21, no. 11, pp. 8–11, 2001. 15

[3] G. Mahesh, R. Ganesan, and S. K. Das, "Effects of power harmonics and its control techniques," in *Electromagnetic Interference and Compatibility'99. Proceedings of the International Conference on*. IEEE, 1999, pp. 400–405. 40

[4] A. Çelebi and M. Çolak, "The effects of harmonics produced by grid connected photovoltaic systems on electrical networks," last date of access 28.03.2014. [Online]. Available: http://www.emo.org.tr/ekler/0172ea66506f59c_ek.pdf xi, 16, 35, 36, 40

[5] H. Abniki, S. Nateghi, R. Ghandehari, and M. N. Razavi, "Harmonic analyzing of wind farm based on harmonic modeling of power system components," in *Environment and Electrical Engineering (EEEIC), 2012 11th International Conference on*. IEEE, 2012, pp. 667–672. 29

[6] G. Azevedo, M. Cavalcanti, F. Neves, L. Limongi, and K. Oliveira, "Grid connected photovoltaic topologies with current harmonic compensation," in *Industrial Electronics (ISIE), 2010 IEEE International Symposium on*. IEEE, 2010, pp. 2394–2399. 35, 36

[7] J. Balcells and J. García, "Impact of plug-in electric vehicles on the supply grid," in *Vehicle Power and Propulsion Conference (VPPC), 2010 IEEE*. IEEE, 2010, pp. 1–4. 32

[8] M. Basu, K. Gaughan, and E. Coyle, "Harmonic distortion caused by ev battery chargers in the distribution systems network and its remedy," in *Universities Power Engineering Conference, 2004. UPEC 2004. 39th International*, vol. 2. IEEE, 2004, pp. 869–873. 32

[9] S. H. Berisha, G. G. Karady, R. Ahmad, R. Hobbs, and D. Karner, "Current harmonics generated by electric vehicle battery chargers," in *Power Electronics, Drives and Energy Systems for Industrial Growth, 1996., Proceedings of the 1996 International Conference on*, vol. 1. IEEE, 1996, pp. 584–589. 32

[10] R. P. Bingham, "Harmonics-understanding the facts," 2001, last date of access 20.05.2013. [Online]. Available: http://www.dranetz-bmi.com/pdf/harmonicsall.pdf 28

[11] M. H. Bollen, L. Yao, S. Ro nnberg, and M. Wahlberg, "Harmonic and interharmonic distortion due to a windpark," in *Power and Energy Society General Meeting, 2010 IEEE*. IEEE, 2010, pp. 1–6.

[12] J. Byrne-Finley, B. K. Johnson, H. Hess, and Y. Xia, "Harmonic distortion mitigation for electric vehicle recharging scheme," in *North American Power Symposium (NAPS), 2011*. IEEE, 2011, pp. 1–7. 32

[13] R. Carter, A. Cruden, A. Roscoe, D. Densley, and T. Nicklin, "Impacts of harmonic distortion from charging electric vehicles on low voltage networks," 2012, eVS26 Los Angeles, California, May 6 - 9, 2012 last date of access 20.05.2013. [Online]. Available: http://strathprints.strath.ac.uk/id/eprint/39621 32

[14] M. Castilla, J. Miret, A. Camacho, J. Matas, and L. de Vicuna, "Reduction of current harmonic distortion in three-phase grid-connected photovoltaic inverters via resonant current control," *Industrial Electronics, IEEE Transactions on*, vol. 60, no. 4, pp. 1464–1472, April 2013. 37, 38, 39

[15] M. Castilla, J. Miret, J. Matas, L. de Vicua, and J. M. Guerrero, "Linear current control scheme with series resonant harmonic compensator for single-phase grid-connected photovoltaic inverters," *Industrial Electronics, IEEE Transactions on*, vol. 55, no. 7, pp. 2724–2733, 2008. 37

[16] G. W. Chang, W. Xu, and P. F. Ribeiro, "Modeling of harmonic sources-power electric converters," *Pulse*, vol. 10, no. 009, p. 008, 1998.

[17] S. Chattopadhyay, M. Mitra, and S. Sengupta, *Electric power quality*. Springer, 2011. vi, 21, 28, 40

[18] Z. Chen, J. M. Guerrero, and F. Blaabjerg, "A review of the state of the art of power electronics for wind turbines," *Power Electronics, IEEE Transactions on*, vol. 24, no. 8, pp. 1859–1875, 2009. 29

[19] G. Chicco, J. Schlabbach, and A. Spertino, "Characterisation and assessment of the harmonic emission of grid-connected photovoltaic systems," in *Power Tech, 2005 IEEE Russia*. IEEE, 2005, pp. 1–7. 36

[20] K. Dartawan, L. Hui, R. Austria, and M. Suehiro, "Harmonics issues that limit solar photovoltaic generation on distribution circuits," last date of access 12.06.2013. [Online]. Available: https://ases.conference-services.net/resources/252/2859/pdf/SOLAR2012_0482_full20paper.pdf

[21] A. C. Delaiba, J. C. de Oliveira, A. Vilaca, and J. Cardoso, "The effect of harmonics on power transformers loss of life," in *Circuits and Systems, 1995., Proceedings., Proceedings of the 38th Midwest Symposium on*, vol. 2. IEEE, 1995, pp. 933–936. 40

[22] A. Domijan, G. Heydt, A. Meliopoulos, S. Venkata, and S. West, "Directions of research on electric power quality," *Power Delivery, IEEE Transactions on*, vol. 8, no. 1, pp. 429–436, 1993.

[23] L. Duarte and M. Alves, "The degradation of power capacitors under the influence of harmonics," in *Harmonics and Quality of Power, 2002. 10th International Conference on*, vol. 1. IEEE, 2002, pp. 334–339. 40

[24] R. G. Ellis, "Power system harmonics: a reference guide to causes, effects and corrective measures," Allen-Bradley, Tech. Rep., last date of access 22.04.2013. [Online]. Available: http://literature.rockwellautomation.com/idc/groups/literature/documents/wp/mvb-wp011_-en-p.pdf vi, 21, 40

[25] A. Estanqueiro, J. Tande, and J. P. Lopes, "Assessment of power quality characteristics of wind farms," in *Power Engineering Society General Meeting, 2007. IEEE*. IEEE, 2007, pp. 1–4. 30

[26] M. Fioretto, G. Raimondo, L. Rubino, N. Serbia, and P. Marino, "Evaluation of current harmonic distortion in wind farm application based on synchronous active front end converters," in *AFRICON, 2011*, 2011, pp. 1–6.

[27] C. C. FOK, "Electric vehicle battery chargers: harmonics, modeling and charging strategies," Master's thesis, The Hong Kong Polytechnic University, 2001. 32, 34

[28] E. Fuchs and M. Masoum, *Power quality in power systems and electrical machines, 2008*. Academic Press. vi, xix, 20, 21, 27, 42, 44, 45

[29] E. Fuchs and Y. You, "Measurement of lambda;-i characteristics of asymmetric three-phase transformers and their applications," *Power Delivery, IEEE Transactions on*, vol. 17, no. 4, pp. 983–990, 2002.

[30] F. Ghassemi and K.-L. Koo, "Equivalent network for wind farm harmonic assessments," *Power Delivery, IEEE Transactions on*, vol. 25, no. 3, pp. 1808–1815, 2010.

[31] J. C. Gomez and M. M. Morcos, "Impact of ev battery chargers on the power quality of distribution systems," *Power Delivery, IEEE Transactions on*, vol. 18, no. 3, pp. 975–981, 2003. 32

[32] J. Guo, Z. G. Li, Y. P. Cheng, K. Huang, and C. Y. Cui, "A method of harmonic current suppression in photovoltaic grid-connected systems," *Applied Mechanics and Materials*, vol. 303, pp. 1145–1148, 2013. 35

[33] Z. Z. H. Cheng, Q. Ai and Z. Zhu, *Power quality*. Tsinghua University Press, 2006.

[34] L. Hai Xue, "Review for the engineering recommendation g5/4 by eleelectric association in the uk," *Power system technology*, vol. 30, no. 13, 2006. 45

[35] G. Hensman, "Harmonic standard er g5/4 engineering technical report 122," IEE(HK Specialist Power Division), CIBSE ESG, and IEE BETNET, Tech. Rep. 42, 45

[36] B. Kedra, "Grid modelling for purposes of wind farm harmonic voltages evaluation," in *Electrical Power Quality and Utilisation, 2009. EPQU 2009. 10th International Conference on*. IEEE, 2009, pp. 1–5.

[37] R. King and J. Ekanayake, "Harmonic modelling of offshore wind farms," in *Power and Energy Society General Meeting, 2010 IEEE*, 2010, pp. 1–6. 29

[38] L. H. Kocewiak, J. Hjerrild, and C. L. Bak, "The impact of harmonics calculation methods on power quality assessment in wind farms," in *Harmonics and Quality of Power (ICHQP), 2010 14th International Conference on*. IEEE, 2010, pp. 1–9. 29, 30

[39] K. L. Koo, "Harmonic assessments for filter design specifications at uk national grid electricity transmission system for large wind farms," in *Universities Power Engineering Conference (UPEC), 2010 45th International*. IEEE, 2010, pp. 1–6. 30

[40] A. Latheef, V. Gosbell, and V. Smith, "Harmonic impact of residential type photovoltaic inverters on 11kv distribution system," in *Australian Universities Power Engineering Conference*, 2006.

[41] J. Li, N. Samaan, and S. Williams, "Modeling of large wind farm systems for dynamic and harmonics analysis," in *Transmission and Distribution Conference and Exposition, 2008. T&D. IEEE/PES*. IEEE, 2008, pp. 1–7. 28, 29, 30

[42] S. Liang, Q. Hu, and W.-J. Lee, "A survey of harmonic emissions of a commercially operated wind farm," *Industry Applications, IEEE Transactions on*, vol. 48, no. 3, pp. 1115–1123, 2012. 30

[43] Y. Liu and Z. Wang, "Modeling of harmonic sources magnetic core saturation," *Virginia Tech, Blacksburg, USA*, 1998, last date of access 20.05.2013. [Online]. Available: https://www.calvin.edu/~pribeiro/IEEE/ieee_cd/chapters/pdffiles/c4pdf.pdf 28

[44] E. Lo, D. Sustanto, and C. Fok, "Harmonic load flow study for electric vehicle chargers," in *Power Electronics and Drive Systems, 1999. PEDS'99. Proceedings*

of the IEEE 1999 International Conference on, vol. 1. IEEE, 1999, pp. 495–500. 32

[45] J. Lundquist, "On harmonic distortion in power systems," Ph.D. dissertation, Chalmers University of Technology, 2001, last date of access 22.04.2013. [Online]. Available: http://webfiles.portal.chalmers.se/et/Lic/LundquistJohanLic.pdf vi, 21, 28

[46] G. W. Massey, "Estimation methods for power system harmonic effects on power distribution transformers," in *Rural Electric Power Conference, 1993. Papers Presented at the 37th Annual Conference*. IEEE, 1993, pp. B4–1. 40

[47] F. Medeiros, D. Brasil, C. A. G. Marques, C. Duque, and P. Ribeiro, "Considerations on the aggregation of harmonics produced by large wind farms," in *Harmonics and Quality of Power (ICHQP), 2012 IEEE 15th International Conference on*, 2012, pp. 364–369. 30

[48] R. Melício, V. Mendes, and J. Catalão, "Computer simulation of wind power systems: power electronics and transient stability analysis," in *Proceedings of the 2009 International Conference on Power Systems Transients PST 2009*, 2009, pp. 3–6.

[49] G. Mendonça, H. Pereira, and S. Silva, "Wind farm and system modelling evaluation in harmonic propagation studies," *International Conference on Renewable Energies and Power Quality (ICREPQ12)*, March 2012. xix, 30, 31

[50] K. Meng Goh, "Harmonic analysis for electrical power systems," Master's thesis, University of Strathclyde, December 1984.

[51] A. F. Moreira, P. M. Santos, T. A. Lipo, and G. Venkataramanan, "Filter networks for long cable drives and their influence on motor voltage distribution and common-mode currents," *Industrial Electronics, IEEE Transactions on*, vol. 52, no. 2, pp. 515–522, 2005.

[52] E. Muljadi, C. Butterfield, A. Ellis, J. Mechenbier, J. Hochheimer, R. Young, N. Miller, R. Delmerico, R. Zavadil, and J. Smith, "Equivalencing the collec-

tor system of a large wind power plant," in *Power Engineering Society General Meeting, 2006. IEEE*. IEEE, 2006, pp. 9–pp.

[53] E. Muljadi and A. Ellis, "Final project report wecc wind generator development," 2010, last date of access 20.05.2013. [Online]. Available: http://uc-ciee.org/downloads/WGM_Final_Report_Appendix6.pdf 29

[54] K. K. Munji and R. Bhimasingu, "Mitigation of harmonics in grid integrated wind farms," in *Power and Energy Systems (ICPS), 2011 International Conference on*. IEEE, 2011, pp. 1–5. xix, 29, 30, 31

[55] H. Novanda, P. Regulski, V. Stanojevic, and V. Terzija, "Assessment of frequency and harmonic distortions during wind farm rejection test," last date of access 23.05.2013. [Online]. Available: http://ieeexplore.ieee.org/xpls/abs_all.jsp?arnumber=6469194 30

[56] J. Orr, A. Emanuel, and K. Oberg, "Current harmonics generated by a cluster of electric vehicle battery chargers," *Power Apparatus and Systems, IEEE Transactions on*, no. 3, pp. 691–700, 1982. 32

[57] S. A. Papathanassiou and M. P. Papadopoulos, "Harmonic analysis in a power system with wind generation," *Power Delivery, IEEE Transactions on*, vol. 21, no. 4, 2006.

[58] S. Papathanassiou and M. Papadopoulos, "A study case on harmonic distortion created by wind turbines," 2005, last date of access 23.05.2013. [Online]. Available: http://digital-library.theiet.org/content/conferences/10.1049/cp_20051016

[59] F. Peng, "Harmonic sources and filtering approaches," *Industry Applications Magazine, IEEE*, vol. 7, no. 4, pp. 18–25, 2001. 27, 28

[60] T. Petru and T. Thiringer, "Modeling of wind turbines for power system studies," *Power Systems, IEEE Transactions on*, vol. 17, no. 4, pp. 1132–1139, 2002.

[61] J. Plotkin, R. Hanitsch, and U. Schaefer, "Power conditioning of a 132 mw wind farm," in *Power Electronics and Applications, 2007 European Conference on*. IEEE, 2007, pp. 1–9. 30

[62] J. Plotkin, D. Schulz, and R. Hanitsch, "Influence of long high voltage cables on total harmonic distortion of currents in wind farms," in *IEEE Industrial Electronics, IECON 2006-32nd Annual Conference on*. IEEE, 2006, pp. 3189–3194. 30

[63] L. Sainz and J. Cunill-Solà, "Currents physical components (cpc) concept in wind farm harmonic current studies," last date of access 06.06.2013. [Online]. Available: http://upcommons.upc.edu/e-prints/handle/2117/12733 30

[64] L. Sainz, J. J. Mesas, R. Teodorescu, and P. Rodriguez, "Deterministic and stochastic study of wind farm harmonic currents," *Energy Conversion, IEEE Transactions on*, vol. 25, no. 4, pp. 1071–1080, 2010.

[65] L. Sainz Sapera, J. Balcells Sendra *et al.*, "Experimental measurements about harmonic current mitigation of electric vehicle battery chargers," 2011, last date of access 06.06.2013. [Online]. Available: http://upcommons.upc.edu/handle/2117/12734 32

[66] L. Sainz Sapera, J. J. Mesas García, J. Balcells Sendra *et al.*, "On electric vehicle battery charger modeling," 2012, last date of access 06.06.2013. [Online]. Available: http://www.icrepq.com/icrepq'11/350-sainz.pdf 32

[67] J. Schlabbach, "Harmonic current emission of photovoltaic installations under system conditions," in *Electricity Market, 2008. EEM 2008. 5th International Conference on European*. IEEE, 2008, pp. 1–5. 35

[68] J. Schlabbach, A. Grob, and G. Chicco, "Influence of harmonic system voltages on the harmonic current emission of photovoltaic inverters," in *Power Engineering, Energy and Electrical Drives, 2007. POWERENG 2007. International Conference on*. IEEE, 2007, pp. 545–550. 35

[69] J. Schlabbach and A. Gross, "Harmonic current emission of photovoltaic inverters," in *19th Int. Conf. Electricity Distribution, Vienna, Austria*, 2007.

[70] M. A. SLONIM, "Distortion power in linear and non-linear systems," *International Journal of Electronics*, vol. 68, no. 5, pp. 769–778, 1990.

[71] P. Staats, W. Grady, A. Arapostathis, and R. Thallam, "A statistical method for predicting the net harmonic currents generated by a concentration of electric vehicle battery chargers," *Power Delivery, IEEE Transactions on*, vol. 12, no. 3, pp. 1258–1266, 1997. 32, 33, 34

[72] J. Stevens, "The issue of harmonic injection from utility integrated photovoltaic systems. i. the harmonic source," *Energy Conversion, IEEE Transactions on*, vol. 3, no. 3, pp. 507–510, 1988. 35

[73] ——, "The issue of harmonic injection from utility integrated photovoltaic systems. ii. study results," *Energy Conversion, IEEE Transactions on*, vol. 3, no. 3, pp. 511–515, 1988.

[74] J. SubJak, J.S. and J. McQuilkin, "Harmonics-causes, effects, measurements, and analysis: an update," *Industry Applications, IEEE Transactions on*, vol. 26, no. 6, pp. 1034–1042, 1990. 28

[75] S. Tentzerakis, N. Paraskevopoulou, S. Papathanassiou, and P. Papadopoulos, "Measurement of wind farm harmonic emissions," in *Power Electronics Specialists Conference, 2008. PESC 2008. IEEE.* IEEE, 2008, pp. 1769–1775. 29, 30

[76] S. T. Tentzerakis and S. A. Papathanassiou, "An investigation of the harmonic emissions of wind turbines," *Energy Conversion, IEEE Transactions on*, vol. 22, no. 1, pp. 150–158, 2007. 30

[77] E. Vasanasong and E. Spooner, "The effect of net harmonic currents produced by numbers of the sydney olympic village's pv systems on the power quality of local electrical network," in *Power System Technology, 2000. Proceedings. PowerCon 2000. International Conference on*, vol. 2. IEEE, 2000, pp. 1001–1006.

[78] V. Wagner, J. Balda, D. Griffith, A. McEachern, T. Barnes, D. Hartmann, D. Phileggi, A. Emannuel, W. Horton, W. Reid *et al.*, "Effects of harmonics on equipment," *Power Delivery, IEEE Transactions on*, vol. 8, no. 2, pp. 672–680, 1993. 40

[79] G. J. Wakileh, *Power systems harmonics fundamentals, analysis and filter design*. China machine press, 2003. 20, 42

[80] L. Yanxia and J. Jiuchun, "Harmonic-study of electric vehicle chargers," in *Electrical Machines and Systems, 2005. ICEMS 2005. Proceedings of the Eighth International Conference on*, vol. 3. IEEE, 2005, pp. 2404–2407. 32

[81] "Engineering recommendation draft, emission limits for harmonic voltage distortion and the connection of non-linear and resonant equipment to transmission systems and distribution networks in the united kingdom," National grid, Tech. Rep., 2012. 45

[82] "Engineering recommendation g5/4, planning levels for harmonic votalge distortion and the connection of non-linear equipment to transmission systems and distribution networks in the united kingdom," Electricity Association (CA), Tech. Rep., Feb 2001. 45, 46

[83] "Ieee recommended practices and requirements for harmonic control in electric power systems," IEEE-519, Tech. Rep., 1992. 16, 44

[84] M. Castilla, J. Miret, J. Matas, L. Garcia de Vicuna, and J. M. Guerrero, "Control design guidelines for single-phase grid-connected photovoltaic inverters with damped resonant harmonic compensators," *Industrial Electronics, IEEE Transactions on*, vol. 56, no. 11, pp. 4492–4501, 2009. 38

Chapter 3

Review of Harmonic Power Flow Evaluation Methods

3.1 Introduction

Due to the increase of non-linear devices in electric power networks, there has been a growing interest in obtaining steady state network voltages at harmonic frequencies, which is regarded as harmonic penetration evaluation. The large number of unknowns to solve in the studies leads authors to tackle the problem in several ways in order to achieve a compromise between the simplicity and reliability of the formulation.

Many different approaches have been proposed and implemented to solve the harmonic power flow problems until now. These approaches can be classified by different criteria:

- The modelling techniques of power system and non-linear loads simulations such as time domain, frequency domain, and hybrid time-frequency domain.
- System conditions such as single-phase and three-phase, as well as balanced and unbalanced power system.
- Solution approaches such as coupled and decoupled approaches.
- The modelling parameters of non-linear loads and power system components such as deterministic and stochastic.

Time domain approaches have high accuracy. However, they usually require long computing times especially for a large power system containing many non-linear loads with strong harmonic couplings. Frequency domain approaches evaluate the frequency response of power systems with shorter computing times. The disadvantage of these approaches is that it is difficult to obtain accurate frequency models for non-linear loads. Hybrid time-frequency domain approaches use a combination of time domain and frequency domain approaches to simulate the power system and non-linear loads, respectively. Hence, they can achieve the benefits of the accuracy of the time domain and the simplicity of the frequency domain.

In electric power system operation, the three-phase voltage at the terminals of the load is expected to be symmetric. For this reason, the harmonic power flow problem study in balanced conditions is the usual procedure. However, the power network is sometimes under unbalanced conditions, imposed by the system configuration, disturbances and non-linear loads. The unbalanced harmonic power flow requires long computing times and considerable memory storage.

Coupled approaches give more accurate simulation results, for they impose the couplings between harmonics of both non-linear loads and power system components. However, they require more computing time and account for convergence problems. Decoupled approaches can simplify the simulation by neglecting the harmonic couplings under this condition, if they are not too strong.

The deterministic harmonic power flow is usually used to analyse and assess the planning and operating of power systems. It uses specific values of power generations and load demands of a selected network configuration to calculate system states and power flows. However, due to dispersed generation units, such as wind turbines and photovoltaic being integrated into modern power systems, they introduce uncertainties such as wind speed. In order to take the uncertainties into consideration, the mathematical approaches such as probabilistic and fuzzy are applied to the evaluation.

Based on the above mentioned criteria, this chapter classifies the harmonic power flow algorithm as follows:

- Newton-Raphson based harmonic power flow method [1–5].
- Decoupled harmonic power flow method [6–13].
- Fast decoupled harmonic power flow method. [4, 14–18]
- Fast harmonic power flow method. [5, 19, 20]
- Fuzzy harmonic power flow method. [5, 21, 22]
- Probabilistic harmonic power flow method. [5, 23–31]
- Modular harmonic power flow method. [32–34]

This chapter gives a literature review of the above evaluation methods.

In section two the different bus types of a power system are described. Section three indicates the models of the power system components. Section four gives the Newton-Raphson based harmonic power flow approach in detail. Then, the other approaches are briefly denoted in section five. Finally, the Newton-Raphson based method and the decoupled method are applied to a simple five bus power system with a six pulse line commutated converter to calculate the harmonic power flow. The results will be compared and discussed. Section seven is the conclusion.

3.2 The Bus Type of Power System

It is very important to define the bus type in order to simplify the computation of harmonic power flow during the harmonic power flow analysis. The buses in the power system with non-linear loads can be categorized into four types. They are the slack bus or swing bus, the voltage control (PV) bus, the linear load (PQ) bus and the non-linear (PS) load bus. These bus types are briefly explained as follows: [1, 4, 5]

Slack bus or swing bus It is regarded as the reference bus because the fundamental voltage magnitude $\mid V^{(1)} \mid$ and its phase angle $\mid \theta^{(1)} \mid$ are known. It is necessary to select one reference bus during the harmonic power flow analysis because all other bus fundamental voltage angles are measured with respect to the phase

angle of this reference bus. However, the active and reactive powers (P and Q) of this slack bus should be calculated.

Voltage control (PV) buses The PV buses are usually the generation buses. The real powers $\overline{P}$ and the fundamental voltage magnitudes $|\overline{V}^{(1)}|$ are specified for PV buses. Normally, a voltage regulator holds $|\overline{V}^{(1)}|$ fixed at PV buses by automatically varying the generator field excitation. But, both the fundamental voltage phase angles $|\overline{\theta}^{(1)}|$ and reactive powers $\overline{Q}$ are unknown. Thus, their upgraded values need to be computed.

Linear load (PQ) buses These are mostly linear loads of the power system at which the real and reactive powers ($\overline{P}$ and $\overline{Q}$) are specified. Therefore, computations must be preformed to yield upgraded values for both fundamental voltage magnitudes and phase angles ($|\overline{V}^{(1)}|$ and $|\overline{\theta}^{(1)}|$).

Non-linear load (PS) buses The non-linear loads connected to the power system are regarded as PS buses. The real and apparent powers ($\overline{P}$ and $\overline{S}$) are both specified. When modern devices such as electric vehicle battery chargers (EVCs) are regarded as harmonic sources, these PS buses are converted to PQ buses in the fundamental power flow calculation. While renewable generators such as wind turbines (WTs) and photovoltaic generators are connected, these PS buses are regarded as PV buses in the fundamental power flow calculation. The power balance on PS buses is $P^2+Q^2+D^2=S^2$, which is denoted in chapter 2.

It is noted that the specified active and reactive powers contain only fundamental frequency components at linear buses, but contain all harmonic components at non-linear buses.

3.3 Power System Component Models [4, 8, 11, 19, 35–42]

In harmonic analysis, it is very important to achieve accurate harmonic models of power network components. Hence, this section will introduce several typical representations of common power network components.

3.3.1 Generators

Synchronous machines are usually regarded as the generators in practice. When a h^{th} positive or negative sequence harmonic current passes through stator windings, it creates positive and negative rotating magnetic fields with h times synchronous rotating speed. These rotating magnetic fields will generate $(h-1)^{th}$ and $(h+1)^{th}$ harmonic currents in rotor windings. In the case of the stator windings the property of these harmonic currents is in accordance with the response of the rotor windings when a negative harmonic sequence current passes through the stator windings. In other words, in the case of the stator windings the equivalent inductance of the synchronous machine nearly equals the negative sequence inductance. Therefore, at harmonic frequencies the equivalent reactance of the synchronous machine can be expressed by:

$$X_{eq}(h) = h * X_f \tag{3.1}$$

where $X_{eq}(h)$ represents the equivalent reactance of the synchronous machine at the h^{th} harmonic frequency. X_f represents the fundamental negative sequence reactance of the synchronous machine [35, 37]. It can be defined by:

$$X_f = \frac{(X_d^{''} + X_q^{''})}{2} \tag{3.2}$$

where $X_d^{''}$ and $X_q^{''}$ represent the d and q axis sub-transient reactance respectively [36].

The equivalent resistance of the synchronous machine normally increases with frequency in the form of:

$$R_{eq}(h) = h^a * R_f \tag{3.3}$$

where $R_{eq}(h)$ is the equivalent resistance at the h^{th} harmonic frequency. R_f is the fundamental resistance of the synchronous machine and h represents the harmonic frequency. a is in the range 0.5 to 1.5 [35].

Hence, the equivalent impedance of the synchronous machine is defined as follows,

when considering the skin effect (the value of a is taken to be 0.5):

$$Z_{eq}(h) = \sqrt{h}R_f + jhX_f \tag{3.4}$$

The equivalent circuit of the synchronous machine is shown in Figure 3.1.

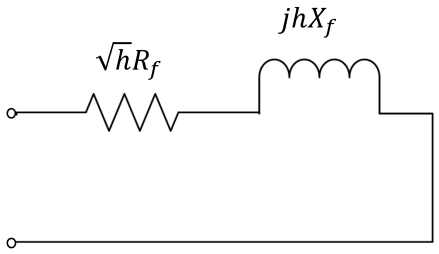

Figure 3.1: The harmonic equivalent impedance of the synchronous machine

3.3.2 Transformers

The characteristics of a transformer that affect harmonic flows are the short circuit impedance, magnetizing characteristics and winding connections [35]. In most applications, transformers are modelled by their series harmonic impedances. Each series harmonic impedance can be expressed as:

$$Z_{eq}(h) = R_{eq}(h) + jhX_f \tag{3.5}$$

where Z_{eq} represents the equivalent impedance of the transformer at the h^{th} harmonic frequency. R_{eq} and X_f represent the equivalent resistance at the h^{th} harmonic frequency and the fundamental reactance respectively [8, 36, 37]. The authors in [36] defined R_{eq} as follows:

$$R_{eq}(h) = R_f(c_0 + c_1h^b + c_2h^2) \tag{3.6}$$

where R_f represents the fundamental resistance of the transformer, h is the harmonic order, c_0, c_1, c_2 and b are parameters of the transformer. The values of these parameters are shown in Table 3.1.

Table 3.1: Parameter values of transformers [36]

	c_0	c_1	c_2	b
small T/F	0.85 - 0.90	0.05 - 0.08	0.05 - 0.08	0.9 - 1.4
large T/F	0.75 - 0.80	0.10 - 0.13	0.10 - 0.13	0.9 - 1.4
	under the constraint $c_0 + c_1 + c_2 = 1$			

If the skin effect is considered in the calculation, the equivalent impedance at the h^{th} harmonic frequency can be defined as [8] (the values of c_0, c_1, c_2 and b are taken to be 0.8, 0.1, 0.1 and 1 respectively):

$$Z_{eq}(h) = \sqrt{h}R_{eq} + jhX_f \tag{3.7}$$

3.3.3 Transmission Lines

Transmission lines include overhead lines and underground cables. They can be modelled by multiple nominal π circuits as shown in Figure 3.2, connected in series [35–37].

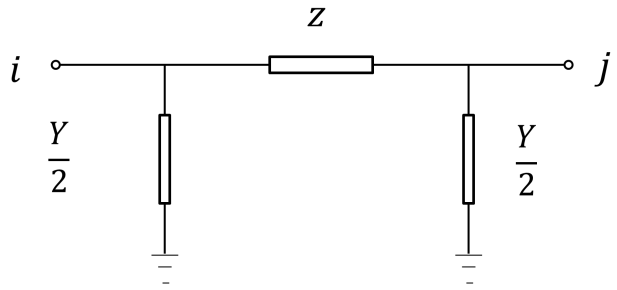

Figure 3.2: The equivalent π circuit

The main concerns for modelling transmission lines are [35]:

i The frequency dependency of the unit length series impedance. Major causes are the earth return effect and the conductor skin effect.

ii The distributed parameter nature (long line effects) of the unit length series impedance and shunt capacitance.

The unit length series impedance and shunt admittance parameters should be computed first according to the physical arrangement of the line conductors, in order to construct

a line model as shown in Figure 3.2. The series impedance is composed of external and internal impedance when considering the earth return effect and the conductor skin effect. The external impedance is a function of the earth return condition and the frequency of interest. The internal impedance is dependent on the conductor skin effect. Hence the h^{th} harmonic resistance $R(h)$ can be calculated by the following equation:

$$R(h) = 0.288R_f + 0.138\sqrt{hR_f} \qquad (\Omega/Km) \tag{3.8}$$

where R_f represents the fundamental resistance.

The inductance and capacitance of the line can be considered as constant, which have a relation with frequency, i.e., the harmonic reactance is h times the value of the fundamental frequency. The H^{th} harmonic series impedance $Z(h)$ and parallel admittance $Y(h)$ per unit length are formulated as:

$$Z(h) = R(h) + jhX_f \qquad (\Omega/Km) \tag{3.9}$$

$$Y(h) = j\frac{B_f}{h} \qquad (S/Km) \tag{3.10}$$

where X_f and B_f are the fundamental reactance and susceptance of the transmission line per unit length [8].

3.3.4 System Loads

The system loads have a significant effect on system frequency response primarily near resonant frequencies. Although the proper selection of the load model is very important for correctly assessing the magnitude of harmonic resonances, no generally applicable harmonic model exists and case-specific measurements and evaluations are needed for detailed studies [36].

The author in [41] described three types of loads: motive, power electronic and passive.

- The motive loads are usually used to represent induction motors, which the rotating magnetic field created by a stator harmonic rotates at a speed significantly

different from that of the rotor. There are various models of them due to the boundary of system representation.

- The power electronic loads are more difficult to be modelled as these loads do not present a constant R, L, C configuration and their non-linear characteristics cannot fit within the linear harmonic equivalent model.
- There are two types of passive load models as shown in Figure 3.3 [35, 37, 41].

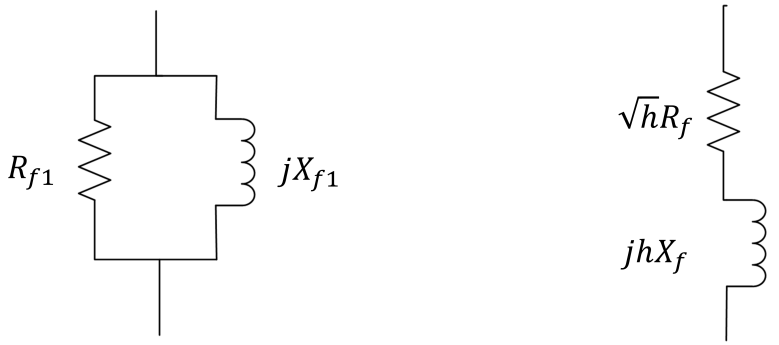

(a) Model A (b) Model B

Figure 3.3: Alternative harmonic models of passive loads

Typically domestic passive loads can be represented approximately by a series R, X impedance as shown in Figure 3.3(b). R_f is load resistance at the fundamental frequency, X_f is load reactance at the fundamental frequency and h is harmonic order. Reference [43] gives their mathematical equations as:

$$R_f = \frac{V_f^2}{P_L} \tag{3.11}$$

$$X_f = \frac{R_f}{2\pi f_0 6.7 \frac{Q_L}{P_L} - 0.74} \tag{3.12}$$

where V_f represents the fundamental bus voltage. P_L and Q_L represent the fundamental frequency active and reactive powers and f_0 is the fundamental frequency.

In studies concerning mainly the transmission network the loads are usually equivalent parts of the distribution network, specified by the consumption of active and reactive power. Normally a parallel model is used as shown in Figure 3.3(a). R_{f1} and X_{f1} represent the fundamental frequency resistance and reactance. There are many variations of this parallel form of load representation. Reference [43] suggests a parallel load model whose values are:

$$R_{f1} = \frac{V_f^2}{(0.1h+0.9)P_L} \tag{3.13}$$

$$X_{f1} = \frac{V_f^2}{2\pi f_0(0.1h+0.9)Q_L} \tag{3.14}$$

3.4 Newton-Raphson Based Harmonic Power Flow [1–5]

This section presents the Newton-Raphson based harmonic power flow algorithm in detail. The principle of Newton-Raphson iterative approach is explained in Appendix E. The Newton-Raphson based harmonic power flow algorithm is based on similar principles and equations to the conventional fundamental Newton-Raphson power flow algorithm. It was the first proposed approach for power system harmonic power flow. It is capable of including any type of non-linear load by assuming the $v-i$ characteristic of non-linearity is available in the frequency or time domain. The Newton-Raphson based harmonic power flow algorithm is very accurate because harmonic coupling of all frequencies is considered. However, this approach might encounter convergence problems and a large amount of calculating time for large power systems with many non-linear loads.

3.4.1 Unknowns and Available Equations

In order to apply the Newton-Raphson method to predict harmonic power flow in the power system, several unknowns and their relative solving equations should be considered.

It is assumed that a power system has n buses. Bus number one is regarded as the slack (swing) bus. The number of non-linear buses is from m to n. Therefore, the number of linear buses is from 1 to $(m-1)$. "H" represents the number of harmonics which excludes the slack bus (e.g. for $h = 1,3,5,7, H = 3$). Based on these assumptions, the number and detail of unknowns are shown in Table 3.2.

Table 3.2: The specifications of unknowns

Unknowns	**Number**
Fundamental frequency bus voltage magnitudes and phase angles for all buses except slack bus	$2(n-1)$
Fundamental frequency active and reactive powers at the slack bus	2
Harmonic voltage magnitudes and phase angles at each bus for each harmonic frequency (excluding fundamental frequency)	$2nH$
Total reactive powers at each non-linear bus	$n-m+1$
Total number of unknowns	$3n-m+2nH+1$

The specifications of available independent equations are shown in Table 3.3.

Table 3.3: The specifications of available equations

Available Equations	**Number**
Fundamental frequency active and reactive power mismatches at each linear bus except the slack bus	$2(m-2)$
Fundamental frequency voltage magnitude and phase angle at the slack bus	2
Total active and reactive power mismatches at each non-linear bus	$2(n-m+1)$
Real and imaginary current balance for each harmonic frequency (excluding fundamental frequency) at each bus	$2nH$
Apparent voltampere balance at each non-linear bus to calculate the reactive power	$n-m+1$
Total number of equations	$3n-m+2nH+1$

This shows that the total number of available equations equals to the total number of unknowns. Hence, the unknowns of the Newton-Raphson harmonic power flow algorithm can be established.

3.4.2 The Admittance Matrix

The admittance matrix is a mathematical model to describe the power system. It is involved to simplify the power system calculation as well. It consists of fundamental power system admittance matrix and harmonic power system admittance matrix during the harmonic power flow calculation.

Fundamental power system admittance matrix

An admittance matrix based equation is usually used to calculate the bus voltage or injection current in the fundamental frequency as shown:

$$\overline{I}_{bus}^{(1)} = \overline{Y}_{bus}^{(1)} \overline{V}_{bus}^{(1)} \tag{3.15}$$

where $\overline{Y}_{bus}^{(1)}$ is the n by n fundamental admittance matrix of an n-bus power system. It is defined as:

$$\overline{Y}_{bus}^{(1)} = \begin{bmatrix} Y_{11}^{(1)} & Y_{12}^{(1)} & \cdots & Y_{1n}^{(1)} \\ Y_{21}^{(1)} & Y_{22}^{(1)} & \cdots & Y_{2n}^{(1)} \\ \vdots & \vdots & \ddots & \vdots \\ Y_{n1}^{(1)} & Y_{n2}^{(1)} & \cdots & Y_{nn}^{(1)} \end{bmatrix} \tag{3.16}$$

The diagonal entries of $\overline{Y}_{bus}^{(1)}$, $Y_{ii}^{(1)}$, are formed by summing the total line admittances and the total shunt capacitor admittances connected to the terminal bus i. The mathematical equation is:

$$Y_{ii}^{(1)} = \sum_{i \neq j}^{j} \left(y_{ci}^{(1)} + y_{ij}^{(1)} \right) \tag{3.17}$$

where $y_{ci}^{(1)}$ is the fundamental shunt capacitor admittances. And $y_{ij}^{(1)}$ denotes the fundamental line admittances between bus i and bus j.

While the off-diagonal entries of $\overline{Y}_{bus}^{(1)}$, $Y_{ij}^{(1)}$, are the negatives of the line admittances between bus i and bus j. The mathematical expression of off-diagonal entries is:

$$Y_{ij}^{(1)} = -y_{ij}^{(1)} \tag{3.18}$$

If there is no line between i and j, $Y_{ij}^{(1)} = 0$. Since $y_{ij}^{(1)}$ equals $y_{ji}^{(1)}$, the admittance matrix is symmetric.

If there is a transformer connected between bus i and bus j, the single-phase diagram and its equivalent π circuit are shown in Figure 3.4(a) and Figure 3.4(b), respectively. It is assumed that the ratio of the transformer is k.

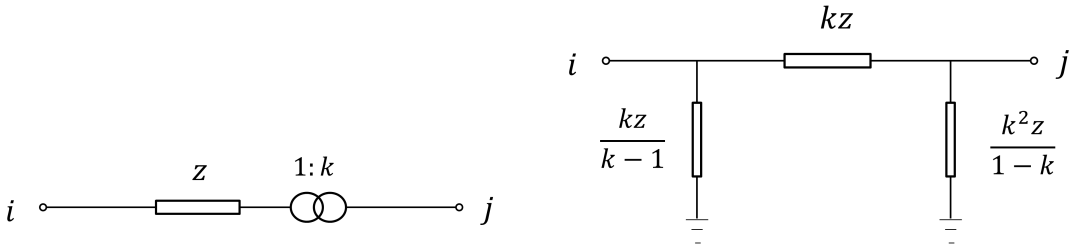

(a) The single-phase diagram

(b) The equivalent π circuit

Figure 3.4: The diagram of transmission line with a transformer connected [44]

According to Figure 3.4:

$$y_{ii}^{(1)} = \frac{1}{kz^{(1)}} + \frac{k-1}{kz^{(1)}} = \frac{1}{z^{(1)}} \tag{3.19}$$

$$y_{jj}^{(1)} = \frac{1}{kz^{(1)}} + \frac{1-k}{k^2 z^{(1)}} = \frac{1}{k^2 z^{(1)}} \tag{3.20}$$

$$y_{ij}^{(1)} = y_{ji}^{(1)} = -\frac{1}{kz^{(1)}} \tag{3.21}$$

Harmonic power system admittance matrix

For non-sinusoidal operating conditions, the power system admittance matrix will be defined at harmonic frequencies, $\overline{Y}_{bus}^{(h)}$. The pattern and the calculation method for the harmonic admittance matrix are identical to the fundamental admittance matrix except that the diagonal entries of $\overline{Y}_{bus}^{(h)}$ are the sum of the load admittances, the shunt capacitor admittances and the line admittances. Also the load admittances, shunt capacitor admittances and line admittances of the harmonic admittance matrix are evaluated at

the h^{th} harmonic frequency $f_h = h \cdot f_1$. Hence:

$$Y_{ii}^{(h)} = y_{li}^{(h)} + y_{ci}^{(h)} + y_{ij}^{(h)} \tag{3.22}$$

where $y_{li}^{(h)}$ represents the h^{th} harmonic frequency load admittance connected to the bus i.

The mathematical expression of off-diagonal entries is:

$$Y_{ij}^{(h)} = -y_{ij}^{(h)} \tag{3.23}$$

3.4.3 Current Balance

The current balance for both fundamental and harmonic frequencies at each non-linear bus is indicated in Figure 3.5.

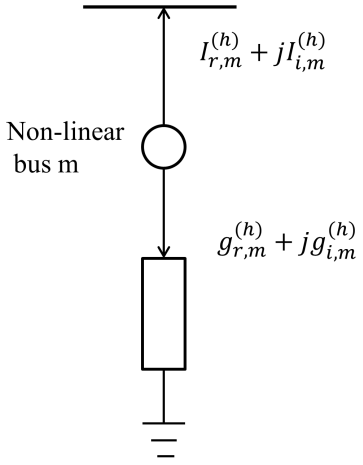

Figure 3.5: Current balance at a non-linear bus

Where $I_{r,m}^{(h)}$ and $I_{i,m}^{(h)}$ are the harmonic (including fundamental frequency) real and reactive line currents at the m^{th} non-linear bus. $g_{r,m}^{(h)}$ and $g_{i,m}^{(h)}$ denote the harmonic (including fundamental frequency) real and reactive non-linear load currents referred to the same bus. Note that the line and non-linear load currents are positive when they leave the non-linear bus. Therefore, the harmonic (including fundamental frequency)

current balance at each non-linear bus can be expressed as below:

$$\begin{bmatrix} I_{r,m}^{(h)} \\ I_{i,m}^{(h)} \\ \vdots \\ I_{r,n}^{(h)} \\ I_{i,n}^{(h)} \end{bmatrix} = - \begin{bmatrix} g_{r,m}^{(h)} \\ g_{i,m}^{(h)} \\ \vdots \\ g_{r,n}^{(h)} \\ g_{i,n}^{(h)} \end{bmatrix} \tag{3.24}$$

According to the $v-i$ characteristic of non-linear loads, the injected harmonic currents of a non-linear load ($I_{injected}^{(h)}$) at bus m will be a function of its fundamental and harmonic voltages:

$$\begin{cases} Real(I_{injected}^{(h)}) = g_{r,m}^{(h)}(\tilde{V}_m^{(1)}, \tilde{V}_m^{(2)}, \ldots, \tilde{V}_m^{(h_{max})}, \alpha_m, \beta_m) \\ Imag(I_{injected}^{(h)}) = g_{i,m}^{(h)}(\tilde{V}_m^{(1)}, \tilde{V}_m^{(2)}, \ldots, \tilde{V}_m^{(h_{max})}, \alpha_m, \beta_m) \end{cases} \tag{3.25}$$

where α_m and β_m are the non-linear load control parameters. The equation 3.25 indicates that the non-linearity of the non-linear load injected current, $g_m^{(h)}$, is due to strong couplings between harmonic currents and voltages.

Figure 3.6 shows a typical non-linear bus m of an n bus power system below.

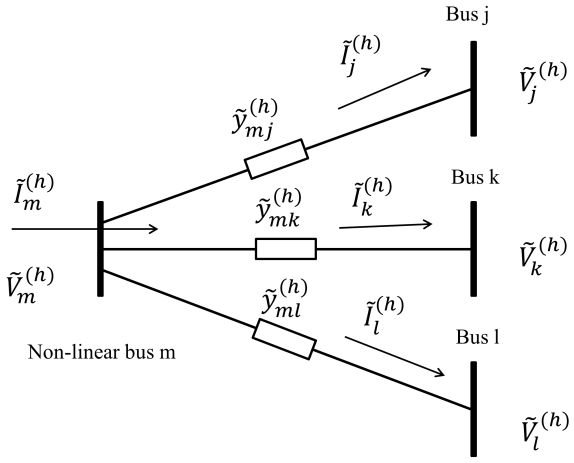

Figure 3.6: Non-linear bus m connected to other buses

This non-linear bus is connected to three other buses j, k, and l. $\tilde{y}_{mj}^{(h)}$, $\tilde{y}_{mk}^{(h)}$ and $\tilde{y}_{ml}^{(h)}$

represent the line admittances evaluated at the h^{th} harmonic frequency between $m-j$, $m-k$ and $m-l$, respectively. Each bus has its own harmonic voltage, $\tilde{V}_m^{(h)}$, $\tilde{V}_j^{(h)}$, $\tilde{V}_k^{(h)}$ and $\tilde{V}_l^{(h)}$.

Hence, the harmonic line current leaving the non-linear bus m through the lines, $\tilde{I}_m^{(h)}$, is defined as:

$$\begin{aligned}
\tilde{I}_m^{(h)} &= \tilde{I}_j^{(h)} + \tilde{I}_k^{(h)} + \tilde{I}_l^{(h)} \\
&= (\tilde{V}_m^{(h)} - \tilde{V}_j^{(h)})\tilde{y}_{mj}^{(h)} + (\tilde{V}_m^{(h)} - \tilde{V}_k^{(h)})\tilde{y}_{mk}^{(h)} + (\tilde{V}_m^{(h)} - \tilde{V}_l^{(h)})\tilde{y}_{ml}^{(h)} \\
&= (\tilde{y}_{mj}^{(h)} + \tilde{y}_{mk}^{(h)} + \tilde{y}_{ml}^{(h)})\tilde{V}_m^{(h)} - \tilde{y}_{mj}^{(h)}\tilde{V}_j^{(h)} - \tilde{y}_{mk}^{(h)}\tilde{V}_k^{(h)} - \tilde{y}_{ml}^{(h)}\tilde{V}_l^{(h)} \\
&= (\overline{Y}_{bus}^{(h)})_{mm}\tilde{V}_m^{(h)} + (\overline{Y}_{bus}^{(h)})_{mj}\tilde{V}_j^{(h)} + (\overline{Y}_{bus}^{(h)})_{mk}\tilde{V}_k^{(h)} + (\overline{Y}_{bus}^{(h)})_{ml}\tilde{V}_l^{(h)} \\
&= (\text{the row } m \text{ of})\overline{Y}_{bus}^{(h)}\overline{V}_{bus}^{(h)}
\end{aligned} \tag{3.26}$$

where the $\overline{V}_{bus}^{(h)}$ is the complex vector of the h^{th} harmonic bus voltages.

3.4.4 Apparent Power Balance

The apparent power balance at each linear bus is:

$$(S_i)^2 = (P_i)^2 + (Q_i)^2 \tag{3.27}$$

where $i = 1,2,3,\ldots,m-1$.

While the apparent power balance at each non-linear bus is:

$$\left(S_i\right)^2 = \left(\sum P_i^{(h)}\right)^2 + \left(\sum Q_i^{(h)}\right)^2 + \left(D_i\right)^2 \tag{3.28}$$

where $i = m,m+1,\ldots,n$.

3.4.5 Newton-Raphson Based Harmonic Power Flow Algorithm

The Newton-Raphson based harmonic power flow calculation method is achieved by forcing the appropriate mismatches, $\Delta\overline{M}$, to zero using the Jacobian matrix, $\overline{J}$, and

obtaining appropriate correction terms, $\Delta\overline{V}$. The mathematical equation is:

$$\begin{bmatrix} \Delta\overline{W} \\ \Delta\overline{I}^{(2)} \\ \Delta\overline{I}^{(3)} \\ \vdots \\ \Delta\overline{I}^{(h_{max})} \\ \Delta\overline{I}^{(1)} \end{bmatrix} = \begin{bmatrix} \overline{J}_{sub}^{(1)} & \overline{J}_{sub}^{(2)} & \overline{J}_{sub}^{(3)} & \cdots & \overline{J}_{sub}^{(h_{max})} & 0 \\ \overline{CG}^{(2,1)} & \overline{CG}^{(2,2)} & \overline{CG}^{(2,3)} & \cdots & \overline{CG}^{(2,h_{max})} & \overline{T}^{(2)} \\ \overline{CG}^{(3,1)} & \overline{CG}^{(3,2)} & \overline{CG}^{(3,3)} & \cdots & \overline{CG}^{(3,h_{max})} & \overline{T}^{(3)} \\ \vdots & \vdots & \vdots & \cdots & \vdots & \vdots \\ \overline{CG}^{(h_{max},1)} & \overline{CG}^{(h_{max},2)} & \overline{CG}^{(h_{max},3)} & \cdots & \overline{CG}^{(h_{max},h_{max})} & \overline{T}^{(h_{max})} \\ \overline{CG}^{(1,1)} & \overline{CG}^{(1,2)} & \overline{CG}^{(1,3)} & \cdots & \overline{CG}^{(1,h_{max})} & \overline{T}^{(1)} \end{bmatrix} \begin{bmatrix} \Delta\overline{V}^{(1)} \\ \Delta\overline{V}^{(2)} \\ \Delta\overline{V}^{(3)} \\ \vdots \\ \Delta\overline{V}^{(h_{max})} \\ \Delta\overline{\Phi} \end{bmatrix} \tag{3.29}$$

The appropriate $2(nH+n-1)+2(n-m+1)\times 1$ mismatch vector, $\Delta\overline{M}$ is defined as:

$$\Delta\overline{M} = [\Delta\overline{W}, \Delta\overline{I}^{(2)}, \Delta\overline{I}^{(3)} \ldots, \Delta\overline{I}^{(h_{max})}, \Delta\overline{I}^{(1)}]^T \tag{3.30}$$

where $\Delta\overline{W}$ is the fundamental frequency power mismatch vector at all buses (except the slack bus). Also $(\Delta\overline{I}^{(2)}, \Delta\overline{I}^{(3)} \ldots, \Delta\overline{I}^{(h_{max})}, \Delta\overline{I}^{(1)})$ is the harmonic current mismatch (including the fundamental frequency) vector at each bus.

Assuming bus one is the slack bus. In equation 3.30,

$$\begin{aligned} \Delta\overline{W} =& [P_2^{sp} - P_2^{(1)}, Q_2^{sp} - Q_2^{(1)}, P_3^{sp} - P_3^{(1)}, Q_3^{sp} - Q_3^{(1)}, \cdots, P_{m-1}^{sp} - P_{m-1}^{(1)}, Q_{m-1}^{sp} - Q_{m-1}^{(1)}, \\ & P_m^{sp} - P_m^{(total)}, Q_m^{sp} - Q_m^{(total)}, \cdots, P_n^{sp} - P_n^{(total)}, Q_n^{sp} - Q_n^{(total)}]^T \end{aligned} \tag{3.31}$$

$$\Delta\overline{I}^{(1)} = [I_{r,m}^{(1)} + G_{r,m}^{(1)}, I_{i,m}^{(1)} + G_{i,m}^{(1)}, \cdots, I_{r,n}^{(1)} + G_{r,n}^{(1)}, I_{i,n}^{(1)} + G_{i,n}^{(1)}]^T \tag{3.32}$$

$$\Delta\overline{I}^{(h)} = [I_{r,1}^{(h)}, I_{i,1}^{(h)}, \cdots, I_{r,m-1}^{(h)}, I_{i,m-1}^{(h)}, I_{r,m}^{(h)} + G_{r,m}^{(h)}, I_{i,m}^{(h)} + G_{i,m}^{(h)}, \cdots, I_{r,n}^{(h)} + G_{r,n}^{(h)}, I_{i,n}^{(h)} + G_{i,n}^{(h)}]^T \tag{3.33}$$

where $(P_2^{sp}, P_3^{sp}, \cdots, P_{m-1}^{sp})$ and $(Q_2^{sp}, Q_3^{sp}, \cdots, Q_{m-1}^{sp})$ are the specified active and reactive powers applied to the linear buses (except the slack bus). These specified active and reactive powers include fundamental components only. $(P_m^{sp}, \cdots, P_n^{sp})$ and $(Q_m^{sp}, \cdots, Q_n^{sp})$ represent the specified active and reactive powers for non-linear buses, which consist of all harmonic components. $(P_2^{(1)}, \cdots, P_{m-1}^{(1)})$ and $(Q_2^{(1)}, \cdots, Q_{m-1}^{(1)})$ denote the calculated fundamental active and reactive powers for linear buses (excluding the slack bus) by using equations 2.20 and 2.21 in chapter 2. $(P_m^{(total)}, \cdots, P_n^{(total)})$ and

$(Q_m^{(total)}, \cdots, Q_n^{(total)})$ denote the calculated total active and reactive powers for non-linear buses, which consist of all harmonic components. There is no reactive power mismatch at a PV bus for the fundamental frequency because the bus voltage magnitude is already known.

The fundamental current mismatch is defined for non-linear buses only as shown in equation 3.32, whereas the harmonic current mismatch is defined for all the buses (including the slack bus) as shown in equation 3.33, where $I_{r,j}^{(h)}$ and $I_{i,j}^{(h)}(j = 1,2,\ldots,n)$ are the real and imaginary part of the harmonic line currents (including the fundamental frequency) established by equation 3.26. $G_{r,j}^{(h)}$ and $G_{i,j}^{(h)}(j = m,m+1,\ldots,n)$ represent the real and imaginary non-linear load injected harmonic currents (including the fundamental frequency) calculated by equation 3.25.

The $2(nH+n-1)+2(n-m+1) \times 1$ correction vector, $\Delta\overline{V}$, in equation 3.29 consist of the correction vector of fundamental voltage magnitude and phase angle at each bus (excluding the slack bus), $\Delta\overline{V}^{(1)}$, the correction vectors of harmonic voltage magnitude and phase angle at each bus, $(\Delta\overline{V}^{(2)}, \Delta\overline{V}^{(3)}, \ldots, \Delta\overline{V}^{(h_{max})})$ and the correction vector of non-linear load control parameters, $\Delta\overline{\Phi}$. These correction sub-vectors are defined below:

$$\Delta\overline{V}^{(1)} = [\Delta\theta_2^{(1)}, \Delta \mid V \mid_2^{(1)}, \Delta\theta_3^{(1)}, \Delta \mid V \mid_3^{(1)} \cdots, \Delta\theta_n^{(1)}, \Delta \mid V \mid_n^{(1)}]^T \tag{3.34}$$

$$\Delta\overline{V}^{(h)} = [\Delta\theta_1^{(h)}, \Delta \mid V \mid_1^{(h)}, \Delta\theta_2^{(h)}, \Delta \mid V \mid_2^{(h)}, \cdots, \Delta\theta_n^{(h)}, \Delta \mid V \mid_n^{(h)}]^T \quad (h = 2,3,\ldots,h_{max}) \tag{3.35}$$

$$\Delta\overline{\Phi} = [\Delta\alpha_m, \Delta\beta_m, \cdots, \Delta\alpha_n, \Delta\beta_n]^T \tag{3.36}$$

The Jacobian matrix of equation 3.29 is a $2(nH+n-1)+2(n-m+1)$ square matrix. It contains four sub-matrices, $\overline{J}_{sub}$, 0, $\overline{CG}$ and $\overline{T}$. The details of $\overline{J}_{sub}$, $\overline{CG}$ and $\overline{T}$ are listed below:

- $\overline{J}_{sub}$ has two parts, $\overline{J}_{sub}^{(1)}$ and $\overline{J}_{sub}^{(h)}$. $\overline{J}_{sub}^{(1)}$ is the Jacobian $2(n-1)$ square matrix of partial derivatives of the fundamental active and reactive powers with respect to the fundamental bus voltage phase angles and magnitudes for all buses except the slack bus, as shown in equation 3.37. The derivatives of the fundamental

reactive powers with respect to the fundamental bus voltage phase angles and magnitudes are equal to zero at PV buses.

$$\overline{J}_{sub}^{(1)} = \begin{bmatrix} \frac{\partial \Delta P_2^{(1)}}{\partial \theta_2^{(1)}} & \frac{\partial \Delta P_2^{(1)}}{\partial V_2^{(1)}} & \cdots & \frac{\partial \Delta P_2^{(1)}}{\partial \theta_n^{(1)}} & \frac{\partial \Delta P_2^{(1)}}{\partial V_n^{(1)}} \\ \frac{\partial \Delta Q_2^{(1)}}{\partial \theta_2^{(1)}} & \frac{\partial \Delta Q_2^{(1)}}{\partial V_2^{(1)}} & \cdots & \frac{\partial \Delta Q_2^{(1)}}{\partial \theta_n^{(1)}} & \frac{\partial \Delta Q_2^{(1)}}{\partial V_n^{(1)}} \\ \vdots & \vdots & \vdots & \vdots & \vdots \\ \frac{\partial \Delta P_n^{(1)}}{\partial \theta_2^{(1)}} & \frac{\partial \Delta P_n^{(1)}}{\partial V_2^{(1)}} & \cdots & \frac{\partial \Delta P_n^{(1)}}{\partial \theta_n^{(1)}} & \frac{\partial \Delta P_n^{(1)}}{\partial V_n^{(1)}} \\ \frac{\partial \Delta Q_n^{(1)}}{\partial \theta_2^{(1)}} & \frac{\partial \Delta Q_n^{(1)}}{\partial V_2^{(1)}} & \cdots & \frac{\partial \Delta Q_n^{(1)}}{\partial \theta_n^{(1)}} & \frac{\partial \Delta Q_n^{(1)}}{\partial V_n^{(1)}} \end{bmatrix} \tag{3.37}$$

$\overline{J}_{sub}^{(h)}$ is the Jacobian $2(n-1) \times 2n$ matrix of the similar partial derivatives to $\overline{J}_{sub}^{(1)}$. However, there are zero entries for $(m-1)$ linear buses. The mathematical equation is shown in equation 3.38 below.

$$\overline{J}_{sub}^{(h)} = \begin{bmatrix} \overline{0}_{2(n-2)\times 2n} \\ \hline \frac{\partial \Delta P_m^{(h)}}{\partial \theta_1^{(h)}} & \frac{\partial \Delta P_m^{(h)}}{\partial V_1^{(h)}} & \cdots & \frac{\partial \Delta P_m^{(h)}}{\partial \theta_n^{(h)}} & \frac{\partial \Delta P_m^{(h)}}{\partial V_n^{(h)}} \\ \frac{\partial \Delta Q_m^{(h)}}{\partial \theta_1^{(h)}} & \frac{\partial \Delta Q_m^{(h)}}{\partial V_1^{(h)}} & \cdots & \frac{\partial \Delta Q_m^{(h)}}{\partial \theta_n^{(h)}} & \frac{\partial \Delta Q_m^{(h)}}{\partial V_n^{(h)}} \\ \vdots & \vdots & \vdots & \vdots & \vdots \\ \frac{\partial \Delta P_n^{(h)}}{\partial \theta_1^{(h)}} & \frac{\partial \Delta P_n^{(h)}}{\partial V_1^{(h)}} & \cdots & \frac{\partial \Delta P_n^{(h)}}{\partial \theta_n^{(h)}} & \frac{\partial \Delta P_n^{(h)}}{\partial V_n^{(h)}} \\ \frac{\partial \Delta Q_n^{(h)}}{\partial \theta_1^{(h)}} & \frac{\partial \Delta Q_n^{(h)}}{\partial V_1^{(h)}} & \cdots & \frac{\partial \Delta Q_n^{(h)}}{\partial \theta_n^{(h)}} & \frac{\partial \Delta Q_n^{(h)}}{\partial V_n^{(h)}} \end{bmatrix} \tag{3.38}$$

Each element of $\overline{J}_{sub}^{(h)}$ (including the fundamental frequency) is established in Appendix A.

- The sub-matrix $\overline{CG}^{(h,j)}$ is defined as:

$$\overline{CG}^{(h,j)} = \begin{cases} \overline{C}^{(h,h)} + \overline{G}^{(h,h)} & \text{for} h = j \\ \overline{0} + \overline{G}^{(h,j)} & \text{for} h \neq j \end{cases} \tag{3.39}$$

where $\overline{C}^{(h,h)}$ is an array of partial derivatives of the h^{th} real and imaginary harmonic line currents with respect to the h^{th} harmonic bus voltage phase angles and magnitudes, as illustrated in equation 3.40. Each element of $\overline{C}^{(h,h)}$ is defined in Appendix B.

$$\overline{C}^{(h,h)} = \begin{bmatrix} \frac{\partial I_{r,1}^{(h)}}{\partial \theta_1^{(h)}} & \frac{\partial I_{r,1}^{(h)}}{\partial V_1^{(h)}} & \cdots & \frac{\partial I_{r,1}^{(h)}}{\partial \theta_n^{(h)}} & \frac{\partial I_{r,1}^{(h)}}{\partial V_n^{(h)}} \\ \frac{\partial I_{i,1}^{(h)}}{\partial \theta_1^{(h)}} & \frac{\partial I_{i,1}^{(h)}}{\partial V_1^{(h)}} & \cdots & \frac{\partial I_{i,1}^{(h)}}{\partial \theta_n^{(h)}} & \frac{\partial I_{i,1}^{(h)}}{\partial V_n^{(h)}} \\ \vdots & \vdots & \vdots & \vdots & \vdots \\ \frac{\partial I_{r,n}^{(h)}}{\partial \theta_1^{(h)}} & \frac{\partial I_{r,n}^{(h)}}{\partial V_1^{(h)}} & \cdots & \frac{\partial I_{r,n}^{(h)}}{\partial \theta_n^{(h)}} & \frac{\partial I_{r,n}^{(h)}}{\partial V_n^{(h)}} \\ \frac{\partial I_{i,n}^{(h)}}{\partial \theta_1^{(h)}} & \frac{\partial I_{i,n}^{(h)}}{\partial V_1^{(h)}} & \cdots & \frac{\partial I_{i,n}^{(h)}}{\partial \theta_n^{(h)}} & \frac{\partial I_{i,n}^{(h)}}{\partial V_n^{(h)}} \end{bmatrix} \tag{3.40}$$

While $\overline{G}^{(h,j)}$ represents an array of partial derivatives of the h^{th} real and imaginary parts of non-linear load harmonic currents with respect to the j^{th} harmonic bus voltage phase angles and magnitudes (for $j = h$, is $\overline{G}^{(h,h)}$). The mathematical equation is shown below:

$$\overline{G}^{(h,j)} = \left[\begin{array}{cc:ccc} \overline{0}_{2(m-1)\times 2(m-1)} & & \overline{0}_{2(m-1)\times 2(n-m+1)} & & \\ \hdashline & & \frac{\partial G_{r,m}^{(h)}}{\partial \theta_m^{(j)}} & \frac{\partial G_{r,m}^{(h)}}{\partial V_m^{(j)}} & \cdots & 0 & 0 \\ & & \frac{\partial G_{i,m}^{(h)}}{\partial \theta_m^{(j)}} & \frac{\partial G_{i,m}^{(h)}}{\partial V_m^{(j)}} & \cdots & 0 & 0 \\ \overline{0}_{2(n-m+1)\times 2(m-1)} & & \vdots & \vdots & \vdots & \vdots & \vdots \\ & & 0 & 0 & \cdots & \frac{\partial G_{r,n}^{(h)}}{\partial \theta_n^{(j)}} & \frac{\partial G_{r,n}^{(h)}}{\partial V_n^{(j)}} \\ & & 0 & 0 & \cdots & \frac{\partial G_{i,n}^{(h)}}{\partial \theta_n^{(j)}} & \frac{\partial G_{i,n}^{(h)}}{\partial V_n^{(j)}} \end{array}\right] \tag{3.41}$$

Note that $\overline{CG}^{(h,j)}$ is a $2n$ square matrix. However, only the last $2(n-m+1)$ rows exist at the fundamental frequency due to the fact that the fundamental current

balance is not applied to linear buses ($\overline{CG}^{(1,j)} = 2(n-m+1) \times 2n$ matrix). Also for $j = 1$, $\overline{CG}^{(h,1)}$ is a $2n \times 2(n-1)$ matrix because the fundamental bus voltage magnitude and phase angle are known at the slack bus.

- $\overline{T}^{(h)}$ is an array of partial derivatives of real and imaginary parts of non-linear load harmonic currents with respect to the control parameters α and β. The expression of $\overline{T}^{(h)}$ is:

$$\overline{T}^{(h)} = \begin{bmatrix} \overline{0}_{2(m-1)\times 2(n-m+1)} & \\ \hline \frac{\partial G_{r,m}^{(h)}}{\partial \alpha_m} & \frac{\partial G_{r,m}^{(h)}}{\partial \beta_m} & \cdots & 0 & 0 \\ \frac{\partial G_{i,m}^{(h)}}{\partial \alpha_m} & \frac{\partial G_{i,m}^{(h)}}{\partial \beta_m} & \cdots & 0 & 0 \\ \vdots & \vdots & \vdots & \vdots & \vdots \\ 0 & 0 & \cdots & \frac{\partial G_{r,n}^{(h)}}{\partial \alpha_n} & \frac{\partial G_{r,n}^{(h)}}{\partial \beta_n} \\ 0 & 0 & \cdots & \frac{\partial G_{i,n}^{(h)}}{\partial \alpha_n} & \frac{\partial G_{i,n}^{(h)}}{\partial \beta_n} \end{bmatrix} \tag{3.42}$$

Based on the equations given, the Newton-Raphson based harmonic power flow algorithm is the calculation of bus voltage vector $\Delta\overline{V}$ for a given system configuration with both linear and non-linear loads. It is used to force the mismatch vector $\Delta\overline{M}$ to zero by using the harmonic Jacobian matrix and obtaining the appropriate correction terms $\Delta\overline{V}$. Therefore, it is defined mathematically:

$$\Delta\overline{V}^{(itr)} = \overline{J}^{-1}\Delta\overline{M}^{(itr)} \tag{3.43}$$

$$\overline{V}^{(itr+1)} = \overline{V}^{(itr)} + \Delta\overline{V}^{(itr)} \tag{3.44}$$

where itr is the iteration number.

The Newton-Raphson based harmonic power flow algorithm is illustrated in the flow chart shown below (see Figure 3.7).

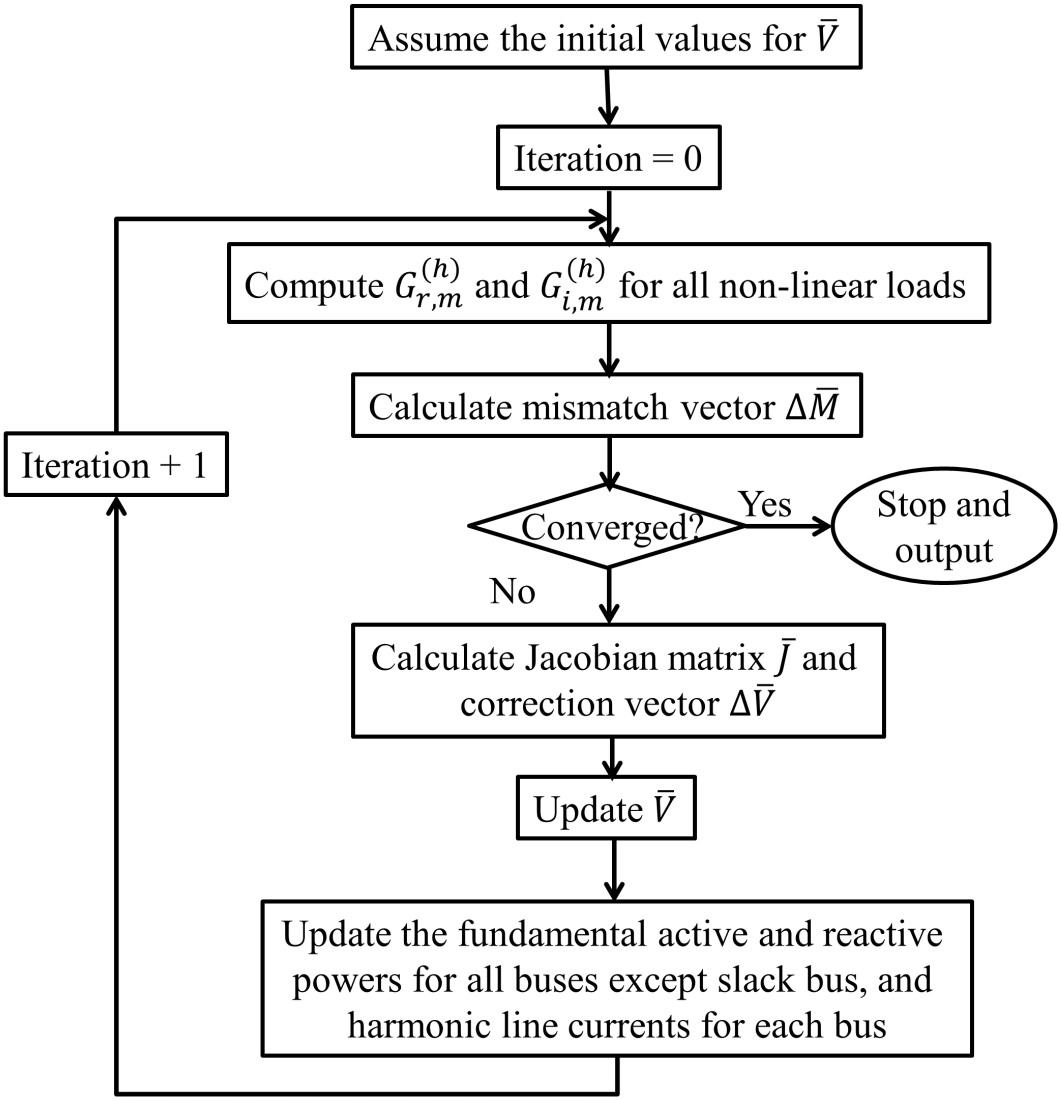

Figure 3.7: Newton-Raphson based harmonic power flow algorithm flow chart

Step one: The fundamental voltage magnitudes fluctuate around $1.0p.u.$, while the harmonic voltage magnitudes are between $0.01p.u.$ and $0.05p.u.$ according to simulation experiments. Hence, it is assumed that the fundamental voltage magnitudes are $1.0p.u.$ for all buses except the slack bus. Because the fundamental voltage magnitude and phase angle of the slack bus are already known. While the harmonic voltage magnitudes are set to any desired value between $0.01p.u.$ and $0.05p.u.$. The phase angles in all harmonics (including fundamental frequency) are assumed to be 0.0 degrees for each bus except the slack bus.

Step two: Compute the non-linear device real and imaginary harmonic currents $G_{r,m}^{(h)}$ and $G_{i,m}^{(h)}$ respectively. Moreover, the control parameters α and β are established during this step.

Step three: Calculate the fundamental active and reactive powers for each linear bus (excluding the slack bus), $P_i^{(1)}$ and $Q_i^{(1)}$ $(i = 2,3,\ldots,m-1)$, and the total harmonic active and reactive powers for each non-linear bus, $P_i^{(total)}$ and $Q_i^{(total)}$ $(i = m,m+1,\ldots,n)$. The harmonic line currents $I_{r,j}^{(h)}$ and $I_{i,j}^{(h)}$ $(j = 1,2,\ldots,n)$ should be calculated as well. Then, use equations 3.30 to 3.33 to consider the mismatch vector $\Delta\overline{M}$.

Step four: The convergence criterion $\max(|\Delta\overline{W},\Delta\bar{I}^{(2)},\Delta\bar{I}^{(3)}\ldots,\Delta\bar{I}^{(h_{max})},\Delta\bar{I}^{(1)}|) < \varepsilon$ is used to determine whether the mismatch vector is converged. ε is usually set to be 10^{-5}. If it is under convergence criterion, the procedure stops and outputs the results. Otherwise, the procedure goes to the next step.

Step five: Evaluate the Jacobian matrix $\bar{J}$ using equations 3.37, 3.38, 3.40, 3.41 and 3.42. Then calculate the correction vector $\Delta\overline{V}$ using equation 3.43.

Step six: Use equation 3.44 to update bus voltage magnitudes and phase angles. These updated values will be the initial values in the next iteration.

Step seven: Update the fundamental active and reactive powers for each bus except the slack bus. Moreover, the harmonic line currents for all buses are updated during this step.

Step eight: Go to step two for another iteration.

3.5 Other Harmonic Power Flow Techniques

3.5.1 Decoupled Harmonic Power Flow [4, 6–13]

The calculated results of the Newton-Raphson based power flow algorithm are accurate because of the harmonic couplings included at all frequencies. However, it might encounter convergence problems and require long computing time for large power systems with many non-linear loads and strong harmonic couplings. Therefore, the decoupled harmonic power flow algorithm is determined to solve the problems.

The decoupled approach is designed to calculate the harmonic power flow by ignoring the harmonic couplings between harmonic orders. As a result, the calculation procedure is carried out separately for each harmonic order. Therefore, it can reduce the computing time and solve the convergence problems. Although the decoupled harmonic power flow calculation approach is not as accurate as the coupled harmonic power flow technique (e.g. Newton-Raphson based power flow algorithm), it gives a benefit of balancing the computational complexity and the result accuracy. [11]

The decoupled harmonic power flow algorithm is composed of two calculation procedures. One is the calculation of fundamental power flow; the other is the harmonic power flow calculation. The details of these two procedures are indicated as follows:

The calculation of fundamental power flow

The Newton-Raphson based conventional power flow algorithm is usually used to evaluate the fundamental power flow, which is similar to the one mentioned in section 3. Its mathematical definition is shown below:

$$\begin{bmatrix} \Delta\overline{P}^{(1)} \\ \Delta\overline{Q}^{(1)} \end{bmatrix} = - \begin{bmatrix} \overline{H}^{(1)} & \overline{N}^{(1)} \\ \overline{K}^{(1)} & \overline{L}^{(1)} \end{bmatrix} \begin{bmatrix} \Delta\overline{\theta}^{(1)} \\ \Delta\overline{|V|}^{(1)} \end{bmatrix} \tag{3.45}$$

where $\overline{H}^{(1)}$, $\overline{N}^{(1)}$, $\overline{K}^{(1)}$, and $\overline{L}^{(1)}$ are the sub-matrices of fundamental Jacobian matrix $\overline{J}^{(1)}_{sub}$. The element expressions of each sub-matrix are $H^{(1)}_{(i,j)} = \frac{\partial \Delta P_i^{(1)}}{\partial \theta_j^{(1)}}$, $N^{(1)}_{(i,j)} = \frac{\partial \Delta P_i^{(1)}}{\partial V_j^{(1)}}$,

$K^{(1)}_{(i,j)} = \frac{\partial \Delta Q_i^{(1)}}{\partial \theta_j^{(1)}}$ and $L^{(1)}_{(i,j)} = \frac{\partial \Delta Q_i^{(1)}}{\partial V_j^{(1)}}$ respectively. $\Delta\overline{P}^{(1)}$ and $\Delta\overline{Q}^{(1)}$ represent the fundamental active and reactive power mismatches for all buses except the slack bus (assuming bus one is the slack bus). They are defined as:

$$\Delta\overline{P}^{(1)} = [P_2^{sp} - P_2^{(1)}, P_3^{sp} - P_3^{(1)}, \cdots, P_{m-1}^{sp} - P_{m-1}^{(1)}, P_m^{sp} - P_m^{(1)}, \cdots, P_n^{sp} - P_n^{(1)}]^T \quad (3.46)$$

$$\Delta\overline{Q}^{(1)} = [Q_2^{sp} - Q_2^{(1)}, Q_3^{sp} - Q_3^{(1)}, \cdots, Q_{m-1}^{sp} - Q_{m-1}^{(1)}, Q_m^{sp} - Q_m^{(1)}, \cdots, Q_n^{sp} - Q_n^{(1)}]^T \quad (3.47)$$

where the harmonic couplings at higher frequencies ($h = 2, 3, \ldots, h_{max}$) are ignored. Hence, the fundamental active and reactive power mismatches at non-linear buses equal the specified active and reactive powers minus the fundamental calculated active and reactive powers.

The correction vectors $\Delta\overline{\theta}^{(1)}$ and $\Delta\overline{|V|}^{(1)}$ are expressed by:

$$\Delta\overline{\theta}^{(1)} = [\Delta\theta_2^{(1)}, \Delta\theta_3^{(1)}, \ldots, \Delta\theta_n^{(1)}]^T \quad (3.48)$$

$$\Delta\overline{|V|}^{(1)} = [\Delta\,|V|_2^{(1)}, \Delta\,|V|_3^{(1)}, \ldots, \Delta\,|V|_n^{(1)}]^T \quad (3.49)$$

The convergence criterion for the fundamental power flow calculation is

$$\max(|\,\Delta P_2^{(1)}, \Delta Q_2^{(1)}, \ldots, \Delta P_n^{(1)}, \Delta Q_n^{(1)}\,|) < \varepsilon \quad (3.50)$$

where ε is usually set to be 10^{-5}.

Figure 3.8 shows the flow chart of fundamental power flow calculation below.

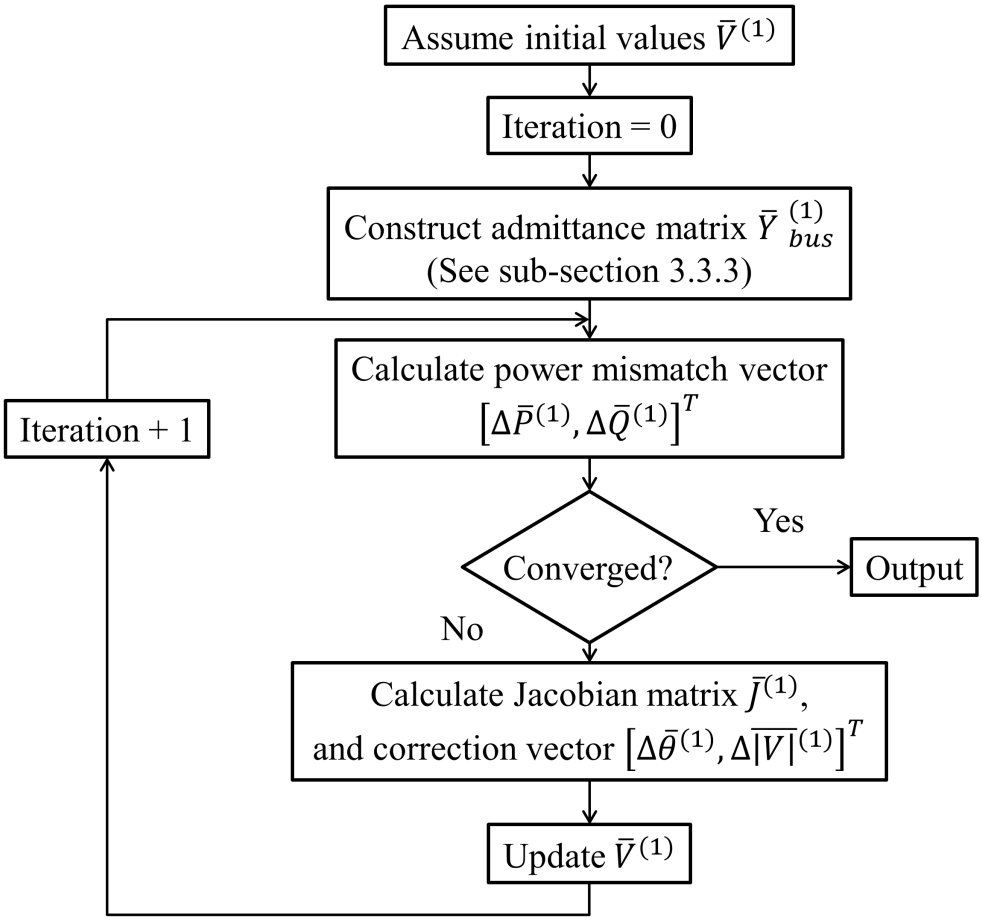

Figure 3.8: Fundamental power flow calculation flow chart

The calculation of harmonic power flow

At higher frequencies, the whole power system is modelled as the combination of harmonic current sources and passive elements. Non-linear loads are treated as decoupled harmonic current sources that inject harmonic currents into the system by neglecting harmonic couplings between all harmonics.

The harmonic admittance matrix is modified for each harmonic order, as the admittance of power system components will vary with the harmonic order. After modifying

the harmonic admittance matrix and the associated harmonic currents, the harmonic power flow problem can be calculated by using the following admittance-matrix-based equation:

$$\overline{I}^{(h)} = \overline{Y}^{(h)}\overline{V}^{(h)} \tag{3.51}$$

This simple and fast approach for the calculation of harmonic voltages and currents provides acceptable solutions as compared with the Newton-Raphson based power flow algorithm, which considers harmonic couplings.

3.5.2 Fast Decoupled Harmonic Power Flow [4, 14–18]

The fast decoupled harmonic power flow algorithm is an improved method based on the decoupled harmonic power flow technique. It is achieved by reducing and simplifying the fundamental Jacobian matrix, $\overline{J}^{(1)}_{sub}$. This approach is more simple, reliable and faster than decoupled harmonic power flow algorithm. Also, it is attractive for networks of any size. The author in [15] applied this modified method in 118 and 1080 bus power systems to evaluate the harmonic power flow. After some time he obtained acceptable solutions and faster computing time.

The fast decoupled harmonic power flow algorithm is composed of two decoupled calculation procedures similar to those used in the decoupled harmonic power flow calculation method. They are the fundamental power flow and the harmonic power flow calculations. The harmonic power flow calculation of this fast decoupled method is very similar to the one used in the decoupled approach. The only difference is in the fundamental power flow calculation.

In the decoupled harmonic power flow calculation method, the fundamental power flow is solved by the generalised Newton-Raphson based iterative algorithm (See equation 3.45). In general, for a small change in the fundamental magnitude of bus voltage, the fundamental active power at the bus does not change appreciably. Likewise, for a small change in the fundamental phase angle of the bus voltage the fundamental reactive power does not change appreciably. Moreover, practical experience indicates that the elements of the sub-matrices, $\overline{N}^{(1)}$ and $\overline{K}^{(1)}$ are much smaller than those of $\overline{H}^{(1)}$ and $\overline{L}^{(1)}$ respectively. Hence, it assumes that $\overline{N}^{(1)}$ and $\overline{K}^{(1)}$ are neglected. As a result,

the fundamental power flow calculation equation (equation 3.45) is decomposed into two separate equations:

$$\Delta\overline{P}^{(1)} = -\overline{H}^{(1)}\Delta\overline{\theta}^{(1)} \tag{3.52}$$

$$\Delta\overline{Q}^{(1)} = -\overline{L}^{(1)}\Delta\overline{|V|}^{(1)} \tag{3.53}$$

According to Appendix A, the diagonal elements of $\overline{H}^{(1)}$ are:

$$H_{(i,i)}^{(1)} = \frac{\partial\Delta P_i^{(1)}}{\partial\theta_i^{(1)}} = Q_i^{(1)} + (V_i^{(1)})^2 B_{(i,i)}^{(1)} \tag{3.54}$$

The off-diagonal elements of $\overline{H}^{(1)}$ are:

$$H_{(i,j)}^{(1)} = \frac{\partial\Delta P_i^{(1)}}{\partial\theta_j^{(1)}} = -V_i^{(1)}V_j^{(1)}(G_{(i,j)}^{(1)}\sin\theta_{(i,j)}^{(1)} - B_{(i,j)}^{(1)}\cos\theta_{(i,j)}^{(1)}) \tag{3.55}$$

The diagonal elements of $\overline{L}^{(1)}$ are:

$$L_{(i,i)}^{(1)} = \frac{\partial\Delta Q_i^{(1)}}{\partial V_i^{(1)}} = -Q_i^{(1)} + (V_i^{(1)})^2 B_{(i,i)}^{(1)} \tag{3.56}$$

The off-diagonal elements of $\overline{L}^{(1)}$ are:

$$L_{(i,j)}^{(1)} = \frac{\partial\Delta Q_i^{(1)}}{\partial V_i^{(1)}} = -V_i^{(1)}(G_{(i,j)}^{(1)}\sin\theta_{(i,j)}^{(1)} - B_{(i,j)}^{(1)}\cos\theta_{(i,j)}^{(1)}) \tag{3.57}$$

From practical experience the actual difference in harmonic voltage phase angles between two buses in a power system is very small, the following assumptions are made:

$$\cos\theta_{(i,j)}^{(1)} \approx 1, \qquad G_{(i,j)}^{(1)}\sin\theta_{(i,j)}^{(1)} \ll B_{(i,j)}^{(1)}$$

Moreover, the admittance corresponding to the fundamental reactive power at each bus, $B_{LDi}^{(1)}$, is much smaller than the imaginary part of the bus self-admittance $B_{(i,i)}^{(1)}$.

Therefore:

$$B_{LDi}^{(1)} = \frac{Q_i^{(1)}}{(V_i^{(1)})^2} \ll B_{(i,i)}^{(1)} \qquad \text{or} \qquad Q_i^{(1)} \ll (V_i^{(1)})^2 B_{(i,i)}^{(1)}$$

As a result of the above assumptions, equations 3.54, 3.55, 3.56 and 3.57 can be modified to:

$$H_{(i,i)}^{(1)} = (V_i^{(1)})^2 B_{(i,i)}^{(1)} \tag{3.58}$$

$$H_{(i,j)}^{(1)} = V_i^{(1)} V_j^{(1)} B_{(i,j)}^{(1)} \tag{3.59}$$

$$L_{(i,i)}^{(1)} = (V_i^{(1)})^2 B_{(i,i)}^{(1)} \tag{3.60}$$

$$L_{(i,j)}^{(1)} = V_i^{(1)} B_{(i,j)}^{(1)} \tag{3.61}$$

Then, matrices $\overline{B'}^{(1)}$ and $\overline{B''}^{(1)}$ are used instead of $\overline{H}^{(1)}$ and $\overline{L}^{(1)}$ respectively. Finally, the equations to calculate the fast decoupled fundamental power flow are:

$$\Delta\overline{P}^{(1)} = -\overline{B'}^{(1)} \Delta\overline{\theta}^{(1)} \tag{3.62}$$

$$\Delta\overline{Q}^{(1)} = -\overline{B''}^{(1)} \Delta\overline{|V|}^{(1)} \tag{3.63}$$

There are two possible procedures for solving the fast decoupled fundamental power flows. Their flow charts are shown in Figure 3.9 and Figure 3.10.

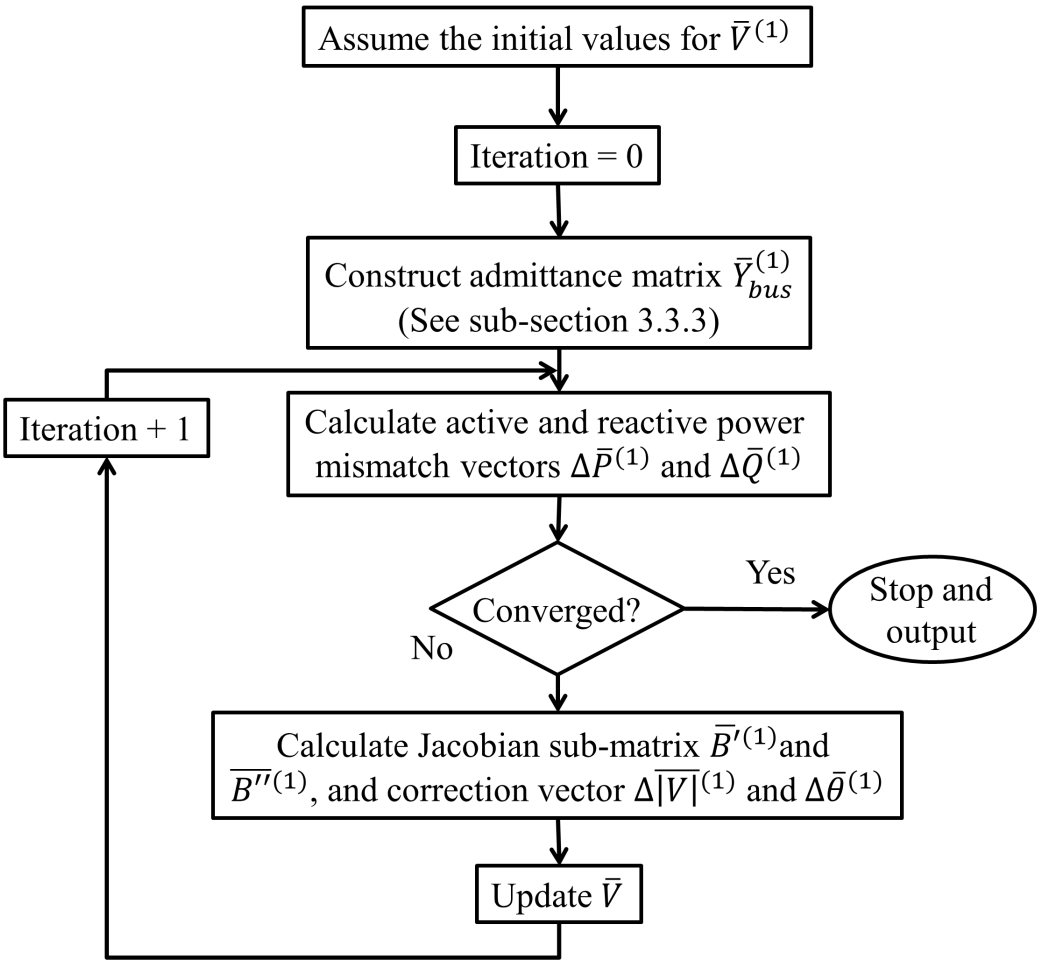

Figure 3.9: Fast decoupled fundamental power flow calculation flow chart: method one

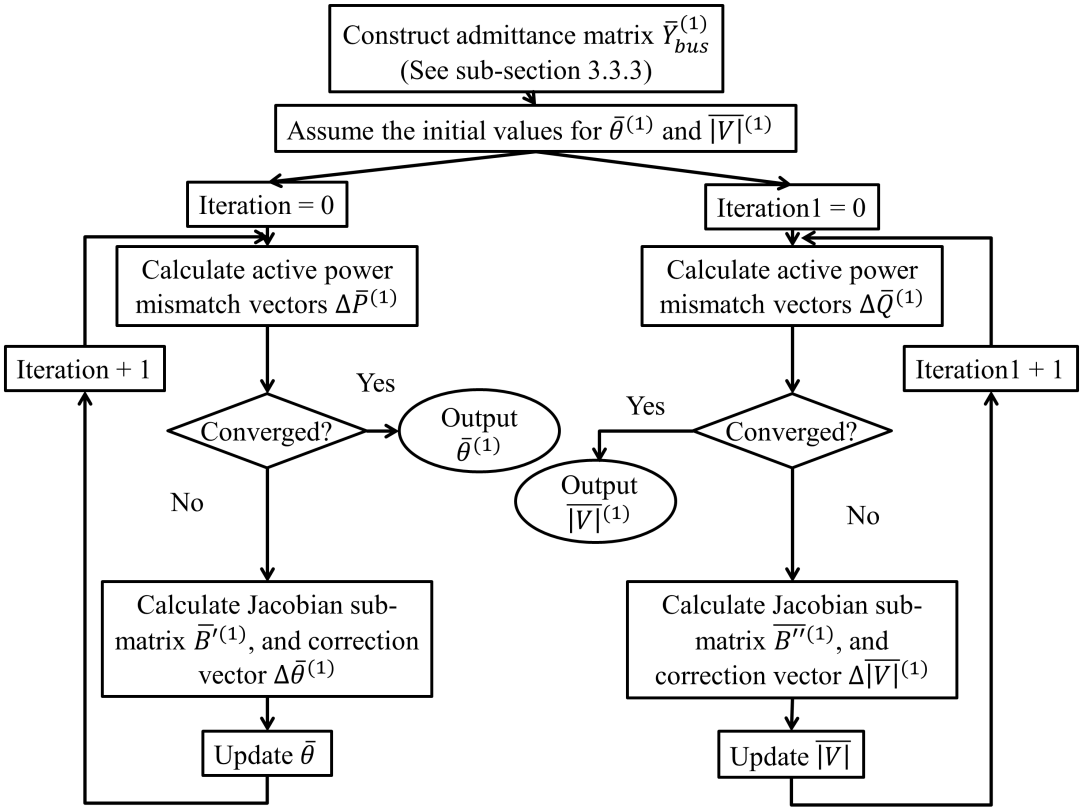

Figure 3.10: Fast decoupled fundamental power flow calculation flow chart: method two

3.5.3 Fast Harmonic Power Flow [5, 19, 20]

The fast harmonic power flow algorithm is designed for distribution systems. This method has the benefits of saving computing time. Based on the network structures of distribution systems, current injection evaluations and Kirchhoff's Law, the relationships between the bus voltages, branch currents and harmonic sources can be formulated. Then, the fundamental and harmonic voltages for each bus of a power system can be solved by the simple forward/backward sweep techniques. [19]

Equivalent current injections are widely used for the applications of distribution systems. For any bus i (both linear and non-linear) of a distribution power system, the equivalent current injection $I_i^{(1,k)}$ at the k^{th} iteration is:

$$I_i^{(1,k)} = \left(\frac{P_i^{sp} + jQ_i^{sp}}{V_i^{(1,k)}} \right)^* \tag{3.64}$$

where $V_i^{(1,k)}$ represents the voltage of linear bus i at the k^{th} iteration. P_i^{sp} and Q_i^{sp} are the specified active and reactive powers at bus i respectively. The symbol "$*$" represents the conjugate value.

For fundamental power flow, the equivalent current injection $I_i^{(1,k)}$ needs to be updated at each iteration. In other words, the fundamental equivalent current injection $I_i^{(1,k)}$ is modified at the end of each iteration k using equation 3.64 from the updated voltage $V_i^{(1,k)}$. However, the harmonic injection currents of each non-linear load do not require to be updated at the end of each iteration such as the ones used in fundamental equivalent current injections, for they have already been obtained based on harmonic analysis.

Parts of a distribution system and the harmonic injection currents are shown in Figure 3.11 below.

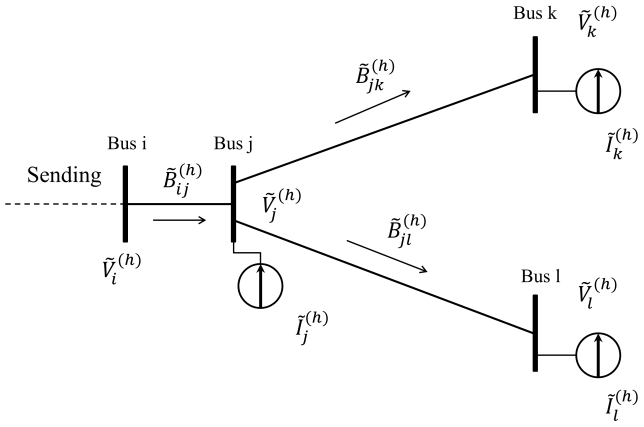

Figure 3.11: Parts of a distribution system

The harmonic injection currents are expressed as $\tilde{I}_j^{(h)}$, $\tilde{I}_k^{(h)}$ and $\tilde{I}_l^{(h)}$. $\tilde{B}_{ij}^{(h)}$, $\tilde{B}_{jk}^{(h)}$ and $\tilde{B}_{jl}^{(h)}$ are the harmonic branch currents. $\tilde{V}_i^{(h)}$, $\tilde{V}_j^{(h)}$, $\tilde{V}_k^{(h)}$ and $\tilde{V}_l^{(h)}$ denote the harmonic bus voltages. Then, the relationships between the harmonic branch currents and the harmonic injection currents of Figure 3.11 are:

$$\tilde{B}_{jk}^{(h)} = -\tilde{I}_k^{(h)} \tag{3.65}$$

$$\tilde{B}_{jl}^{(h)} = -\tilde{I}_l^{(h)} \tag{3.66}$$

$$\tilde{B}_{ij}^{(h)} = \tilde{B}_{jk}^{(h)} + \tilde{B}_{jl}^{(h)} - \tilde{I}_j^{(h)} \tag{3.67}$$

where $h = 1, 2, \ldots, h_{max}$.

It shows that the relationship between harmonic branch currents and harmonic injection currents of a radial feeder can be evaluated by summing the harmonic injection currents from the receiving bus toward the sending bus of the feeder. This calculation procedure is called backward current sweep. The general formulation of this procedure can be expressed as:

$$\tilde{B}_{ij}^{(h)} = -\tilde{I}_j^{(h)} + \sum_{n=j}^{n} \tilde{B}_{jn}^{(h)} \tag{3.68}$$

where n is the number of buses connected to bus j.

From Figure 3.11, the relationships between harmonic branch currents and harmonic bus voltages can be defined as:

$$\tilde{V}_j^{(h)} = \tilde{V}_i^{(h)} - \tilde{B}_{ij}^{(h)} \tilde{Z}_{ij}^{(h)} \tag{3.69}$$

$$\tilde{V}_k^{(h)} = \tilde{V}_j^{(h)} - \tilde{B}_{jk}^{(h)} \tilde{Z}_{jk}^{(h)} \tag{3.70}$$

$$\tilde{V}_l^{(h)} = \tilde{V}_j^{(h)} - \tilde{B}_{jl}^{(h)} \tilde{Z}_{jl}^{(h)} \tag{3.71}$$

where $\tilde{Z}_{ij}^{(h)}$, $\tilde{Z}_{jk}^{(h)}$ and $\tilde{Z}_{jl}^{(h)}$ are the branch equivalent impedances for the h^{th} harmonic order.

It is assumed that bus i at the sending end in the distribution system is the reference bus. Then, it is evident for a radial distribution system that if the harmonic branch current between buses i and j, $\tilde{B}_{ij}^{(h)}$, has been calculated by using the backward current sweep approach, then the harmonic voltage at bus j, $\tilde{V}_j^{(h)}$, can be established from equation 3.69. Finally, the harmonic voltages at the other buses can be obtained in the same way. Hence, the procedure that calculates the voltage from the sending bus forward to the receiving bus of the distribution feeder is called forward voltage sweep.

Therefore, the fast harmonic power flow algorithm combines the equivalent current injections, backward current sweep method and forward voltage sweep method together to evaluate the harmonic power flow in a distribution system. The calculation steps of this approach are illustrated below:

Step one Assume the initial bus voltages at fundamental frequency, $\tilde{V}^{(1)}$.

Step two Set harmonic frequency to be one, $h = 1$.

Step three Calculate fundamental equivalent current injections $I_i^{(1)}$ by using equation 3.64.

Step four Calculate fundamental branch currents by using equation 3.68.

Step five Calculate fundamental bus voltages.

Step six Set the convergence criterion to be whether the fundamental bus voltages at iteration k equal those at iteration $(k+1)$. If it is converged, go to next step;

otherwise, use the $(k+1)^{th}$ iteration fundamental bus voltages instead of the k^{th} iteration values, and go to step three.

Step seven Set $h = 2, 3, \ldots, h_{max}$.

Step eight Calculate equivalent branch impedance at each harmonic order.

Step nine Calculate harmonic branch currents by using equation 3.68.

Step ten Calculate harmonic bus voltages.

Step eleven If the harmonic order equals the maximum one, output the results; otherwise, go to step seven.

3.5.4 Fuzzy Harmonic Power Flow [5, 21, 22]

In the fuzzy harmonic power flow algorithm, the fuzzy set theory is employed to represent the harmonic injection currents. For an n bus power system the solution is achieved by solving a set of $4n \times 4n$ linear equations. The fuzzy solutions for both harmonic voltage magnitudes and phase angles can be individually expressed by two explicit linear equations. The solutions for each harmonic level can be obtained from these equations.

The harmonic sources are regarded as voltage independent current sources generated from non-linear loads. Harmonic penetration is a steady state phenomenon, hence monitoring the harmonics requires a long period of time for accurate results. It can be shown that the value of the harmonic injection current at a bus is most likely near the centre of a monitored range. Therefore, it is suitable to model the harmonic current sources with a triangle fuzzy number, denoted by $\tilde{I}^{(h)}$. Then, with a proper fuzzy model, the new fuzzy harmonic power flow equation can be expressed as follow:

$$\left[\overline{\Psi}^{(h)}\right] \begin{bmatrix} \tilde{V}_r^{(h)} \\ \tilde{V}_i^{(h)} \end{bmatrix} = \begin{bmatrix} \tilde{I}_r^{(h)} \\ \tilde{I}_i^{(h)} \end{bmatrix} \tag{3.72}$$

where $\overline{\Psi}^{(h)}$ is a $2n \times 2n$ matrix modified from the power system admittance matrix $\overline{Y}_{bus}^{(h)}$. $\tilde{V}_r^{(h)}$ and $\tilde{V}_i^{(h)}$ represent the fuzzy numbers of real and imaginary parts of the

harmonic bus voltages. $\tilde{I}_r^{(h)}$ and $\tilde{I}_i^{(h)}$ denote the fuzzy numbers of real and imaginary parts of the harmonic injection currents, respectively.

According to [21, 22], an arbitrary fuzzy number can be represented by an ordered pair of functions $(u_{min}(r), u_{max}(r))$, where $0 \leq r \leq 1$ and r is considered as the membership function value, which meet the following conditions:

- $u_{min}(r)$ is a bounded left continuous non-decreasing function during [0, 1].
- $u_{max}(r)$ is a bounded right continuous non-increasing function during [0, 1].
- $u_{min}(r) \leq u_{max}(r)$, $0 \leq r \leq 1$.

Figure 3.12 shows the diagram of a fuzzy number $(1+r, 4-2r)$.

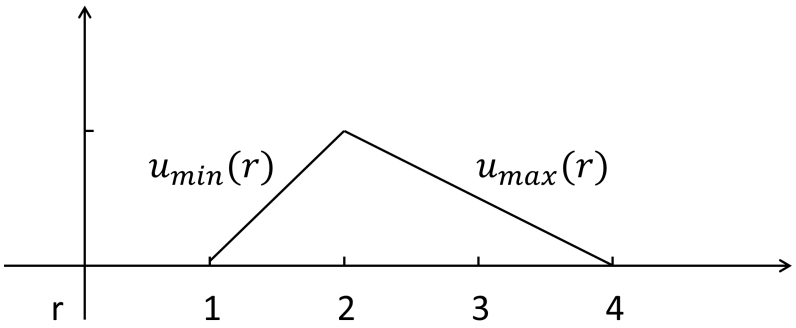

Figure 3.12: A fuzzy number

The author in [21] gives a rule to calculate each element of the modified matrix $\overline{\Psi}^{(h)}$, and it is shown below:

$$\begin{cases} y_{(i,j)} \geq 0 & \Rightarrow \quad \Psi_{(i,j)} = y_{(i,j)}, \Psi_{(i+n,j+n)} = y_{(i,j)} \\ y_{(i,j)} < 0 & \Rightarrow \quad \Psi_{(i,j+n)} = -y_{(i,j)}, \Psi_{(i+n,j)} = -y_{(i,j)} \end{cases} \tag{3.73}$$

Hence, the matrix $\overline{\Psi}^{(h)}$ can be expanded to a $4n \times 4n$ matrix as expressed below:

$$\left[\overline{\Psi}^{(h)}\right] = \begin{bmatrix} \Psi_{11}^{(h)} & \Psi_{12}^{(h)} \\ \Psi_{21}^{(h)} & \Psi_{22}^{(h)} \end{bmatrix} \tag{3.74}$$

where $\Psi_{11}^{(h)}$ contains the positive entries of $\overline{\Psi}^{(h)}$, $\Psi_{12}^{(h)}$ contains the absolute values of the negative entries of $\overline{\Psi}^{(h)}$, moreover, $\Psi_{21}^{(h)} = \Psi_{12}^{(h)}$ and $\Psi_{22}^{(h)} = \Psi_{11}^{(h)}$.

Then, the equation 3.72 can be expressed as a set of $4n \times 4n$ linear equations shown below:

$$\begin{bmatrix} \Psi_{11}^{(h)} & \Psi_{12}^{(h)} \\ \Psi_{21}^{(h)} & \Psi_{22}^{(h)} \end{bmatrix} \begin{bmatrix} V_{(r,min)}^{(h)}(r) \\ V_{(i,min)}^{(h)}(r) \\ -V_{(r,max)}^{(h)}(r) \\ -V_{(i,max)}^{(h)}(r) \end{bmatrix} = \begin{bmatrix} I_{(r,min)}^{(h)}(r) \\ I_{(i,min)}^{(h)}(r) \\ -I_{(r,max)}^{(h)}(r) \\ -I_{(i,max)}^{(h)}(r) \end{bmatrix} \tag{3.75}$$

The equation 3.75 can be uniquely solved for $[V_{(r,min)}^{(h)}(r), V_{(i,min)}^{(h)}(r), -V_{(r,max)}^{(h)}(r), -V_{(i,max)}^{(h)}(r)]^T$ if and only if the matrix in equation 3.74 is non-singular. Moreover, the fuzzy real and imaginary parts of the harmonic voltages at a bus k can each be written with two explicit linear equations:

$$V_{(r,k,min)}^{(h)}(r) = a_{(r,k,min)}^{(h)} r + b_{(r,k,min)}^{(h)} \tag{3.76}$$

$$V_{(i,k,min)}^{(h)}(r) = a_{(i,k,min)}^{(h)} r + b_{(i,k,min)}^{(h)} \tag{3.77}$$

$$V_{(r,k,max)}^{(h)}(r) = a_{(r,k,max)}^{(h)} r + b_{(r,k,max)}^{(h)} \tag{3.78}$$

$$V_{(i,k,max)}^{(h)}(r) = a_{(i,k,max)}^{(h)} r + b_{(i,k,max)}^{(h)} \tag{3.79}$$

where $a_{(r,k,min)}^{(h)}$, $a_{(i,k,min)}^{(h)}$, $a_{(r,k,max)}^{(h)}$, $a_{(i,k,max)}^{(h)}$ and $b_{(r,k,min)}^{(h)}$, $b_{(i,k,min)}^{(h)}$, $b_{(r,k,max)}^{(h)}$, $b_{(i,k,max)}^{(h)}$ are the coefficients of fuzzy numbers of the real and imaginary parts of the harmonic voltages at bus k.

3.5.5 Probabilistic Harmonic Power Flow [5, 23–31]

Unavoidable uncertainties (e.g. the wind speed) affect the input data of the modelling for the evaluation of harmonic voltages and currents caused by non-linear loads in the power system. These uncertainties are mainly caused by time variations of linear load demands, network configurations and operating modes of non-linear loads [5, 24, 27]. The variations have a random character, and therefore, the probabilistic method is used to describe the behaviour of such characteristics. There are two methods to evaluate

the supply voltage distortions in the field of probabilistic models:

Direct method the probabilistic functions of harmonic voltages are calculated for the assigned probabilistic functions of harmonic currents injected into the power network by non-linear loads.

Integrated method the probabilistic functions of both harmonic voltages and currents are calculated together by properly taking into account the interactions between voltage distortions and harmonic currents.

The probabilistic method was first proposed to calculate the fundamental power flow in 1974 [28]. It has been further developed and applied into power system normal operation [29–31]. Then, the authors in [24, 26, 27] developed the probabilistic method and applied it to harmonic power flow evaluation.

A probabilistic steady state analysis of a harmonic power flow can be performed by either iterative probabilistic methods such as Monte Carlo or analytical approaches. The iterative probabilistic procedures require knowledge of probability density functions of the input variables. For each random input a value is generated according to its proper probability density function. Then, due to the generated input values, the operating steady state conditions of harmonic power flow are evaluated by solving the non-linear equations based on iterative numerical methods such as the Newton-Raphson approach and the decoupled approach. Once the convergence has been achieved, the state of the power system is completely known and the values of all the variables of interest are stored. The procedure is repeated to achieved an accurate probability of the output variables. Unfortunately, the iterative probabilistic procedures require long computing time and may encounter convergence problems. An analytical approach is a method that uses convolution techniques with probability density functions of stochastic variables of power inputs to calculate the probability density functions of stochastic variables of system states and line flows. However, it is difficult to solve probabilistic harmonic power flow equations by the convolution of probability density functions of input power variables.[23]

Hence, the authors in [24, 27] indicate a new probabilistic method for harmonic analysis in a power system which takes into account, in closed-form, the interactions

between the supply voltage distortions and the harmonic currents of non-linear loads. It linearises the non-linear equation system that describes the system steady state behaviour around an expected value region. Then, the first-order approximations, based on Taylor equations, are used to directly establish the means and the covariance matrix of the output probability density functions, starting from knowledge of the means and the covariance matrix of the input probability density functions.

A vector of input parameters $\overline{T}_a = [\overline{T}_1 \overline{T}_2 \overline{T}_3]^T$ is assigned as input data. $\overline{T}_1$, $\overline{T}_2$ and $\overline{T}_3$ are defined as follows:

$$\overline{T}_1 = [P_2^{(1)}, \cdots, P_{N_g}^{(1)}]^T \tag{3.80}$$

$$\begin{aligned} \overline{T}_2 = & [P_{N_g+1}^{(1)}, Q_{N_g+1}^{(1)}, \cdots, P_{N_g+N_1}^{(1)}, Q_{N_g+N_1}^{(1)}, \\ & P_{N_g+N_1+1}, S_{N_g+N_1+1}, \cdots, P_N, S_N]^T \end{aligned} \tag{3.81}$$

$$\overline{T}_3 = [|\, V \,|_1^{(1)}, \cdots, |\, V \,|_{N_g}^{(1)}]^T \tag{3.82}$$

where $1, 2, \ldots, N_g$ represent the number of PV buses; $(N_g + 1), \ldots, (N_g + N_1)$ are the number of PQ buses; and $(N_g + N_1 + 1), \ldots, (N)$ denote the number of PS buses. Hence, the input vector $\overline{T}_1$ includes the active generator powers at fundamental frequency (with exception of the slack bus, numbered as bus one); input vector $\overline{T}_2$ includes the active and reactive linear load powers at fundamental frequency and the total active and apparent non-linear load powers; and input vector $\overline{T}_3$ includes the generator voltage magnitudes.

Two requirements are needed for every probabilistic formulation. One is the statistical characterization of the input data; the other is the evaluation of the statistical features of the output variables of interest. The statistical characterization of the input data consists of checking:

(i) which components of vector $\overline{T}_a$ have to be considered as random and which ones can be kept fixed.

(ii) what are the statistical features to characterize the randomness of the variables identified in step (i).

The most realistic method to solve the problem is to refer to past experience, looking at both available historical data collections and technical knowledge of the electrical power system under study. With reference to problem (i), the generator voltage magnitudes can be considered determined if the set points of the regulator are not deliberately changed. With reference to problem (ii), the random nature appearing in $\overline{T}_1$ and $\overline{T}_2$ is applied.

It is assumed that the harmonic power flow equation is expressed as:

$$f(N) = \overline{T}_a \tag{3.83}$$

where $\overline{N}$ represents the output variable random vector which includes the fundamental and harmonic voltage magnitudes and phase angles and the non-linear loads variables.

Let the vector $\mu(\overline{T}_a)$ be the expected values of $\overline{T}_a$. If a deterministic power flow is calculated by using $\mu(\overline{T}_a)$ as input data, the solution of equation 3.83 will be given by the vector $\overline{N}_o$ such that:

$$f(N_o) = \mu(\overline{T}_a) \tag{3.84}$$

Then, linearising the equation around the point N_o:

$$\overline{N} \cong \overline{N}_o + \overline{A}\Delta\overline{T}_a = \overline{N'}_o + \overline{A}\overline{T}_a \tag{3.85}$$

where

$$\Delta\overline{T}_a = \overline{T}_a - \mu(\overline{T}_a) \tag{3.86}$$

$$\overline{N'}_o = \overline{N}_o - \overline{A}\mu(\overline{T}_a) \tag{3.87}$$

$$\overline{A} = \begin{bmatrix} \frac{\partial P_1^{(1)}}{\partial |V|} & \frac{\partial P_1^{(1)}}{\partial \Phi} & 0 \\ \frac{\partial Q_1^{(1)}}{\partial |V|} & \frac{\partial Q_1^{(1)}}{\partial \Phi} & 0 \\ \frac{\partial P_{nl}}{\partial |V|} & \frac{\partial P_{nl}}{\partial \Phi} & 0 \\ \frac{\partial S_{nl}}{\partial |V|} & \frac{\partial S_{nl}}{\partial \Phi} & 0 \\ \frac{\partial P_{gen}^{(1)}}{\partial |V|} & \frac{\partial P_{gen}^{(1)}}{\partial \Phi} & 0 \\ \frac{\partial |V|_{gen}^{(1)}}{\partial |V|} & 0 & 0 \\ \frac{\partial I_r}{\partial |V|} & \frac{\partial I_r}{\partial \Phi} & 0 \\ \frac{\partial I_i}{\partial |V|} & \frac{\partial I_i}{\partial \Phi} & 0 \\ \frac{\partial (I_r+g_r)}{\partial |V|} & \frac{\partial I_r+g_r)}{\partial \Phi} & \frac{\partial I_r+g_r)}{\partial X} \\ \frac{\partial (I_i+g_i)}{\partial |V|} & \frac{\partial I_i+g_i)}{\partial \Phi} & \frac{\partial I_i+g_i)}{\partial X} \end{bmatrix}^{-1}_{N=N_o} \tag{3.88}$$

The parameter X in the above equation represents the non-linear load variable.

Equation 3.85 expresses each random element of the vector $\overline{N}$ as a linear combination of the random elements of the input vector $\overline{T}_a$. Hence, the vector of mean (expected) values can be defined as:

$$\mu(\overline{N}) = \overline{N}_o \tag{3.89}$$

The vector of the covariance matrix of $\overline{N}$ is established by:

$$cov(\overline{N}) = \overline{A} cov(\overline{T}_a) \overline{A}^T \tag{3.90}$$

Once the statistical features of the random output vector $\overline{N}$ are known, the statistics of other variables on which it depends can also be evaluated.

3.5.6 Modular Harmonic Power Flow [32–34]

As mentioned in the introduction of this chapter, the time domain approach based on transient analysis has high accuracy. But it usually requires long computing times especially for a large power system with many non-linear loads. However, the frequency domain can overcome this problem. Hence, the time domain approach is convenient to apply to a small power system; while the frequency domain usually applies to a large

power system. But, the non-linear loads are best modelled using direct time domain methods, and it is difficult to consider a large power system using pure time domain. Therefore, the authors in [32–34] denoted a hybrid methodology with both time domain and frequency domain computations to apply a faster and more flexible solution to the problem. This hybrid methodology is called modular harmonic power flow.

This approach categorises the power system components into two distinct groups. The first group presents an easily predictable change of harmonic impedance with operating point. Such components are termed linear and are assumed not to couple harmonics. In the second group, the harmonic impedances of such power system components cannot be easily predetermined. They are usually calculated by direct or iterative methods. These components are termed non-linear and are modelled within the harmonic power flow as dependent harmonic sources.

In modular approaches, all the linear components can be represented as frequency dependent with a harmonic admittance matrix, $\overline{Y}^{(h)}$, representing their terminal behaviour for a given harmonic order h. However, non-linear components (loads) are included within the harmonic power flow as black boxes. In a black box, it is the model of a non-linear component which is carried out individually in the time domain using a best-suited method. Its input is periodic harmonic bus voltage, and the output of the black box is the corresponding periodic harmonic injection current.

The modular harmonic power flow is performed iteratively. Each step consists of two stages:

(i) *Updating the periodic steady state of the individual components using voltage correction from stage (ii).* The inputs to a component are the terminal voltages and the outputs are the terminal currents. This stage provides accurate outputs for the given inputs. For linear components, the calculations are performed in frequency domain. For non-linear components, the calculations are performed in time domain, and the process is accelerated to steady state by means of the Poincaré procedure illustrated in [32]. The initial input voltages are usually achieved from the fundamental power flow algorithm at the first iteration.

(ii) *Calculation of voltage corrections for stage (i).* The currents obtained from stage (i) are combined for buses with adjacent components into the current mismatch $\Delta\bar{I}$, expressed in the frequency domain. This is achieved by performing fast Fourier transform (FFT) on the periodic terminal currents of each of the time-varying components. These current mismatches become injections into a system-wide incremental harmonic admittance matrix $\overline{Y}_{bus}$, calculated in advance from such matrices for all individual components. Then, the following equation is applied to solve voltage correction vector $\Delta\overline{V}$, to be used to update all bus voltages in stage (i):

$$\Delta\bar{I} = \overline{Y}_{bus}\Delta\overline{V} \tag{3.91}$$

The approach is modular at stage (i). The voltage correction vector $\Delta\overline{V}$ in stage (ii) is calculated globally for the whole power system.

The main procedures of the modular harmonic power flow algorithm are:

- A fundamental power flow algorithm is used to establish the initial voltages at all buses.
- The incremental harmonic admittance matrix $\overline{Y}_{bus}$ is identified by assembling a separate admittance matrix for each component (black box).
- Currents and their mismatches $\Delta\bar{I}$ for all the buses are achieved by the following: frequency domain calculations are used for the linear and largest parts of the power system such as transmission lines and time domain calculations supplemented by Poincaré acceleration for non-linear and time-varying components at stage (i).
- Use equation 3.91 to obtain the voltage correction vector $\Delta\overline{V}$ to update the bus voltages for the next iteration.

3.6 Computation and Results

In this section, the Newton-Raphson based harmonic power flow algorithm and the decoupled harmonic power flow algorithm are applied to a simple five-bus power sys-

tem. A simple six pulse line commutated converter is used as the harmonic source. Its harmonic injection current of each harmonic level is given. The computing time, the iterations, the harmonic bus voltage magnitudes and phase angles and the total harmonic voltage distortion are calculated by each of two approaches. Then, the results are compared to investigate the difference between two methods.

The computer which is used for the simulation has an i7 quad-core CPU with 3.4 GHz and a 12G RAM. Its operation system is Windows 8.

3.6.1 Power System and Harmonic Source

A simple five-bus power system is applied to the calculation as shown in Figure3.13 [45].

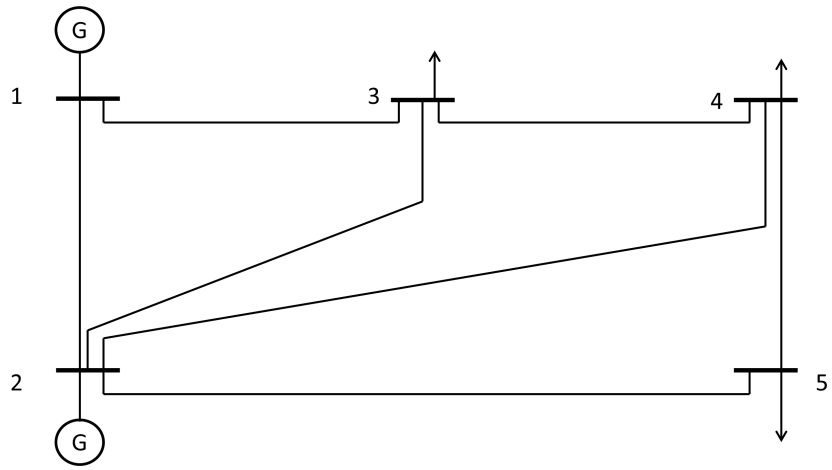

Figure 3.13: A five-bus power system

It has two generators which are located at bus one and bus two, respectively. Bus one is regarded as the reference bus (slack bus). Bus two is a PV bus. Buses three and four are both PQ bus. Bus five is a non-linear bus (PS). The bus data is presented in Table 3.4 and the line and transformer data of this power system is shown in Table 3.5.

Table 3.4: The bus data of a five-bus power system

Bus	Type	Voltage (p.u.)	Load			Generator	
			MW	MVar	MVA	MW	MVar
1	Slack	1.06	0.0	0.0	-	-	-
2	PV	1.046	20.0	10.0	-	40.0	-
3	PQ	-	45.0	45.0	-	0.0	0.0
4	PQ	-	40.0	5.0	-	0.0	0.0
5	PS	-	60.0	-	65.0	0.0	0.0
"-" means the value needs to be calculated.							

Table 3.5: The line and transformer data of a five-bus power system

Line No.	Line data					Transformer tap	
	From	To	R (p.u.)	X (p.u.)	B (p.u.)	Magnitude	Angle
1	1	2	0.02	0.06	0.06	1	0
2	1	3	0.08	0.24	0.05	1	0
3	2	3	0.06	0.18	0.04	1	0
4	2	4	0.06	0.18	0.04	1	0
5	2	5	0.04	0.12	0.03	1	0
6	3	4	0.01	0.03	0.02	1	0
7	4	5	0.08	0.24	0.05	1	0

A simple six pulse line commutated converter is applied as the harmonic source which is located at bus five. The harmonic injection current for each harmonic level (including fundamental frequency) is listed in Table 3.6. The highest harmonic order of this converter is assumed 29^{th}.

Table 3.6: Harmonic currents generated by a simple six pulse line commutated converter [11]

Harmonic order'h'	Magnitude (p.u.)	Angle degree	Harmonic order'h'	Magnitude (p.u.)	Angle degree
1	0.1	0	17	0.0059	0
5	0.02	0	19	0.0053	0
7	0.0143	0	23	0.0043	0
11	0.0091	0	25	0.004	0
13	0.0077	0	29	0.0034	0

3.6.2 Results and Discussions

The Newton-Raphson method (NRM) spends 0.1813 seconds and generates 5 iterations to accomplish the calculation. However the decoupled method (DM) only spends 0.0549 seconds to complete the calculation, and just generates 3 iterations in the end. It indicates that the DM is much faster than the NRM with one simple harmonic source in a five bus power system.

Because the bus voltage magnitude at the fundamental frequency is much bigger than that at each harmonic frequency, the results of fundamental bus voltage magnitude generated by two methods are illustrated separately to the harmonic ones. The fundamental ones are shown in Figure 3.14 below.

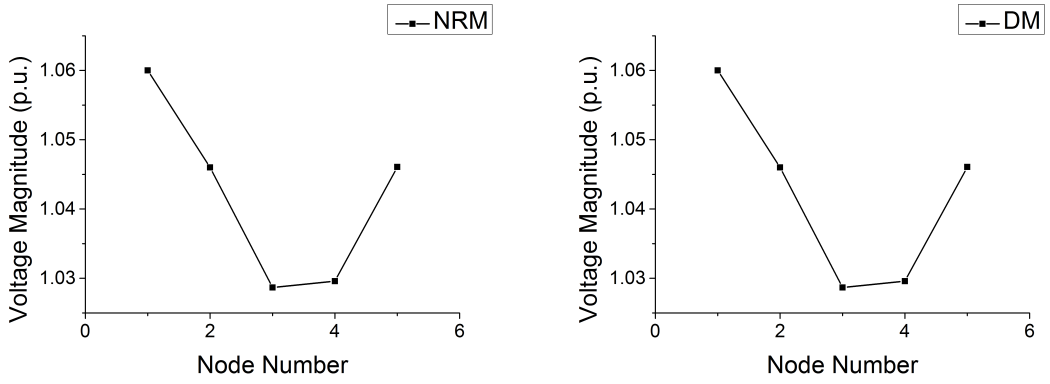

(a) Generated by the NRM

(b) Generated by the DM

Figure 3.14: Fundamental voltage magnitudes generated by two methods

The results of fundamental bus voltage magnitudes calculated by two different methods are nearly the same through the above two diagrams. Bus one is the slack bus with fixed voltage magnitude. Bus two is PV bus and its voltage magnitude is also fixed. Bus three gets the minimum voltage magnitude after the calculation.

The results of bus voltage magnitudes at higher harmonic frequencies (greater than one) are denoted in the three dimension diagram shown in Figure 3.15. The horizontal axis represents the harmonic frequencies, the vertical axis represents the voltage magnitude and the depth axis represents the bus number.

The harmonic voltage magnitudes only exists at the 5^{th}, 7^{th}, 11^{th}, 13^{th}, 17^{th}, 19^{th},

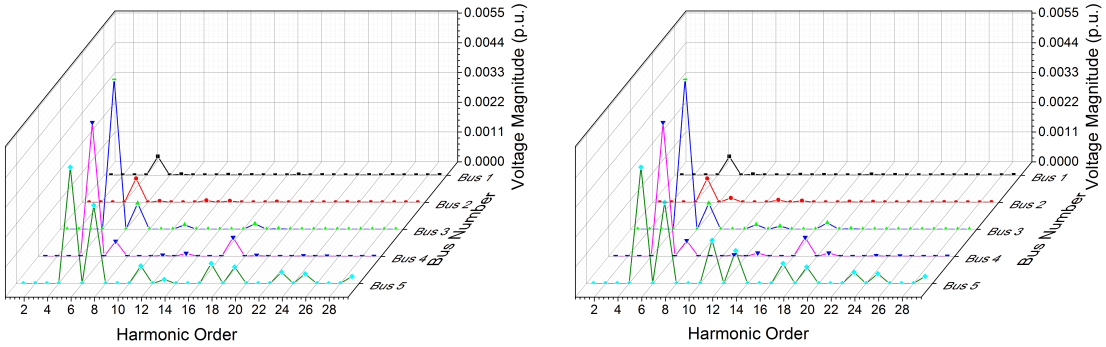

(a) Generated by the NRM

(b) Generated by the DM

Figure 3.15: Harmonic voltage magnitudes generated by two methods

23^{rd}, 25^{th} and 29^{th} harmonic orders. The harmonic voltage magnitudes at non-linear bus five, generated by the harmonic source, are bigger than those at other buses except the 5^{th} harmonic voltage magnitude. At bus three it has the biggest value, $0.0059 p.u.$. The result errors between two different methods is shown in Figure 3.16 below.

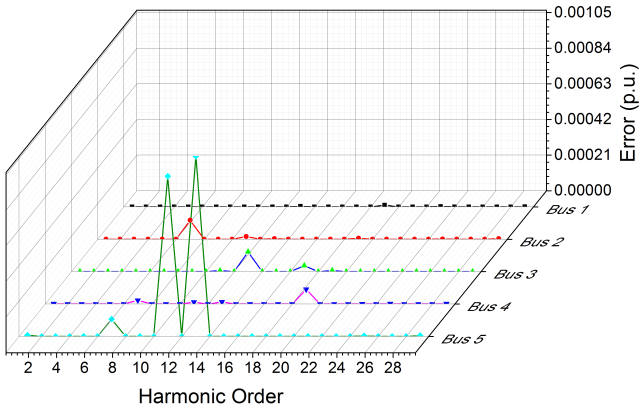

Figure 3.16: Voltage magnitude error between two different methods at all harmonic frequencies

It shows that the results obtained by the DM are nearly the same with those generated by the NRM. However the voltage magnitudes at 13th and 15th harmonic orders on bus five give obvious differences according to the above figure. Nevertheless, the error values are only $0.0009 p.u.$ and $0.001 p.u.$ which are acceptable.

The bus voltage phase angles at all harmonic orders are illustrated in a 3D diagram shown in Figure 3.17 below. The horizontal axis represents the harmonic orders, the vertical axis represents bus voltage angles in degree and the depth axis represents the bus number.

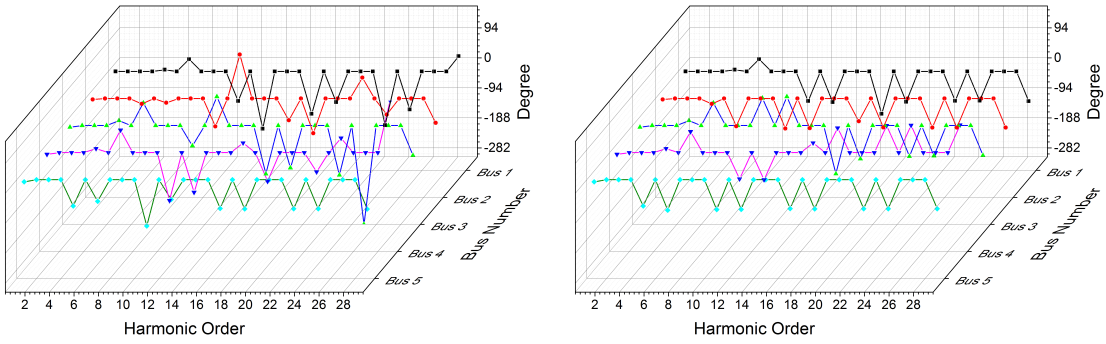

(a) Generated by the NRM

(b) Generated by the DM

Figure 3.17: Harmonic voltage phase angles generated by two methods (including fundamental frequency)

It shows that most voltage phase angles at each bus fluctuate between 0° and -132°. Moreover, most results achieved by two different methods are nearly the same. However, several values are obviously different, especially at the 13^{th}, 23^{rd} and 29^{th} harmonic orders on bus one, the 7^{th}, 13^{th} and 23^{rd} harmonic orders on bus two, the 11^{th}, 23^{rd} and 25^{th} harmonic orders on bus three, the 11^{th}, 19^{th} and 23^{rd} harmonic orders on bus four and the 11^{th} harmonic order on bus five.

The NRM and the DM generate nearly the same bus voltage magnitudes at all harmonic levels (including fundamental frequency) on each bus. However, they give different bus voltage phase angles at higher harmonic orders (excluding fundamental frequency). The reason leads to these differences is that the DM calculates bus voltage magnitudes and phase angles using admittance-matrix-based equation $I = Y * V$ directly at each higher harmonic level without considering harmonic couplings, while the NRM establishes them using whole iterative loop with considering harmonic couplings. The bus voltage magnitude must converge to a specific value, while the phase

angle rotates between $-180°$ and $180°$. Hence, different calculation methods may generate different phase angles at higher harmonic levels.

The total harmonic voltage distortions (THD_v) generated by two different methods are shown in Figure 3.18.

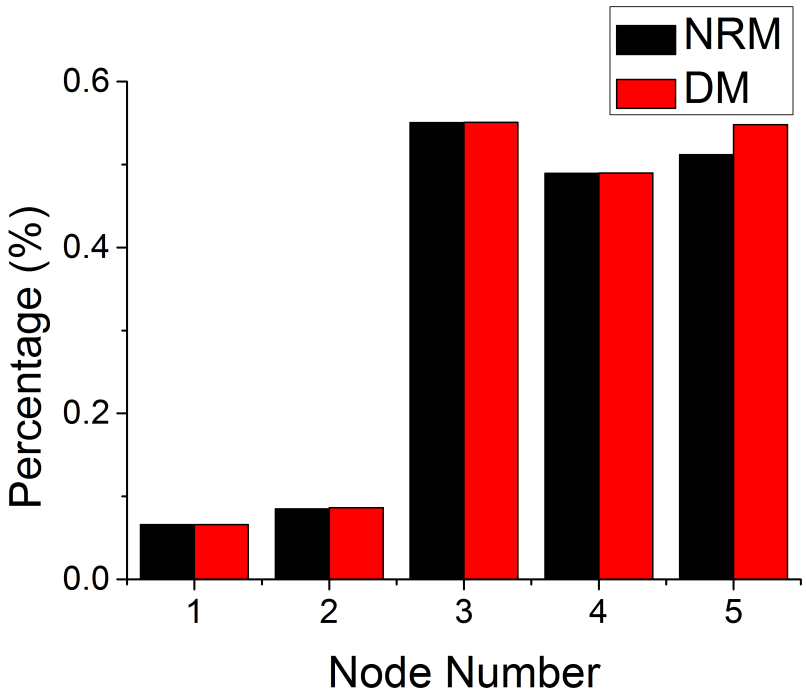

Figure 3.18: Total harmonic voltage distortion

It indicates that two different methods give the same THD values from bus one to bus four. But a mismatch that equals $0.0004 p.u.$ exists on bus five, for the little voltage magnitude differences exist at the 11^{th} and 13^{th} harmonic orders on bus five. As mentioned in chapter 2, the THD only depends on the voltage magnitudes at all harmonic levels on each bus. Hence, if the harmonic voltage magnitudes generated by different methods are equal, the values of THD are also the same.

3.7 Conclusion

This chapter described several harmonic power flow evaluation methods. The Newton-Raphson based algorithm is the first proposed method for the harmonic power flow

evaluation. It provides an accurate calculation by considering the harmonic couplings. However, it requires long computing time for a large power network with many non-linear loads and strong harmonic couplings.

The decoupled approach was designed to overcome these problems. It considers the harmonic injection currents generated by non-linear loads as the voltage independent harmonic sources and it ignores the couplings between all harmonics. Hence, the decoupled approach provides a faster calculation. But, it cannot obtain as accurate results as the Newton-Raphson based method. The author in [15] modified the decoupled approach by reducing the Jacobian matrix, and finally got acceptable solutions.

The fast harmonic power flow formulation described in sub-section 3.4.3 is especially for a distribution system by applying the equivalent current injection and the simple forward/backward sweep techniques. The fuzzy and probabilistic harmonic power flow calculation approaches are both for the uncertain harmonic power flow evaluations.

The last method mentioned in this chapter was the modular harmonic power flow algorithm. It is a hybrid methodology with both time domain and frequency domain computations to apply a faster and more flexible solution to the problem. The modular approach facilitates the development of new component models and the formation of a wide range of system configurations. It is also appropriate for an unbalanced system with asymmetric loads.

Finally, the Newton-Raphson based method and the decoupled method were each applied to a simple five bus power system with a six pulse line commutated converter for harmonic power flow calculation. It was shown that the results calculated by the decoupled method were almost the same as those calculated by the Newton-Raphson based method. However, the Newton-Raphson method requires longer computing time which is three times the decoupled method.

References

[1] C. S. Tan, "An analysis of lmp decomposition for financial settlement and economic upgrades," Ph.D. dissertation, PhD Thesis, University of Strathclyde, 2007. vi, 64, 71

[2] D. Xia and G. T. Heydt, "Harmonic power flow studies part i-formulation and solution," *Power Apparatus and Systems, IEEE Transactions on*, no. 6, pp. 1257–1265, 1982.

[3] D. Xia and G. Heydt, "Harmonic power flow studies-part ii implementation and practical application," *Power Apparatus and Systems, IEEE Transactions on*, no. 6, pp. 1266–1270, 1982.

[4] K. Meng Goh, "Harmonic analysis for electrical power systems," Master's thesis, University of Strathclyde, December 1984. vi, vii, 64, 65, 85, 88

[5] E. Fuchs and M. Masoum, *Power quality in power systems and electrical machines, 2008*. Academic Press. vi, vii, 64, 71, 93, 96, 98

[6] T. Chung and H. Leung, "A genetic algorithm approach in optimal capacitor selection with harmonic distortion considerations," *International Journal of Electrical Power & Energy Systems*, vol. 21, no. 8, pp. 561–569, 1999. vii, 64, 85

[7] K. L. Lian and T. Noda, "A time-domain harmonic power-flow algorithm for obtaining nonsinusoidal steady-state solutions," *Power Delivery, IEEE Transactions on*, vol. 25, no. 3, pp. 1888–1898, 2010.

[8] L. Gengyin, X. Chunxia, L. Guanqi, and Z. Chengyong, "Calculation of three-phase harmonic power flow in power systems with traction loads," in *Power System Technology, 1998. Proceedings. POWERCON'98. 1998 International Conference on*, vol. 2. IEEE, 1998, pp. 1565–1570. vi, 65, 67, 68, 69

[9] Y. Baghzouz, "Effects of nonlinear loads on optimal capacitor placement in radial feeders," *Power Delivery, IEEE Transactions on*, vol. 6, no. 1, pp. 245–251, 1991.

[10] Z. Marinos, J. Pereira, and S. J. Carneiro, "Fast harmonic power flow calculation using parallel processing," *IEE Proceedings-Generation, Transmission and Distribution*, vol. 141, no. 1, pp. 27–32, 1994.

[11] A. Ulinuha, M. Masoum, and S. Islam, "Harmonic power flow calculations for a large power system with multiple nonlinear loads using decoupled approach," in *Power Engineering Conference, 2007. AUPEC 2007. Australasian Universities*. IEEE, 2007, pp. 1–6. vi, xx, 65, 85, 106

[12] H.-C. Chin, "Optimal shunt capacitor allocation by fuzzy dynamic programming," *Electric Power Systems Research*, vol. 35, no. 2, pp. 133–139, 1995.

[13] V. Sharma, R. Fleming, and L. Niekamp, "An iterative approach for analysis of harmonic penetration in the power transmission networks," *Power Delivery, IEEE Transactions on*, vol. 6, no. 4, pp. 1698–1706, 1991. vii, 64, 85

[14] B. Stott, "Decoupled newton load flow," *Power Apparatus and Systems, IEEE Transactions on*, no. 5, pp. 1955–1959, 1972. vii, 64, 88

[15] B. Stott and O. Alsaç, "Fast decoupled load flow," *power apparatus and systems, ieee transactions on*, no. 3, pp. 859–869, 1974. 88, 111

[16] R. D. Zimmerman and H.-D. Chiang, "Fast decoupled power flow for unbalanced radial distribution systems," *Power Systems, IEEE Transactions on*, vol. 10, no. 4, pp. 2045–2052, 1995.

[17] J. Arrillaga and B. Harker, "Fast-decoupled three-phase load flow," *Electrical Engineers, Proceedings of the Institution of*, vol. 125, no. 8, pp. 734–740, 1978.

[18] I. M. Elamin, "Fast decoupled harmonic loadflow method," in *Industry Applications Society Annual Meeting, 1990., Conference Record of the 1990 IEEE*. IEEE, 1990, pp. 1749–1756. vii, 64, 88

[19] J.-H. Teng and C.-Y. Chang, "A fast harmonic load flow method for industrial distribution systems," in *Power System Technology, 2000. Proceedings. PowerCon 2000. International Conference on*, vol. 3. IEEE, 2000, pp. 1149–1154. vi, vii, 64, 65, 93

[20] ——, "Fast harmonic analysis method for unbalanced distribution systems," in *Power Engineering Society General Meeting, 2003, IEEE*, vol. 2. IEEE, 2003. vii, 64, 93

[21] M. Friedman, M. Ming, and A. Kandel, "Fuzzy linear systems," *Fuzzy sets and systems*, vol. 96, no. 2, pp. 201–209, 1998. vii, 64, 96, 97

[22] Y.-Y. Hong, J.-S. Lin, and C.-H. Liu, "Fuzzy harmonic power flow analyses," in *Power System Technology, 2000. Proceedings. PowerCon 2000. International Conference on*, vol. 1. IEEE, 2000, pp. 121–125. vii, 64, 96, 97

[23] P. Chen, Z. Chen, and B. Bak-Jensen, "Probabilistic load flow: A review," in *Electric Utility Deregulation and Restructuring and Power Technologies, 2008. DRPT 2008. Third International Conference on*. IEEE, 2008, pp. 1586–1591. vii, 64, 98, 99

[24] G. Carpinelli, T. Esposito, P. Varilone, and P. Verde, "First-order probabilistic harmonic power flow," *IEE Proceedings-Generation, Transmission and Distribution*, vol. 148, no. 6, pp. 541–548, 2001. 98, 99

[25] A. Romero, H. Zini, G. Rattá, and R. Dib, "Harmonic load-flow approach based on the possibility theory," *IET Generation, Transmission & Distribution*, vol. 5, no. 4, pp. 393–404, 2011.

[26] P. Caramia, G. Carpinelli, T. Esposito, P. Varilone, R. Chiumeo, L. Mastandrea, and F. Tarsia, "Probabilistic harmonic power flow for assessing waveform distortions in distribution systems with wind embedded generation," in *Power Electronics, Electrical Drives, Automation and Motion, 2006. SPEEDAM 2006. International Symposium on*. IEEE, 2006, pp. 818–823. 99

[27] T. Esposito, G. Carpinelli, P. Varilone, and P. Verde, "Probabilistic harmonic power flow for percentile evaluation," in *Electrical and Computer Engineering, 2001. Canadian Conference on*, vol. 2. IEEE, 2001, pp. 831–838. 98, 99

[28] B. Borkowska, "Probabilistic load flow," *Power Apparatus and Systems, IEEE Transactions on*, no. 3, pp. 752–759, 1974. 99

[29] P. Jorgensen, J. Christensen, and J. Tande, "Probabilistic load flow calculation using monte carlo techniques for distribution network with wind turbines," in *Harmonics and Quality of Power Proceedings, 1998. Proceedings. 8th International Conference On*, vol. 2. IEEE, 1998, pp. 1146–1151. 99

[30] A. Leite da Silva, V. Arienti, and R. Allan, "Probabilistic load flow considering dependence between input nodal powers," *power apparatus and systems, ieee transactions on*, no. 6, pp. 1524–1530, 1984.

[31] S. Conti and S. Raiti, "Probabilistic load flow using monte carlo techniques for distribution networks with photovoltaic generators," *Solar Energy*, vol. 81, no. 12, pp. 1473–1481, 2007. vii, 64, 98, 99

[32] A. Semlyen and M. Shtash, "Principles of modular harmonic power flow methodology," in *Generation, Transmission and Distribution, IEE Proceedings-*, vol. 147, no. 1. IET, 2000, pp. 1–6. vii, 64, 102, 103

[33] G. Bathurst, B. Smith, N. Watson, and J. Arillaga, "A modular approach to the solution of the three-phase harmonic power-flow," in *Harmonics and Quality of Power Proceedings, 1998. Proceedings. 8th International Conference On*, vol. 2. IEEE, 1998, pp. 653–659.

[34] M. Shlash and A. Semlyen, "Efficiency issues of modular harmonic power flow," *IEE Proceedings-Generation, Transmission and Distribution*, vol. 148, no. 2, pp. 123–127, 2001. vii, 64, 102, 103

[35] A. Bonner, T. Grebe, E. Gunther, L. Hopkins, M. Marz, J. Mahseredjian, N. Miller, T. Ortmeyer, V. Rajagopalan, S. Ranade *et al.*, "Modeling and simulation of the propagation of harmonics in electric power networks. 1. concepts, models, and simulation techniques," *IEEE Transactions on Power Delivery*, vol. 11, no. 1, pp. 452–465, 1996. vi, 65, 66, 67, 68, 70

[36] S. A. Papathanassiou and M. P. Papadopoulos, "Harmonic analysis in a power system with wind generation," *Power Delivery, IEEE Transactions on*, vol. 21, no. 4, 2006. xx, 66, 67, 68, 69

[37] S. Ranade and W. Xu, "An overview of harmonics modeling and simulation," *IEEE Task Force on Harmonics Modeling and Simulation*, p. 1, 2007. 66, 67, 68, 70

[38] H. Yang, F. Wen, L. Wang, and S. Singh, "Newton-downhill algorithm for distribution power flow analysis," in *Power and Energy Conference, 2008. PECon 2008. IEEE 2nd International*. IEEE, 2008, pp. 1628–1632.

[39] T. Koike, "Electric power transmission and distribution," *Youkendo. Co. Ltd, Tokyo, Japan*, 1979.

[40] G. Deb, "Ferranti effect in transmission line," *International Journal of Electrical and Computer Engineering (IJECE)*, vol. 2, no. 4, pp. 447–451, 2012.

[41] J. Arrillaga and N. R. Watson, *Power system harmonics*. Wiley. com, 2004. 69, 70

[42] L. Tongfu, K. Zhaomin, and F. Xiunan, *Numerical computational method*. Tsinghua University press, 2008. vi, 65

[43] W. CIGRE, "36-05:" harmonics, characteristic parameters, methods of study, estimates of existing values in the network," *Electra*, vol. 77, pp. 35–54, 1981. 70, 71

[44] Y. He and Z. Wen, *Power system analysis (1)*. Huazhong University of Science & Technology Press Co., Ltd, 2002. xi, 74

[45] A. H. El-Abiad, *Computer methods in power system analysis*. Tata McGraw-Hill Education, 2006. 105

Chapter 4

A Fast Hybrid Harmonic Power Flow Calculation Method

4.1 Introduction

Several harmonic penetration evaluation methods were described in Chapter 3. They have some shortcomings. They require long computing time especially for large power systems with many non-linear loads. The Jacobian matrix needs to be calculated in each iteration. It also leads to long computing time and makes the calculation process more complicated. The convergence problem with poor initial value at fundamental frequency is a vital issue. The initial value at fundamental frequency is usually randomly selected. If they are not close to the expected value. It leads to failure to converge. $1.0p.u.$ is generally considered to be initial value according to the result of experiment. However it still fails to converge especially in large power systems. In addition, previous approaches are just applied to small or medium power systems with single type of harmonic source and narrow harmonic frequency range (i.e. integer-harmonics). This chapter will introduce a new method to solve these problems.

The new method is called fast hybrid method (FHM). It is a frequency domain method. It is used to calculate steady state harmonic power flow in single phase balanced power systems with discrete frequencies. Harmonic couplings are not considered in this proposed method. Each harmonic injection current of harmonic source is

assumed to be known. The word "hybrid" represents the proposed method consists of three methods: the secant method, the Newton-Downhill method and the decoupled method.

The performance of this proposed method is illustrated by the block diagram shown in Figure 4.1.

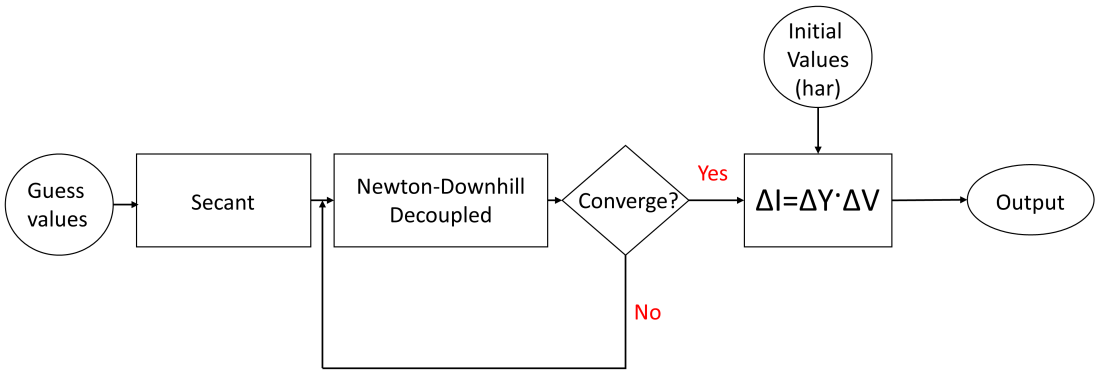

Figure 4.1: The performance block diagram of the proposed method

As shown in Figure 4.1, the inputs (two guess values) enter the secant method first in order to establish the initial values for the calculation at fundamental frequency. It combines the Newton-Downhill and the decoupled method together to calculate the power flow at fundamental frequency in order to reduce the calculation process and converge successfully. If it converges, it moves to the next step. The initial values at higher harmonic frequencies are included in the calculation. An admittance-matrix-base equation is used to calculate the harmonic penetration directly. The detail will be explained in the next several sections.

This chapter consists of five sections. The first section is the introduction. The second and third section indicates the principle of the secant method and the Newton-Downhill method respectively. Then the fourth section describes the fast hybrid method in detail. Finally, the last section is the conclusion.

4.2 Secant Method

The secant method is an iterative approach of solving non-linear equations. It uses a succession of roots of secant lines to better approximate a root of non-linear function f.

It assumes a non-linear equation $f(x) = 0$. $f(x)$ is continuous for interval $[a,b]$. Taking two initial guesses of this interval, x^{k-1} and x^k (where k represents the number of iteration.) that make $f(x^{k-1})f(x^k) < 0$, and drawing a straight line passing through $(x^{k-1}, f(x^{k-1}))$ and $(x^k, f(x^k))$, the intersection, x^{k+1}, between the straight line and the x-axis is regarded as an approximate solution for the non-linear equation $f(x) = 0$. However, if $f(x^{k-1})\ f(x^k) > 0$, the secant method may not achieve an approximate solution. The secant line can be formulated by:

$$y = f(x^k) + \frac{f(x^k) - f(x^{k-1})}{x^k - x^{k-1}}(x - x^k) \tag{4.1}$$

Let $y = 0$, then the horizontal ordinate at the intersection, x^{k+1}, is:

$$x^{k+1} = x^k - \frac{x^k - x^{k-1}}{f(x^k) - f(x^{k-1})} f(x^k), \qquad k = 1,2,\ldots. \tag{4.2}$$

where x^{k-1} and x^k are regarded as the two initial guesses and k represents the number of iteration.

The secant method can be explained geometrically as shown in Figure 4.2. $f(x)$ is a non-linear equation and it is continuous for interval $[a,b]$. x^* is the root of $f(x) = 0$. Assume x^{k-1} and x^k are two initial guesses of interval $[a,b]$. if $f(x^{k-1})f(x^k) < 0$, as shown in blue, one draws a straight line between $(x^{k-1}, f(x^{k-1}))$ and $(x^k, f(x^k))$, the intersection, x^{k+1}, is an approximate solution. However, if $f(x^{k-1})f(x^{k'}) > 0$, as shown in red, drawing a straight line passing through $(x^{k-1}, f(x^{k-1}))$ and $(x^{k'}, f(x^{k'}))$, there is no intersection between the straight line and x-axis. Hence, it has no solution.

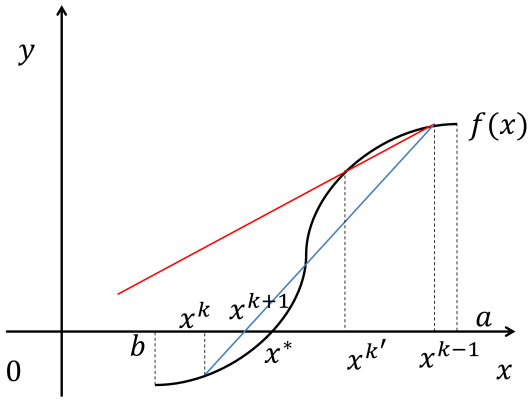

Figure 4.2: The geometrical expression of the secant method

4.3 Newton-Downhill Algorithm

Newton-Downhill algorithm is usually used in the optimization problem. It is well known that in order to make the Newton-Raphson method converge, the initial iterative value must be close to the expected value. However sometimes it is very difficult to choose the initial value to meet the convergence conditions. Hence the Newton-Downhill algorithm is provided to solve this problem with a large scale convergence [1].

The Newton-Downhill algorithm is developed based on the Newton-Raphson method. It introduces a downhill factor, λ, to make the iterative process monotonic decrease, that can be formulated by $\mid f(x^{k+1}) \mid < \mid f(x^k) \mid$ (where k represents the number of iteration.), in order to improve the convergence and decrease the iterations.

As mentioned in chapter 3, the principle of the Newton-Raphson iterative approach can be expressed mathematically as follow:

$$\bar{x}^{k+1} = x^k - \frac{f(x^k)}{f'(x^k)} \tag{4.3}$$

where $\bar{x}^{k+1}$ is the next iterative approximate solution and k represents the number of iteration.. The weighted average method is applied to equation 4.3. Then the Newton-

Raphson approach is revised to:

$$\begin{aligned} x^{k+1} &= \lambda \bar{x}^{k+1} + (1-\lambda)x^k \\ &= x^k - \lambda \frac{f(x^k)}{f'(x^k)} \end{aligned} \tag{4.4}$$

where λ is the downhill factor, and $0 < \lambda \leq 1$. Therefore, the equation 4.4 is defined as the mathematical expression of the Newton-Downhill algorithm [1, 2].

The downhill factor, λ, plays a very important role in the Newton-Downhill algorithm as it expands the convergence scale and decreases the iterations. Hence, it is important to consider its value during the calculation. Normally, let $\lambda = 1$ in the first iteration, then the iterative approximate value x^{k+1} is achieved according to 4.4. If $\mid f(x^{k+1}) \mid < \mid f(x^k) \mid$, it moves to next iteration. Otherwise, the downhill factor, λ, is halved and x^{k+1} is re-calculated until the monotonic decrease of iterative process is satisfied. Although the monotonic condition, $\mid f(x^{k+1}) \mid < \mid f(x^k) \mid$, may not meet at the beginning, as long as λ is small enough, it can be achieved.

4.4 The Fast Hybrid Harmonic Power Flow Calculation Method

The fast hybrid harmonic power flow calculation method (FHM) is an improved iterative approach to calculate harmonic power flow in a power system. It uses the admittance-matrix-based equation to calculate the harmonic power flow directly at higher frequencies ($h > 1$), which is similar to the decoupled method. However it makes improvements in the harmonic power flow evaluation at the fundamental frequency. It introduces the secant method to establish the iterative initial value in order to tackle the convergence problem caused by the poor initial value. It then combines the Newton-Downhill method and the decoupled harmonic power flow calculation approach to evaluate the harmonic penetration at fundamental frequency in power systems. It is proposed to make further efforts to solve the convergence problem and accelerate the calculation. The basic idea and procedure are described as follow.

4.4.1 Computation of Iterative Initial Value

The current balance for the fundamental frequency at each linear bus is indicated in Figure 4.3 below.

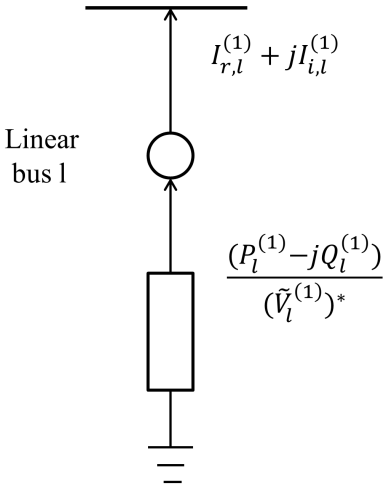

Figure 4.3: Current balance at a linear bus

$I_{r,l}^{(1)}$ and $I_{i,l}^{(1)}$ represent the fundamental real and imaginary line currents at the l^{th} linear bus. $P_l^{(1)}$ and $Q_l^{(1)}$ denote the fundamental real and reactive powers at the same bus. $\left(\tilde{V}_l^{(1)}\right)^*$ is the conjugate value of the fundamental bus voltage at bus l. The subscripts r, i and l represent the real and imaginary parts and the bus number. The superscript (1) of all symbols represents the fundamental frequency. The upper wave line of $\left(\tilde{V}_l^{(1)}\right)^*$ represents that it is a vector and the asterisk means conjugate value.

The fundamental current balance at each linear bus can be formulated as follow:

$$\begin{bmatrix} real(\frac{(P_l^{(1)}-jQ_l^{(1)})}{(\tilde{V}_l^{(1)})^*}) \\ imag(\frac{(P_l^{(1)}-jQ_l^{(1)})}{(\tilde{V}_l^{(1)})^*}) \\ \vdots \\ real(\frac{(P_n^{(1)}-jQ_n^{(1)})}{(\tilde{V}_n^{(1)})^*}) \\ imag(\frac{(P_n^{(1)}-jQ_n^{(1)})}{(\tilde{V}_n^{(1)})^*}) \end{bmatrix} = \begin{bmatrix} I_{r,l}^{(1)} \\ I_{i,l}^{(1)} \\ \vdots \\ I_{r,n}^{(1)} \\ I_{i,n}^{(1)} \end{bmatrix} \tag{4.5}$$

where $l \cdots n$ represent the linear buses. The fundamental current balance at each non-linear bus is described in equation 3.24 in chapter 3. Hence, the non-linear equation $f(x)$ in equation 4.2 can be expressed by

$$f(x) = \begin{cases} real\left(\dfrac{(P_x^{(1)} - jQ_x^{(1)})}{(\tilde{V}_x^{(1)})^*} - (I_{r,x}^{(1)} + jI_{i,x}^{(1)})\right) & \text{for linear bus} \\ real\left(-(g_{r,x}^{(1)} + jg_{i,x}^{(1)}) - (I_{r,x}^{(1)} + jI_{i,x}^{(1)})\right) & \text{for non-linear bus} \end{cases} \tag{4.6}$$

where subscript x of all symbols represents the bus number including both linear and non-linear buses.

According to a simulation experiment, the value of the fundamental bus voltage magnitude is usually between $0.5 p.u.$ and $1.5 p.u.$. Hence the root of the non-linear equation $f(x)$ in equation 4.2 is in the interval $[0.5, 1.5]$ and $f(x)$ is continuous for this interval. Therefore, let 0.5 and 1.5 be the initial guesses for the secant method. If $f(0.5)f(1.5) > 0$, make $0.5+0.1$ and $1.5-0.1$ and get two new further initial guesses 0.6 and 1.4. Then determine whether $f(0.6)f(1.4) < 0$. If not, the calculation of this increase-decrease by 0.1 repeats until achieving two values a' and b' that satisfy $f(a')f(b') < 0$. Then put these two values, a' and b', into equation 4.2 and the expected iterative initial value for the harmonic power flow calculation, $x_{expected}$, can be established by:

$$x_{expected} = b' - \frac{b'-a'}{f(b')-f(a')} f(b') \tag{4.7}$$

4.4.2 Computation of Harmonic Power Penetration

After introducing the Newton-Downhill method to the decoupled harmonic power flow calculation approach, the mathematical equation used to evaluate the fundamental power flow is revised as:

$$\begin{bmatrix} \Delta\overline{P}^{(1)} \\ \Delta\overline{Q}^{(1)} \end{bmatrix} = -\lambda \begin{bmatrix} \overline{H}^{(1)} & \overline{N}^{(1)} \\ \overline{K}^{(1)} & \overline{L}^{(1)} \end{bmatrix} \begin{bmatrix} \Delta\overline{\theta}^{(1)} \\ \Delta\overline{|\,V\,|}^{(1)} \end{bmatrix} \tag{4.8}$$

where θ, $|\,V\,|$, P and Q represent the voltage phase angle, voltage magnitude, active and reactive power respectively. $\overline{H}$, $\overline{N}$, $\overline{K}$ and $\overline{L}$ are the four sub-matrices of Jacobian matrix. λ represents the downhill factor. The superscript (1) of all symbols represents the fundamental frequency and the upper straight line means that it is a matrix.

As the initial values of fundamental bus voltages, $[V_1^{(1)}, V_2^{(1)}, \ldots, V_n^{(1)}]^T$, are considered by the secant method, the fundamental active and reactive power mismatches at each bus (except slack bus) can be calculated by:

$$\Delta P_i^{(1)} = P_i^{sp} - |\,V\,|_i^{(1)} \sum_{j=1}^{n} |\,V\,|_j^{(1)} \left(G_{(i,j)}^{(1)} \cos\theta_{(i,j)}^{(1)} + B_{(i,j)}^{(1)} \sin\theta_{(i,j)}^{(1)}\right) \tag{4.9}$$

$$\Delta Q_i^{(1)} = Q_i^{sp} - |\,V\,|_i^{(1)} \sum_{j=1}^{n} |\,V\,|_j^{(1)} \left(G_{(i,j)}^{(1)} \sin\theta_{(i,j)}^{(1)} - B_{(i,j)}^{(1)} \cos\theta_{(i,j)}^{(1)}\right) \tag{4.10}$$

where $G_{(i,j)}^{(1)}$ and $B_{(i,j)}^{(1)}$ represents the real and imaginary part of fundamental line admittance impedance between bus i and j respectively. $\theta_{(i,j)}^{(1)}$ represents the fundamental voltage phase angle mismatch between bus i and j.

Let $\lambda = 1$ in the beginning. The correction vectors $\Delta\overline{\theta}^{(1)}$ and $\Delta\overline{|\,V\,|}^{(1)}$ can be established by involving the calculated fundamental active and reactive power mismatches in equation 4.8. Then the modified fundamental bus voltages can be achieved. By putting these modified fundamental bus voltages into equations 4.9 and 4.10, the corresponding active and reactive power mismatches, $\Delta P_i^{(1)'}$ and $\Delta Q_i^{(1)'}$, are calculated. If $|\,\Delta\overline{W}^{(1)'}\,| > |\,\Delta\overline{W}^{(1)}\,|$ (where $\overline{W}^{(1)}$ represents the fundamental power mismatch vector, $[\Delta\overline{P}^{(1)}, \Delta\overline{Q}^{(1)}]^T$), the downhill factor λ is halved. The procedure above is repeated

until $|\Delta\overline{W}^{(1)'}| < |\Delta\overline{W}^{(1)}|$. After this, the final modified fundamental bus voltages are regarded as the initial values for the next iteration of fundamental power flow calculation. The iteration stops when the following condition is satisfied:

$$\max(|\Delta P_1^{(1)}, \Delta Q_1^{(1)}, \ldots, \Delta P_n^{(1)}, \Delta Q_n^{(1)}|) < \varepsilon \tag{4.11}$$

where ε is usually set to be 10^{-5}.

At higher frequencies, the harmonic power flow problem can be solved by using the admittance-matrix-based equation directly, which is the same as that in the decoupled harmonic power flow calculation approach:

$$\overline{I}^{(h)} = \overline{Y}^{(h)}\overline{V}^{(h)} \tag{4.12}$$

Hence, the flow chart of the fast hybrid harmonic power flow calculation approach is shown on the next page.

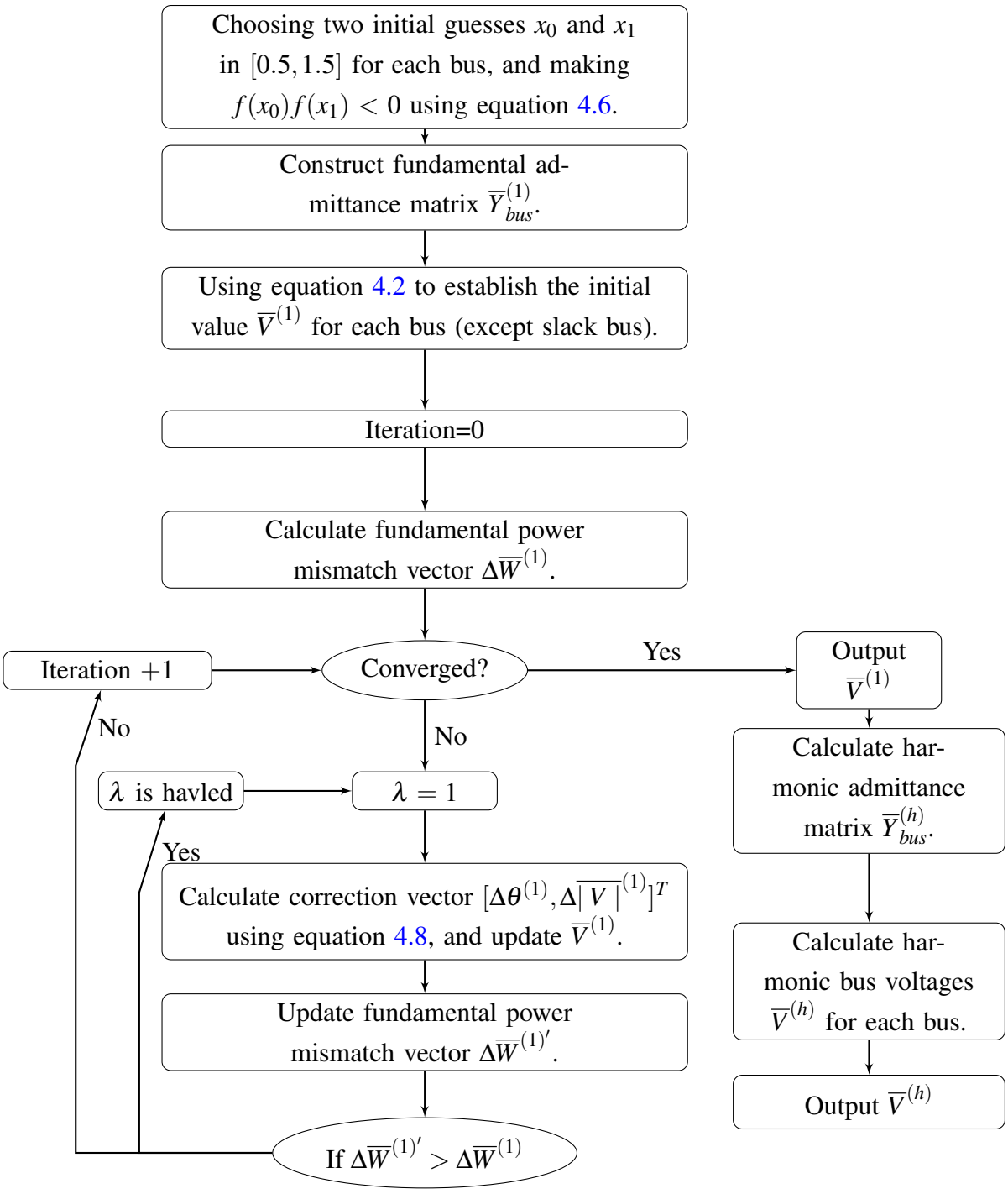
Choosing two initial guesses x_0 and x_1 in $[0.5, 1.5]$ for each bus, and making $f(x_0)f(x_1) < 0$ using equation 4.6.
Construct fundamental admittance matrix $\overline{Y}_{bus}^{(1)}$.
Using equation 4.2 to establish the initial value $\overline{V}^{(1)}$ for each bus (except slack bus).
Iteration=0
Calculate fundamental power mismatch vector $\Delta\overline{W}^{(1)}$.
Converged?
Yes
No
Iteration +1
No
λ is havled
$\lambda = 1$
Yes
Calculate correction vector $[\Delta\theta^{(1)}, \Delta|\overline{V}|^{(1)}]^T$ using equation 4.8, and update $\overline{V}^{(1)}$.
Update fundamental power mismatch vector $\Delta\overline{W}^{(1)'}$.
If $\Delta\overline{W}^{(1)'} > \Delta\overline{W}^{(1)}$
Output $\overline{V}^{(1)}$
Calculate harmonic admittance matrix $\overline{Y}_{bus}^{(h)}$.
Calculate harmonic bus voltages $\overline{V}^{(h)}$ for each bus.
Output $\overline{V}^{(h)}$

4.5 Conclusion

This chapter introduced a fast hybrid harmonic power flow calculation method. Two calculation steps were indicated. One is the calculation at fundamental frequency. The other is the calculation at harmonic frequencies. In the first calculation step, the author used the secant method to establish the iterative initial values. It could make the calculation converge successfully. It then combined the Newton-Downhill and the decoupled method to simplify and accelerate the calculation. In the second calculation step, the admittance-matrix-base equation was used to calculate the harmonic penetration.

This proposed method will be applied in several power systems with single type of harmonic source in the next chapter. The results will be discussed and compared with those generated by traditional methods to investigate whether the proposed method can solve the convergence problem and be fast and accurate.

References

[1] H. Yang, F. Wen, L. Wang, and S. Singh, "Newton-downhill algorithm for distribution power flow analysis," in *Power and Energy Conference, 2008. PECon 2008. IEEE 2nd International*. IEEE, 2008, pp. 1628–1632. 120, 121

[2] L. Tongfu, K. Zhaomin, and F. Xiunan, *Numerical computational method*. Tsinghua University press, 2008. 121

Chapter 5

Harmonic Power Flow Evaluation in Power Systems

5.1 Introduction

Chapter 4 proposed a fast hybrid method (FHM) to calculate static harmonic power flow in power systems. It combined the secant method, the Newton-Downhill method and the decoupled method to solve the convergence problem, reduce the number of iterations and accelerate the computing time. In this chapter, the proposed method is applied to 14-bus, 39-bus, 57-bus and 118-bus power systems respectively. The results of computing time, the number of iterations, the fundamental and the higher harmonic bus voltage magnitudes and the total harmonic voltage distortion are calculated. It also establishes the total active and reactive powers at the sending end, the total active and reactive powers at the receiving end and the total power losses on each branch respectively. Then, these results are compared to those achieved by the Newton-Raphson based method and the decoupled method to investigate whether the proposed method can solve the convergence problem and accomplish the calculation quickly and accurately. The computer which is used for the calculation has an i7 quad-core CPU with 3.4 GHz and a 12G RAM. The operation system is windows 8.

This chapter consists of seven sections. The first section is the introduction. The second section introduces the harmonic source and iterative initial value. The next four

sections are case studies with 14-bus, 39-bus, 57-bus and 118-bus power systems. Each case study includes three sub-sections. Firstly, it introduces the power system with its diagram. Then, it shows and discusses the simulation results. Finally, it compares the results with those obtained by the other two methods. The final section is the result discussion and summary.

5.2 Harmonic Source And Initial Value

5.2.1 Harmonic Source

Twelve-pulse and twenty-four-pulse converters are frequently specified by consulting engineers for heating, ventilating and air conditioning applications because of their theoretical ability to reduce harmonic current distortion [1–3]. Two six-pulse line-commutated converters are regarded as harmonic sources in this chapter. The six-pulse converter is a basic polyphase converter. It is mostly widely use converter in household products. It generates more harmonic injection currents than the twelve and twenty-four pulse converters. Hence, the harmonic penetration could be significant. These two six-pulse converters are represented as six-pulse one and six-pulse two respectively. The six-pulse one is the same converter as used in chapter 3 and its harmonic injection current is shown in Table 3.6. The harmonic injection current for each harmonic level (including the fundamental frequency) of the six-pulse two is illustrated in Table 5.1 below. The highest harmonic order of this converter is also assumed as the 29^{th}.

Table 5.1: Harmonic currents generated by the six-pulse two [4]

Harmonic order'h'	**Magnitude (p.u.)**	**Angle degree**	**Harmonic order'h'**	**Magnitude (p.u.)**	**Angle degree**
1	1	0	17	0.0033	0
5	0.0191	0	19	0.0024	0
7	0.0131	0	23	0.0012	0
11	0.0072	0	25	0.0008	0
13	0.0056	0	29	0.0002	0

5.2.2 Initial Values

The fundamental voltage magnitude and phase angle of the slack bus is known and is kept constant during the iterative calculation. The fundamental voltage magnitudes of the PV buses are specified. Hence it only assumes that the initial values of the fundamental voltage phase angles of these buses are 0.0 degrees.

$0.5\angle 0.0$ and $1.5\angle 0.0$ in the interval $[0.5, 1.5]$ are chosen to calculate the fundamental initial voltages of the PQ and PS buses by the proposed method. For the Newton-Raphson and the decoupled methods, the initial fundamental voltage magnitudes for both PQ and PS bus are assumed to be $0.5p.u.$, $0.6p.u.$, $0.7p.u.$, $0.8p.u.$, $0.9p.u.$, $1.0p.u.$ and $1.5p.u.$ respectively. It is used to investigate the effects of initial values to the convergence situation. Also, the initial fundamental voltage phase angles for these buses are set to 0.0 degree.

It is necessary to consider the initial voltage magnitude for all higher harmonics in the Newton-Raphson method. It is assumed that the initial value of each higher harmonic order is reduced by $0.01p.u.$ than the previous one when the fundamental one is assumed $1.0p.u.$. The details are shown in Table 5.2 below. Also, the voltage phase angles for all higher harmonics are set to 0.0 degree.

Table 5.2: Initial voltage magnitudes for all harmonics

Harmonic order'h'	$\mid V \mid$ (p.u.)	Harmonic order'h'	$\mid V \mid$ (p.u.)	Harmonic order'h'	$\mid V \mid$ (p.u.)
2	0.09	11	0.009	22	0.0007
3	0.08	13	0.007	23	0.0006
4	0.07	14	0.006	25	0.0004
5	0.06	15	0.005	26	0.0003
7	0.04	16	0.004	28	0.0001
8	0.03	17	0.003	29	0.00009
9	0.02	19	0.001		
10	0.01	20	0.0009		

5.3 Case One: In A 14-bus Power System

5.3.1 Power System Diagram

The diagram of an IEEE 14-bus power system is illustrated in Figure 5.1.

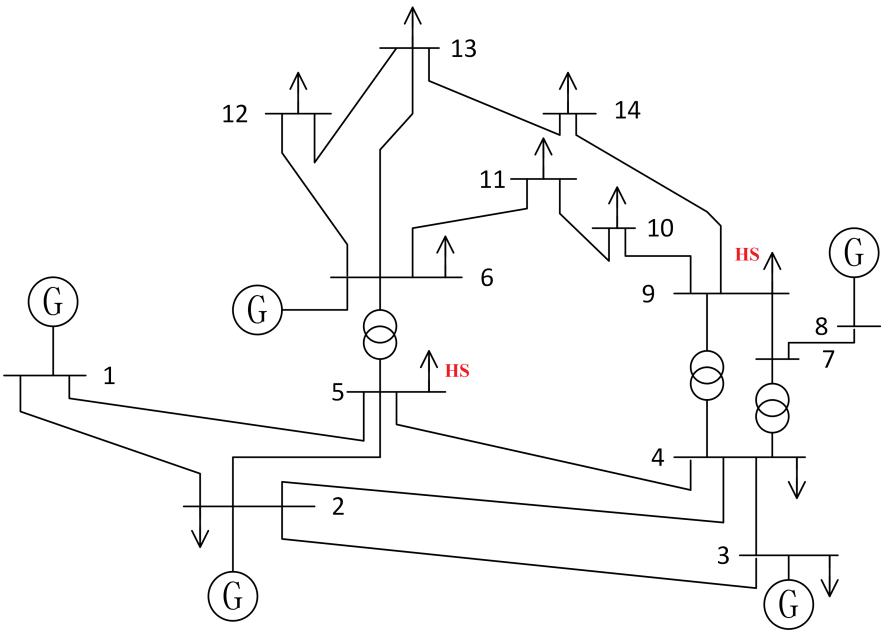

Figure 5.1: The diagram of an IEEE 14-bus power system

As shown in the figure, it has three transformers connected between bus five and bus six, bus four and bus nine and bus four and bus seven. There are five generators located at bus one, bus two, bus three, bus six and bus eight. Bus one is the slack bus. The power system details are described in Appendix D. The bus data is shown in Table D.1. The line and transformer data is shown in Table D.2. Two six-pulse line-commutated converters are connected to bus five and bus nine that are represented by red capital character 'HS'.

5.3.2 Results And Discussion

The fast hybrid method (FHM) takes 0.0313 seconds and 4 iterations to accomplish the harmonic power flow calculation.

The results of the fundamental and the higher harmonic bus voltage magnitudes are shown in Table 5.3 and they are illustrated in Figure 5.2 and 5.3 respectively.

Table 5.3: The fundamental and the higher harmonic bus voltage magnitudes in per unit in a 14-bus power system

Order / Bus	1st	5th	7th	11th	13th
1	1.06	0.0006	0.0004	0.0004	2.14E-05
2	1.045	0.0009	0.0008	0.0014	0.0003
3	1.01	0.0015	0.0025	0.0002	1.21E-05
4	1.0247	0.0024	0.0014	0.0003	0.0003
5	1.0277	0.0033	0.0022	0.0011	0.0009
6	1.07	0.0001	0.0002	0.0001	4.9E-07
7	1.0744	0.0025	0.0014	0.0002	0.0003
8	1.09	0.0008	0.0005	7.73E-05	9.13E-05
9	1.0800	0.0037	0.0020	0.0006	0.0004
10	1.0709	0.0038	0.0027	0.0137	0.0008
11	1.0671	0.0021	0.0017	0.0112	0.0008
12	1.0570	0.0009	0.0060	0.0001	3.34E-05
13	1.0539	0.0015	0.0089	0.0001	2.69E-05
14	1.0509	0.0042	0.0135	0.0006	0.0002
Order / Bus	17th	19th	23rd	25th	29th
1	4.6E-05	4.86E-05	5.08E-05	5.54E-05	8.33E-05
2	5.75E-05	3.43E-05	1.5E-05	1.11E-05	7.53E-06
3	7.63E-06	4.65E-06	1.74E-06	1.12E-06	4.73E-07
4	0.0002	0.0001	6.94E-05	5.36E-05	3.2E-05
5	0.0006	0.0005	0.0004	0.0003	0.0002
6	2.68E-06	2.38E-05	3.64E-06	3.17E-06	2.53E-06

Continued on next page

Table 5.3- *Continued from previous page*

7	0.0001	0.0001	4.7E-05	3.2E-05	1.27E-05
8	4.88E-05	3.71E-05	1.56E-05	1.06E-05	4.2E-06
9	0.0002	0.0001	5.4E-05	3.35E-05	7.4E-06
10	6.29E-05	0.0006	1.95E-05	9E-06	1.28E-06
11	0.0003	0.0026	1.38E-05	3.97E-06	6.1E-07
12	1.58E-05	8.05E-05	2.19E-06	1.29E-06	6.07E-07
13	1.08E-06	5.03E-06	1.88E-07	1.7E-07	1.35E-07
14	3.65E-05	2.1E-05	4.83E-06	2.47E-06	3.9E-07

where the column represents the bus number and the row represents the harmonic order.

The results of the fundamental bus voltage magnitudes are shown in Figure 5.2 below.

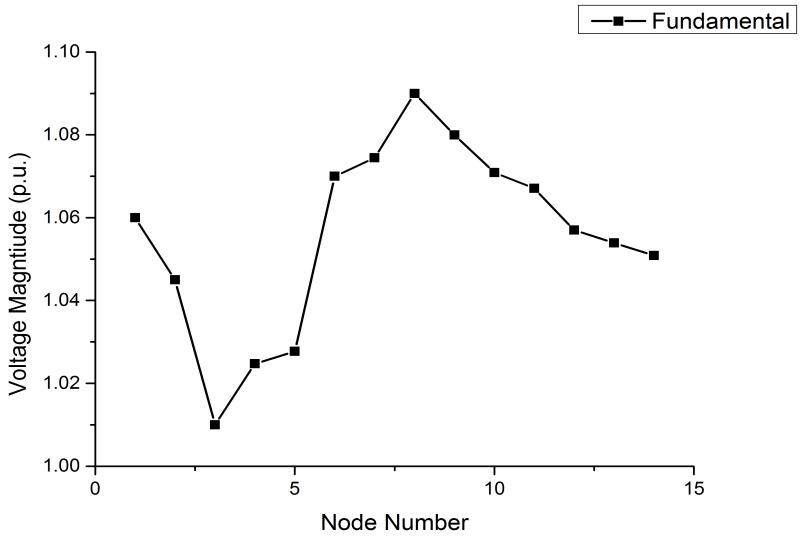

Figure 5.2: The fundamental bus voltage magnitude

The values of the fundamental bus voltage magnitudes fluctuate between $1.01 p.u.$ and $1.09 p.u.$ according to the figure. The minimum value is $1.01 p.u.$ at bus three, and

the maximum value, $1.09p.u.$, occurs at bus eight. They are highlighted in yellow and pink colour respectively in Table 5.3.

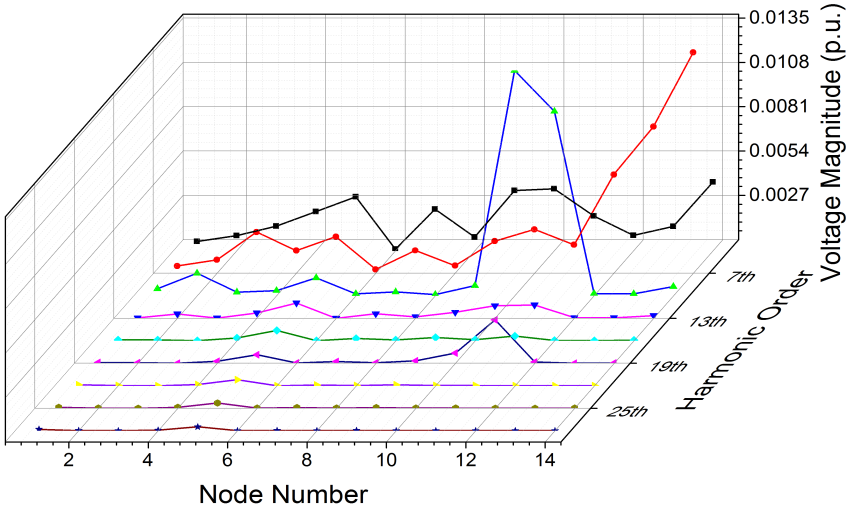

Figure 5.3: The harmonic bus voltage magnitude

The values of the higher harmonic voltage magnitudes are illustrated in a three-dimension diagram in order to investigate and compare the varying curve of each harmonic order. The harmonic order goes up from inside to outside of the depth coordinate as shown in Figure 5.3. The results of the first three higher harmonic orders, 5^{th}, 7^{th} and 11^{th}, are changed significantly on different buses. However the results of the other harmonic orders are too small to be identified in the diagram, except the value on bus 11 of the 19^{th} harmonic. The minimum and maximum value of each higher harmonic order is also highlighted in yellow and pink respectively in Table 5.3. The maximum bus voltage magnitude of the whole higher harmonic orders is $0.0137p.u.$, that occurs on bus 10 in the 11^{th} harmonic order. It is far less than the minimum fundamental voltage magnitude, $1.01p.u.$.

The result of the total harmonic voltage distortion (THDv) in percentage is shown in Table 5.4 and it is illustrated in Figure 5.4 below.

Table 5.4: The total harmonic voltage distortion (THDv)

Bus	1	2	3	4	5	6	7
Percent	0.08	0.18	0.29	0.27	0.42	0.03	0.27
Bus	8	9	10	11	12	13	14
Percent	0.09	0.39	1.36	1.11	0.58	0.86	1.34

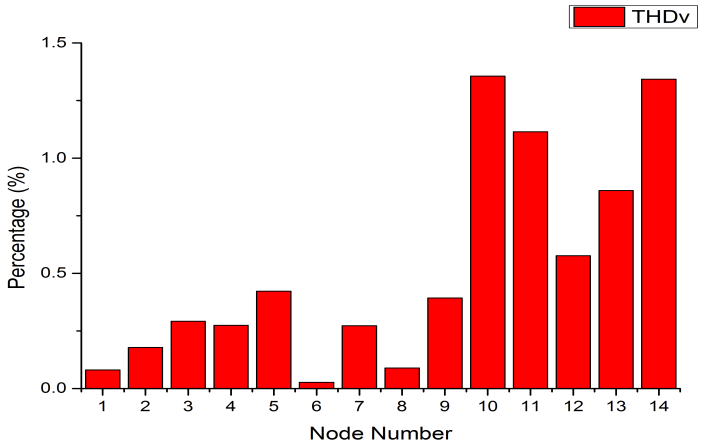

Figure 5.4: The total harmonic voltage distortion

The maximum value of the THDv is 1.36% that is highlighted in pink colour in Table 5.4. It is below the limit level of 3%, in Engineering Recommendation G5/4.

The results of the total active and reactive powers at both sending and receiving ends (Ptotals, Qtotals, Ptotalr and Qtotalr) and the total power losses on each branch (Ptotalloss) are shown in Table 5.5 and they are illustrated in Figures 5.5 to 5.7.

Table 5.5: The results of the total power flows

	Sending End		Receiving End		Total Power Losses
Line No.	P (p.u.)	Q (p.u.)	P (p.u.)	Q (p.u.)	Ptotalloss (p.u.)
1	1.5648	-0.2031	1.5220	-0.2751	0.0428
2	0.7589	0.0002	0.7312	-0.0607	0.0277

Continued on next page

Table 5.5- *Continued from previous page*

3	0.7291	0.0359	0.7061	-0.0148	0.0230
4	0.5626	-0.0566	0.5457	-0.0715	0.0169
5	0.4134	-0.0362	0.4044	-0.0263	0.0089
6	-0.2359	0.0036	-0.2396	0.0075	0.0037
7	-0.6304	0.1365	-0.6357	0.1198	0.0053
8	-0.2910	0.1448	-0.2910	0.1257	0.0000
9	-0.1675	0.0504	-0.1675	0.0358	0.0000
10	-0.4239	-0.1196	-0.4239	-0.1623	0.0000
11	0.0647	-0.0148	0.0644	-0.0157	0.0004
12	0.0752	0.0187	0.0746	0.0173	0.0006
13	0.1719	0.0460	0.1701	0.0423	0.0018
14	0.0000	-0.0949	0.0000	-0.0962	0.0000
15	0.2910	-0.0500	0.2910	-0.0583	0.0000
16	0.0611	0.0928	0.0608	0.0917	0.0003
17	0.1024	0.0686	0.1007	0.0650	0.0017
18	-0.0292	0.0340	-0.0294	0.0336	0.0001
19	0.0136	0.0013	0.0136	0.0013	0.0000
20	0.0487	-0.0143	0.0483	-0.0151	0.0004

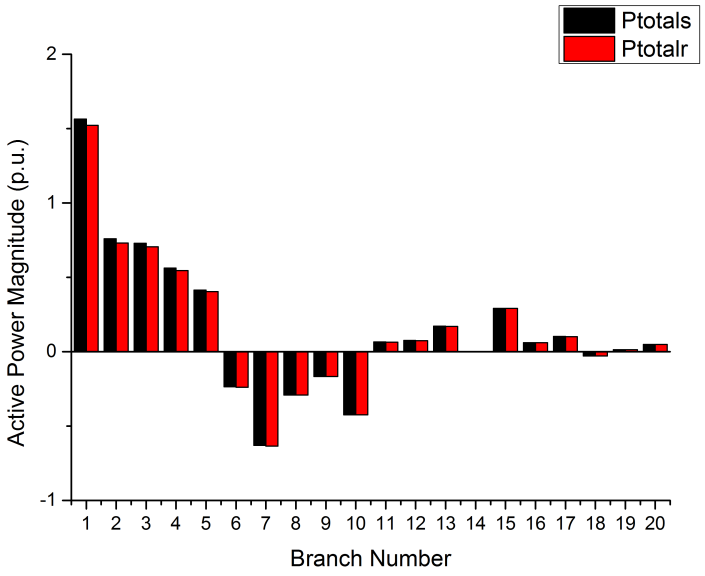

Figure 5.5: The total active powers at both sending and receiving ends

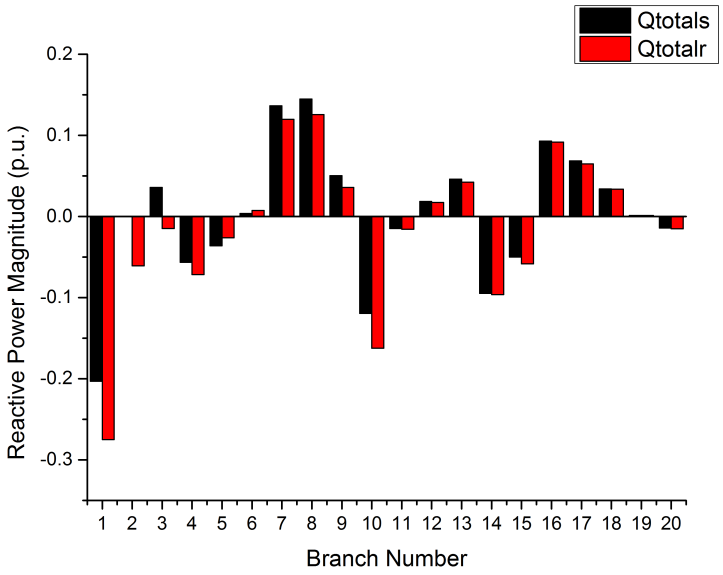

Figure 5.6: The total reactive powers at both sending and receiving ends

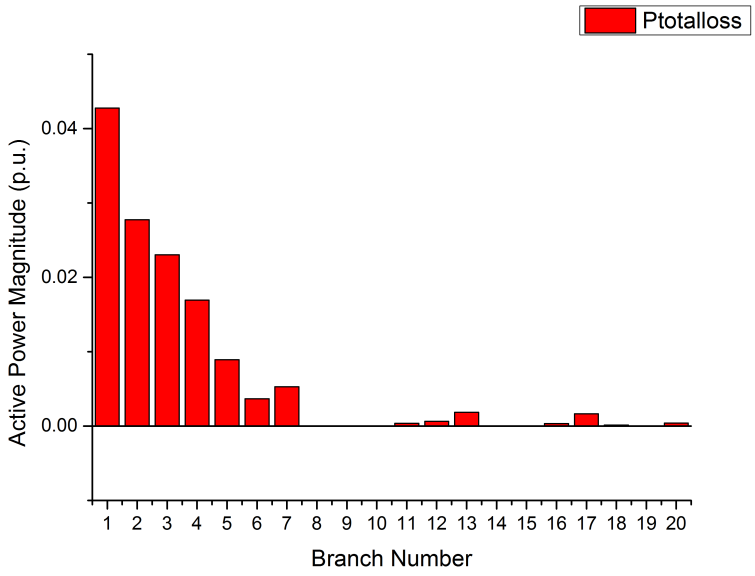

Figure 5.7: The total active power losses

The black and red rectangular column represents the powers at sending and receiving end respectively in Figures 5.5 and 5.6. They are both illustrated in one diagram in order to compare the results at different ends. As shown in Figure 5.5, if the values (both of two different columns) are positive, it denotes that the active powers flow from the sending ends to the receiving ends; otherwise, the active powers flow in the opposite way. In Figure 5.6, if the results are positive, it means that the buses (sending and receiving ends) generate reactive powers; otherwise, they absorb reactive powers. Hence the total active and reactive power flows in the power system can be investigated. Figure 5.7 represents the total power losses on each branch. It denotes that more power losses are produced on the first seven branches. However, the maximum value is only $0.0428 p.u.$. The sending and the receiving ends buses are denoted in Table D.2 in Appendix D. The total active and reactive powers at both sending and receiving ends and the total power losses are the sum of values in all harmonic orders respectively. The calculations of the h^{th} harmonic active and reactive power flow are denoted in Appendix C.

5.3.3 Results Comparison

The computing time, the number of iterations and the convergence conditions calculated with different initial values are described in Table 5.6. In the columns of convergence conditions, 'Yes' represents that it can converge, while 'No' indicates the convergence has failed. It is assumed if the calculation is not finished when the iterations exceed 3000, then it is regarded as not converged. NRM, DM and FHM represent the Newton-Raphson based, the decoupled and the fast hybrid harmonic power flow calculation methods. The computing time and the number of iterations are counted separately during the calculation, as there is no necessary relationship between them.

Table 5.6: Computing time, iterations and convergence conditions comparison

Initial Values (p.u.)	**Computing Time (s)**			**Iterations**			**Convergence Conditions**		
	NRM	**DM**	**FHM**	**NRM**	**DM**	**FHM**	**NRM**	**DM**	**FHM**
1.5	2.6963	0.0229	0.0313	10	4	4	Yes	Yes	Yes
1	0.3919	0.0782	0.0313	10	3	4	Yes	Yes	Yes
0.9	0.3105	0.0267	0.0313	11	3	4	Yes	Yes	Yes
0.8	0.2633	0.0233	0.0313	10	4	4	Yes	Yes	Yes
0.7	0.2553	0.0254	0.0313	10	5	4	Yes	Yes	Yes
0.6	0.3496	0.0315	0.0313	15	15	4	Yes	Yes	Yes
0.5			0.0313			4	No	No	Yes

These show that all the three different harmonic power flow calculation methods converge when the initial bus voltage magnitudes are assumed to be 0.6, 0.7, 0.8, 0.9, 1.0 and $1.5p.u.$ respectively. The NRM and the DM generate different computing time and number of iterations with different initial values. However the results of the computing time and the number of iterations obtained by the FHM are consistent, which indicates that the calculation proceeding of the FHM is not affected by the selection of initial value. The NRM takes more computing time and number of iterations to accomplish the calculation than the other two methods. Especially when the initial value is $1.5p.u.$, the computing time of the NRM is 2.6963 seconds that is one hundred times the other two. When the initial value is set to be $1.5p.u.$, $0.9p.u.$, $0.8p.u.$ and $0.7p.u.$, the DM accomplishes the calculation faster than the FHM. However, the FHM shows its advantage when the initial values are $0.6p.u.$ and $0.5p.u.$ respectively. Only

the FHM is able to converge to a solution when the initial value is $0.5p.u.$. Though it seems that the DM is faster than the FHM when the initial value is between $0.7p.u.$ and $1.5p.u.$, the difference is very small which is in the order of 10^{-4}. Hence the FHM is a better choice, as it makes the calculation converge with any initial voltage magnitude and has nearly the same calculation speed as the DM.

As mentioned in the beginning of this chapter, the author intends to compare the results generated by three different methods to investigate the calculation accuracy of the proposed method. Hence the result differences between each method are illustrated and are represented by "ERROR" in the charts of results. The result achieved by the NRM are regarded as the reference value because of its well-known accuracy. Moreover, it is implemented in MATLAB tool package which can be used directly. As a result, the values of ERROR_1 represent the result differences between the DM and the NRM. ERROR_2 represents the result differences between the FHM and the NRM.

The result differences of the fundamental bus voltage magnitudes between each method are illustrated in Figure 5.8 below.

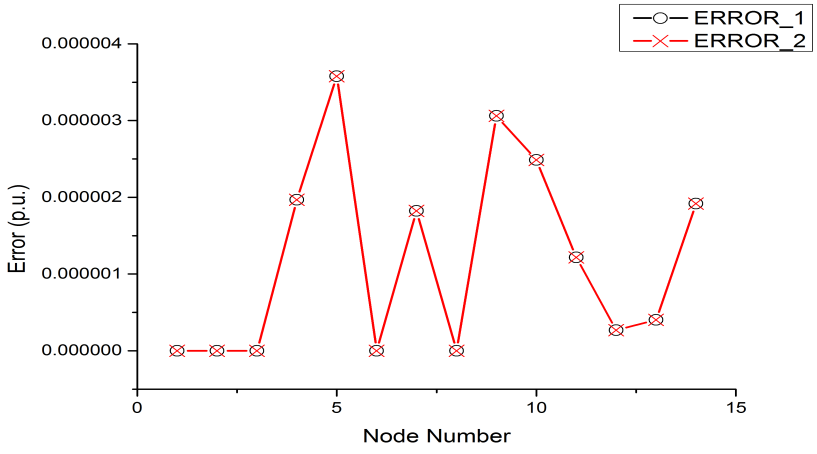

Figure 5.8: The result differences of the fundamental voltage magnitude

The values of ERROR_1 and ERROR_2 are represented by black circles and red crosses respectively in the diagram. It shows that the curves of the ERROR_1 and the ERROR_2 coincide with each other. Hence, the fundamental voltage magnitudes

generated by the FHM are the same as those achieved by the DM. The FHM has the same calculation accuracy of the fundamental voltage magnitudes as the NRM, for the maximum error between these two methods is only $3.58e^{-6}$ that can be ignored.

As mentioned in previous chapter, the FHM calculates higher harmonic voltage magnitudes by the admittance-matrix-based equation directly, which is the same as the DM. Hence, if the results of the fundamental voltage magnitudes generated by these two methods are equal, the higher harmonic voltage magnitudes are also equal.

The result differences of the total harmonic voltage distortion, the total active and reactive powers at both sending and receiving ends and the total power losses on each branch between three different methods are illustrated in the same way as the fundamental voltage magnitudes, and they are shown in Figures F.1 to F.4 in Appendix F. The maximum difference of each result category is summarized in Table 5.7 below.

Table 5.7: The maximum difference of each result category

	THDv	**Ptotals**	**Ptotalr**	**Qtotals**
ERROR_1	$0.0012p.u.$	$-6.75e^{-5}p.u.$	$-5.88e^{-5}p.u.$	$-9.81e^{-5}p.u.$
ERROR_2	$0.0012p.u.$	$-6.75e^{-5}p.u.$	$-5.88e^{-5}p.u.$	$-9.81e^{-5}p.u.$
	Qtotalr	**Ptotalloss**		
ERROR_1	$0.0001p.u.$	$-8.72e^{-6}p.u.$		
ERROR_2	$0.0001p.u.$	$-8.72e^{-6}p.u.$		

where the THDv, Ptotals, Ptotalr, Qtotals, Qtotalr and Ptotalloss represent the total harmonic voltage distortion, the active powers at both sending and receiving ends, the reactive powers at both sending and receiving ends and the total power losses on each branch respectively. The positive value represents the result achieved by the DM or FHM is larger than the reference value, while the negative value represents it less than the base value.

The figures F.1 to F.4 show that the values of ERROR_1 and ERROR_2 also coincide with each other. It means that the FHM generates the same results as the DM. As shown in Table 5.7, the maximum differences of Ptotals, Ptotalr, Qtotals and Ptotalloss are in the order of 10^{-6} and 10^{-7}, which are so small that they can be ignored. Though the THDv and the Qtotalr have the differences in the order of 10^{-4} and 10^{-5}, they are

still acceptable. Hence, the FHM has the same result accuracy with the NRM on these result categories.

5.4 Case Two: In A 39-bus Power System

5.4.1 Power System Diagram

The diagram of the New England 39-bus power system is illustrated in Figure 5.9.

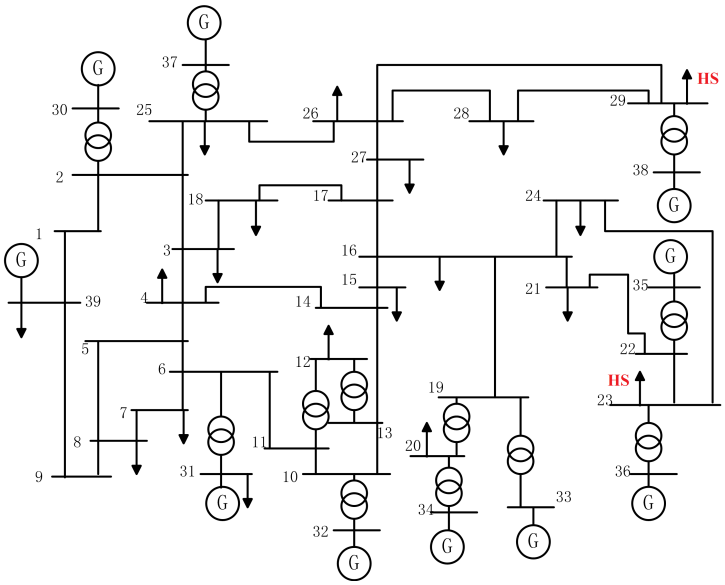

Figure 5.9: The diagram of the New England 39-bus power system

It shows that there are twelve transformers connected between bus 30 and bus 2, bus 37 and bus 25, bus 6 and bus 31, bus 11 and bus 12, bus 12 and bus 13, bus 32 and bus 10, bus 34 and bus 20, bus 20 and bus 19, bus 33 and bus 19, bus 36 and bus 23, bus 22 and bus 35 and bus 38 and bus 29. Ten generators are located at bus 30, bus 39, bus 37, bus 38, bus 35, bus 36, bus 33, bus 34, bus 32 and bus 31 respectively. Bus 31 is regarded as the reference bus. The power system details are described in Appendix D. The bus data is shown in Table D.3. The line and transformer data is shown in Table D.4. Two six-pulse line-commutated converters are connected to bus 23 and bus 29 that are represented by red capital character 'HS'.

5.4.2 Results And Discussion

The FHM takes 0.069 seconds and 4 iterations to accomplish the harmonic power flow calculation with the New England 39-bus power system.

The resutls of the fundamental and the higher harmonic bus voltage magnitudes are not necessary to be shown in the table, for it is in the same way as Table 5.3 in previous section. The results are illustrated in Figures 5.10 and 5.11 directly. However, the maximum and minimum values of each harmonic order (including the fundamental frequency) for all buses are denoted in Table 5.8.

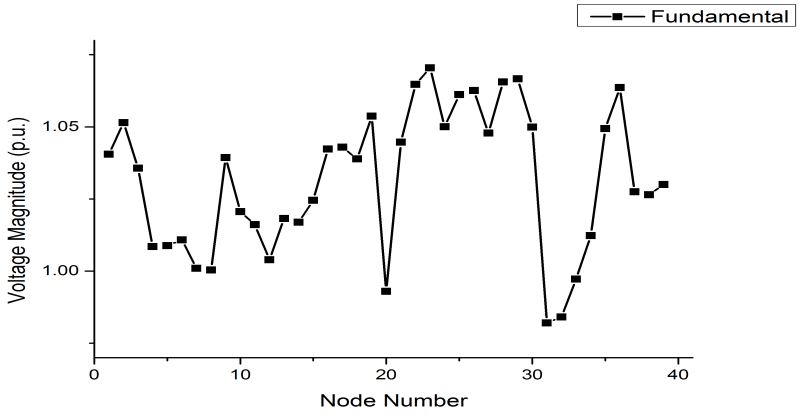

Figure 5.10: The fundamental bus voltage magnitude

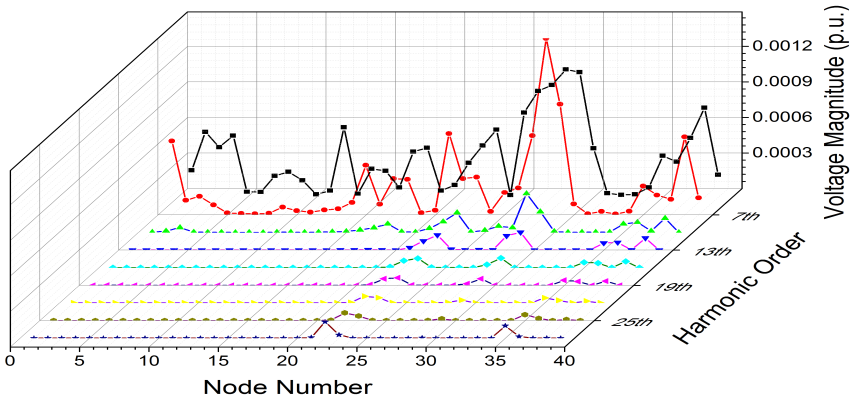

Figure 5.11: The harmonic bus voltage magnitude

Table 5.8: The maximum and minimum values of the fundamental and the higher harmonic voltage magnitudes in a 39-bus power system

	Max		Min	
Order	Bus	Mag. (p.u.)	Bus	Mag. (p.u.)
1st	23	1.0704	31	0.982
5th	28	0.0011	24	1.87E-05
7th	28	0.0015	33	7.06E-06
11th	28	0.0003	9	1.55E-07
13th	29	0.0002	39	1.36E-09
17th	29	8.13E-05	9	2.17E-10
19th	23	6.43E-05	8	6.79E-11
23rd	22	5.62E-05	9	2.44E-12
25th	22	6.54E-05	9	3.77E-12
29th	22	0.0001	29	2.69E-12

The fundamental bus voltage irregularly fluctuates between $0.982p.u.$ and $1.0704p.u.$ as shown in Figure 5.10. The maximum value, $1.0704p.u.$, occurs on bus 23, while the minimum value, $0.982p.u.$, is on bus 31, which is indicated in Table 5.8. The values of the higher harmonic voltage magnitudes are also illustrated in a three-dimension diagram as shown in Figure 5.11 in order to investigate and compare the varying curve of each harmonic order. It shows that the bus voltages of the 5^{th} and 7^{th} harmonic orders are changed significantly. The variation then reduces with increasing of harmonic order. However, the bus voltage magnitudes on bus 22 and bus 35 are still visible at the 29^{th} harmonic order. The maximum bus voltage magnitude of the whole higher harmonic orders is $0.0015p.u.$, that occurs on bus 28 at the 7^{th} harmonic order and is highlighted in pink colour in Table 5.8. It is far less than the minimum fundamental voltage magnitude, $0.982p.u.$.

The result of the total harmonic voltage distortion (THDv) is shown in Table 5.9 and it is illustrated in Figure 5.12 below.

Table 5.9: The total harmonic voltage distortion (THDv)

Bus	1	2	3	4	5	6	7	8
Percent	0.06	0.05	0.04	0.05	0.00	0.00	0.02	0.02
Bus	9	10	11	12	13	14	15	16
Percent	0.02	0.00	0.01	0.06	0.01	0.03	0.05	0.01
Bus	17	18	19	20	21	22	23	24
Percent	0.05	0.05	0.01	0.01	0.07	0.05	0.07	0.00
Bus	25	26	27	28	29	30	31	32
Percent	0.07	0.09	0.11	0.18	0.13	0.04	0.00	0.00
Bus	33	34	35	36	37	38	39	
Percent	0.00	0.01	0.04	0.03	0.05	0.10	0.02	

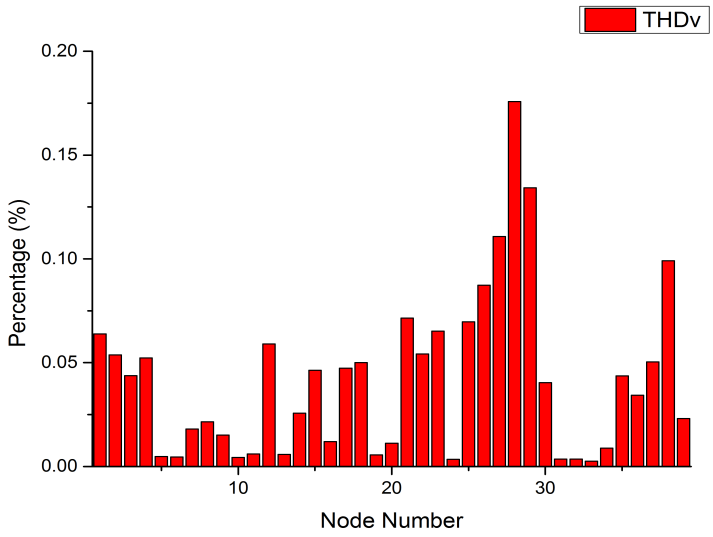

Figure 5.12: The total harmonic voltage distortion

The results in Table 5.9 are approximate values, which are kept three significant figures. Hence, even the value of table is 0.00%, e.g. the THDv value on the bus 5, it may not equal zero and can be illustrated in diagram. The maximum value of the THDv is 0.18% that is highlighted in pink colour in Table 5.9. It is below the limit level of 3%, in Engineering Recommendation G5/4.

The results of the total active and reactive powers at both sending and receiving ends (Ptotals, Qtotals, Ptotalr and Qtotalr) and the total power losses on each branch (Ptotalloss) can be shown in the same way as Table 5.5 in the previous section. Hence, they are illustrated in Figures 5.13 to 5.15 directly.

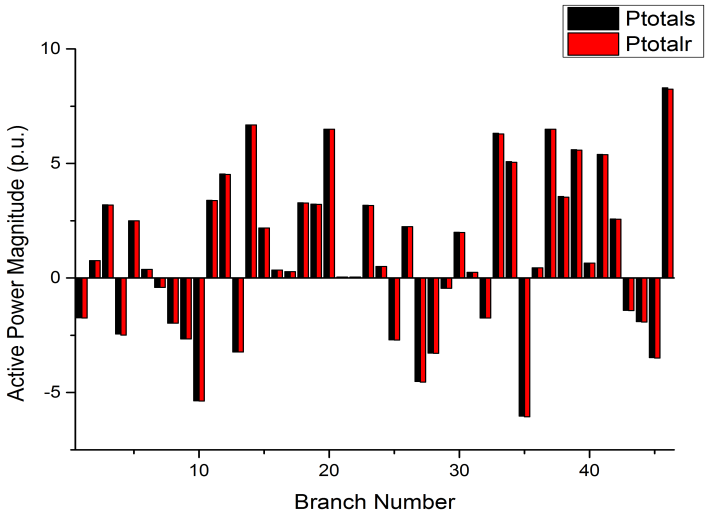

Figure 5.13: The total active powers at both sending and receiving ends

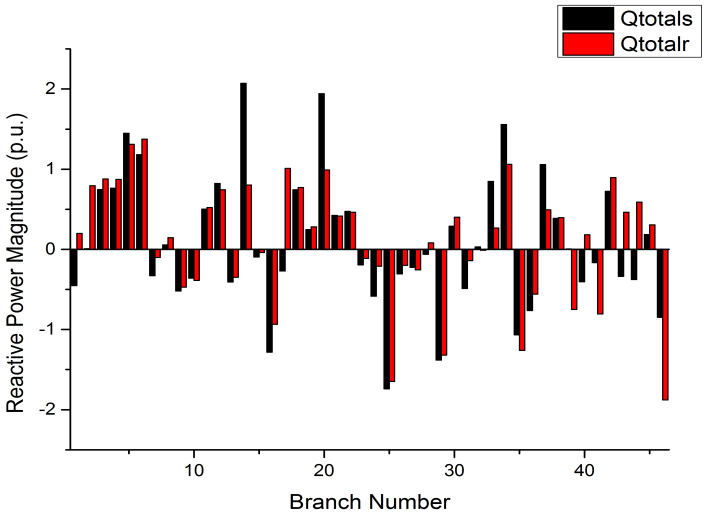

Figure 5.14: The total reactive powers at both sending and receiving ends

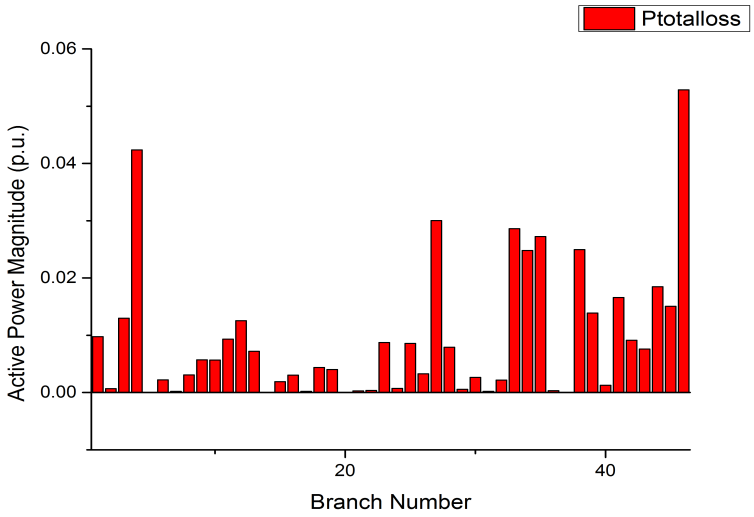

Figure 5.15: The total active power losses

As mentioned in the previous section, in Figure 5.13, if the values (both of two different columns) are positive, it denotes that the active powers flow from the sending ends to the receiving ends; otherwise, the active powers flow in the opposite way. In Figure 5.14, if the results are positive, it means that the buses (sending and receiving ends) generate reactive powers; otherwise, they absorb reactive powers. Hence the total active and reactive power flows in the power system can be investigated. The maximum power loss is $0.0528 p.u.$ that is on the 46^{th} branch.

5.4.3 Results Comparison

The computing time, the number of iterations and the convergence conditions calculated with different initial values are illustrated in Table 5.10 below. As mentioned in the previous section, the NRM, the DM and the FHM represent the Newton-Raphson based, the decoupled and the fast hybrid method respectively. 'Yes' and 'No' in convergence conditions category represent it converged and non-converged respectively. The computing time and the number of iterations are counted separately during the calculation.

Table 5.10: Computing time, iterations and convergence conditions comparison

Initial Values (p.u.)	Computing Time (s)			Iterations			Convergence Conditions		
	NRM	DM	FHM	NRM	DM	FHM	NRM	DM	FHM
1.5	1.3500	0.0602	0.0690	9	4	4	Yes	Yes	Yes
1	1.9609	0.1017	0.0690	19	3	4	Yes	Yes	Yes
0.9	1.6721	0.0739	0.0690	13	4	4	Yes	Yes	Yes
0.8	1.7975	0.0617	0.0690	14	4	4	Yes	Yes	Yes
0.7	1.5052	0.0680	0.0690	12	5	4	Yes	Yes	Yes
0.6	1.8446	0.0875	0.0690	16	8	4	Yes	Yes	Yes
0.5			0.0690			4	No	No	Yes

These show the NRM, the DM and the FHM all converge when the initial values are from $0.6p.u.$ to $1.5p.u.$. The NRM and the DM generate different computing time and number of iterations with different initial values. However, the results of the computing time and the number of iterations achieved by the FHM are consistent, which indicates that the FHM is not affected by the selection of initial value. The DM and the FHM are 25 times faster than the NRM. They generate less number of iterations, especially when the initial values are $1p.u.$ and $0.6p.u.$. The DM is a little bit faster than the FHM when the initial values are $1.5p.u.$, $0.8p.u.$ and $0.7p.u.$. However, the difference is very small which is only in the order of 10^{-3} or less. Hence the FHM performs better than the DM in the whole range of initial values. Moreover it is the only one converged successfully when the initial value is $0.5p.u.$.

The result differences of the fundamental bus voltage magnitudes, the total harmonic voltage distortion, the total active and reactive powers at both sending and receiving ends and the total power losses on each branch between the NRM, the DM and the FHM are calculated to investigate the result accuracy of the FHM. They are illustrated in the same way as the figure of the fundamental bus voltage magnitude in a 14-bus power system. They are shown in Figures F.5 to F.9 in Appendix F. The result achieved by the NRM are also regarded as the reference value. As a result, the values of ERROR_1 and ERROR_2 respectively represent the result generated by the DM minus the reference value and the result obtained by the FHM minus the reference value. The maximum difference of each result category is summarized in Table 5.11 below.

Table 5.11: The maximum difference of each result category

	THDv	**Ptotals**	**Ptotalr**	**Qtotals**
ERROR_1	$8.5e^{-6}p.u.$	$-3.2e^{-5}p.u.$	$-3.3e^{-5}p.u.$	$-5.6e^{-5}p.u.$
ERROR_2	$8.5e^{-6}p.u.$	$-3.2e^{-5}p.u.$	$-3.3e^{-5}p.u.$	$-5.6e^{-5}p.u.$
	Qtotalr	**Ptotalloss**	$\mid V \mid^{(1)}$	
ERROR_1	$-5.7e^{-5}p.u.$	$2.85e^{-7}p.u.$	$9.82e^{-7}$	
ERROR_2	$-5.7e^{-5}p.u.$	$2.85e^{-7}p.u.$	$9.82e^{-7}$	

where the $\mid V \mid^{(1)}$, THDv, Ptotals, Ptotalr, Qtotals, Qtotalr and Ptotalloss represent the fundamental voltage magnitude, the total harmonic voltage distortion, the total active and reactive powers at both sending and receiving ends and the total power losses on each branch respectively. The positive and negative values represent the result generated by the FHM or DM is larger and less than the reference value respectively.

As shown in Figures F.5 to F.9, the curves of ERROR_1 and ERROR_2 coincide in each figure. It means that the FHM generates the same results as the DM. Table 5.11 indicates that the maximum difference of each result category is in the order of 10^{-5}, 10^{-6} and 10^{-8} respectively, which is so small that it can be ignored. Hence, the FHM has the same result accuracy as the NRM, for the base value is the result obtained by the NRM.

5.5 Case Three: In A 57-bus Power System

5.5.1 Power System Diagram

The diagram of an IEEE 57-bus power system is shown in Figure 5.16 below. It illustrates that seven generators are located at bus 1, bus 2, bus 3, bus 6, bus 8, bus 9 and bus 12 respectively. There are a total of seventeen transformers connected in the branches. Bus 1 is regarded as the slack bus. The bus data and the line and transformer data are respectively illustrated in Table D.5 and Table D.6 in Appendix D. Two six-pulse line commutated converters are connected to bus 15 and bus 29 that are represented by red capital character 'HS'.

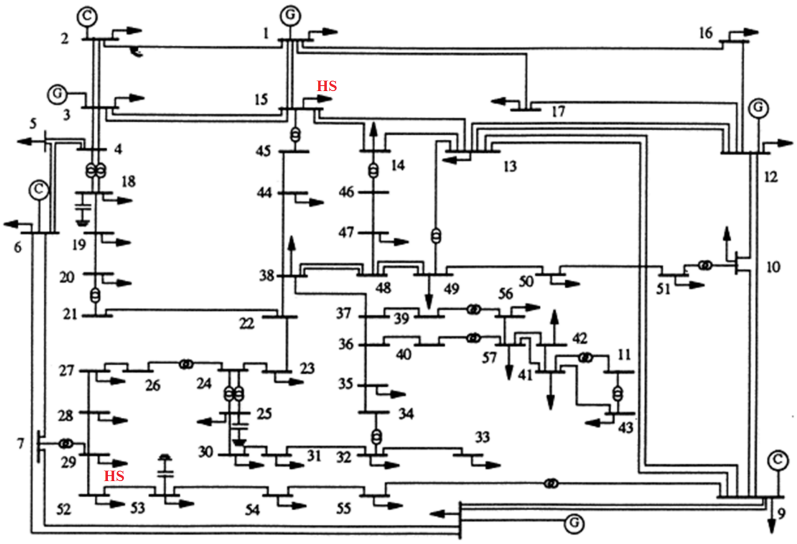

Figure 5.16: The diagram of an IEEE 57-bus power system [5]

5.5.2 Results And Discussion

The fast hybrid method (FHM) takes 0.1045 seconds and 3 iterations to accomplish the harmonic power flow calculation with an IEEE 57-bus power system. The results of the fundamental and the higher harmonic bus voltage magnitudes are illustrated in Figures 5.17 and 5.18 directly, and the maximum and minimum values of each harmonic order (including the fundamental frequency) for all buses are denoted in Table 5.12, which is the same as the previous section.

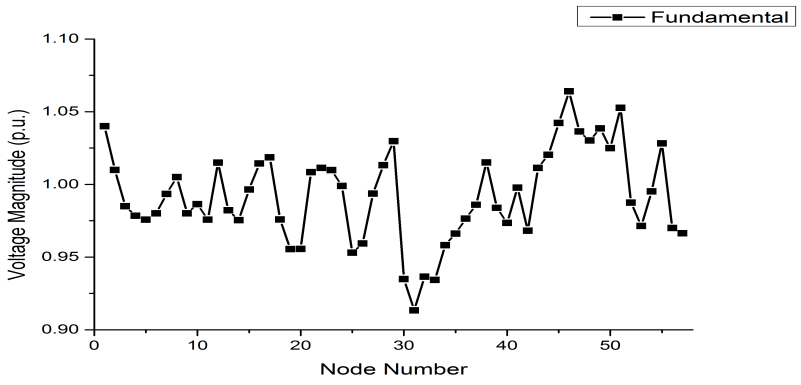

Figure 5.17: The fundamental bus voltage magnitude

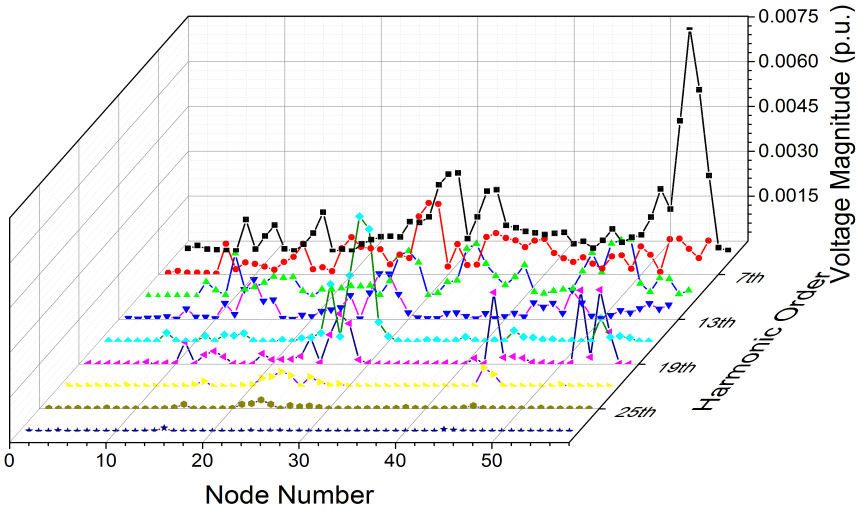

Figure 5.18: The harmonic bus voltage magnitude

Table 5.12: The maximum and minimum values of the fundamental and the higher harmonic voltage magnitudes in a 57-bus power system

	Max		Min	
Order	Bus	Mag. (p.u.)	Bus	Mag. (p.u.)
1st	47	1.0641	32	0.9133
5th	54	0.0075	17	1.66E-05
7th	29	0.0024	7	2.92E-06
11th	52	0.0019	3	8.13E-06
13th	28	0.0015	19	5.31E-06
17th	26	0.0042	37	1.13E-06
19th	55	0.0025	33	3.63E-07
23rd	45	0.0006	57	1.91E-08
25th	24	0.0003	43	9.4E-09
29th	16	0.0001	51	2.6E-10

As shown in Figure 5.17, the fundamental bus voltage magnitude irregularly fluctuates around $1.0 p.u.$. The maximum value is $1.0641 p.u.$, that is on the bus 47, while the minimum value is $0.9133 p.u.$, that occurs on the bus 32, according to Table 5.12. The

results of the higher harmonic voltage magnitudes are illustrated in a three-dimension diagram that is shown in Figure 5.18. It indicates that the bus voltage magnitudes have visual fluctuation at most of harmonic orders, which is different to the values achieved in 14 and 39-bus power systems. It represents that the harmonic injection currents located on the bus 15 and 29 have a great impact on the voltage magnitudes of other buses at most of harmonic orders. However, the variation begins to reduce when the harmonic order is 23^{rd}. The maximum bus voltage magnitude of the whole higher harmonic orders is $0.0075 p.u.$, that is on the bus 54 at the 5^{th} harmonic order.

With increasing of the bus numbers, the table scale that is shown the result of the total harmonic voltage distortion (THDv) also rises. As it has the same format as Tables 5.9 and 5.4, the result of the THDv is directly illustrated in Figure 5.19 below.

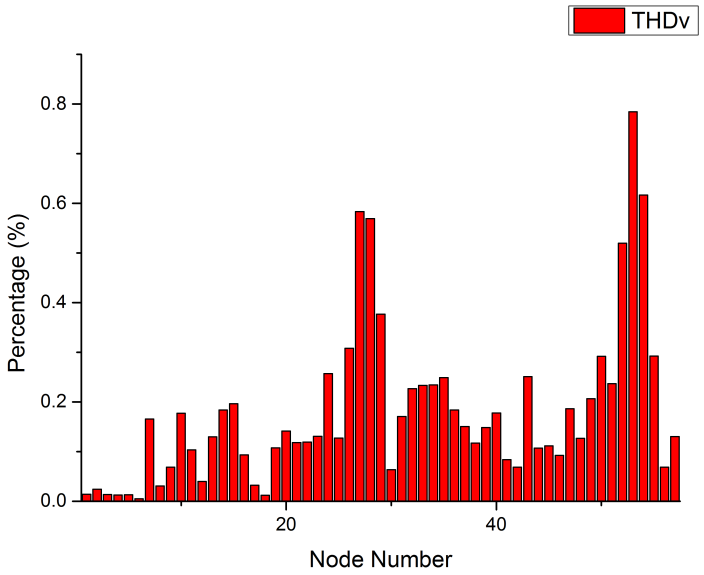

Figure 5.19: The total harmonic voltage distortion

The maximum value of the THDv calculated in a 57-bus power system is 0.78%, that occurs on the bus 53. It is below the limit level of 3% in Engineering Recommendation G5/4.

The results of the total active and reactive powers at both sending and receiving

ends (Ptotals, Qtotals, Ptotalr and Qtotalr) and the total power losses on each branch (Ptotalloss) can be expressed in the same way as Table 5.5. Hence they are illustrated in Figures 5.20 to 5.22 directly.

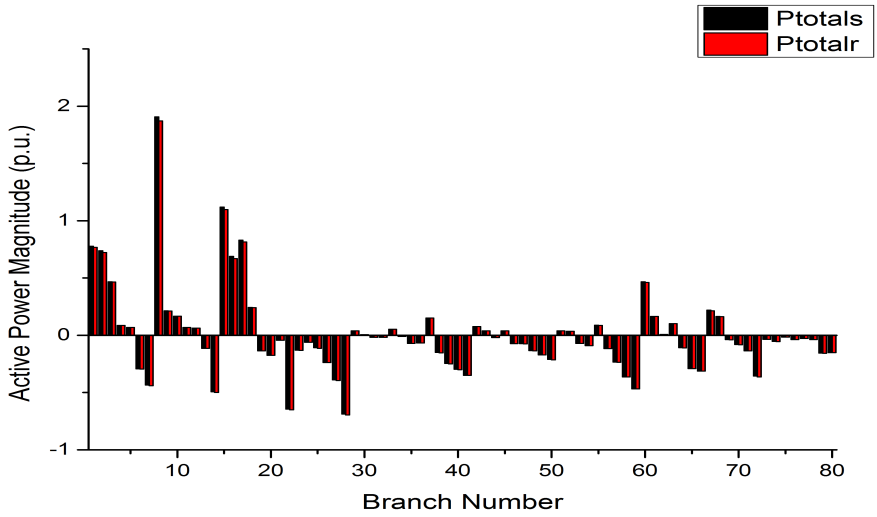

Figure 5.20: The total active powers at both sending and receiving ends

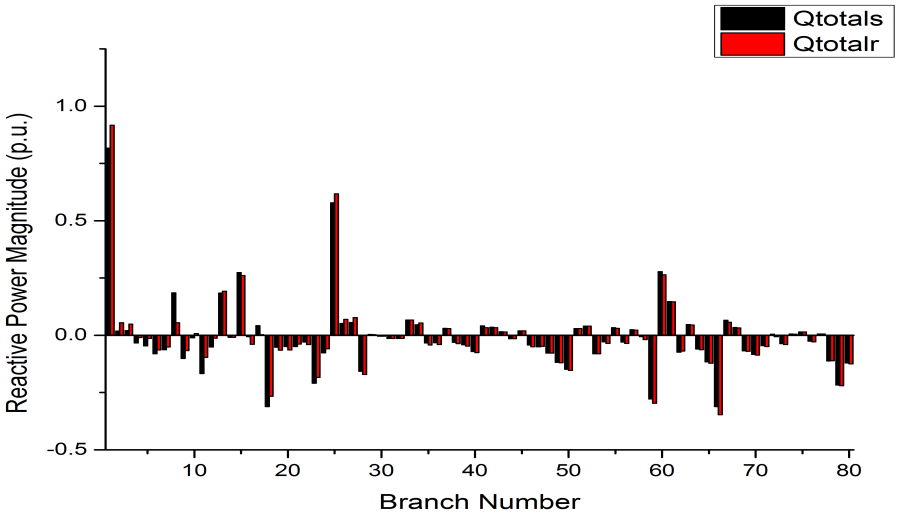

Figure 5.21: The total reactive powers at both sending and receiving ends

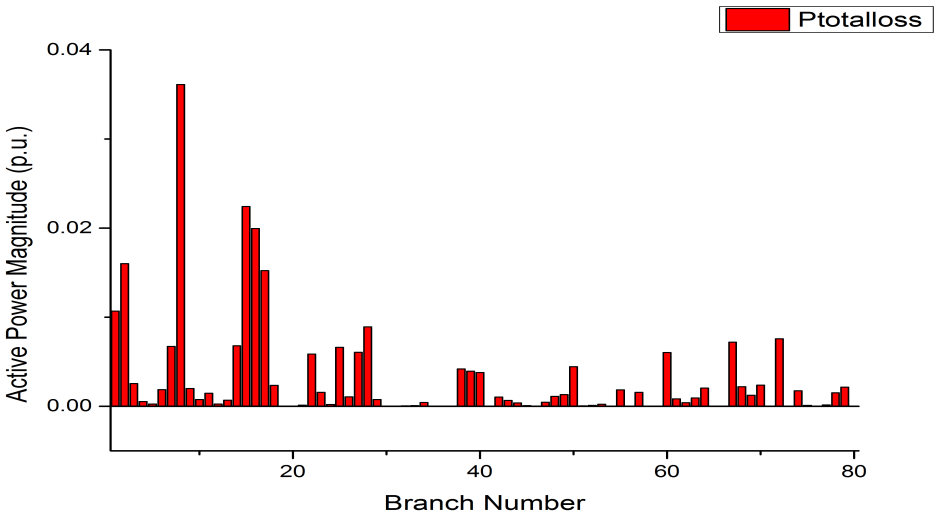

Figure 5.22: The total active power losses

As mentioned before, the active powers, also the reactive powers, at the sending and the receiving ends are respectively represented in black and red bar in a single diagram. For the active powers, if the values (both of two different columns) are positive, it denotes that they flow from the sending ends to the receiving ends; otherwise, they flow in the opposite way. For reactive powers, if the results are positive, it means that the buses (sending and receiving ends) generate reactive powers; otherwise, they absorb reactive powers. Hence, the total active and reactive power flows in the 57-bus power system can be visually explained. The maximum power loss, $0.0361 p.u.$, occurs on the 8^{th} branch, as shown in Figure 5.22.

5.5.3 Results Comparison

The computing time, the number of iterations and the convergence conditions calculated in the 57-bus power system with different initial values are illustrated in Table 5.13 below. Each symbol has the same meaning as Tables 5.6 and 5.10 denoted in the previous two sections.

Table 5.13: Computing time, iterations and convergence conditions comparison

Initial Values (p.u.)	Computing Time (s)			Iterations			Convergence Conditions		
	NRM	DM	FHM	NRM	DM	FHM	NRM	DM	FHM
1.5	8.0009	0.1543	0.1045	8	4	3	Yes	Yes	Yes
1	8.0812	0.0974	0.1045	9	3	3	Yes	Yes	Yes
0.9	5.5704	0.1077	0.1045	6	3	3	Yes	Yes	Yes
0.8	4.8559	0.1394	0.1045	5	4	3	Yes	Yes	Yes
0.7	8.3805	0.1508	0.1045	9	5	3	Yes	Yes	Yes
0.6	6.7363	0.1814	0.1045	7	7	3	Yes	Yes	Yes
0.5			0.1045			3	No	No	Yes

They show that the NRM, the DM and the FHM accomplish the calculation with no convergence problems when the initial values are from $0.6p.u.$ to $1.5p.u.$. The NRM and the DM generate different computing time and number of iterations with different initial values. However, the results of the computing time and the number of iterations obtained by the FHM are fixed at 0.0690 seconds and 4 respectively, no matter what initial value is. It indicates that the calculation procedure of the FHM in the 57-bus power system is not influenced by the selection of the initial value, either. The FHM performs best in this range of initial values though it is a little bit slower than the DM when the initial value is $1.0p.u.$. Moreover the FHM is the only method that converged successfully when the initial value is $0.5p.u.$.

In order to investigate the result accuracy of the FHM, the result differences of the fundamental bus voltage magnitudes, the total harmonic voltage distortion, the total active and reactive powers at both sending and receiving ends and the total power losses on each branch between three different methods (the NRM, the DM and the FHM) are involved to achieve the purpose. They are illustrated in the same format as the figure of the fundamental bus voltage magnitude in a 14-bus power system. Their diagrams are shown in Figures F.10 to F.14 in Appendix F. However, the maximum difference of each result category is summarized in Table 5.14 below.

Table 5.14: The maximum difference of each result category

	THDv	**Ptotals**	**Ptotalr**	**Qtotals**
ERROR_1	$0.0044 p.u.$	$-1.8e^{-5} p.u.$	$-1.8e^{-5} p.u.$	$7.09e^{-5} p.u.$
ERROR_2	$0.0044 p.u.$	$-1.8e^{-5} p.u.$	$-1.8e^{-5} p.u.$	$7.09e^{-5} p.u.$
	Qtotalr	**Ptotalloss**	$\mid V \mid^{(1)}$	
ERROR_1	$7e^{-5} p.u.$	$2.74e^{-6} p.u.$	$7.15e^{-6}$	
ERROR_2	$7e^{-5} p.u.$	$2.74e^{-6} p.u.$	$7.15e^{-6}$	

According to Figures F.10 to F.14, they show that the results of the $\mid V \mid^{(1)}$, THDv, Ptotals, Ptotalr, Qtotals, Qtotalr and Ptotalloss calculated by the DM and the FHM respectively are matched. There are result differences between the NRM and the DM, and the NRM and the FHM. However they are so small, in the order of 10^{-6} and 10^{-7}, that they can be ignored. Some significant mismatches are shown in Figure F.11 and Table 5.14, especially on bus 54. The reason is that the harmonic bus voltage magnitudes (excluding the fundamental frequency) calculated by the NRM are different to those obtained by the other two methods. Because they are calculated directly based on the admittance-matrix-based equation in the DM and the FHM instead of being obtained iteratively through harmonic injection currents in the NRM. However the maximum value is $0.0044 p.u.$ according to Table 5.14, that is small enough to be accepted. Hence, the results calculated by the FHM are accurate based on the NRM.

5.6 Case Four: In A 118-bus Power System

5.6.1 Details of Power System

The diagram of an IEEE 118-bus power system is illustrated in Figure 5.23 below. There are fifty-four generators connected to the system and nine transformers connected in the branches. Bus 69 is represented as the reference bus. The bus data and the line and transformer data are respectively shown in Table D.7 and D.8 in Appendix D. Two six-pulse line-commutated converters are connected to buses 22 and 95 that are represented by red capital character 'HS'.

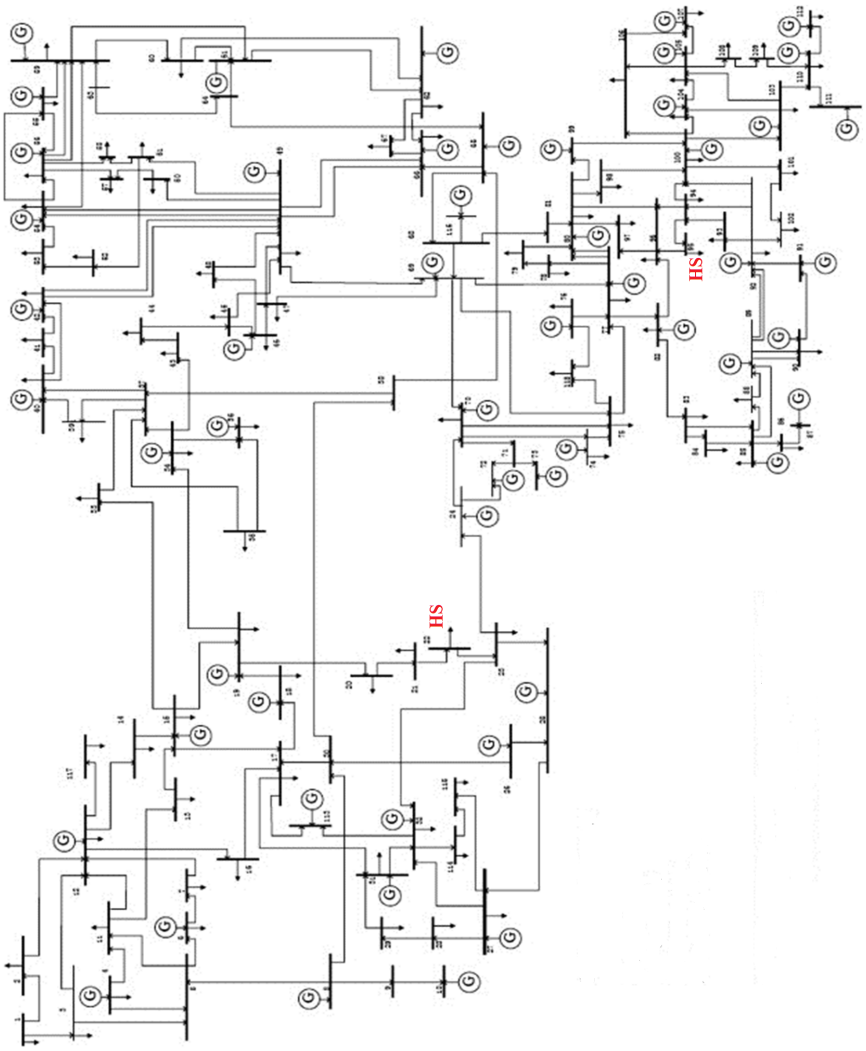

Figure 5.23: The diagram of an IEEE 118-bus power system [6]

5.6.2 Results And Discussion

The fast hybrid method (FHM) takes 0.2794 seconds 3 iterations to accomplish the harmonic power flow calculation with an IEEE 118-bus power system. The results of the fundamental and the higher harmonic bus voltage magnitudes are illustrated in Figures 5.24 and 5.25 directly, and the maximum and minimum values of each harmonic order (including the fundamental frequency) for all buses are denoted in

Table 5.15 below.

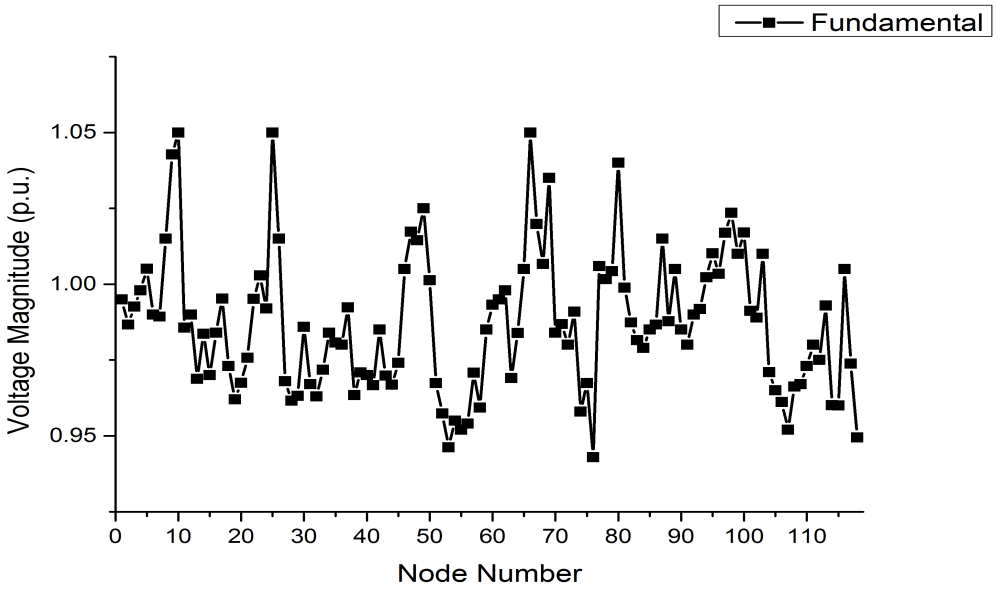

Figure 5.24: The fundamental bus voltage magnitude

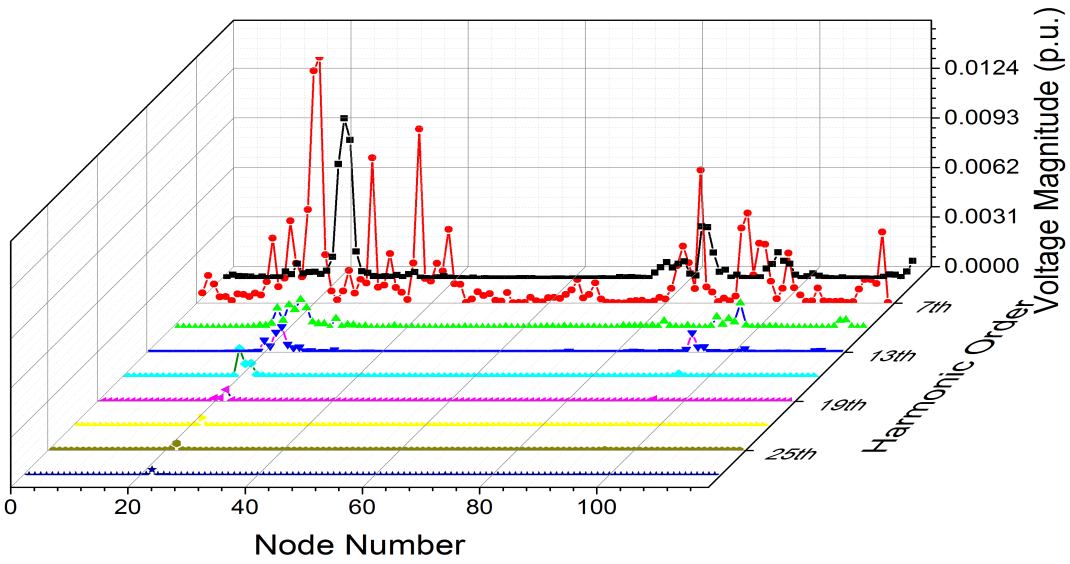

Figure 5.25: The harmonic bus voltage magnitude

Table 5.15: The maximum and minimum values of the fundamental and the higher harmonic voltage magnitudes in a 118-bus power system

	Max		Min	
Order	Bus	Mag. (p.u.)	Bus	Mag. (p.u.)
1st	11, 26 and 67	1.05	77	0.943
5th	22	0.01	56	1.67E-06
7th	22	0.0154	74	1.55E-05
11th	23	0.0018	46	1.61E-07
13th	24	0.0016	52	3.01E-09
17th	21	0.0018	54	1.12E-11
19th	23	0.0007	54	1.2E-11
23rd	23	0.0005	54	9.08E-14
25th	23	0.0005	54	7.88E-14
29th	23	0.0003	54	7.17E-16

As shown in Figure 5.24, the fundamental bus voltage magnitude irregularly fluctuates between $0.943 p.u.$ and $1.05 p.u.$. The maximum value, $1.05 p.u.$, occurs on the bus 11, 26 and 67, while the minimum value, $0.943 p.u.$, is on the bus 77, according to Table 5.15. The values of the higher harmonic voltage magnitudes are illustrated in a three-dimension diagram in order to investigate and compare the varying curve of each harmonic order, that is the same as previous sections, and it is shown in Figure 5.25. The figure indicates that the bus voltage magnitudes of the first two harmonic orders, 5^{th} and 7^{th}, are changed significantly. Then the voltage magnitudes nearly tends to zero with increasing of the harmonic order. However, the values of several buses around the bus 20 are still visible from the 9^{th} to 19^{th} harmonic order. The maximum value of the bus voltage magnitudes for the whole higher harmonic orders (excluding the fundamental frequency) is $0.0154 p.u.$, which occurs on the bus 22 at the 7^{th} harmonic order and is highlighted in pink colour as shown in Table 5.15.

As the same reason described in the previous section, the result of the total harmonic voltage distortion (THDv) is illustrated in Figure 5.26 directly. In order to see each bus value clearly, the result of the THDv is separately shown in two parts: one is from the bus 1 to the bus 60 and the other is from the bus 61 to the bus 118. They have

the same value range in vertical coordinate.

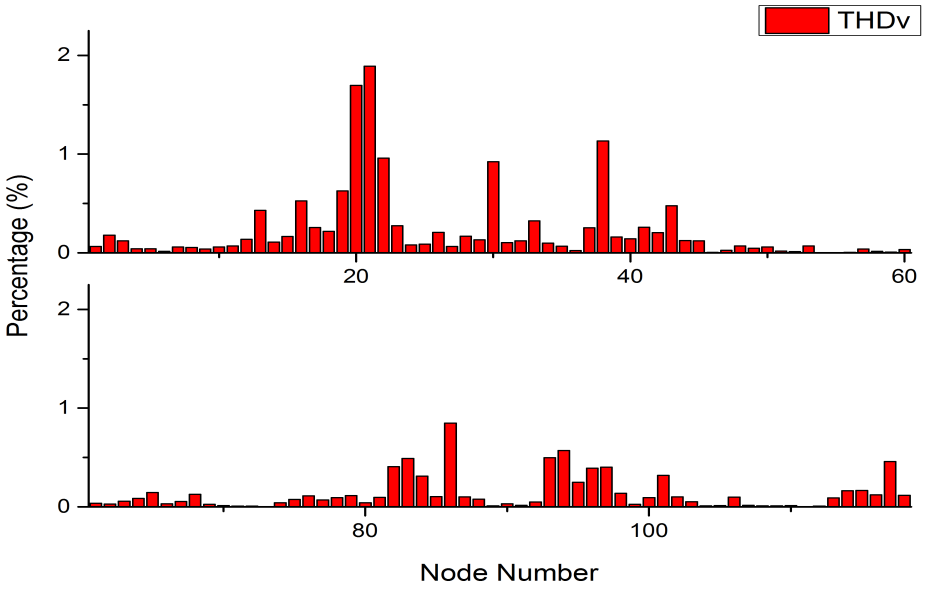

Figure 5.26: The total harmonic voltage distortion

As shown in Figure 5.26, the maximum value of the THDv calculated in a 118-bus power system, 1.89%, is higher than the one in other three cases, but it is still below the limit level, 3%, of the Engineering Recommendation G5/4.

The results of the total active and reactive powers at both sending and receiving ends (Ptotals, Qtotals, Ptotalr and Qtotalr) and the total power losses on each branch (Ptotalloss) can be expressed in the same way as Table 5.5. Hence they are directly illustrated in Figures 5.27 to 5.29. In order to see each branch value clearly, the results of the Ptotals, Ptotalr, Qtotals, Qtotalr and Ptotalloss are separately illustrated in three parts: one is from branch 1 to branch 60, one is from branch 61 to branch 120 and the last is from branch 121 to branch 180. Their vertical scopes are the same.

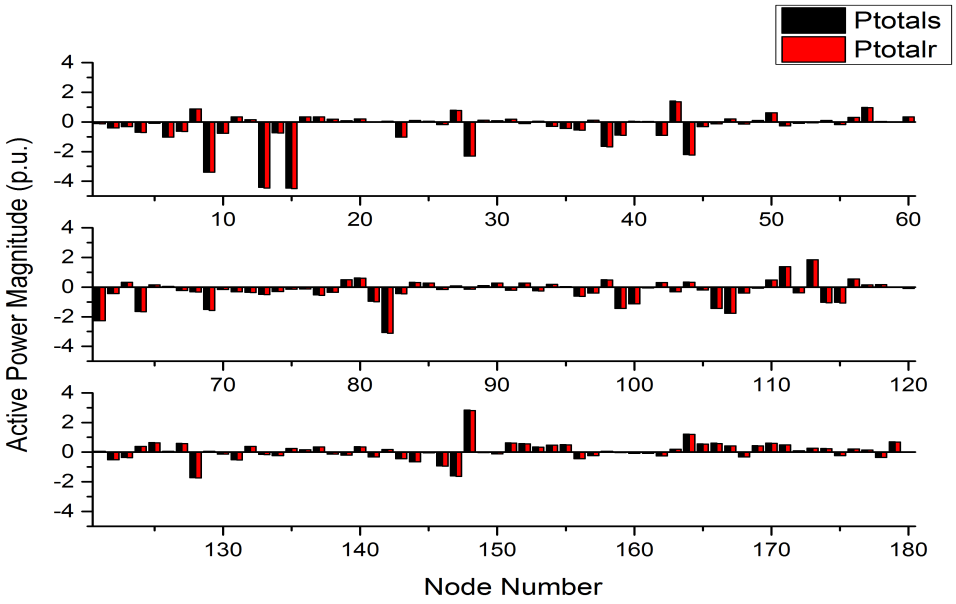

Figure 5.27: The total active powers at both sending and receiving ends

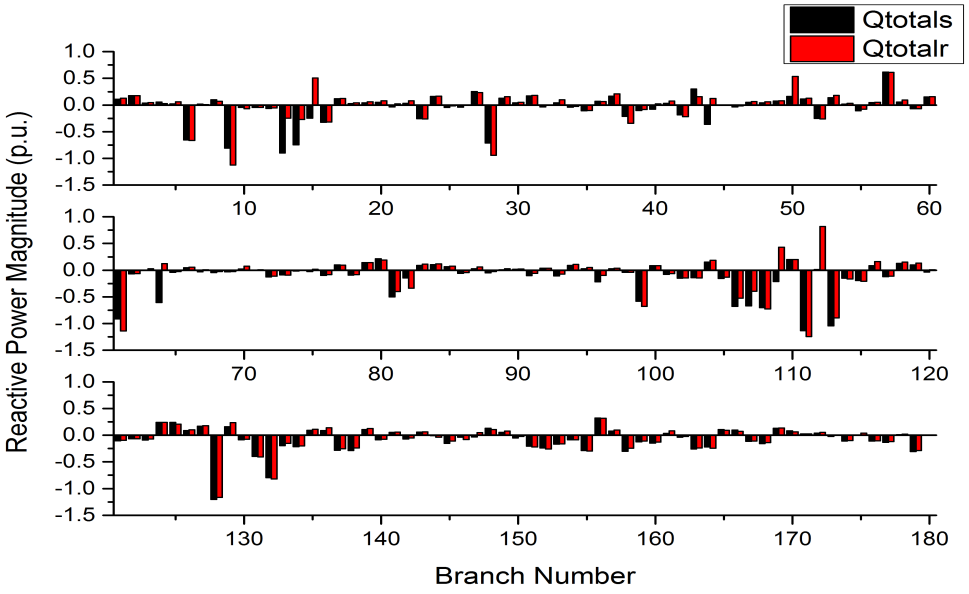

Figure 5.28: The total reactive powers at both sending and receiving ends

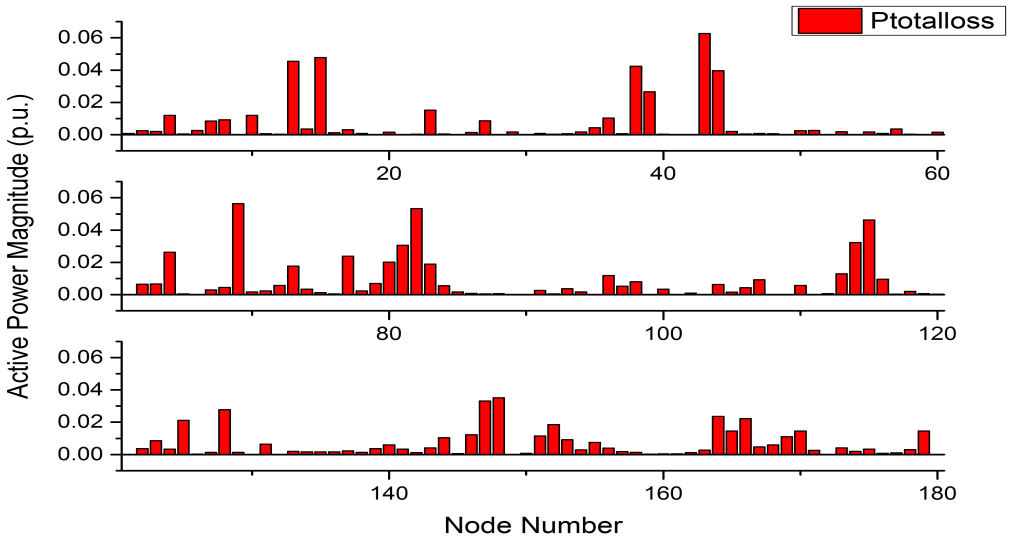

Figure 5.29: The total active power losses

As mentioned in the precious three cases, the active powers, also the reactive powers, at the sending and the receiving ends are respectively represented in black and red bar in a single diagram. For the active powers, if the values (both of two different columns) are positive, it denotes that they flow from the sending ends to the receiving ends; otherwise, they flow in the opposite way. For reactive powers, if the results are positive, it means that the buses (sending and receiving ends) generate reactive powers; otherwise, they absorb reactive powers. Hence, the total active and reactive power flows in the 118-bus power system can be visually explained. The maximum total active power flow is $-4.4522 p.u.$ that occurs on the 15^{th} branch. The power flows from the bus 10 to the bus 9. The maximum value of the total power losses is $0.0626 p.u.$ that is on branch 43.

5.6.3 Results Comparison

The computing time, the number of iterations and the convergence conditions established with different initial values are shown in Table 5.16 below. Each symbol has the same meaning as Tables 5.6, 5.10 and 5.16 denoted in the previous three cases.

Table 5.16: Computing time, iterations and convergence conditions comparison

Initial Values (p.u.)	Computing Time (s)			Iterations			Convergence Conditions		
	NRM	DM	FHM	NRM	DM	FHM	NRM	DM	FHM
1.5	37.9044	0.3690	0.2794	11	5	3	Yes	Yes	Yes
1	32.6356	0.2511	0.2794	10	3	3	Yes	Yes	Yes
0.9	54.1790	0.3343	0.2794	19	4	3	Yes	Yes	Yes
0.8	46.9363	0.3851	0.2794	15	5	3	Yes	Yes	Yes
0.7			0.2794			3	No	No	Yes
0.6			0.2794			3	No	No	Yes
0.5			0.2794			3	No	No	Yes

They show that all the three different harmonic power flow calculation methods converge when the initial bus voltage magnitudes are assumed to be $0.8p.u.$, $0.9p.u.$, $1.0p.u.$ and $1.5p.u.$ respectively. The NRM and the DM generate different computing time and number of iterations with different initial values. However, the results of these values achieved by the FHM are consistent. It indicates that the calculation proceeding of the FHM is not influenced by the selection of initial value. The NRM takes hundred times longer computing time to accomplish the calculation than the other two methods. The DM performs better only when the initial value is $1.0p.u.$. The FHM is the best choice to calculate harmonic power flow in a 118-bus power system because of its fast calculation and less number of iterations. In addition, it is the only one that is able to converge to a solution when the initial values are from $0.5p.u.$ to $0.7p.u.$.

The author still considers to illustrate the result differences between each method to investigate the calculation accuracy of the FHM. The result achieved by the NRM are still regarded as the reference value that is the same as previous three cases. ERROR_1 and EERROR_2, shown in figures, are respectively expressed as the result differences generated by the DM minus the reference value and the result obtained by the FHM minus the reference value. The result differences of the fundamental bus voltage magnitudes, the total harmonic voltage distortion, the total active and reactive powers at both sending and receiving ends and the total power losses on each branch are illustrated to achieve the purpose. They are shown in Figures F.15 to F.21 in Appendix F. In order to see each bus and branch value clearly, the results of the fundamental bus

voltage magnitude $\mid V \mid^{(1)}$ and the THDv are separately illustrated in two parts: one is from the bus 1 to the bus 60 and other is from the bus 61 to the bus 118; and the results of the Ptotals, Ptotalr, Qtotals, Qtotalr and Ptotalloss are separately illustrated in three parts: one is from branch 1 to branch 60, one is from branch 61 to branch 120 and the last is from branch 121 to branch 180. The vertical scopes of each part in one figure are the same. The maximum difference of each result category is summarized in Table 5.17 below.

Table 5.17: The maximum difference of each result category

	THDv	**Ptotals**	**Ptotalr**	**Qtotals**
ERROR_1	$0.0033 p.u.$	$-6.6e^{-5} p.u.$	$-6.9e^{-5} p.u.$	$0.0001 p.u.$
ERROR_2	$0.0033 p.u.$	$-6.6e^{-5} p.u.$	$-6.9e^{-5} p.u.$	$0.0001 p.u.$
	Qtotalr	**Ptotalloss**	$\mid V \mid^{(1)}$	
ERROR_1	$9.65e^{-5} p.u.$	$-3.4e^{-6} p.u.$	$1.61e^{-5}$	
ERROR_2	$9.65e^{-5} p.u.$	$-3.4e^{-6} p.u.$	$1.61e^{-5}$	

As shown in Figures F.15 to F.21, the results of the $\mid V \mid^{(1)}$, THDv, Ptotals, Ptotalr, Qtotals, Qtotalr and Ptotalloss respectively achieved by the DM and the FHM are matched. According to Table 5.17, there are result differences between the NRM and the DM, and the NRM and the FHM. However they are in the order of 10^{-5}, 10^{-6} and 10^{-7} that are small enough to be ignored. Hence, the results calculated by the FHM are accurate based on the NRM.

5.7 Result Discussion and Summary

The fast hybrid method (FHM) was applied to an IEEE 14-bus, the New England 39-bus, an IEEE 57-bus and an IEEE 118-bus power system respectively. Two six-pulse line-commutated converters were connected to be harmonic sources. The results of computing time, the number of iterations, the fundamental bus voltage magnitude, the total harmonic voltage distortion, the total active and reactive powers at both sending and receiving ends, and the total active and reactive power losses on each line were achieved. The results generated by the proposed method were compared to those obtained by the NRM and the DM respectively. It was used to investigate the result accuracy and advantages of the proposed method. The results achieved by the NRM were regarded as the references in this chapter.

5.7.1 Summary Of The Results Achieved By The Proposed Method

The computing time and the number of iterations achieved by the FHM in four different cases are summarized in Figure 5.30 below.

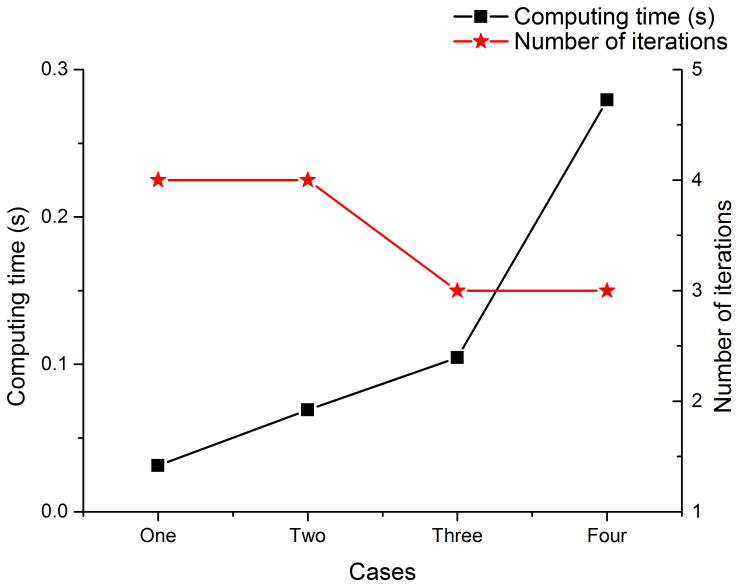

Figure 5.30: The computing time and the number of iterations of four cases

As shown in the figure above, the computing time and the number of iterations are illustrated in black square and red star respectively. The unit of the computing time is second. The horizontal axis represents four different cases from left to right, which are in a 14-bus, 39-bus, 57-bus and 118-bus power system respectively. with increasing of the scale of power system, the computing time rises. However, the number of iterations decreases from 4 to 3. Therefore, the computing time is not depended on the number of iterations.

As the total harmonic voltage distortion (THDv) can explain the influence of harmonics to the bus voltage magnitudes in power systems directly, the average and maximum values of the THDv achieved by the proposed method from four different cases are illustrated in Figure 5.31 below.

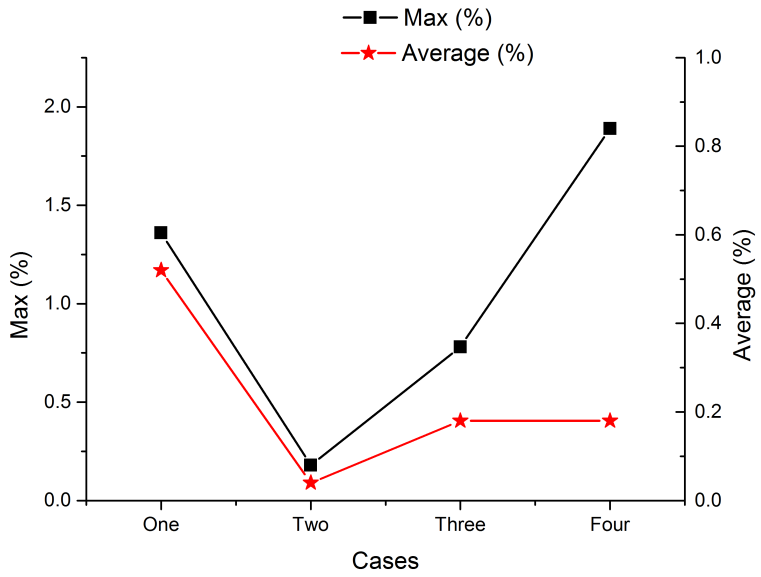

Figure 5.31: The total harmonic voltage distortion (THDv) of four cases

The maximum and average values of the THDv are respectively illustrated in black square and red star. Their units are all percent. The horizontal axis represents four different cases, which are the same as Figure 5.30. As shown in the above figure, the maximum value, either the average value, of the THDv are not dependent on the scale of power system. Actually, they are related to the fundamental and higher harmonic bus voltage magnitudes, also the data of transmission lines. Because the higher harmonic bus voltage magnitudes are generated by the admittance-matrix-based equation, $\overline{I}^{(h)} = \overline{Y}^{(h)}\overline{V}^{(h)}$. However, if the harmonic sources are consistent and the transmission line data of different power systems are in the same order, the maximum and average values of the THDv may rise with increasing of the scale of power system.

5.7.2 Summary Of The Result Comparison

The computing time achieved by the Newton-Raphson method (NRM), the decoupled method (DM) and the fast hybrid method (FHM) in four different power systems is illustrated with three layers in Figure 5.32 below. The results obtained by different power systems are represented by different symbols and different colour, and the details are shown in the legend.

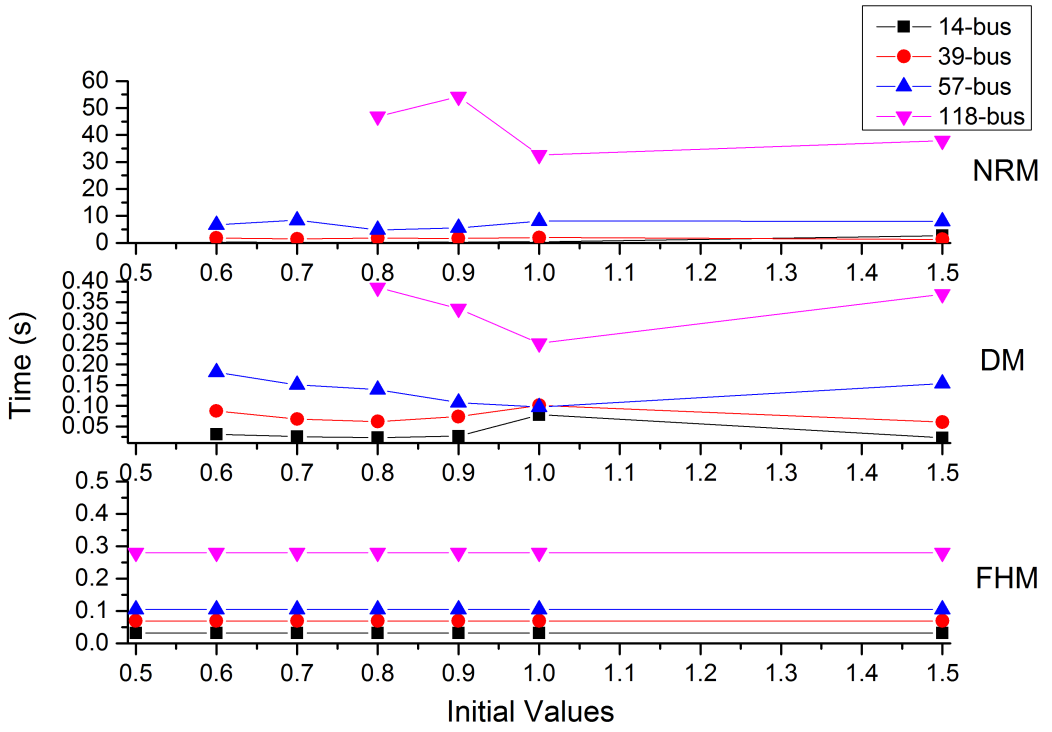

Figure 5.32: The summary of the computing time comparison

As shown in the above figure, the results respectively achieved by the NRM and the DM vary with different initial values. However, the computing time generated by the FHM is consistent. The NRM was very limited in the initial value. The larger the power system was, the more difficult the calculation could be converged. Moreover, the NRM took much more time to accomplish the calculation than the other two methods. The DM was better than the NRM, but it was still limited by the initial value. They did not converge when the initial values were $0.5p.u.$ in 14-bus, 39-bus, 57-bus power systems, and $0.5p.u.$, $0.6p.u.$ and $0.7p.u.$ in 118-bus power system. The FHM was not effected by the initial value setting, as it used the secant method to establish the iterative initial value. Hence, the FHM solved the convergence problem caused by the poor initial value successfully.

Sometimes, the DM accomplished the calculation more quickly than the FHM especially in small power system. However, the larger the power system was, the better

the FHM performed. Even though the FHM was slower than the DM, the difference in computing time was under 0.1 seconds. Hence, the FHM ran the calculation as fast as the DM in a small power system and even faster in a large power system.

The maximum result differences of the fundamental bus voltage magnitude ($|V|^{(1)}$), the total harmonic voltage distortion (THDv), the total active and reactive powers at both sending and receiving ends (Ptotals, Ptotalr, Qtotals and Qtotalr), and the total power loss on each branch (Ptotalloss) between each method in four different power systems are summarized in Table 5.18 in the next page.

As mentioned before, the result achieved by the NRM was regarded as the reference value. ERROR_1 and ERROR_2 represented the result differences between the DM and the NRM, and between the FHM and the NRM respectively. Table 5.18 shows that the DM and the FHM have the same result difference in each result category when they are applied in 14-bus, 39-bus, 57-bus and 118-bus power system respectively. Hence, it indicates that the DM and the FHM have the same calculation accuracy. Though the result differences of $|V|^{(1)}$, THDv, Ptotals, Qtotals, Ptotalr, Qtotalr and Ptotalloss exist, they are in the order of 10^{-4}, 10^{-5}, 10^{-6}, 10^{-7} and 10^{-8} and can be ignored. Hence, the results calculated by the FHM were accurate based on the NRM evaluation.

In conclusion, the FHM can accomplish the harmonic power flow calculation and is not influenced by initial value setting. Hence it succeeds in solving the convergence problems. Moreover, the FHM can complete the calculation quickly and achieve accurate results.

Table 5.18: The summary of the maximum result difference of each category

	14-bus		39-bus		57-bus		118-bus	
	ERROR_1 (p.u.)	ERROR_2 (p.u.)	ERROR_1 (p.u.)	ERROR_2 (p.u.)	ERROR_1 (p.u.)	ERROR_2 (p.u.)	ERROR_1 (p.u.)	ERROR_2 (p.u.)
$\mid V \mid^{(1)}$	$3.58e^{-6}$	$3.58e^{-6}$	$9.82e^{-7}$	$9.82e^{-7}$	$7.15e^{-6}$	$7.15e^{-6}$	$1.61e^{-5}$	$1.61e^{-5}$
THDv	0.0012	0.0012	$8.5e^{-6}$	$8.5e^{-6}$	0.0044	0.0044	0.0033	0.0033
Ptotals	$-6.75e^{-5}$	$-6.75e^{-5}$	$-3.2e^{-5}$	$-3.2e^{-5}$	$-1.8e^{-5}$	$-1.8e^{-5}$	$-6.6e^{-5}$	$-6.6e^{-5}$
Ptotalr	$-5.88e^{-5}$	$-5.88e^{-5}$	$-3.3e^{-5}$	$-3.3e^{-5}$	$-1.8e^{-5}$	$-1.8e^{-5}$	$-6.9e^{-5}$	$-6.9e^{-5}$
Qtotals	$-9.81e^{-5}$	$-9.81e^{-5}$	$-5.6e^{-5}$	$-5.6e^{-5}$	$7.09e^{-5}$	$7.09e^{-5}$	0.0001	0.0001
Qtotalr	0.0001	0.0001	$-5.7e^{-5}$	$-5.7e^{-5}$	$7e^{-5}$	$7e^{-5}$	$9.65e^{-5}$	$9.65e^{-5}$
Ptotalloss	$-8.72e^{-6}$	$-8.72e^{-6}$	$2.85e^{-7}$	$2.85e^{-7}$	$2.74e^{-6}$	$2.74e^{-6}$	$-3.4e^{-6}$	$-3.4e^{-6}$

References

[1] K. M. Hink, "Harmonic mitigation of 12-pulse drives with unbalanced input line voltages," *MTE Corporation, W147*, no. 9525, 2002. 130

[2] C. Francisco, *Harmonics and power systems*. CRC press, 2006.

[3] J. Technologies, "Guide to harmonics with ac variable frequency drives," Variable speed drives & controls, Tech. Rep., last date of access 03.06.2013. [Online]. Available: http://www.joliettech.com/abb_evaluating-harmonics-with-ac-drives.htm 130

[4] A. Ulinuha, M. Masoum, and S. Islam, "Harmonic power flow calculations for a large power system with multiple nonlinear loads using decoupled approach," in *Power Engineering Conference, 2007. AUPEC 2007. Australasian Universities*. IEEE, 2007, pp. 1–6. xx, 130

[5] H. Wan and Y. Song, "Hybrid supervised and unsupervised neural network approach to voltage stability analysis," *Electric power systems research*, vol. 47, no. 2, pp. 115–122, 1998. xiii, 151

[6] L. Wu, M. Shahidehpour, and T. Li, "Stochastic security-constrained unit commitment," *Power Systems, IEEE Transactions on*, vol. 22, no. 2, pp. 800–811, 2007. xiii, 158

Chapter 6

Harmonic Penetration Evaluation With Variable Harmonic Capacities

6.1 Introduction

The importance of green energies is continuously growing in our societies not only due to environmental concerns but also to solve the problem of access to electricity in a number of rural areas in developing countries. In Europe (EU), new renewable power capacity installations were mere 3.6 GW in 2000. Since 2010, annual renewable capacity additions have been between 24.7 GW and 35.2 GW. In 2013, a total of 25.4 GW of renewable power capacity installations were installed in EU [1].

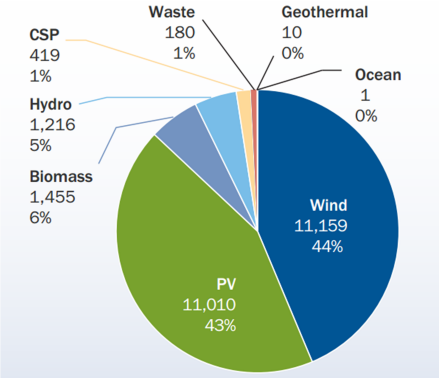

Figure 6.1: 2013 share of new renewable power capacity installations in MW, total 25.450 MW [1]

As shown in Figure 6.1 above, of this 25.4 GW installed in EU, wind power accounted for 44% (11.2 GW) of new installations. Followed by photovoltaic power 43% (11 GW). They have increased from 2.4% in 2000 to 13% in 2013, and from 0% in 2000 to 9% in 2013 respectively, according to Figures 6.2(a) and 6.2(b) [1].

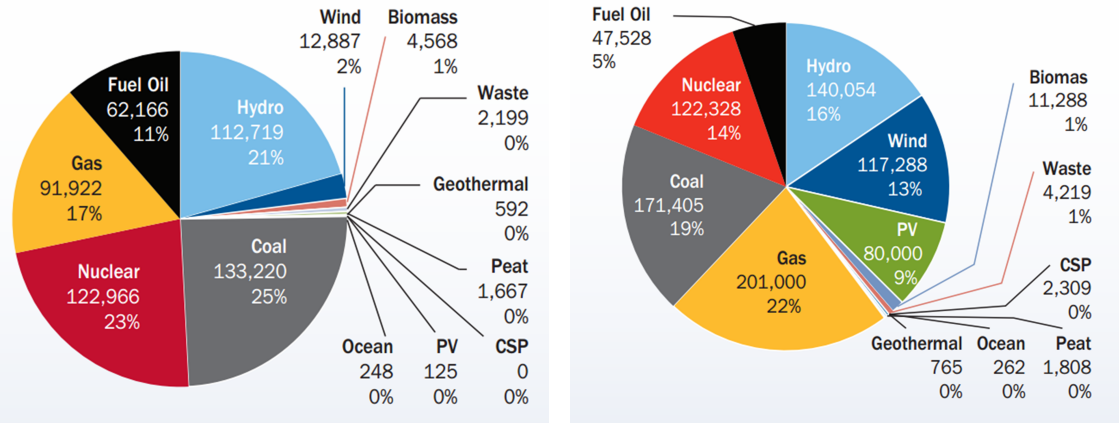

(a) EU power mix 2000

(b) EU power mix 2013

Figure 6.2: EU power mix from 2000 to 2013 [1]

In 2020, 230 GW wind power capacity will be installed in EU: 190 GW onshore and 40 GW offshore declared by European wind energy association (EWEA). It would produce 14% - 17% of EU's electricity depending on total demand. In 2030, 400 GW wind power capacity will be installed in EU: 250 GW onshore and 150 GW offshore, which would produce 26% - 35% of EU's electricity [2–4]. Moreover, European photovoltaic industry association (EPIA) assumed that photovoltaic electricity will become a mainstream power source in EU by 2020 and a major power source in 2050. It could supply up to 12% of the electricity demand in EU by 2020 representing 390 GW of installed capacity and 460 TWh of electricy generation, and reach as much a 962 GW of installed capacity by 2050 in EU [5].

However, with increasing of renewable power generations in power networks, it encounters power quality problems caused by harmonic injections. Hence, these renewable generators are regarded as harmonic sources. Therefore, it is essential to calculate the harmonic penetration and investigate the effects to power networks. This chapter will apply the proposed method, i.e. the fast hybrid method (FHM), to cal-

culate the harmonic power flow in a 2383-bus Polish power system [6] with multiple renewable generators and modern devices. With changing of the power capacities of these harmonic sources the total harmonic capacities are also changed. Hence, it will investigate the effects to the harmonic penetration with variable harmonic capacities following these aspects:

- The effects to the result waveforms of root-mean-square (rms) values of bus voltage magnitudes, total harmonic voltage distortion (THDv), total active and reactive powers at both sending and receiving ends and total power loss on each transmission line. Also, the number of influenced buses and lines in each category are investigated.
- The number of buses that THDv values exceed the level of limit, 3 % are investigated.
- The effects to the neighborhood buses of harmonic sources in different harmonic penetration level are investigated based on THDv.

The wind turbine (WT), the electric vehicle battery charger (EVC) and the Photovoltaic generator (PG) described in chapter 2 will be connected to the power system as harmonic sources in order to achieve the above purpose. A converter with sub-harmonic and inter-harmonic frequencies will be connected to the power system as harmonic sources as well. The investigation of the effects of integrating these harmonic sources to the harmonic penetration is achieved by changing their power capacities. The computer which is used for the calculation has an i7 quad-core CPU with 3.4 GHz and a 12G RAM. The operation system is windows 8.

This chapter is arranged as follows: Section one is the introduction. The 2383-bus Polish power system and the harmonic sources are introduced in section two. Section three presents the scenarios. Section four investigate the effects of changing power capacities of harmonic sources to the harmonic power flow through three aspects. The final section is the conclusion.

6.2 Power System And Harmonic Sources

6.2.1 Power System

The Polish 2383-bus power system is applied in this chapter. Its network diagram is shown in Figure 6.3 on next page. It contains 2896 branches and 327 generators. Bus 18 is the slack bus. The bus data and the line and transformer data of this power system can be found from **MATPOWER4.1** [6].

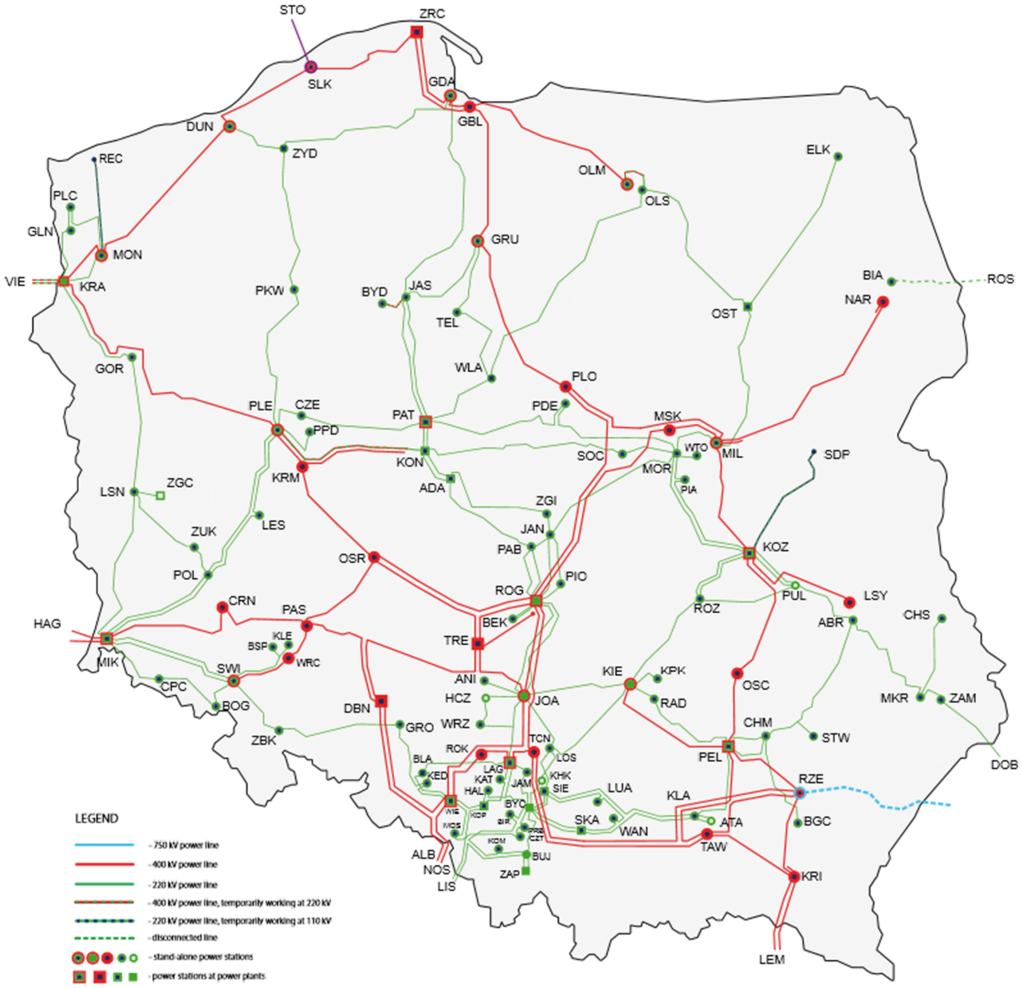

Figure 6.3: Polish 2383-bus power network diagram [7]

6.2.2 Harmonic Sources

The wind turbine (WT), the electric vehicle battery charger (EVC) and the photovoltaic generator (PG) are regarded as harmonic sources in this chapter. Their harmonic injection currents of each harmonic level (including fundamental frequency) are shown in Table 2.3, 2.4 and 2.5 in chapter 2.

Moreover, a converter with sub-harmonic and inter-harmonic frequencies is also used as harmonic source. It expands the range of harmonic frequency, which is not only on integer-harmonic, and makes the simulation more practical. Its harmonic injection current of each harmonic level (including fundamental frequency) is shown in Table 6.1 below.

Table 6.1: Harmonic injection current of a converter [8]

Harmonic order'h'	**Magnitude (p.u.)**	**Angle degree**	**Harmonic order'h'**	**Magnitude (p.u.)**	**Angle degree**
0.3	$2.8875e^{-3}$	0	5.5	$2.0493e^{-3}$	0
0.6	$3.5442e^{-3}$	0	6.6	$2.1417e^{-3}$	0
1	$146.92e^{-3}$	0	7	$0.8052e^{-3}$	0
1.9	$0.5049e^{-3}$	0	8	$0.7821e^{-3}$	0
2	$0.2112e^{-3}$	0	8.6	$1.0692e^{-3}$	0
2.6	$1.8216e^{-3}$	0	9.5	$1.3563e^{-3}$	0
3	$0.9009e^{-3}$	0	11	$1.3365e^{-3}$	0
3.5	$2.3034e^{-3}$	0	13	$0.9669e^{-3}$	0
5	$1.1088e^{-3}$	0			
$I_{base} = 3030.3$A					

6.3 Scenarios

In order to achieve the research purpose in this chapter, four scenarios are designed and shown in Tables 6.2 to 6.5 below.

Table 6.2: Scenario One

Scenario one: 304 Harmonic sources		
Harmonic Source	**No. of Units**	**Power Capacities**
Electric Vehicle Charger (EVC)	108	5 %
Converter	93	5 %
Wind Turbine (WT)	84	20 %
Photovoltaic Generator (PG)	19	5 %
Total power capacities of harmonic sources = 35 %		

Table 6.3: Scenario Two

Scenario two: 304 Harmonic sources		
Harmonic Source	**No. of Units**	**Power Capacities**
Electric Vehicle Charger (EVC)	108	5 %
Converter	93	5 %
Wind Turbine (WT)	84	40 %
Photovoltaic Generator (PG)	19	5 %
Total power capacities of harmonic sources = 55 %		

Table 6.4: Scenario Three

Scenario three: 304 Harmonic sources		
Harmonic Source	**No. of Units**	**Power Capacities**
Electric Vehicle Charger (EVC)	108	5 %
Converter	93	5 %
Wind Turbine (WT)	84	40 %
Photovoltaic Generator (PG)	19	20 %
Total power capacities of harmonic sources = 70 %		

Table 6.5: Scenario Four

Scenario four: 541 Harmonic sources		
Harmonic Source	**No. of Units**	**Power Capacities**
Electric Vehicle Charger (EVC)	433	15 %
Converter	93	5 %
Wind Turbine (WT)	84	40 %
Photovoltaic Generator (PG)	19	20 %
Total power capacities of harmonic sources = 80 %		

All the scenarios comply with the following assumptions and rules:

- The power capacities of wind turbines (WTs) and photovoltaic generators (PGs) are defined as power generation capacities.

- The number and power capacity of converter are fixed.
- The position and number of both WTs and PGs are fixed. With increasing of their power generation capacities the total power generation capacities of all generators raise.
- All loads (linear and non-linear loads) are assumed fully loaded.
- The wind turbines and photovoltaic generators are connected in parallel respectively. Hence, with increasing of their power generation capacities, their injection currents (fundamental and higher harmonic orders) are increased in the same proportion.
- The number and location of electric vehicle chargers (EVCs) are randomly generated until it reaches the proposed power capacity rate.
- The total power generation capacities of WTs and PGs are defined as the percentage of their total active powers to the total active powers of all generators respectively.
- The total power capacities of EVCs and converters are defined as the percentage of their total active powers to the total active powers of all loads respectively.

6.4 Results And Discussions

As mentioned in the introduction, the author is interest in investigating the effects of changing harmonic capacities to the harmonic penetration. It is achieved by changing power capacities of harmonic sources following three aspects:

- Change capacity of wind energy (combined scenario one and two): only the power capacity of wind turbines (WTs) is increased from 20 % to 40 %.
- Change capacity of multiple renewable energy (i.e. wind and solar) (combined scenario one and three): the power capacities of both wind turbines (WTs) and photovoltaic generators (PGs) are increased from 20 % to 40 % and from 5 % to 20 % respectively.

- Change capacity of electric vehicle charger (EVC) (combined scenario three and four): only the power capacity of EVC is increased from 5 % to 15 %.

Therefore, the author presented and discussed the results through these three aspects in this section.

6.4.1 Change Capacity Of Wind Energy

In this section, results achieved from scenario one and two are presented and compared to investigate the effects of changing power capacities of WTs to the harmonic penetration. The number, position and power capacities of PGs, converters and EVCs are fixed respectively. The power capacities of WTs increase by 20 %, from 20 % to 40 %. Their fundamental and higher harmonic injection currents increase by 20 % accordingly.

Computing Time And Number Of Iterations

The results of computing time and number of iterations are listed in Table 6.6 below.

Table 6.6: Computing time and iterations

Scenarios	One	Two
Computing time (s)	45.51	45.74
Iterations	5	5

The computing time and number of iterations in two different scenarios are counted independently during the calculation. The computing time excludes the time consumption of data import and export. It indicates that the numbers of iterations stay at 5 in the two different scenarios. However, there are slightly differences of computing time between each scenario, and it rises with increasing of power capacities of WTs. Hence, when the power capacities of WTs increase, it may not affect the number of iterations, but the computing time can be affected.

Voltage Magnitudes

The results of rms values of voltage magnitudes achieved from two different scenarios are illustrated in Figure 6.4, 6.5, 6.6 and 6.7 respectively.

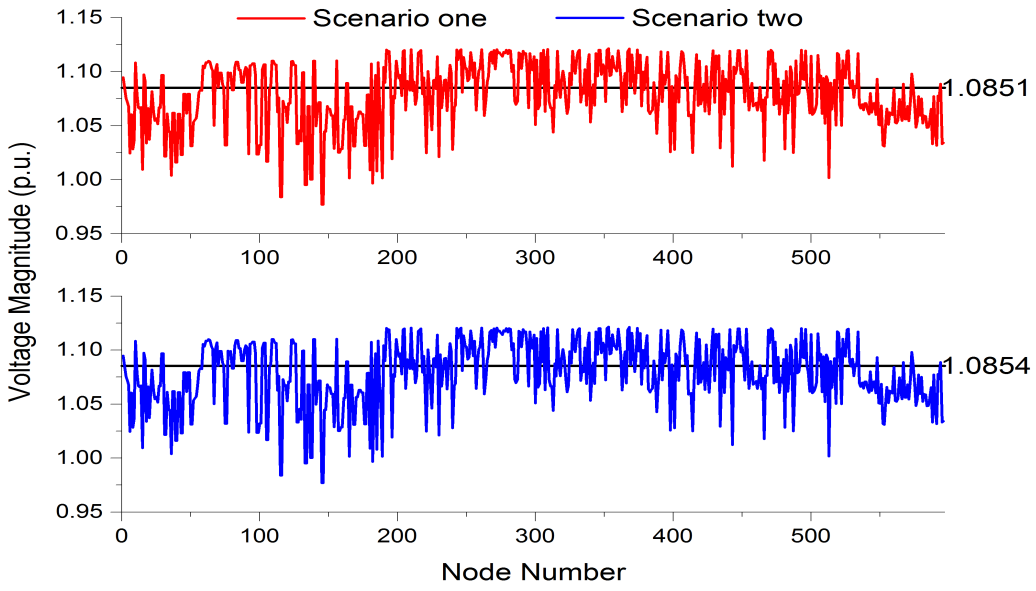

Figure 6.4: The rms values of voltage magnitudes from two different scenarios (part 1)

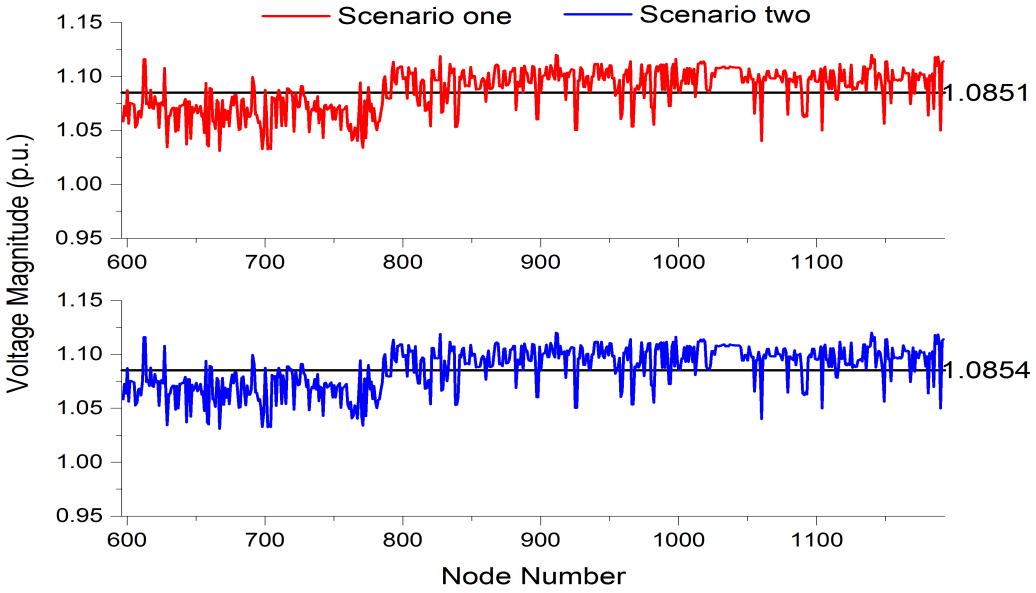

Figure 6.5: The rms values of voltage magnitudes from two different scenarios (part 2)

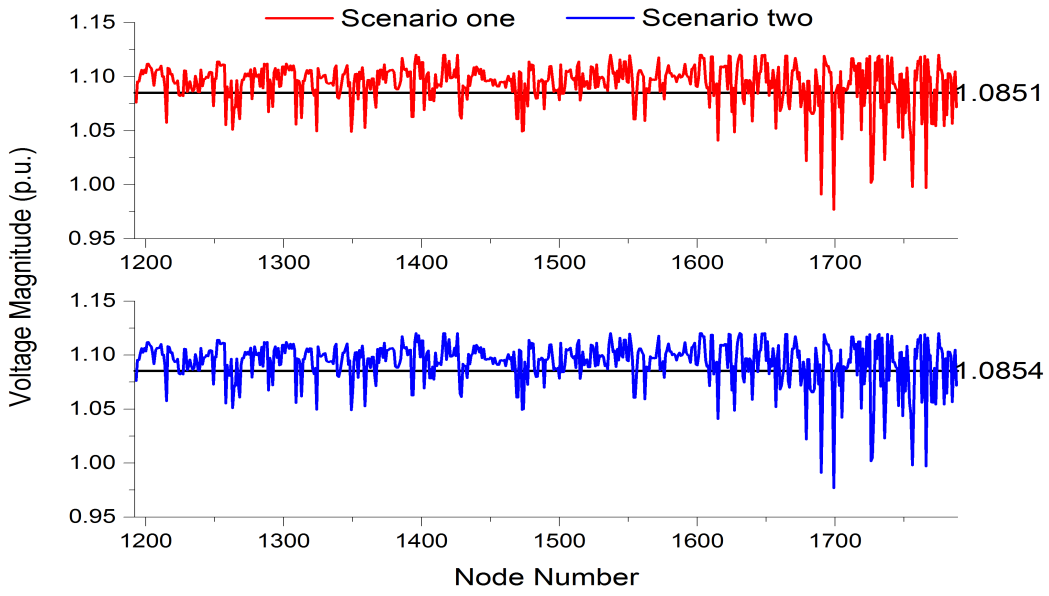

Figure 6.6: The rms values of voltage magnitudes from two different scenarios (part 3)

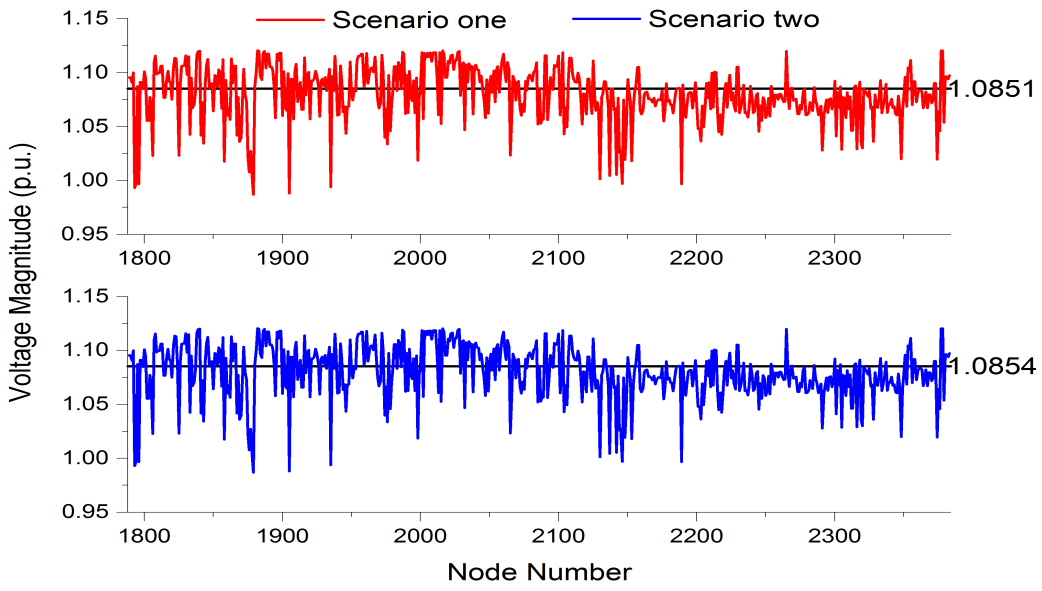

Figure 6.7: The rms values of voltage magnitudes from two different scenarios (part 4)

The results of rms values of voltage magnitudes achieved from two different scenarios are illustrated in two different layers with different colours, in order to investigate the difference and varying regularity. The black straight line in each layer represents the average value of each scenario in per unit. However, it is too many to show the results of 2383 buses clearly in a single diagram. Hence, the diagram is separated into four parts. Part 1 represents the results from bus 1 to bus 596. Part 2 indicates the results from bus 597 to bus 1192. The results of bus 1193 to bus 1788 and bus 1789 to bus 2383 are shown in part 3 and part 4 respectively. These four parts have same vertical scope.

The results show that the rms values of bus voltage magnitudes achieved from two different scenarios all fluctuate between $0.9770p.u.$ and $1.1277p.u.$. Most of them assemble around their average values, $1.0851p.u.$ and $1.0854p.u.$ respectively. According to the above figures, two different scenarios almost have the same result waveforms. Though their average values are different, the difference is only $0.0003p.u.$, which is small enough to be ignored. Hence, it may have no influence on the rms values of bus voltage magnitudes with increasing of power capacities of WTs. The maximum and minimum values of the rms values of voltage magnitudes of each scenario are shown in Table 6.7 below.

Table 6.7: The maximum and minimum rms values of bus voltage magnitudes

Scenarios	One		Two	
	Bus	Mag. (p.u.)	Bus	Mag. (p.u.)
Max	353	1.1215	368	1.1277
Min	145 146	0.9770	1699	0.9773

It shows that each scenario has different minimum and maximum values. They occur on different buses either. However, the result differences are only in the order of 10^{-4} and 10^{-5} respectively.

In order to investigate slight result differences between each scenario, the numerical comparison is required. The result difference between scenario one and scenario two is considered as the error. It is represented by ERROR_1. When the absolute value of ERROR_1 is less than $0.01p.u.$, the error is considered as negligible and the results

of scenario one and two are considered as identical. The results achieved from scenario one is regarded as reference values. If the result of ERROR_1 is positive, it represents that the result of scenario two is larger than that of scenario one. Hence, the values of 32 buses are changed when increasing the power capacities of WTs. The result differences between each scenario are illustrated in Figure 6.8 and Table 6.8 below.

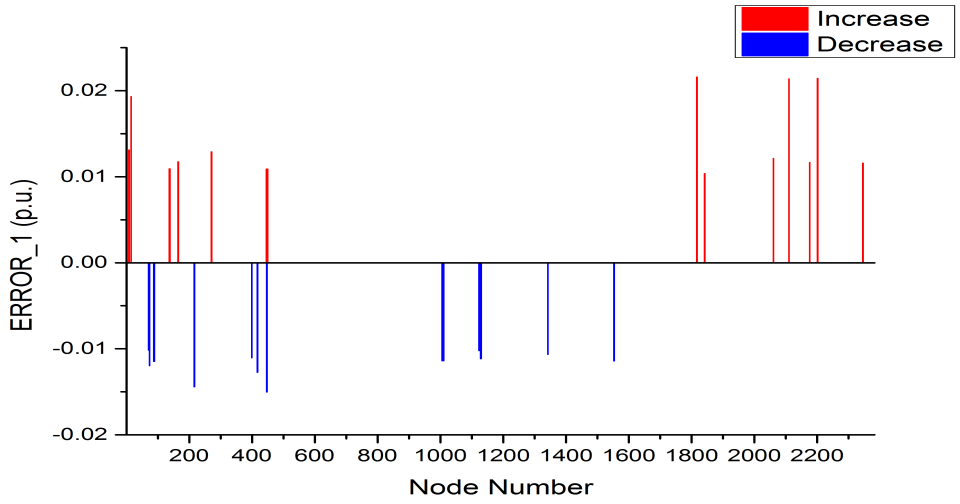

Figure 6.8: The result differences between two different scenarios

Table 6.8: Summary of result differences between two different scenarios

No. of increasing: 16				No. of decreasing: 16			
Maximum		Minimum		Maximum		Minimum	
Bus	Mag. (p.u.)	Bus	Mag. (p.u.)	Bus	Mag. (p.u.)	Bus	Mag. (p.u.)
1817	0.0216	1842	0.0104	447	-0.0150	1123	-0.0102

With increasing of the power capacities of WTs the values of 16 buses increase. The values of another 16 buses decrease. They are illustrated in red and blue rectangular bars respectively as shown in Figure 6.8. The rms value of voltage magnitude on bus 1817 has a great influence when increasing the power capacities of WTs. It may be relative to its fundamental and harmonic bus voltage magnitudes. The result difference of its fundamental voltage magnitude is only $0.00026 p.u.$ which is small enough to be ignored. The values of harmonic voltage magnitudes are compared in Figure 6.9 below.

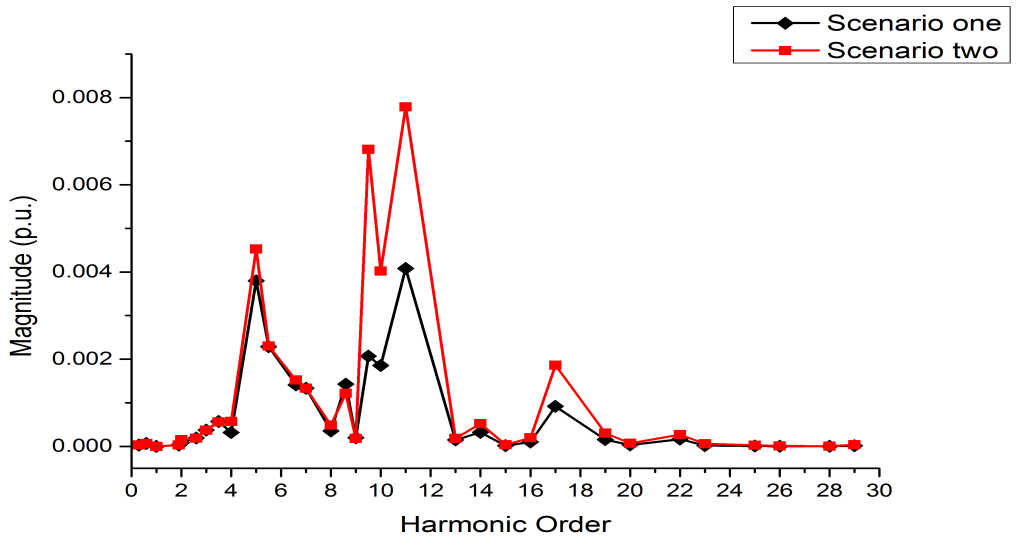

Figure 6.9: The result comparison of harmonic voltage magnitudes

The harmonic emission currents contain thirty-two harmonic orders (including the fundamental frequency). Hence, the results of the harmonic bus voltage magnitudes also have thirty-two harmonic orders (including the fundamental frequency). The values of the fundamental voltage magnitudes (the 1^{st} harmonic order) in both scenarios are not considered and are assumed to be zero. The result shows that the harmonic voltage magnitudes on the bus 1817 increase when raising the power capacities of WTs, especially in the 5^{th}, 9.5^{th}, 10^{th}, 11^{th} and 17^{th} harmonic orders. Its total harmonic voltage magnitude is changed significantly, which is from $0.1554 p.u.$ to $0.3276 p.u.$. Therefore, the great change of total harmonic voltage magnitude leads to the maximum change of rms value of voltage magnitude on the bus 1817.

However, it encounters a problem: is it influenced by any neighbourhood buses that are connected to WTs, as the power capacities and harmonic injection currents of only WTs are changed in this section? In order to achieve the answer, three levels of neighbourhood connection diagram of the bus 1817 is illustrated in Figure 6.10 below.

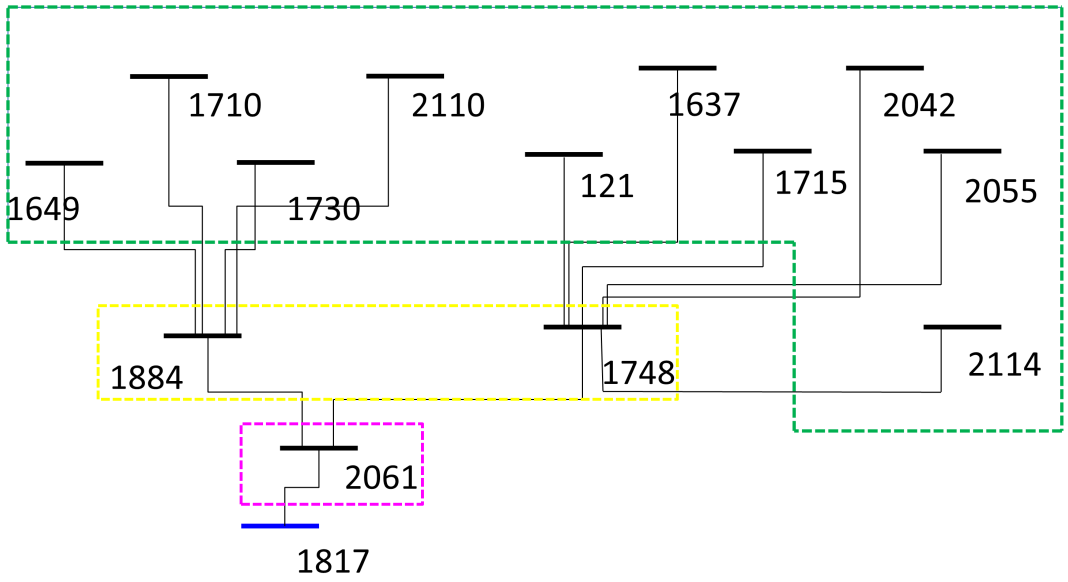

Figure 6.10: The neighbourhood connection diagram of the bus 1817

As shown in the above figure, the first neighbourhood, second neighbourhood and third neighbourhood buses of the bus 1817 are marked in pink, yellow and green dashed box respectively. The bus 1817 is highlighted in blue. The other harmonic source buses that are connected to WTs are highlighted in red. However, there is no WTs connected to the neighbourhood buses of the bus 1817. Hence, the maximum change of rms value of voltage magnitude on the bus 1817 is not influenced by any neighbourhood buses connected to WTs.

As mentioned in chapter 4, the harmonic (excluding fundamental frequency) bus voltage magnitudes are obtained using admittance-matrix-based equation $\bar{I}^{(h)} = \overline{Y}^{(h)}\overline{V}^{(h)}$ directly. The harmonic injection current of linear buses in vector $\bar{I}^{(h)}$ equals zeros, while it equals $-g_m^{(h)}$ for non-linear buses (where $g_m^{(h)}$ represents the harmonic emission current of harmonic source on non-linear bus m). The diagonal elements of power

system harmonic admittance matrix $\overline{Y}^{(h)}$ are related to harmonic load admittance that varies with different fundamental bus voltage magnitudes. Both harmonic injection currents, $-g_m^{(h)}$, and $\overline{Y}^{(h)}$ are changed with increasing of the power capacities of WTs. Therefore, the harmonic bus voltage magnitudes should be changed. However, the variation is irregular. The harmonic sources may not generate great influence on their neighbourhood buses.

Total Voltage Harmonic Distortion (THDv)

The results of the total harmonic voltage distortion (THDv) from two different scenarios are illustrated in Figures 6.11, 6.12, 6.13 and 6.14 below.

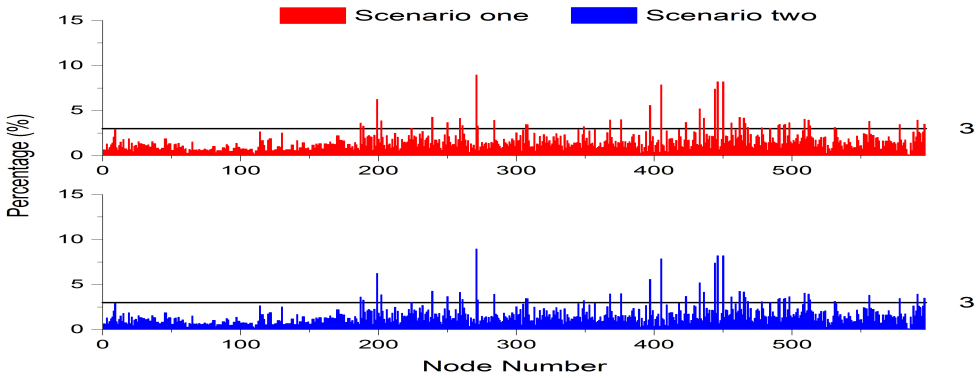

Figure 6.11: THDv of two different scenarios (part 1)

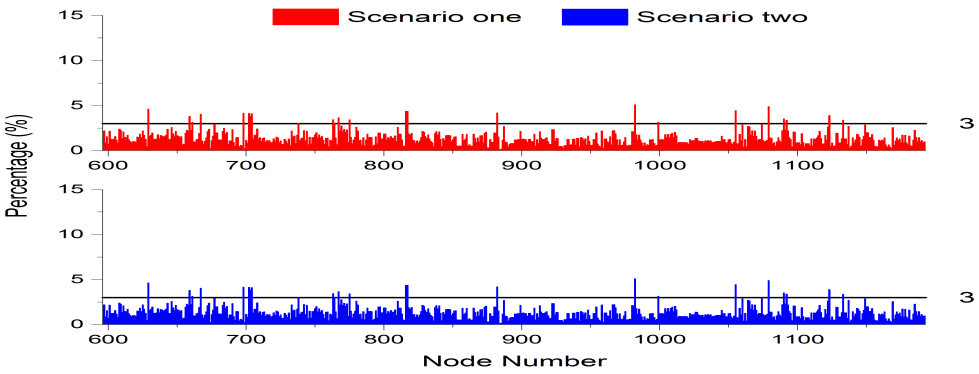

Figure 6.12: THDv of two different scenarios (part 2)

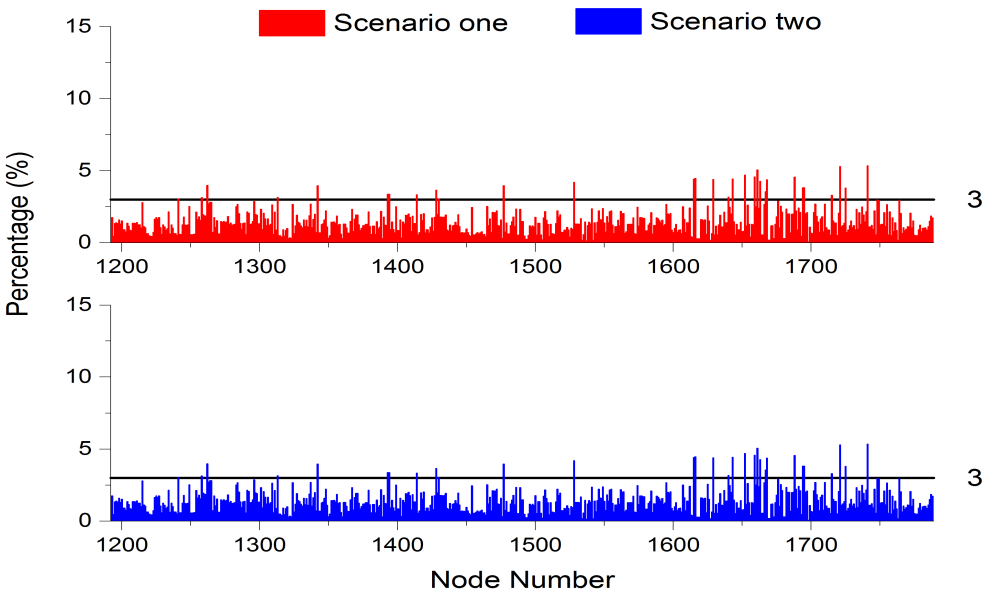

Figure 6.13: THDv of two different scenarios (part 3)

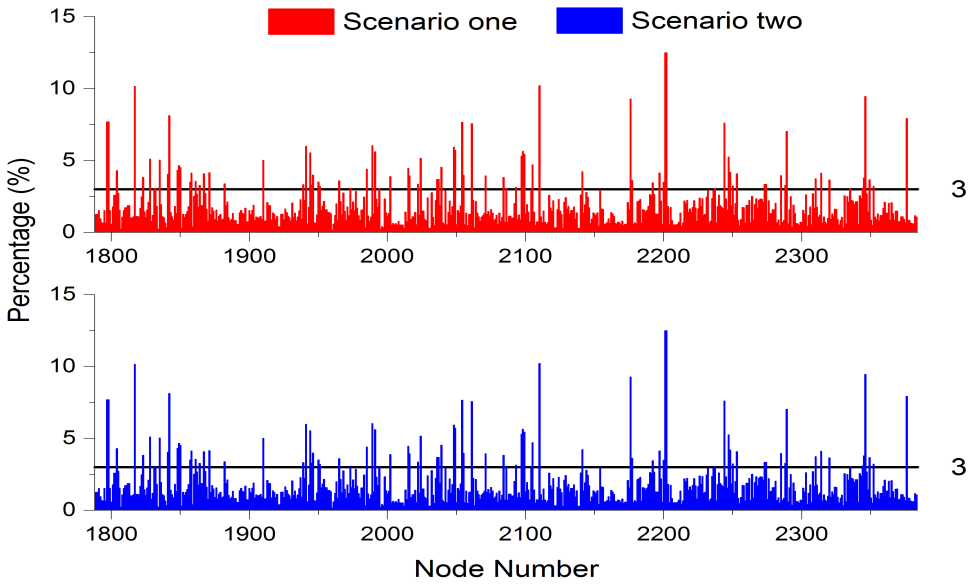

Figure 6.14: THDv of two different scenarios (part 4)

They are also illustrated in four parts in order to investigate and compare the results clearly. The results achieved from different scenarios are illustrated in different panels with different colours. The black horizontal straight line in each panel represents the THDv limit level, 3% [9], derived from Engineering Recommendation G5/4 in chapter 2 in percentage. Two scenarios have the same vertical scope in each figure in order to compare the results and investigate the effects of increasing of the power capacities of WTs. All the results achieved from each scenario can be categorized into four penetration levels: under 3 %, between 3 % and 6 %, between 6 % and 10 % and over 10 %. Therefore, the numbers of THDv values in different penetration levels are summarized in Table 6.9.

Table 6.9: The summary of numbers of THDv values in different penetration levels

Categories	No. of Buses	
	Scenario one	Scenario two
0 - 3 %	2198	1570
3 - 6 %	164	616
6 - 10 %	17	143
$>$ 10%	4	54
$>$ 3%	185	813

The average and maximum values of the THDv of two scenarios are shown in Table 6.10.

Table 6.10: The maximum and average values of the THDv

Scenarios	One	Two
Average (%)	1.55	2.97
Max. (%)	12.48	23.99

Figures 6.11 to 6.14 denote that two scenarios have nearly the same waveforms. It is difficult to find out any result differences between two scenarios according to the figures. However, the average and maximum values raise from 1.55 % to 2.97 % and from 12.48 % to 23.99 % respectively when the power capacities of WTs increase by 20 %, according to Table 6.10. In addition, Table 6.9 indicates that the numbers of THDv values under 3 % decrease but increase in other three penetration levels when the power capacities of WTs increase. Also, the total numbers of buses whose THDv values exceed the level of limit, 3 % [9], increase from 185 to 813. Hence, the THDv values of most buses encounter a great influence by changing the power capacities of

harmonic sources (WTs).

Therefore, several buses connected to WTs are selected to investigate the influence. They are buses 192, 2248 and 2376. Their THDv values in different scenarios are shown in Table 6.11 below.

Table 6.11: THDv values of selected buses in two scenarios

Bus	Scenario one	Scenario two
192	2.12 %	5.96 %
2248	4.18 %	8.19 %
2376	7.92 %	15.23 %

As shown in Table 6.11, the results of THDv on these buses are in three different penetration levels in scenario one: 0 - 3 %, 3 - 6 % and 6 - 10 % respectively. However, after increasing the power capacities of WTs, their values raise and move to the next penetration level respectively. In order to investigate the influence on their neighbourhood buses, three levels of neighbourhood connection diagram of buses 192, 2248 and 2376 are illustrated in Figures 6.15 to 6.19.

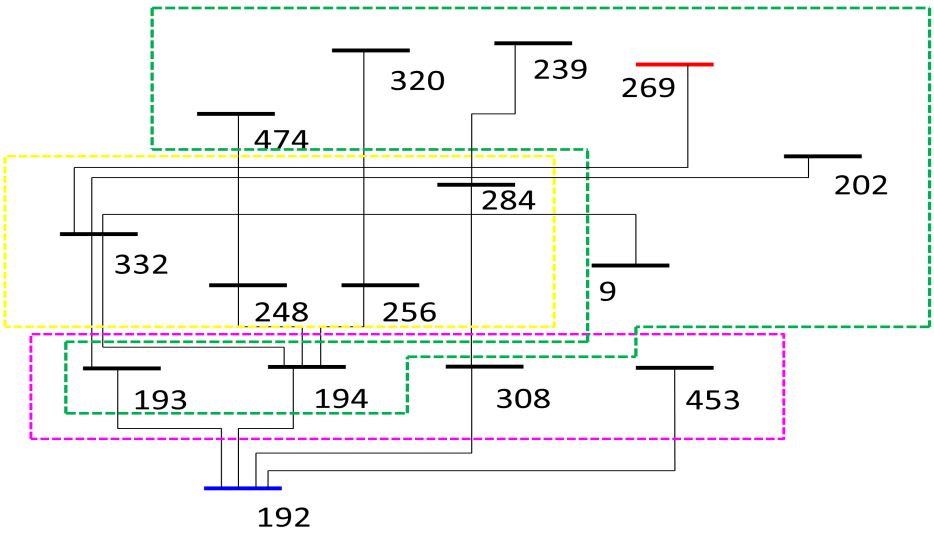

Figure 6.15: The neighbourhood connection diagram of the bus 192

The first neighbourhood, second neighbourhood and third neighbourhood buses are marked in pink, yellow and green dashed box respectively. The buses 192, 2248 and 2376 are highlighted in blue. The harmonic source buses connected to WTs are highlighted in red.

The THDv values of neighbourhood buses of the bus 192 in two different scenarios are shown in Table 6.12.

Table 6.12: THDv values of neighbour buses of the bus 192 in percentage

Bus	193	194	308	453	332	284	248
Scenario one	2.24	2.11	3.44	2.16	2.18	3.94	2.33
Scenario two	6.29	5.98	9.95	6.06	6.11	11.37	6.03
Bus	256	474	320	239	9	269	202
Scenario one	2.25	2.14	2.34	4.27	2.94	1.17	3.88
Scenario two	6.40	5.18	6.59	12.38	6.96	3.20	11.35

The maximum value in each scenario is highlighted in pink and yellow respectively. Hence, the maximum values both occur on the bus 239, which is the third neighbourhood bus of the bus 192. In order to investigate the result variation of each neighbourhood bus with increasing the power capacities of WTs, the numerical comparison is required. ERROR_1 is assumed to represent the result differences between two scenarios. If it is positive, it represents that the result increases; otherwise, the result decreases. Hence, the result differences are illustrated in Figure 6.16 below.

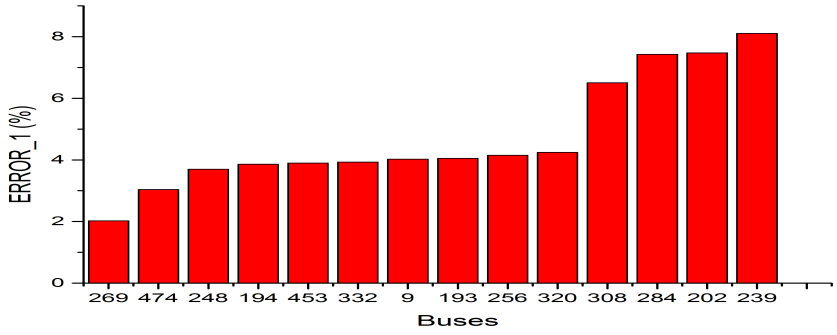

Figure 6.16: The result differences of neighbourhood buses of the bus 192

It indicates that all the results are positive. It represents that the THDv values of all these buses increase when the power capacities of WTs raise. It has a great influence on buses 308, 284, 202 and 239 as they generate larger result differences. Buses 308 and 284 are in the first and second neighbourhood area respectively. However, buses 202 and 239 are in the third neighbourhood area. Though their THDv values change significantly, it may not influenced by the bus 192. It is because that buses 202 and 239 may connect to other harmonic source buses (i.e. WTs) which are not shown in Figure 6.15. Though the bus 269 is also harmonic source connected bus, it has less influence (i.e. the result difference is only 2 %).

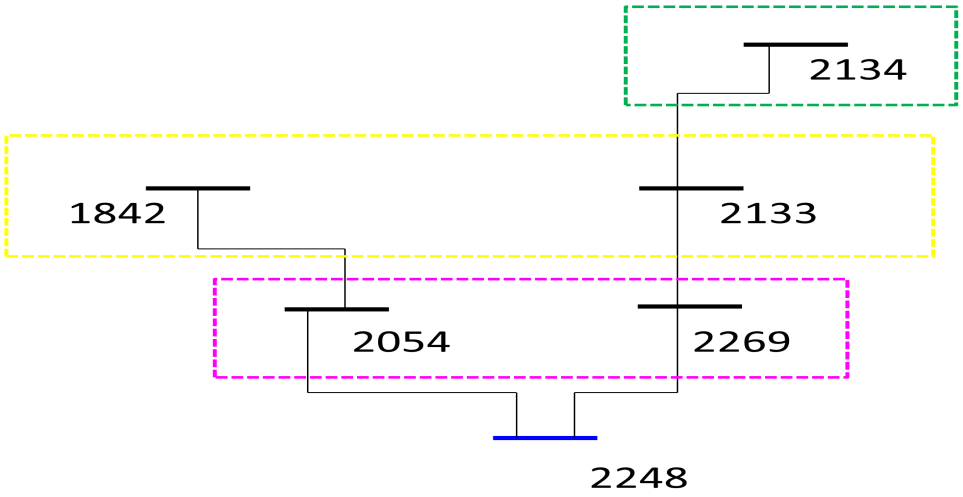

Figure 6.17: The neighbourhood connection diagram of the bus 2248

The THDv values of neighbourhood buses of the bus 2248 in two different scenarios are shown in Table 6.13 below.

Table 6.13: THDv values of neighbourhood buses of the bus 2248 in percentage

Bus	2054	2269	1842	2133	2134
Scenario one	7.65	2.23	8.12	1.53	1.53
Scenario two	15.23	4.06	16.18	2.51	2.51

The maximum value in each scenario is also highlighted in pink and yellow respectively. Therefore, the maximum values both occur on the bus 1842, which is in the second neighbourhood area. The result differences are illustrated in Figure 6.18.

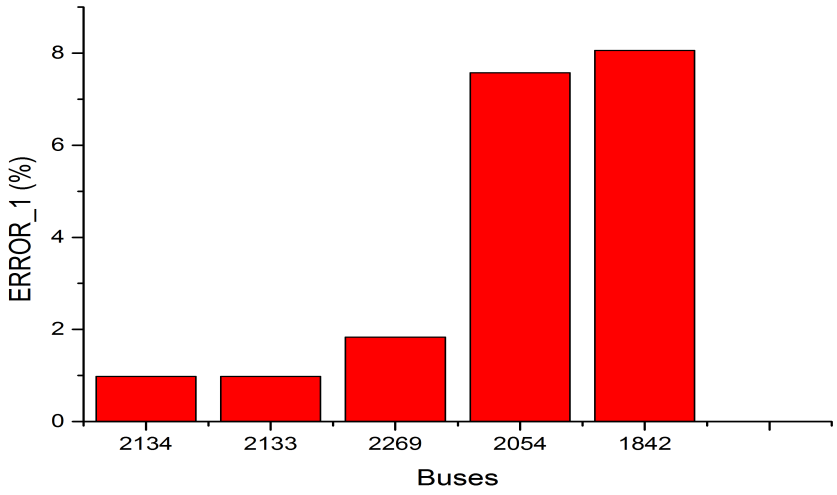

Figure 6.18: The result differences of neighbourhood buses of the bus 2248

All the results are positive. Hence, the THDv values of all neighbourhood buses of the bus 2248 increase when the power capacities of WTs raise. It has a great influence on the values of buses 1842 and 2054 which are in the second and first neighbourhood area respectively. Their values are 16.18 % and 15.23 % respectively, which are both in the fourth penetration level ($>$ 10%). Though the bus 2269 is also the first neighbourhood bus of the bus 2248, it has less influence than the bus 2054. On the right-hand-side branch of the bus 2248 as shown in Figure 6.17, the influence on the values of THDv to each neighbourhood bus weakens with increasing of the distance to the bus 2248.

The THDv values of neighbourhood buses of the bus 2376 in two different scenarios are shown in Table 6.14 below. The maximum value in each scenario is highlighted in pink and yellow colour respectively. In order to investigate the result variation of each neighbourhood bus with increasing of the power capacities of WTs by 20 %, the numerical comparison is required as well. Hence, the values of result differences between two scenarios are illustrated in Figure 6.20.

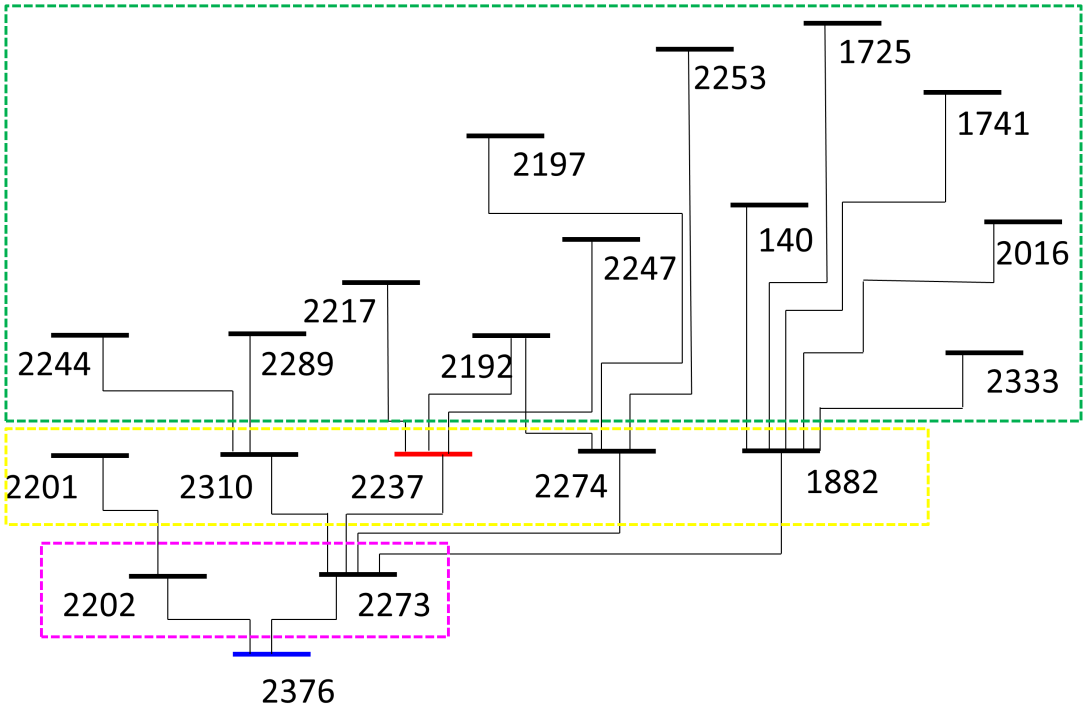

Figure 6.19: The neighbourhood connection diagram of the bus 2376

Table 6.14: THDv values of neighbourhood buses of the bus 2376 in percentage

Bus	2273	2202	2201	1882	2274	2237	2310	2244	2289	2217
Scenario one	3.33	12.48	12.48	3.37	3.34	3.04	3.73	7.59	7.02	2.22
Scenario two	6.47	23.99	23.99	6.45	6.48	5.86	7.26	14.16	13.55	4.27
Bus	2192	2247	2197	2253	140	1725	1741	2016	2333	
Scenario one	3.44	5.25	4.12	4.07	0.58	3.81	5.36	3.93	2.49	
Scenario two	6.66	10.01	7.92	7.89	1.00	7.28	10.23	7.51	4.78	

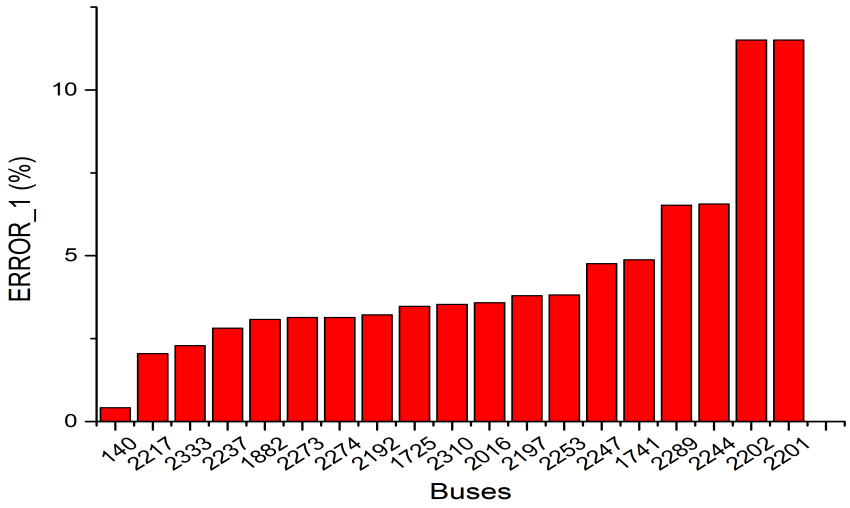

Figure 6.20: The result differences of neighbourhood buses of the bus 2376

Table 6.14 indicates that the maximum values of two scenarios are both on the buses 2201 and 2202. In addition, the THDv values of nearly 37 % neighbourhood buses reach to the fourth penetration level ($>$ 10%) after increasing of the power capacities of WTs. Figure 6.20 shows that the THDv values of buses 2202 and 2201 change significantly, whose result differences reach to 11.5 %. They are both on the first left-hand-side branch, but are separated in the first and second neighbourhood area of the bus 2376 respectively. However, the other first and second neighbourhood buses have less influence than several fourth neighbourhood buses (i.e. buses 2289, 2244, 2247 and 1741). It may be because that those fourth neighbourhood buses were influenced by other connected harmonic source (WTs) buses which were not shown in Figure 6.20. Though the bus 2237 is also harmonic source connected bus, it also has less influence when the power capacities of WTs increase by 20 %. The bus 140 which is in the fourth neighbourhood area has smallest influence on the value of THDv.

Harmonic Powers

The total active and reactive powers at both sending and receiving ends (Ptotals, Ptotalr, Qtotals and Qtotalr) and the total power losses on each branch (Ptotalloss) are shown in Figures 6.21 to 6.25.

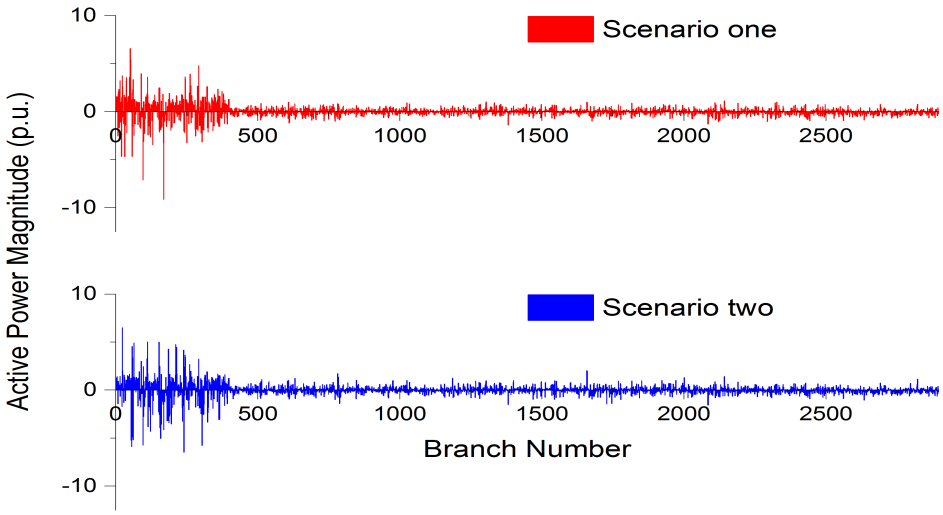

Figure 6.21: Total active powers at the sending end

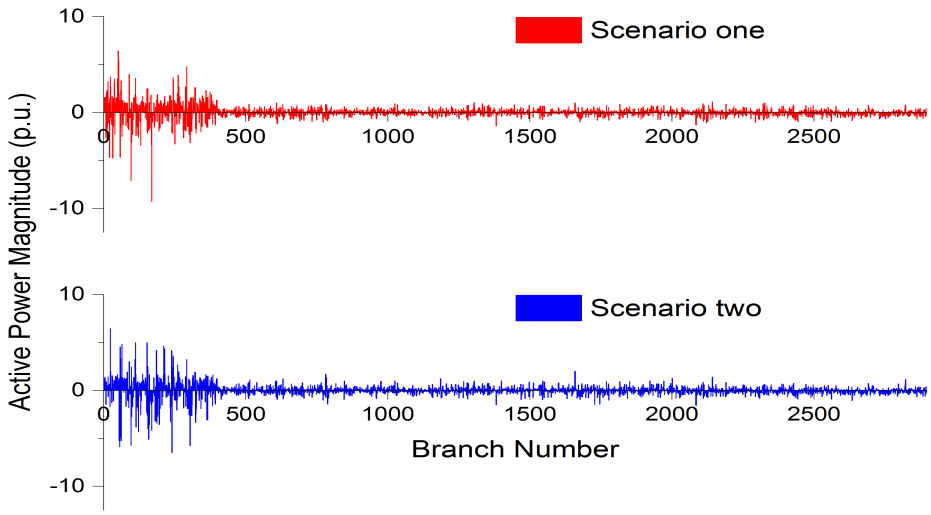

Figure 6.22: Total active powers at the receiving end

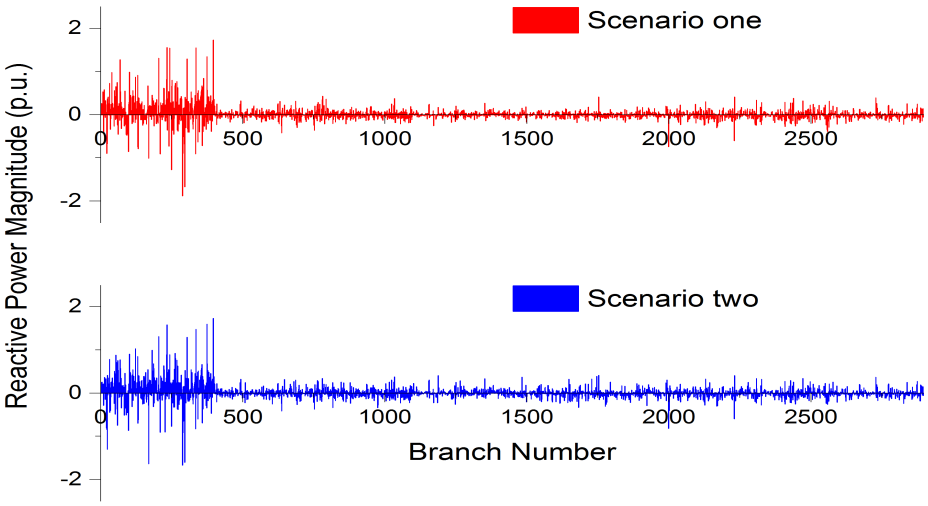

Figure 6.23: Total reactive powers at the sending end

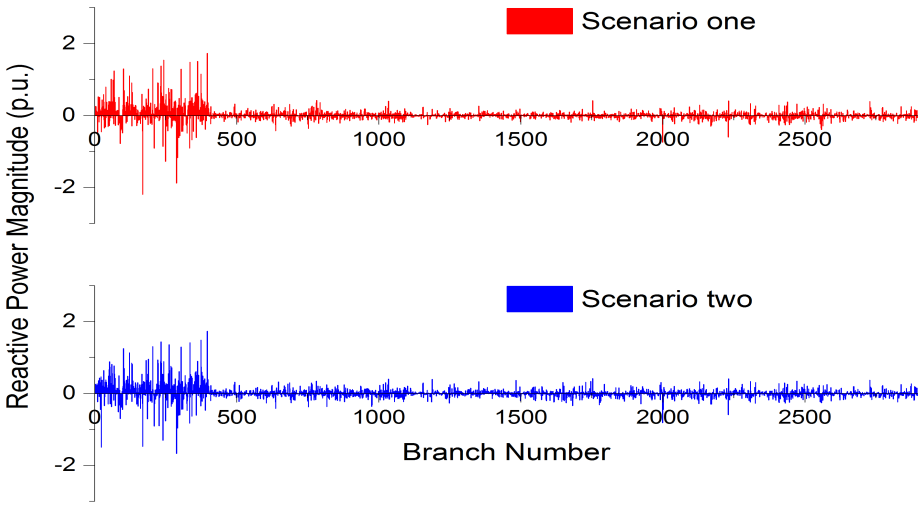

Figure 6.24: Total reactive powers at the receiving end

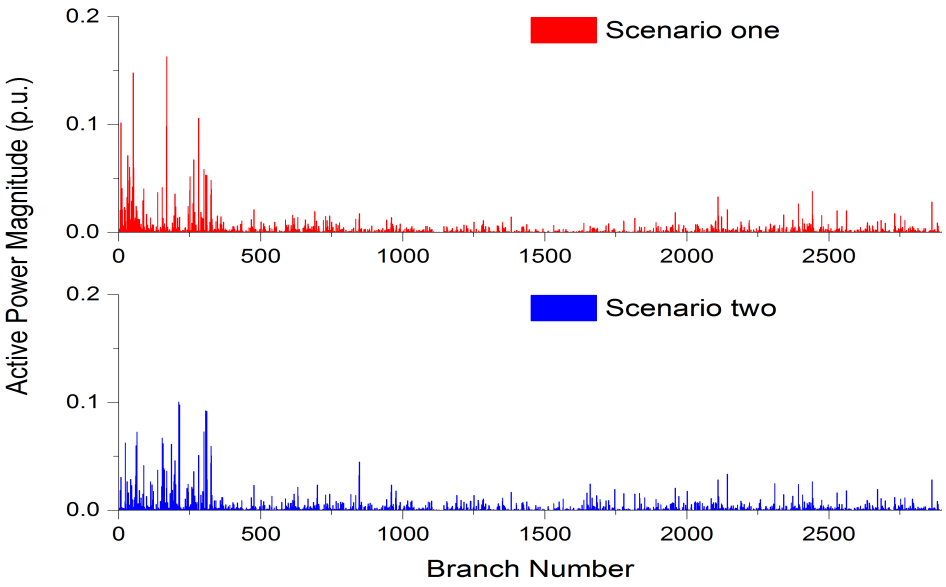

Figure 6.25: Total power losses on each branch

The results achieved from two different scenarios are illustrated in two layers with red and blue colour respectively in each diagram. Each scenario has the same vertical scope in each result category. The results of the Ptotals, Ptotalr, Qtotals and Qtotalr contain both positive and negative values. As mentioned in chapter 5, for the total active powers, if the values are positive, it denotes that the active powers flow from the sending ends to the receiving ends; otherwise, the active powers flow in the opposite way. For the total reacitve powers, if the results are positive, it means that the buses (sending and receiving ends) generate reactive powers; otherwise, they absorb reactive powers. The results show that the larger total active and reactive powers at both sending and receiving ends and power losses on each line are generated on the first 400 transmission lines. It means more powers are transmitted on these lines during the harmonic penetration. The maximum values of these result categories are shown in Table 6.15 below.

Table 6.15: The maximum values of the Ptotals, Ptotalr, Qtotals, Qtotalr and Ptotalloss

Scenarios	Ptotals (p.u.)	Ptotalr (p.u.)	Qtotals (p.u.)	Qtotalr (p.u.)	Ptotalloss (p.u.)
One	-9.1374	-9.3004	-1.8810	-2.1932	0.1630
Two	6.4991	-6.4998	1.7306	1.7303	0.1003

Most of result waveforms that calculated from two different scenarios are nearly the same, except Ptotalloss. Its top three values decrease with increasing of the power capacities of WTs. Hence, it represents that increasing of the power capacities of WTs may have less effects to the total active and reactive powers at both sending and receiving ends, but more effects to the total power loss on each branch. The reason is that they are basically related to the fundamental bus voltages, which are changed. In order to prove the above conclusion, the differences between each scenario are numerically illustrated in Figures 6.26 to 6.30, and the maximum values of them are shown in Table 6.16 below.

Table 6.16: The maximum difference values of the Ptotals, Ptotalr, Qtotals, Qtotalr and Ptotalloss

	Ptotals (p.u.)	Ptotalr (p.u.)	Qtotals (p.u.)	Qtotalr (p.u.)	Ptotalloss (p.u.)
ERROR_1	9.2027	9.2038	-1.1234	-1.1113	-0.1467

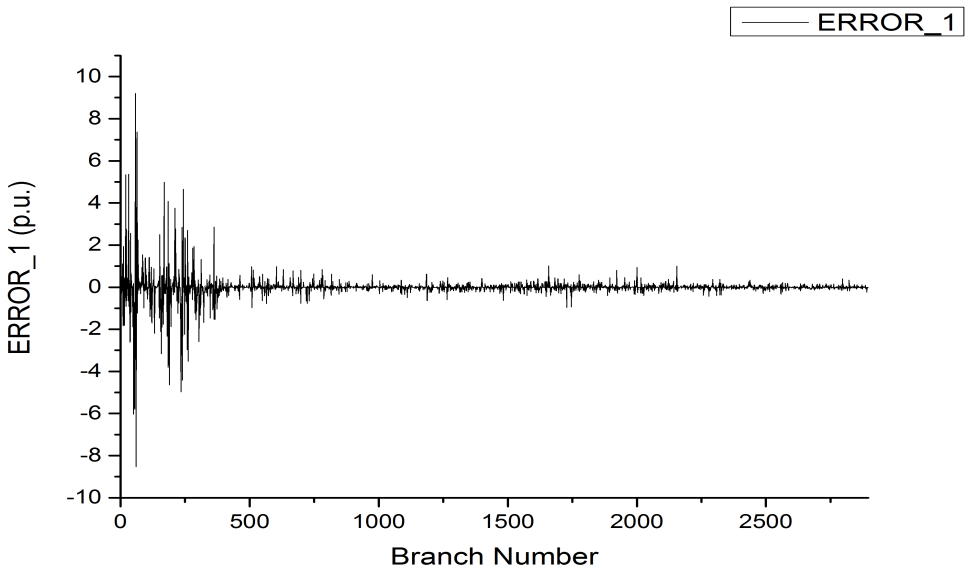

Figure 6.26: Total active powers at the sending end

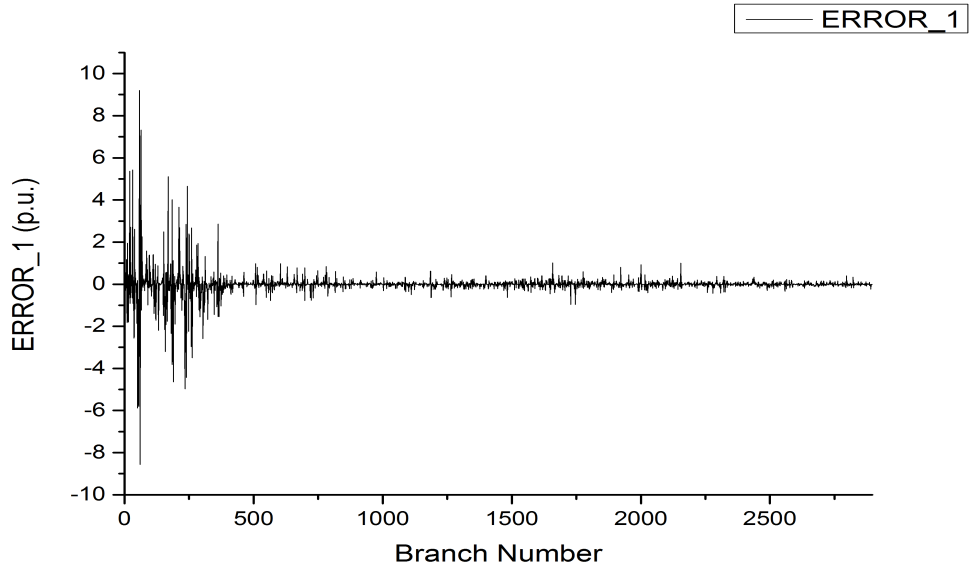

Figure 6.27: Total active powers at the receiving end

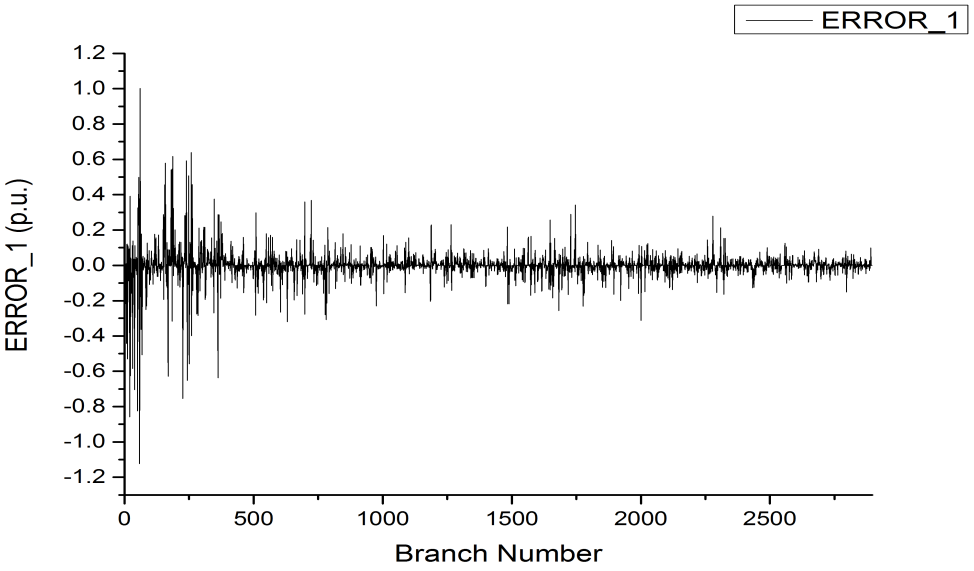

Figure 6.28: Total reactive powers at the sending end

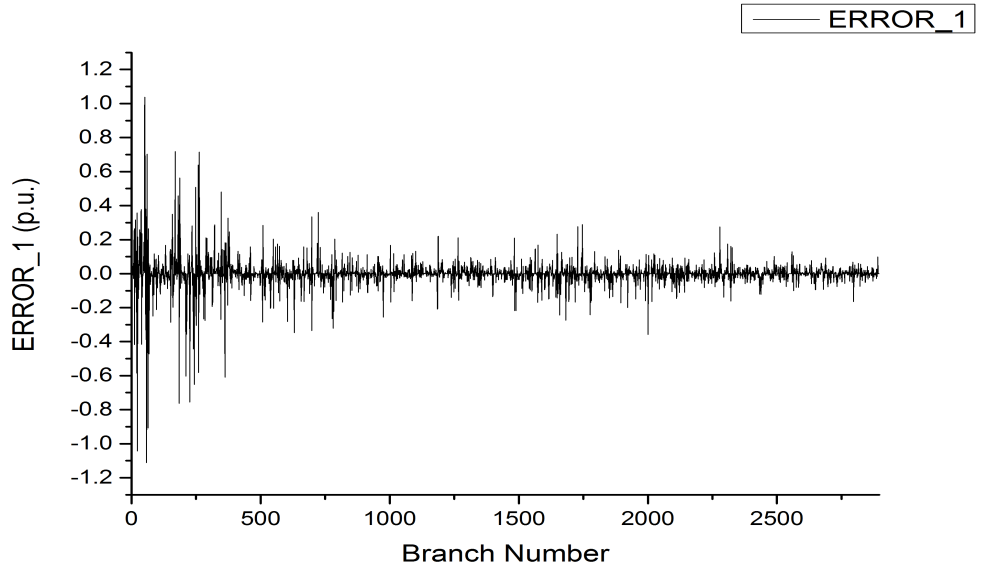

Figure 6.29: Total reactive powers at the receiving end

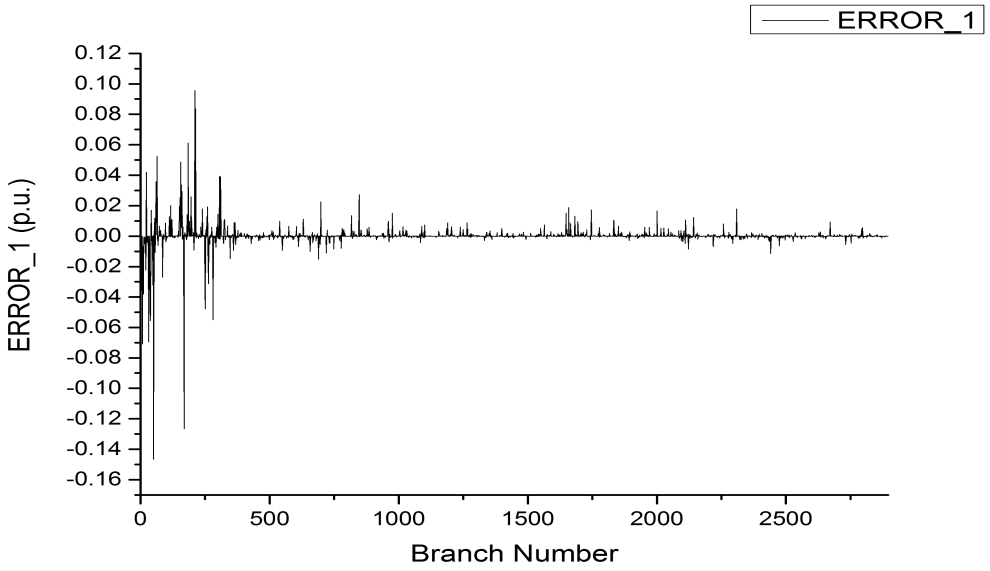

Figure 6.30: Total power losses on each branch

ERROR_1 in the figures above represent the result differences between scenario one and two. If the results are positive, it means the value achieved by scenario two is larger than that of scenario one. When the absolute value of ERROR_1 is less than $0.01p.u.$, the result difference is considered as negligible and the results of two scenarios are considered as identical. Hence, raising of the power capacities of WTs influences 2041 lines of Ptotals, 2041 lines of Ptotalr, 1618 lines of Qtotals, 1629 lines of Qtotalr and 79 lines of Ptotalloss. The greatest influence occurs on lines 58, 58, 58, 58 and 51 of Ptotals, Ptotalr, Qtotals, Qtotalr and Ptotalloss with increasing of $9.2027p.u.$, $9.2038p.u.$, $-1.1234p.u.$, $-1.1113p.u.$ and $-0.1467p.u.$ respectively, as shown in Table 6.16. Therefore, raising of the power capacities of WTs by 20 % has more influence on total active and reactive powers at both sending and receiving ends and total power loss on each transmission line with no regularity.

6.4.2 Change Capacity Of Multiple Renewable Energy: Wind And Solar

In this section, results achieved from scenario one and three are presented and compared to investigate the effects of changing power capacities of both wind turbines (WTs) and photovoltaic generators (PGs) to the harmonic penetration. The number, position and power capacities of converters and EVCs are constant respectively. The power capacities of WTs and PGs increase by 20 % and 15 %, from 20 % to 40 % and from 5 % to 20 %, respectively. Their fundamental and higher harmonic injection currents of WTs and PGs also increase by 20 % and 15 % respectively.

Computing Time And Number Of Iterations

The results of computing time and number of iterations are listed in Table 6.17 below.

Table 6.17: Computing time and iterations

Scenarios	One	Three
Computing time (s)	45.51	45.89
Iterations	5	5

The computing time and number of iterations in two different scenarios are counted independently during the calculation. The computing time excludes the time consumption of data import and export. It indicates that the numbers of iterations stay on 5 in

two different scenarios. However, there are slightly differences of computing time between each scenario, and it raises with increasing of power capacities of WTs and PGs. Hence, when the power capacities of both WTs and PGs increase, it may not affect the number of iterations, but the computing time can be affected.

Voltage Magnitudes

The results of rms values of voltage magnitudes achieved from two different scenarios are illustrated in two different layers with different colours, in order to investigate the difference and varying regularity. The black straight line in each layer represents the average value of each scenario in per unit. However, it is too many to show the results of 2383 buses clearly in a single diagram. Hence, the diagram is also separated into four parts. Part 1 represents the results from bus 1 to bus 596. Part 2 indicates the results from bus 597 to bus 1192. The results of bus 1193 to bus 1788 and bus 1789 to bus 2383 are shown in part 3 and part 4 respectively. These four parts have same vertical scope, and they are illustrated in Figure 6.31, 6.32, 6.33 and 6.34 respectively.

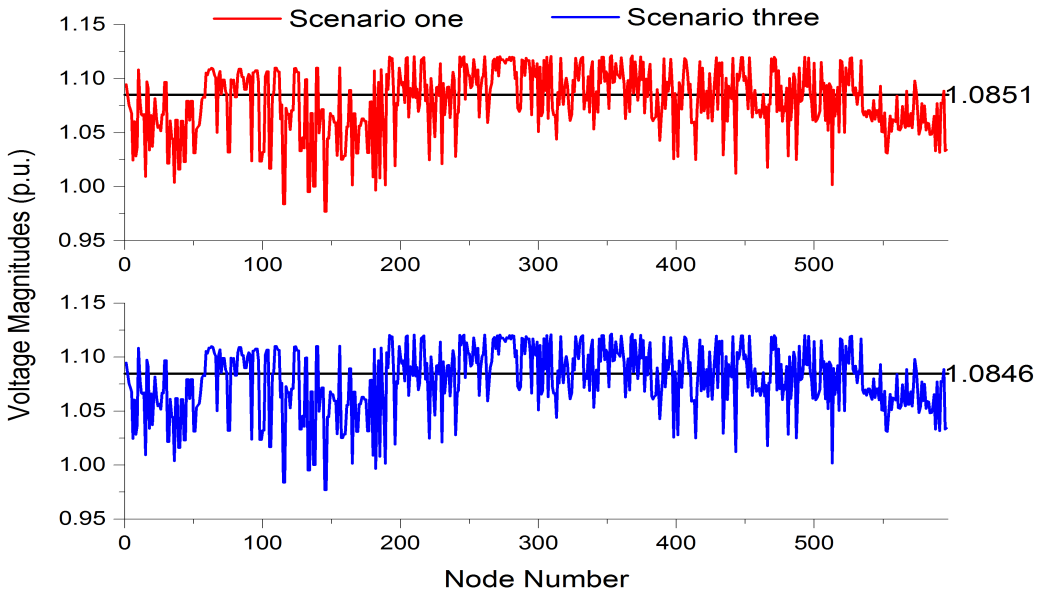

Figure 6.31: The rms values of voltage magnitudes from two different scenarios (part 1)

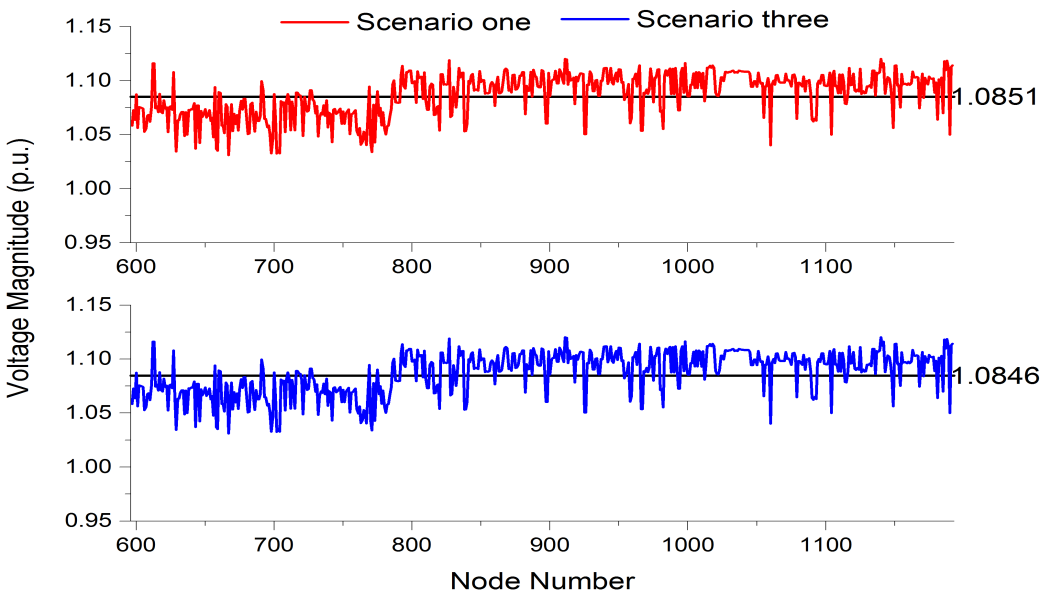

Figure 6.32: The rms values of voltage magnitudes from two different scenarios (part 2)

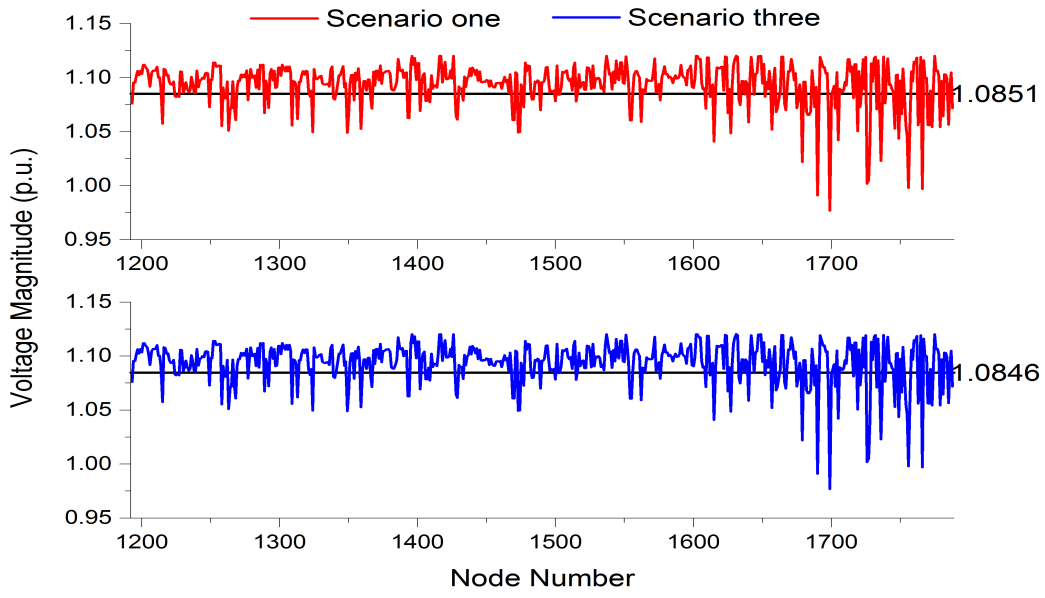

Figure 6.33: The rms values of voltage magnitudes from two different scenarios (part 3)

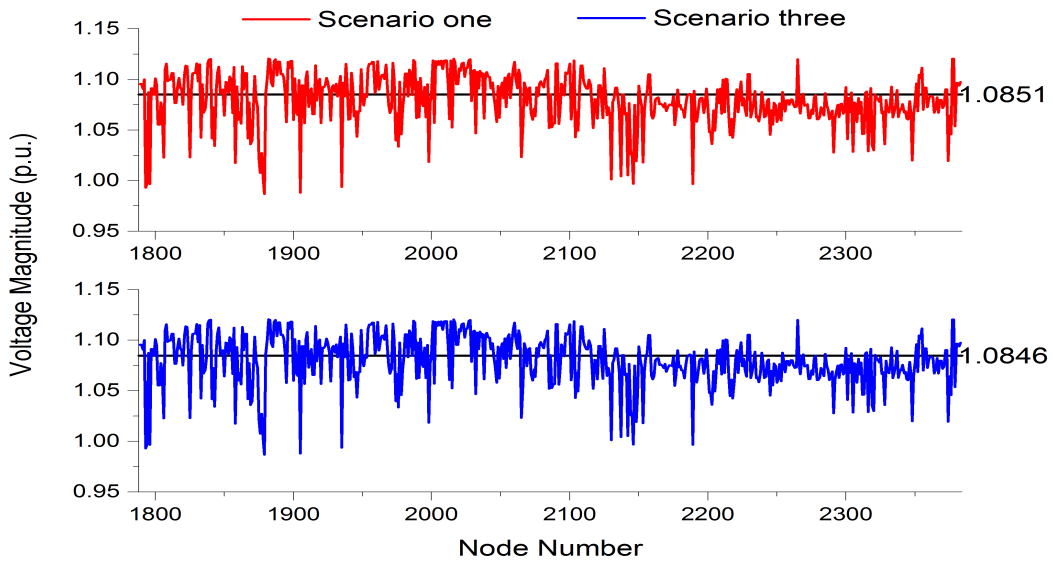

Figure 6.34: The rms values of voltage magnitudes from two different scenarios (part 4)

The results show that the rms values of bus voltage magnitudes achieved from two different scenarios all fluctuate between $0.9546p.u.$ and $1.1420p.u.$. Most of them assemble around their average values, $1.0851p.u.$ and $1.0846p.u.$, respectively. According to the above figures, two different scenarios almost have the same result waveforms. Though the average value decreases to $1.0846p.u.$ when increasing the power capacities of both WTs and PGs, the difference is only $0.0005p.u.$ which is in the order of 10^{-5}. It is small enough to be ignored. Hence, it may have no influence on the rms values of bus voltage magnitudes with increasing of the power capacities of both WTs and PGs. The maximum and minimum values of the rms values of voltage magnitudes of each scenario are shown in Table 6.18 below.

Table 6.18: The maximum and minimum rms values of bus voltage magnitudes

Scenarios	One		Three	
	Bus	Mag. (p.u.)	Bus	Mag. (p.u.)
Max	353	1.1215	1817	1.1420
Min	145 146	0.9770	145 146	0.9546

It shows that each scenario has different minimum and maximum values. However, the minimum values occur on the same buses 145 and 146. The result differences of

maximum and minimum values are both in the order of 10^{-3}.

ERROR_1 is also used to represent the result difference of rms values of voltage magnitudes between scenario one and three. When the absolute value of ERROR_1 is less than $0.01 p.u.$, the result difference is considered as negligible and the results of scenario one and three are considered as identical. Hence, the values of 67 buses are changed when increasing the power capacities of both WTs and PGs. The result differences between each scenario are illustrated in Figure 6.35 and Table 6.19 below.

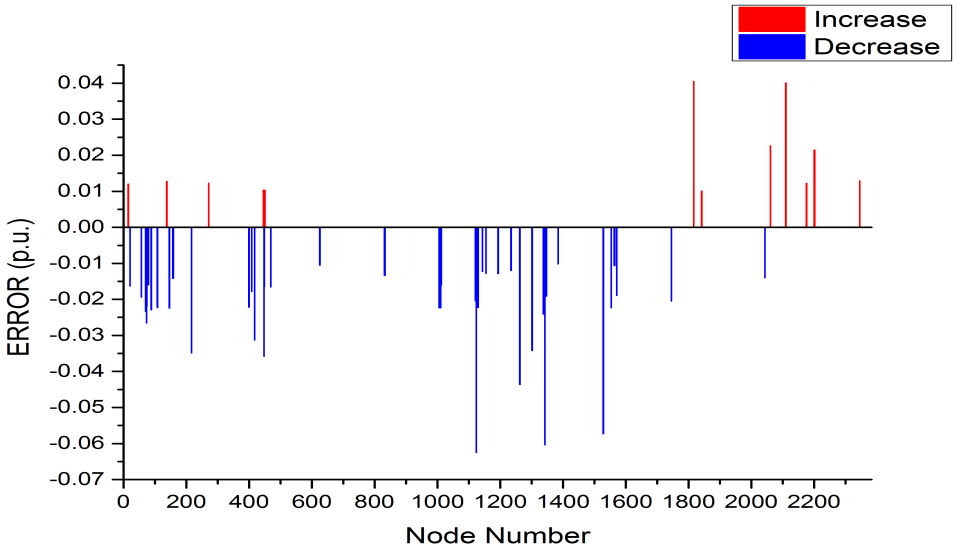

Figure 6.35: The result differences between two different scenarios

Table 6.19: Summary of result differences between two different scenarios

No. of increasing: 14				No. of decreasing: 53			
Maximum		Minimum		Maximum		Minimum	
Bus	Mag. (p.u.)	Bus	Mag. (p.u.)	Bus	Mag. (p.u.)	Bus	Mag. (p.u.)
1817	0.0405	1842	0.0100	1123	-0.0625	1384	-0.0101

It has more influence on the rms values of voltage magnitudes with increasing of the power capacities of both WTs and PGs, as more values are changed as shown in Table 6.19. The numbers of increased and decreased values are 14 and 53 respectively. They are illustrated in red and blue rectangular bars respectively in Figure 6.35. The rms value of voltage magnitude on the bus 1123 changes significantly according to

Table 6.19. It may be relative to its fundamental and harmonic bus voltage magnitudes. According to the calculating results, its fundamental voltage magnitude decreases from $1.0911 p.u.$ to $1.0230 p.u.$ when increasing the power capacities of both WTs and PGs. The result difference is $-0.07 p.u.$. The results of harmonic voltage magnitudes are compared in Figure 6.36 below.

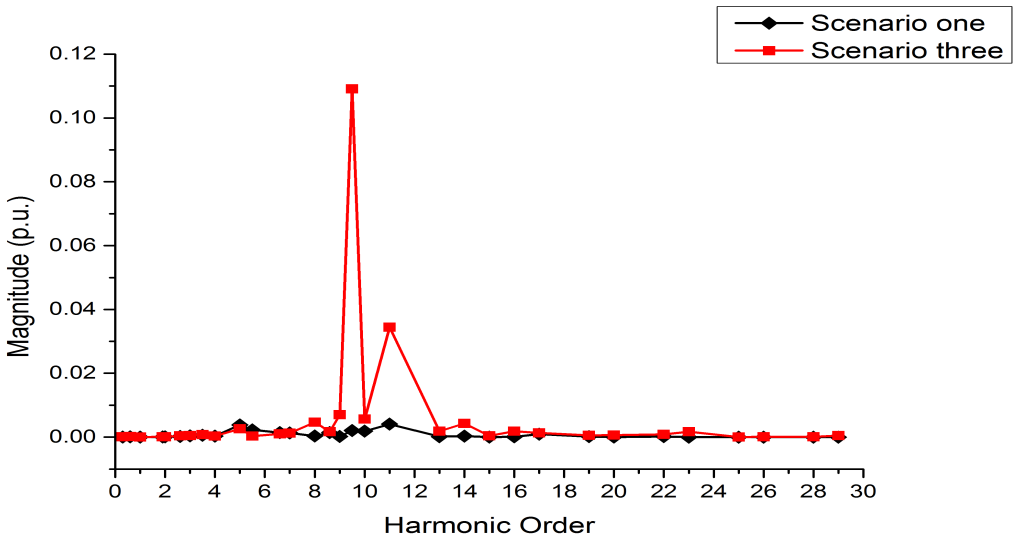

Figure 6.36: The result comparison of harmonic voltage magnitudes

The results of the harmonic bus voltage magnitudes have thirty-one harmonic orders (excluding the fundamental frequency). It contains sub-harmonics, inter-harmonics and integer-harmonics. The maximum harmonic order is the 29^{th} order. The values of the fundamental voltage magnitudes (the 1^{st} harmonic order in the figure) in both scenarios are not considered and are assumed to be zero. The result shows that the most harmonic voltage magnitudes on the bus 1123 increase when raising the power capacities of both WTs and PGs, especially in the 8^{th}, 9^{th}, 9.5^{th}, 10^{th}, 11^{th} and 14^{th} harmonic orders. However, it has a little change of the total harmonic magnitude, from $0.1554 p.u.$ to $0.185 p.u.$. It is smaller than the result difference of fundamental voltage magnitude. Therefore, the change of fundamental voltage magnitude leads to the maximum change of rms value of voltage magnitude on the bus 1123, and makes it decrease.

A three levels of neighbourhood connection diagram of the bus 1123 is illustrated in Figure 6.37, in order to investigate whether it is influenced by any neighbourhood harmonic source (WTs and PGs) connected bus. The first neighbourhood, second neighbourhood and third neighbourhood buses are marked in pink, yellow and green dashed box respectively. The bus 1123 is highlighted in blue as in section 6.4.1. The other harmonic source connected buses are highlighted in red.

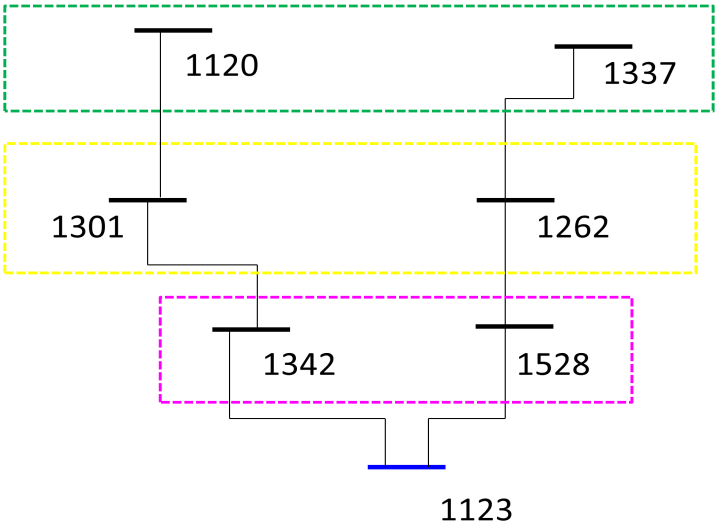

Figure 6.37: The neighbourhood connection diagram of the bus 1123

The above figure shows that there is no harmonic source connected buses in three neighbourhood areas. Hence, the maximum change of rms value of voltage magnitude on the bus 1123 is not influenced by any neighbourhood buses connected to WTs and PGs.

Total Voltage Harmonic Distortion (THDv)

The results of the total harmonic voltage distortion (THDv) from two different scenarios are also illustrated in four parts, that are from bus 1 to bus 596, form bus 597 to bus

1192, from bus 1193 to bus 1788 and from bus 1789 to bus 2383, and they are shown in Figure 6.38, 6.39, 6.40 and 6.41 below. The result values achieved by different scenarios are illustrated in different panels with different colours, in order to investigate the differences between each scenario clearly. The black horizontal straight line in each panel represents the THDv limit level, 3%, in percentage [9].

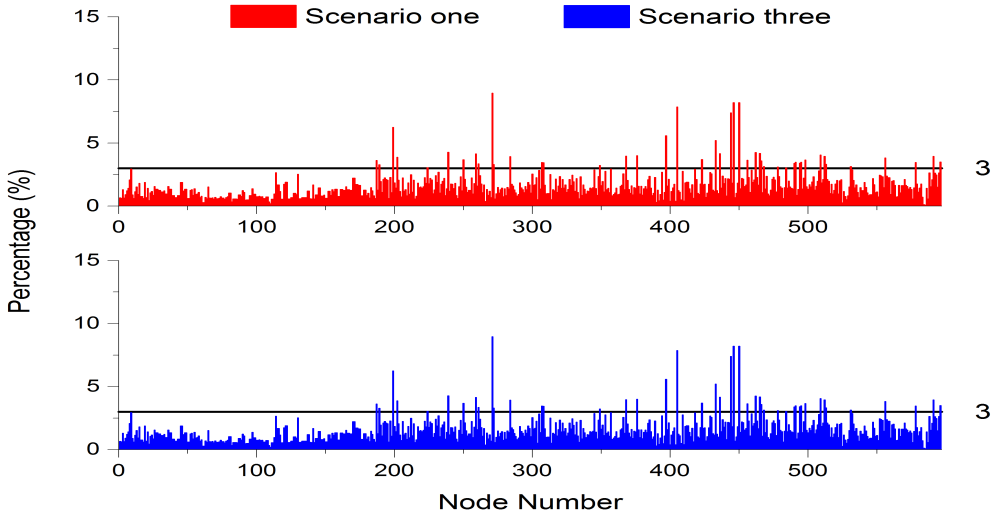

Figure 6.38: THDv of two different scenarios (part 1)

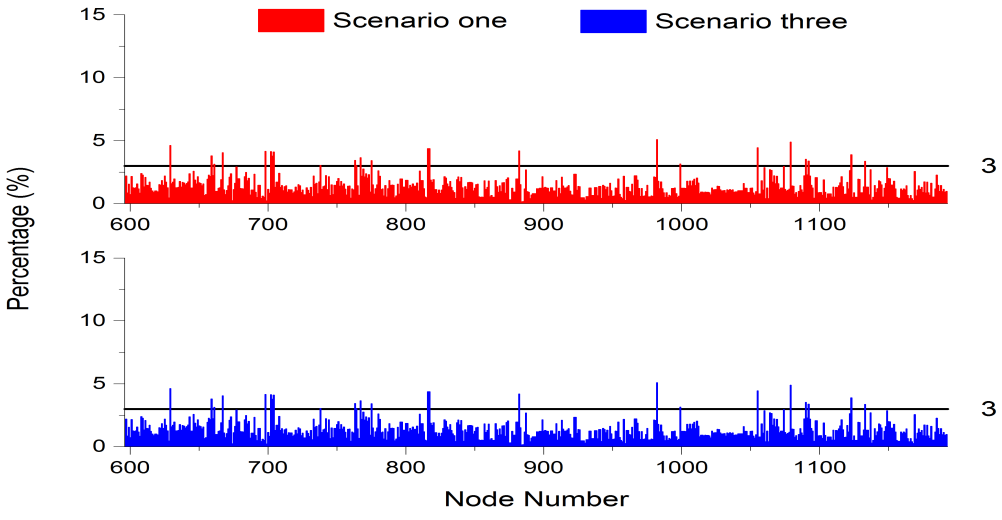

Figure 6.39: THDv of two different scenarios (part 2)

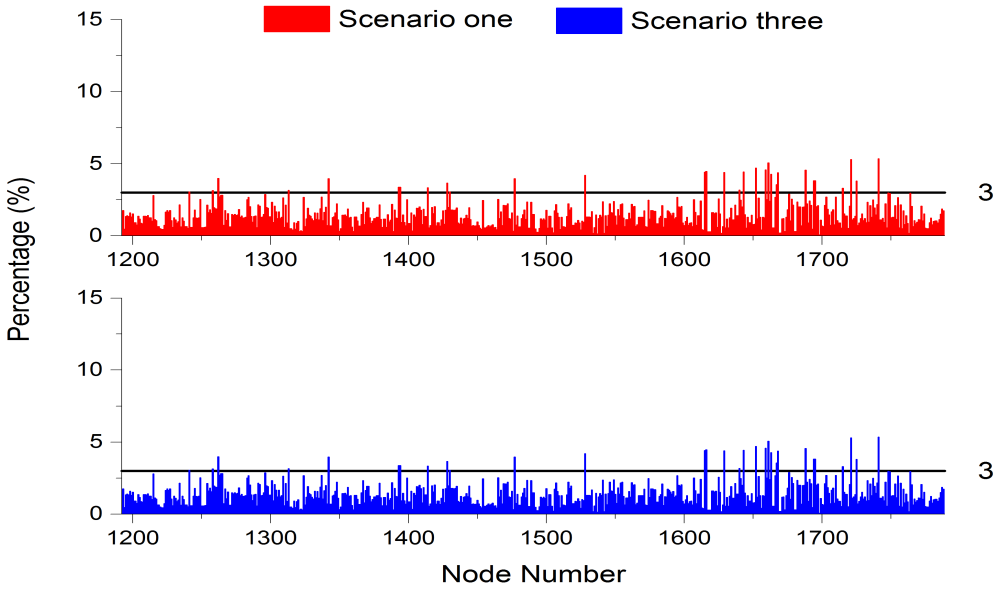

Figure 6.40: THDv of two different scenarios (part 3)

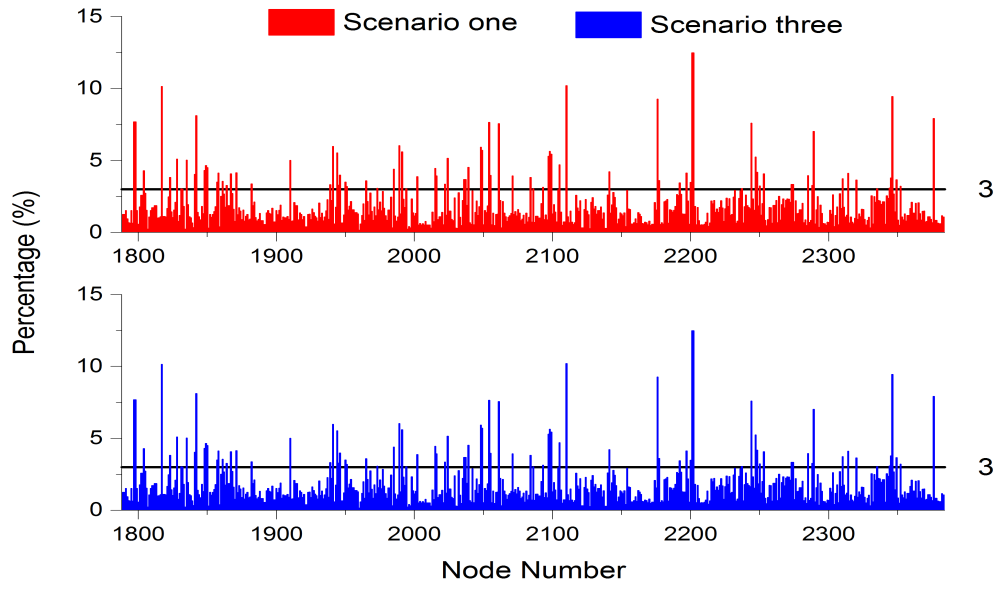

Figure 6.41: THDv of two different scenarios (part 4)

Two scenarios have the same vertical scope in each figure in order to compare the results and investigate the effects of increasing of the power capacities of both WTs and PGs. All the results achieved from each scenario are also categorized into four penetration levels: under 3 %, between 3 % and 6 %, between 6 % and 10 % and over 10 %. Therefore, the numbers of THDv values in different penetration levels are summarized in Table 6.20.

Table 6.20: The summary of numbers of THDv values in different penetration levels

Categories	No. of Buses	
	Scenario one	Scenario three
0 - 3 %	2198	1568
3 - 6 %	164	607
6 - 10 %	17	138
$>$ 10%	4	70
$>$ 3%	185	815

The average and maximum values of the THDv of two scenarios are shown in Table 6.21.

Table 6.21: The maximum and average values of the THDv

Scenarios	One	Three
Average (%)	1.55	2.99
Max. (%)	12.48	29.25

Figures 6.38 to 6.41 denote that two scenarios have nearly the same result waveforms. It is difficult to find out any result differences between two scenarios according to the figures. However, the average and maximum values respectively raise from 1.55 % to 2.99 % and from 12.48 % to 29.25 % when the power capacities of both WTs and PGs increase by 20 % and 15 % respectively. Moreover, the numbers of THDv values increase in the last three penetration levels (i.e. 3 - 6 %, 6 - 10 % and $>$ 10%). Also, the number of buses whose THDv values exceed the level of limit, 3 % [9], increase from 185 to 815. Hence, the THDv values of most buses are greatly influenced by changing the power capacities of harmonic sources (WTs and PGs).

Buses 192, 2248 and 2376 are also selected to investigate the influence. Their THDv values in different scenarios are shown in Table 6.22.

Table 6.22: THDv values of selected buses in two scenarios

Bus	Scenario one	Scenario three
192	2.12 %	5.77 %
2248	4.18 %	8.03 %
2376	7.92 %	15.23 %

As shown in Table 6.22, after increasing the power capacities of both WTs and PGs, the THDv value of each selected bus increases and moves to higher penetration level respectively. In order to investigate the influence on their neighbourhood buses, three levels of neighbourhood connection diagram of buses 192, 2248 and 2376 are illustrated in Figures 6.42 to 6.46.

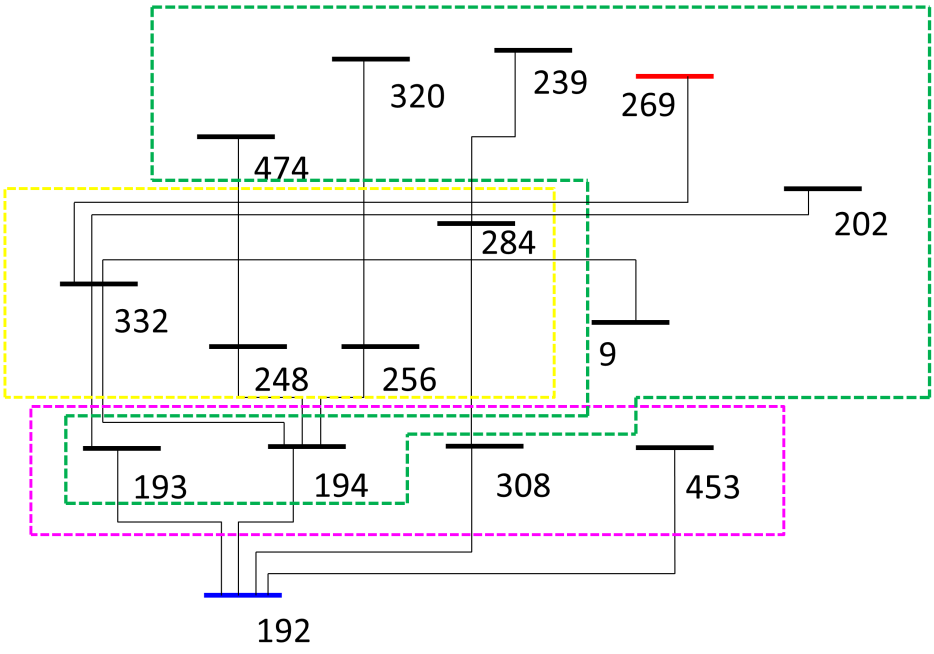

Figure 6.42: The neighbourhood connection diagram of the bus 192

The THDv values of neighbourhood buses of the bus 192 in two different scenarios are shown in Table 6.23.

Table 6.23: THDv values of neighbourhood buses of the bus 192 in percentage

Bus	193	194	308	453	332	284	248
Scenario one	2.24	2.11	3.44	2.16	2.18	3.94	2.33
Scenario three	6.07	5.78	9.65	5.86	5.86	11.04	5.94
Bus	256	474	320	239	9	269	202
Scenario one	2.25	2.14	2.34	4.27	2.94	1.17	3.88
Scenario three	6.28	5.18	6.51	12.04	6.70	3.15	11.04

The maximum value in each scenario is highlighted in pink and yellow respectively. Hence, the maximum values both occur on the bus 239, which is the third neighbourhood bus of the bus 192. In order to investigate the result variation of each neighbourhood bus with increasing the power capacities of both WTs and PGs, ERROR_1 is assumed to represent the result differences between two scenarios. Hence, the result differences are illustrated in Figure 6.43 below.

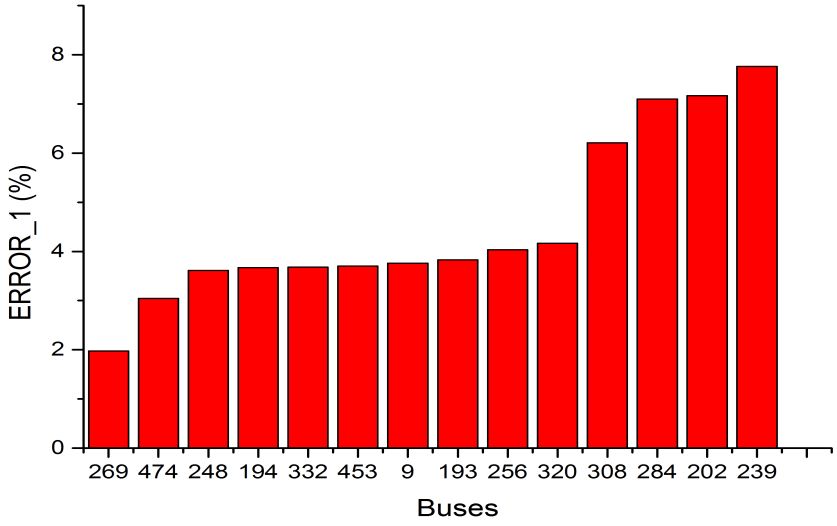

Figure 6.43: The result differences of neighbor buses of the bus 192

It indicates that all the results are positive. It represents that the THDv values of all these buses increase when the power capacities of both WTs and PGs raise. It has a great influence on buses 308, 284, 202 and 239 as they generate larger result differ-

ences. Buses 308 and 284 are in the first and second neighbourhood area respectively. However, buses 202 and 239 are in the third neighbourhood area. Though their THDv values change significantly, it may not influenced by the bus 192. It is because that buses 202 and 239 may connect to other harmonic source buses (i.e. WTs and PGs) which are not shown in Figure 6.15. Though the bus 269 is also harmonic source connected bus, it has less influence (i.e. the result difference is only 2 %).

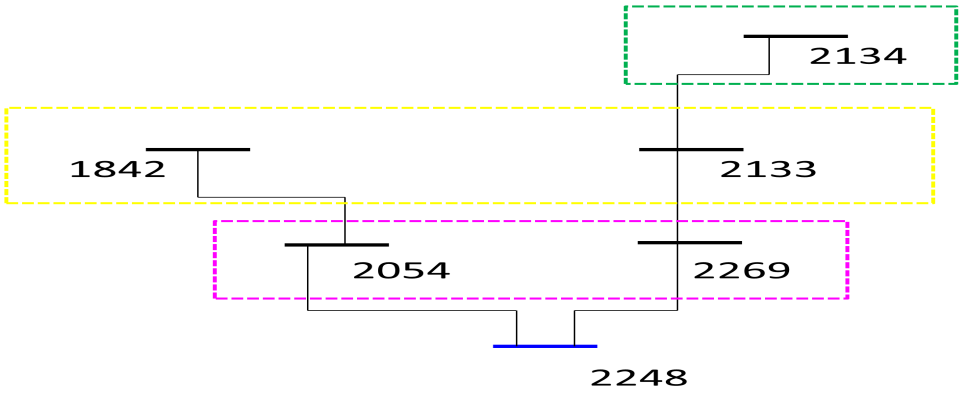

Figure 6.44: The neighbourhood connection diagram of the bus 2248

The THDv values of neighbourhood buses of the bus 2248 in two different scenarios are shown in Table 6.24. In addition, the result differences are illustrated in Figure 6.45.

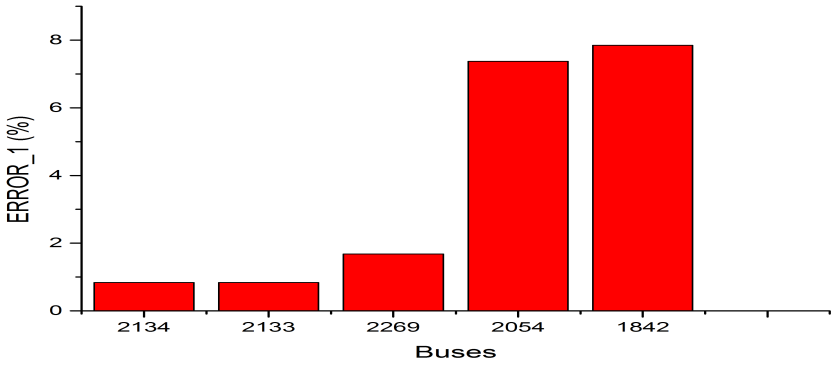

Figure 6.45: The result differences of neighbourhood buses of the bus 2248

The maximum value in each scenario is also highlighted in pink and yellow re-

Table 6.24: THDv values of neighbourhood buses of the bus 2248 in percentage

Bus	2054	2269	1842	2133	2134
Scenario one	7.65	2.23	8.12	1.53	1.53
Scenario three	15.02	3.91	15.97	2.37	2.37

spectively as shown in Table 6.24. Therefore, the maximum values both occur on the bus 1842, which is in the second neighbourhood area. According to Figure 6.45, all the results are positive. Hence, the THDv values of all neighbourhood buses of the bus 2248 increase when the power capacities of both WTs and PGs raise. It has a great influence on the values of buses 1842 and 2054 which are in the second and first neighbourhood area respectively. Their values are 15.97 % and 15.02 % respectively, which are both in the fourth penetration level ($>$ 10%). Though the bus 2269 is also the first neighbourhood bus of the bus 2248, it has less influence than the bus 2054. On the right-hand-side branch of the bus 2248 as shown in Figure 6.17, the influence on the values of THDv to each neighbourhood bus weakens with increasing of the distance to the bus 2248. The buses 2133 and 2134 have the same value change.

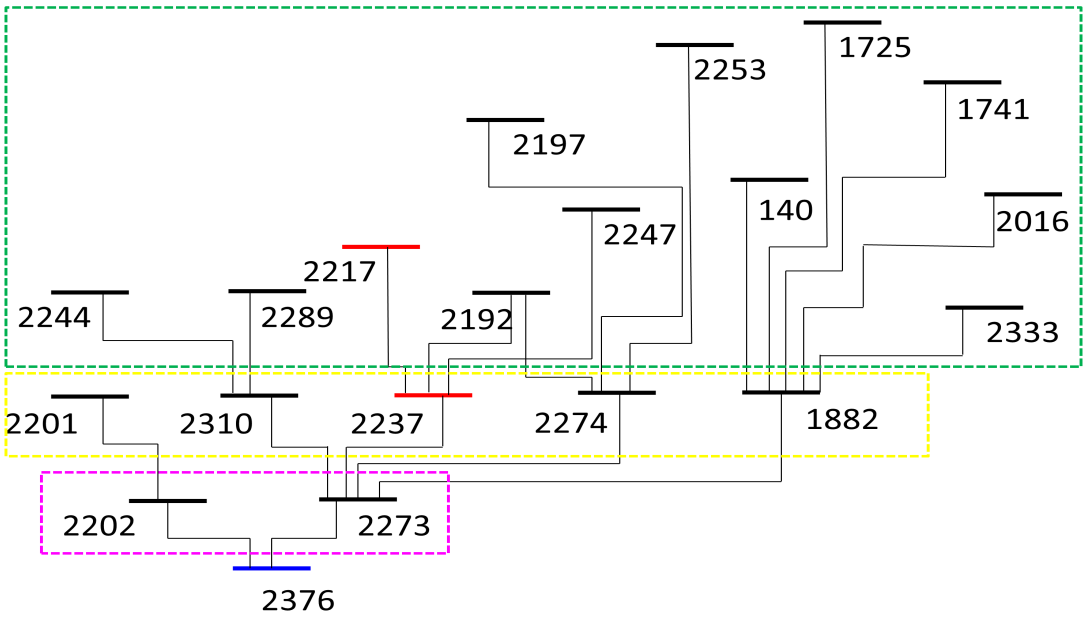

Figure 6.46: The neighbourhood connection diagram of the bus 2376

The THDv values of neighbourhood buses of the bus 2376 in two different scenarios are shown in Table 6.25 below. The maximum value in each scenario is highlighted in pink and yellow colour respectively.

Table 6.25: THDv values of neighbourhood buses of the bus 2376 in percentage

Bus	2273	2202	2201	1882	2274	2237	2310	2244	2289	2217
Scenario one	3.33	12.48	12.48	3.37	3.34	3.04	3.73	7.59	7.02	2.22
Scenario three	6.57	23.97	23.98	6.46	6.58	6.05	7.40	14.72	13.70	4.38
Bus	2192	2247	2197	2253	140	1725	1741	2016	2333	
Scenario one	3.44	5.25	4.12	4.07	0.58	3.81	5.36	3.93	2.49	
Scenario three	6.82	10.29	7.98	8.00	0.94	7.30	10.24	7.52	4.83	

The values of result differences between two scenarios are illustrated in Figure 6.47.

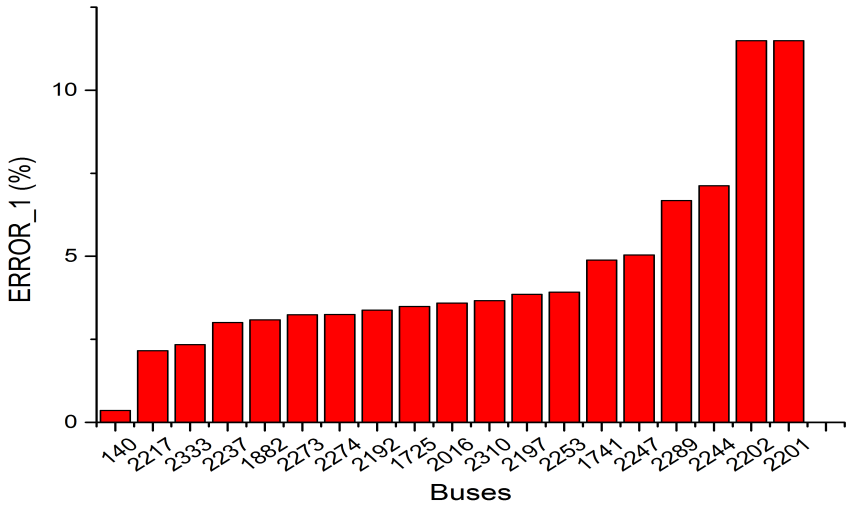

Figure 6.47: The result differences of neighbourhood buses of the bus 2376

Table 6.25 indicates that the maximum values of scenario one are both on the buses 2201 and 2202. However, the maximum value of scenario three is only on the bus 2201. In addition, the THDv values of nearly 37 % neighbourhood buses reach to the fourth penetration level ($>$ 10%) after increasing of the power capacities of both WTs and PGs. Figure 6.47 shows that the THDv values of buses 2202 and 2201 change

significantly, whose result differences reach to 11.5 %. They are along the first left-hand-side branch, but are separated in the first and second neighbourhood area of the bus 2376 respectively. However, the other first and second neighbourhood buses have less influence than several fourth neighbourhood buses (i.e. buses 2289, 2244, 2247 and 1741). It may be because that those fourth neighbourhood buses were influenced by other connected harmonic source (WTs and PGs) buses which were not shown in Figure 6.47. Though the buses 2237 and 2217 are also harmonic source connected bus, a little influence occurs on their THDv values when the power capacities of WTs and PGs increase by 20 % and 15 % respectively. The bus 140 which is in the fourth neighbourhood area has smallest influence on the value of THDv.

Harmonic Powers

The total active and reactive powers at both sending and receiving ends (Ptotals, Ptotalr, Qtotals and Qtotalr) and the total power losses on each branch (Ptotalloss) are shown in Figures 6.48 to 6.52 below. The results achieved from two different scenarios are illustrated in two layers with red and blue colour respectively in each diagram. Each scenario has the same vertical scope in each result category.

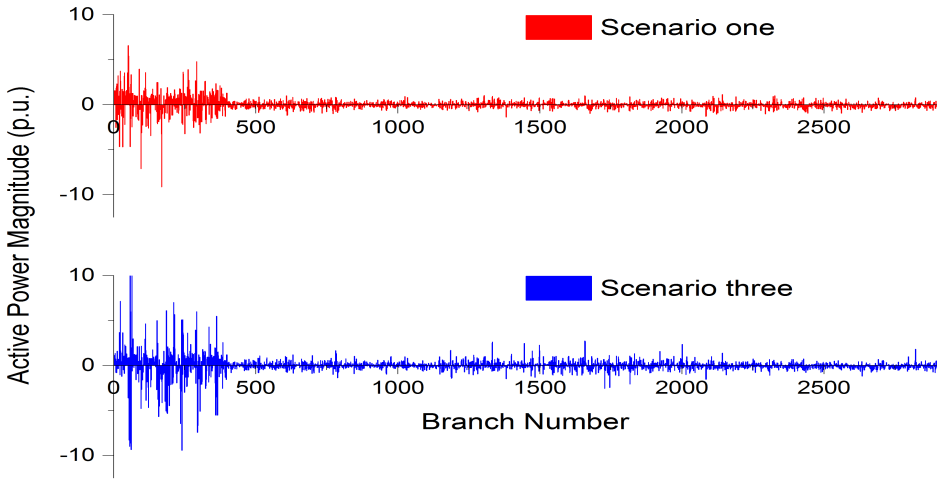

Figure 6.48: Total active powers at the sending end

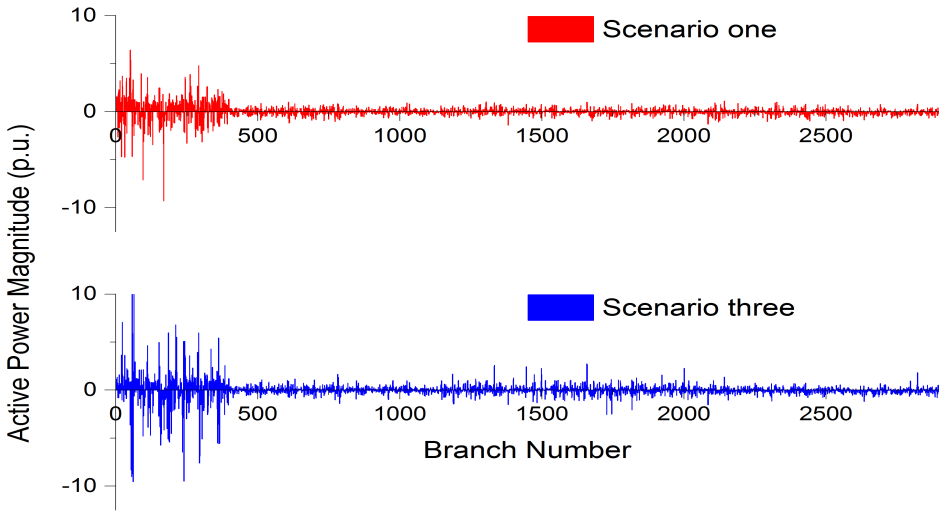

Figure 6.49: Total active powers at the receiving end

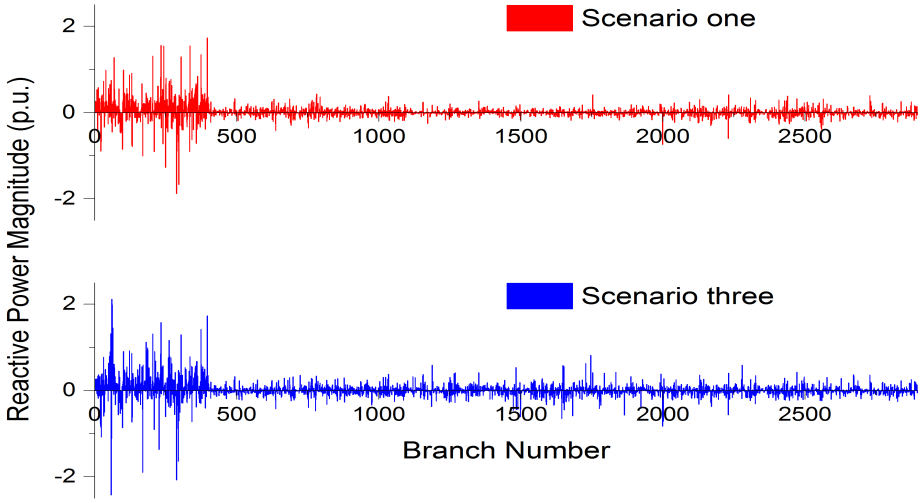

Figure 6.50: Total reactive powers at the sending end

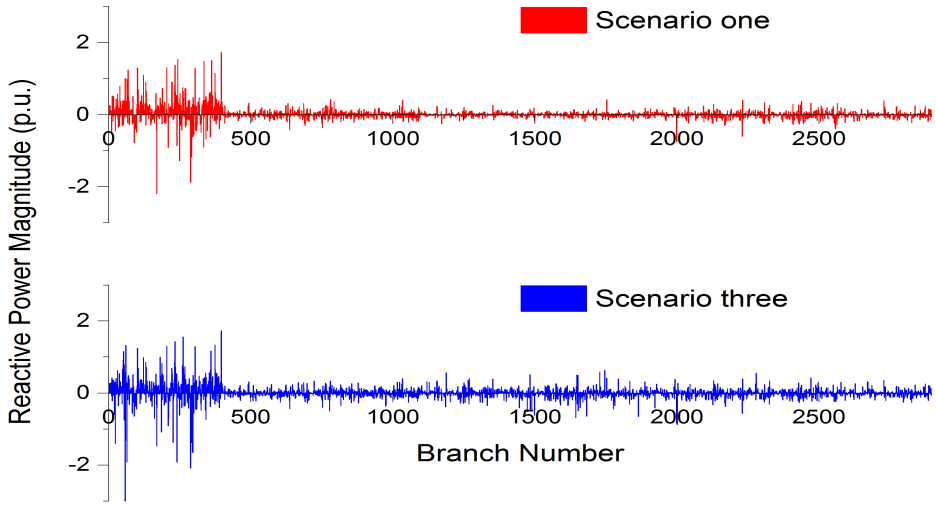

Figure 6.51: Total reactive powers at the receiving end

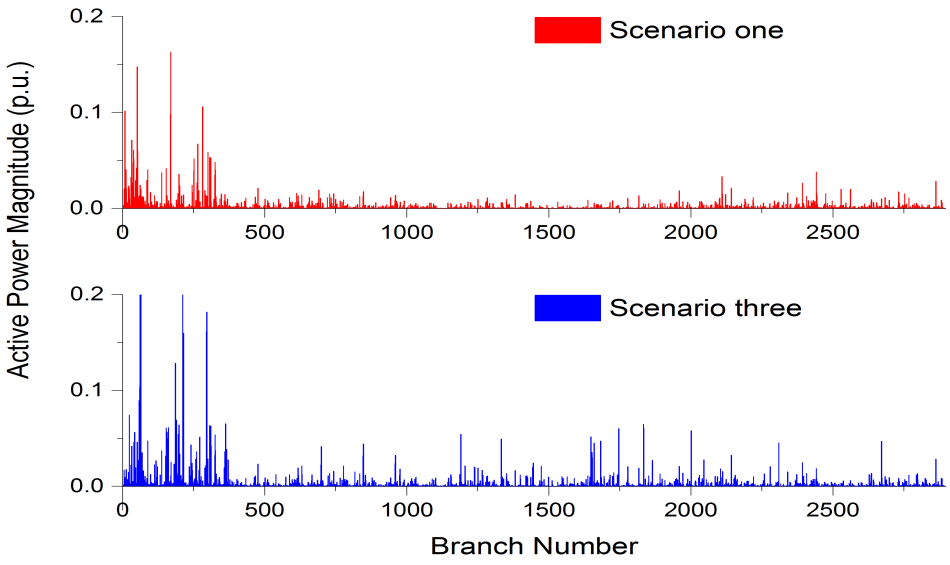

Figure 6.52: Total power losses on each branch

The results of the Ptotals, Ptotalr, Qtotals and Qtotalr contain both positive and negative values. As mentioned in chapter 5, for the total active powers, if the values are positive, it denotes that the active powers flow from the sending ends to the receiving ends; otherwise, the active powers flow in the opposite way. For the total reacitve powers, if the results are positive, it means that the buses (sending and receiving ends) generate reactive powers; otherwise, they absorb reactive powers. The results show that the larger total active and reactive powers at both sending and receiving ends and power losses on each line are generated on the first 400 transmission lines. It means more powers are transmitted on these lines during the harmonic penetration. The maximum values of these result categories are shown in Table 6.26 below.

Table 6.26: The maximum values of the Ptotals, Ptotalr, Qtotals, Qtotalr and Ptotalloss

Scenarios	Ptotals (p.u.)	Ptotalr (p.u.)	Qtotals (p.u.)	Qtotalr (p.u.)	Ptotalloss (p.u.)
One	-9.1374	-9.3004	-1.8810	-2.1932	0.1630
Three	11.9709	11.8813	-2.4262	-3.0772	0.4144

The result waveforms of active and reactive powers at both sending and receiving ends and total power loss on each line that calculated from two different scenarios have significant changes. The values of scenario three are larger than those of scenario one. It represents that increasing of the power capacities of both WTs and PGs raises the total active powers at both sending and receiving ends and the total power loss on each branch. The reason is that increasing of the power capacities on several buses influences the fundamental power flow on each transmission line. In order to prove the above conclusion, the differences between each scenario are numerically illustrated in Figures 6.53 to 6.57, and the maximum values of them are shown in Table 6.27 below.

Table 6.27: The maximum difference values of the Ptotals, Ptotalr, Qtotals, Qtotalr and Ptotalloss

	Ptotals (p.u.)	Ptotalr (p.u.)	Qtotals (p.u.)	Qtotalr (p.u.)	Ptotalloss (p.u.)
ERROR_1	16.6309	16.5546	-3.1748	-4.0889	0.3944

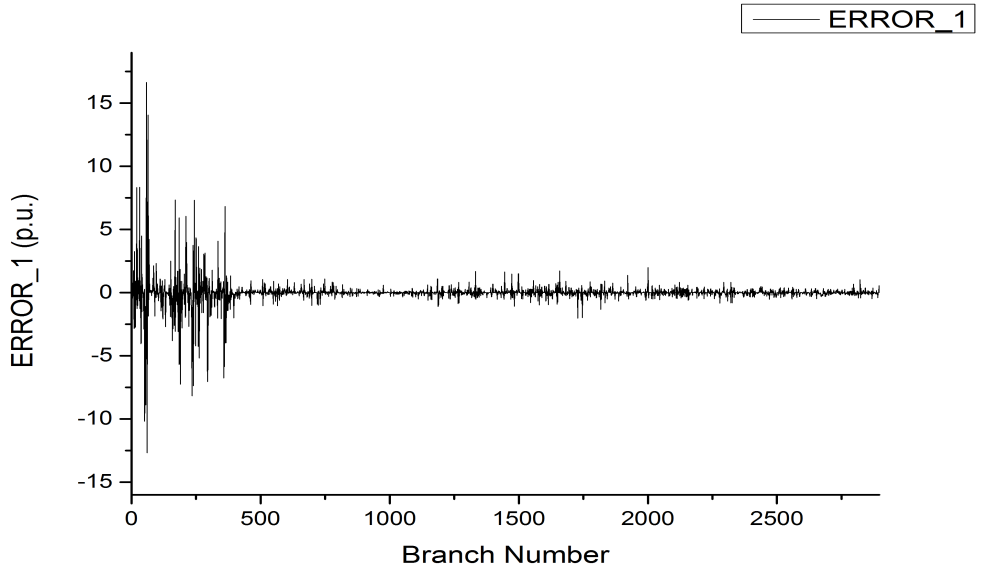

Figure 6.53: Total active powers at the sending end

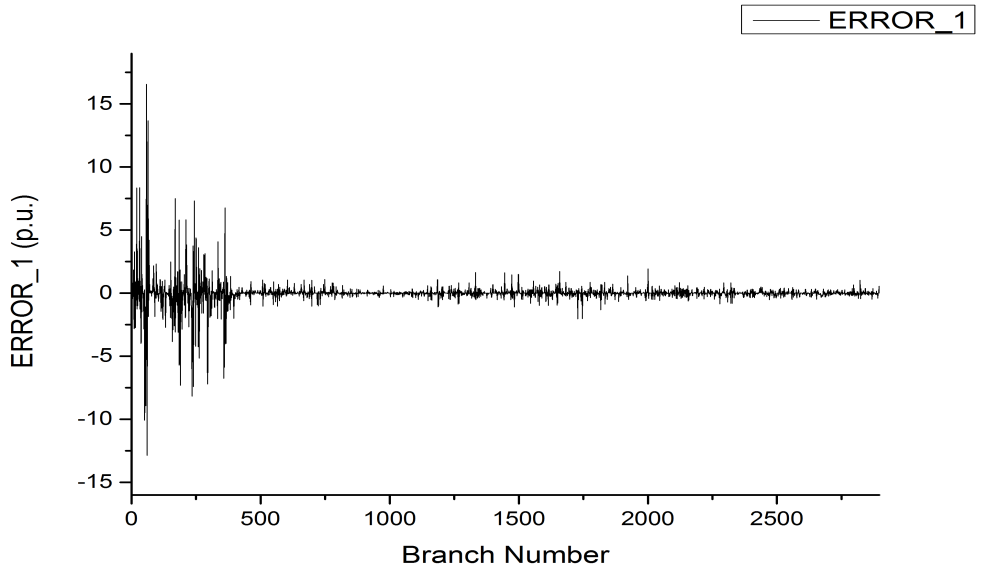

Figure 6.54: Total active powers at the receiving end

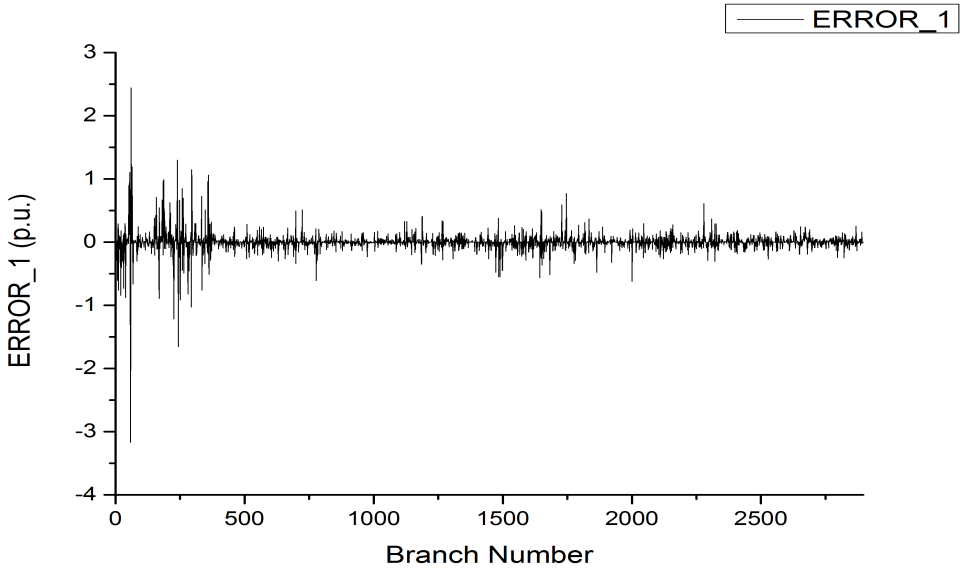

Figure 6.55: Total reactive powers at the sending end

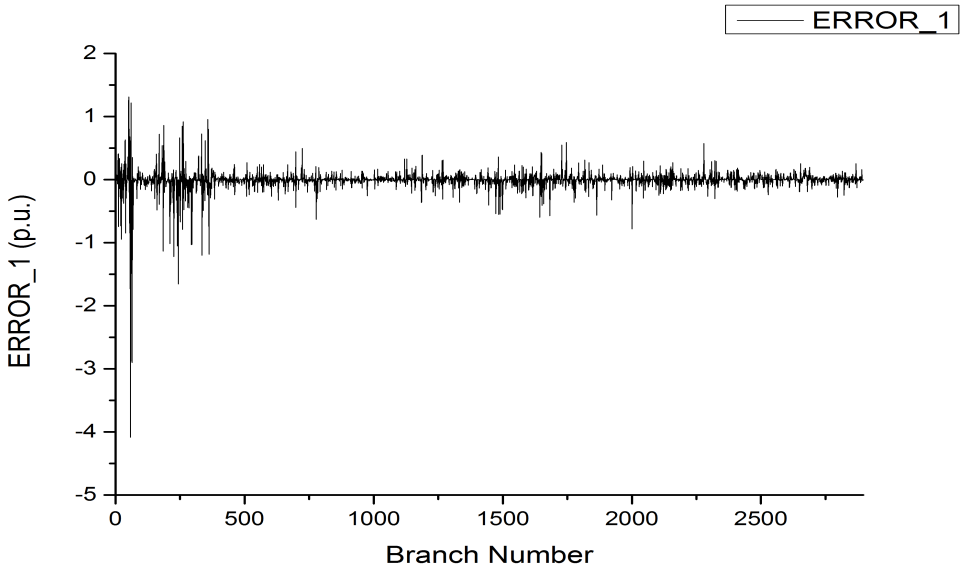

Figure 6.56: Total reactive powers at the receiving end

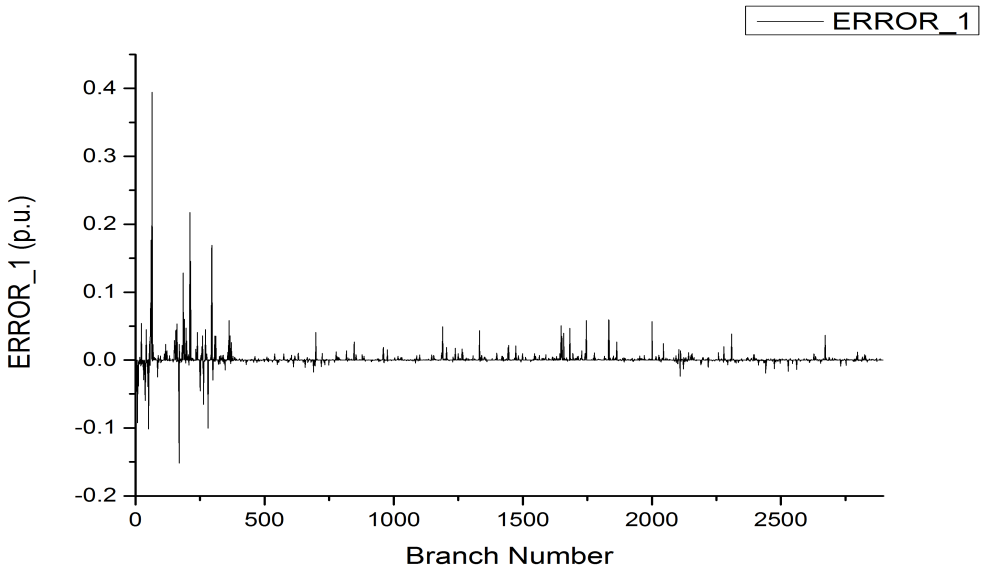

Figure 6.57: Total power losses on each branch

The results of scenario one are regarded as the fundamental values. ERROR_1 in the figures above represent the result differences between scenario one and three. If the results are positive, it means the value achieved by scenario three is larger than that of scenario one. When the absolute value of ERROR_1 is less than $0.01 p.u.$, the result differences between two scenarios are considered negligible and the results of two scenarios are considered as identical. Hence, raising of the power capacities of both WTs and PGs influences 2125 lines of Ptotals, 2122 lines of Ptotalr, 1873 lines of Qtotals, 1865 lines of Qtotalr and 131 lines of Ptotalloss. The greatest influence occurs on lines 58, 58, 58, 58 and 64 of Ptotals, Ptotalr, Qtotals, Qtotalr and Ptotalloss with increasing of $16.6309 p.u.$, $16.5546 p.u.$, $-3.1748 p.u.$, $-4.0889 p.u.$ and $0.3944 p.u.$ respectively, as shown in Table 6.27. Therefore, raising of the power capacities of both WTs and PGs by 20 % and 15 % respectively has great influence on total active and reactive powers at both sending and receiving ends with no regularity. It has less influence on total power loss on each line than others as 131 lines are effected.

6.4.3 Change Power Capacity Of Electrical Vehicle Charger

In this section, results achieved from scenario three and four are presented and compared to investigate the effects of changing power capacities of electric vehicle chargers (EVCs) to the harmonic penetration. The number, position and power capacities of WTs, PGs and converters are constant respectively. However, the power capacities of EVCs increase by 15 %, from 5 % to 20 %. It is achieved by randomly increasing the number of EVC connection, from 108 to 345. Its fundamental and higher harmonic injection currents on each connection bus are constant.

Computing Time And Number Of Iterations

The results of computing time and number of iterations are listed in Table 6.28 below.

Table 6.28: Computing time and iterations

Scenarios	Three	Four
Computing time (s)	45.89	46.01
Iterations	5	5

The computing time and number of iterations in two different scenarios are counted independently during the calculation. The computing time also excludes the time consumption of data import and export. It indicates that the numbers of iterations stay on 5 in two different scenarios. However, the computing time has a slightly increase from 45.89s to 46.01s. Hence, when the power capacities of EVCs increase, it may not affect the number of iterations, but the computing time can be affected.

Voltage Magnitudes

The results of rms values of bus voltage magnitudes achieved from two different scenarios are illustrated in two different layers with red and blue colour respectively, in order to investigate the difference and varying regularity. The black straight line in each layer represents the average value of each scenario in per unit. The results are separated into four parts to be illustrated, in order to get a clear comparison. Part 1 represents the results from bus 1 to bus 596. Part 2 indicates the results from bus 597 to bus 1192. The results of bus 1193 to bus 1788 and bus 1789 to bus 2383 are shown in part 3 and part 4 respectively. These four parts have same vertical scope, and they are shown in Figure 6.58, 6.59, 6.60 and 6.61 respectively.

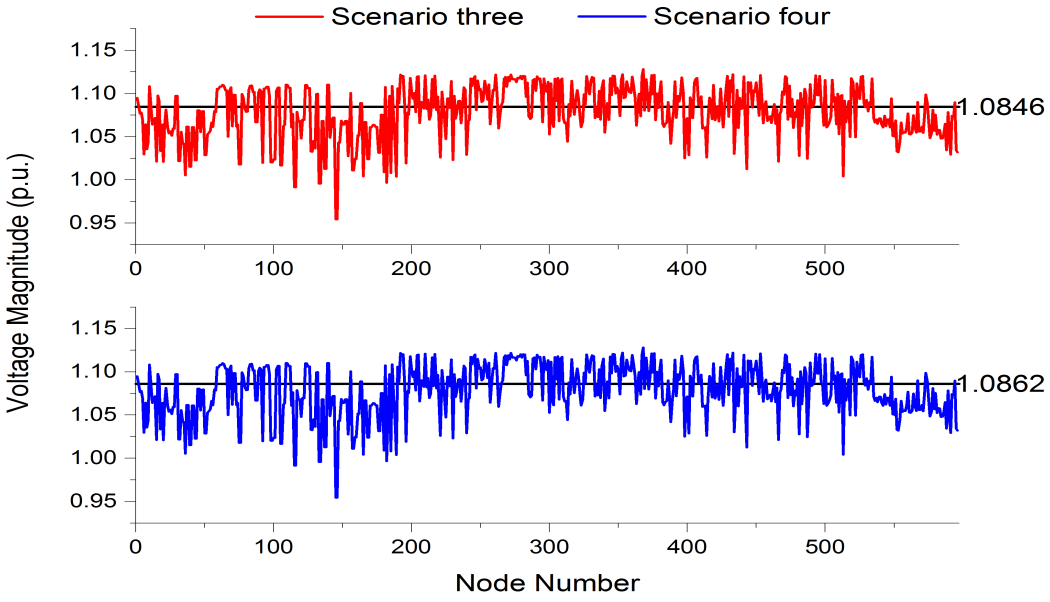

Figure 6.58: The rms values of voltage magnitudes from two different scenarios (part 1)

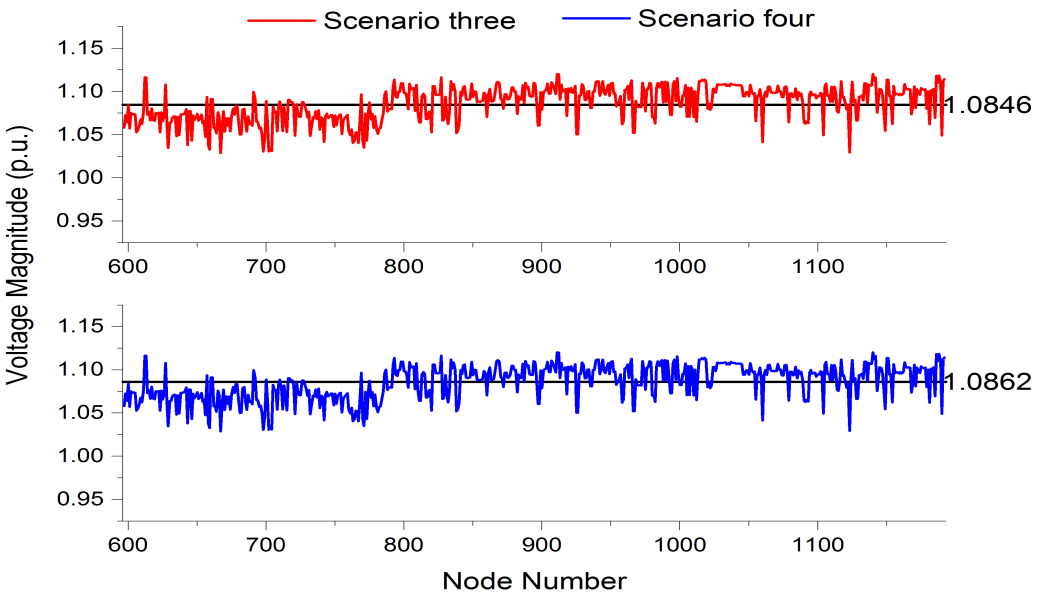

Figure 6.59: The rms values of voltage magnitudes from two different scenarios (part 2)

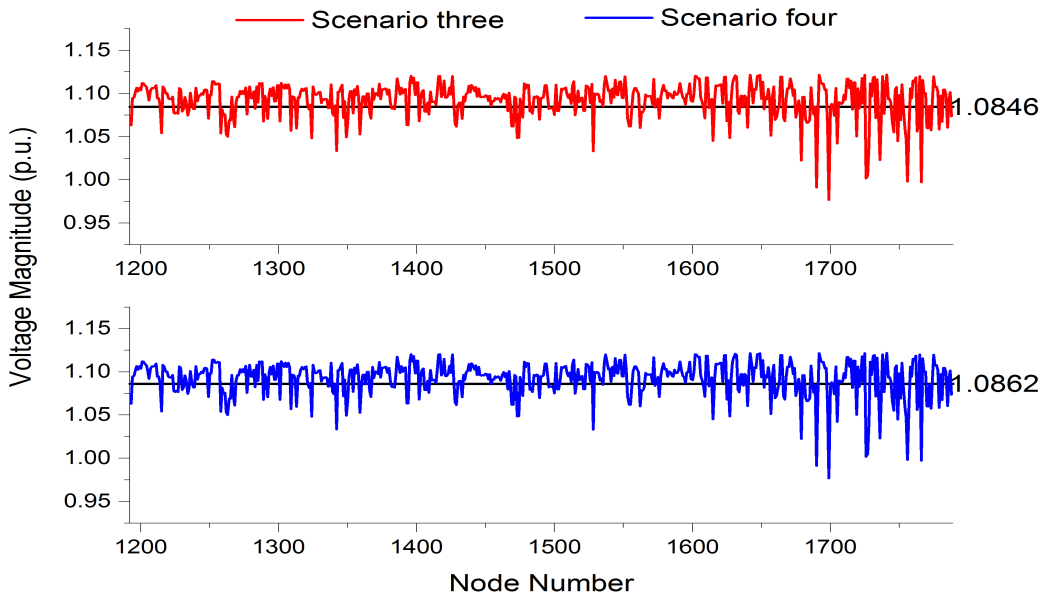

Figure 6.60: The rms values of voltage magnitudes from two different scenarios (part 3)

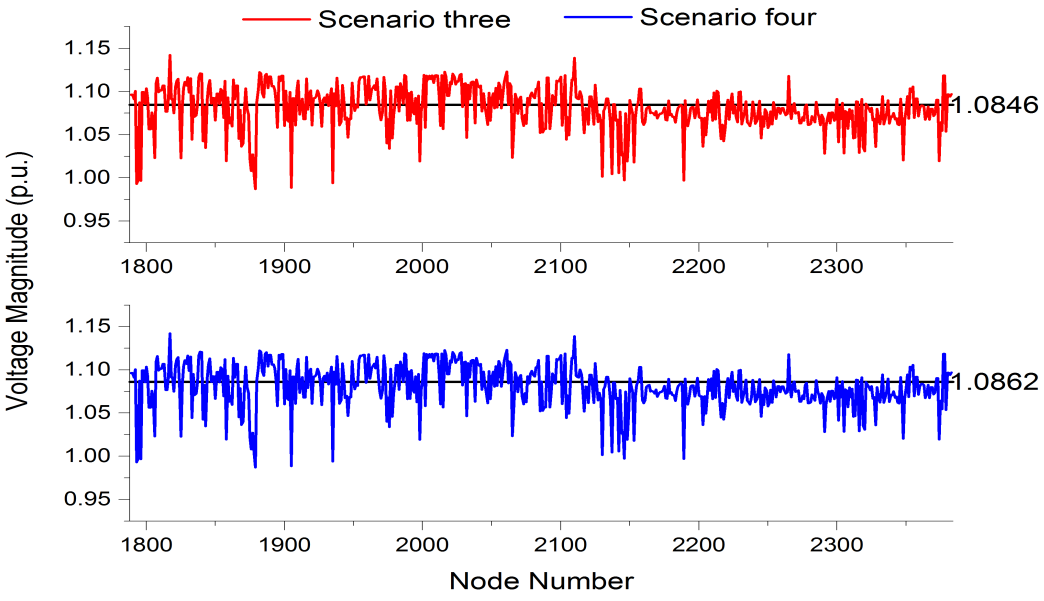

Figure 6.61: The rms values of voltage magnitudes from two different scenarios (part 4)

According to the above figures, the rms values of bus voltage magnitudes achieved from two different scenarios all fluctuate between $0.9546p.u.$ and $1.2583p.u.$. Most of them assemble around their average values, $1.0846p.u.$ and $1.0862p.u.$ respectively. Two different scenarios have nearly the same result waveforms and values. Though there is $0.0016p.u.$ difference of average value between each scenario, it is small enough to be ignored. Hence, it may have no influence on the rms values of bus voltage magnitudes with increasing of power capacities of EVCs. The maximum and minimum values of the rms values of voltage magnitudes of each scenario are shown in Table 6.29 below.

Table 6.29: The maximum and minimum values of the fundamental bus voltage magnitudes

Scenarios	Three		Four	
	Bus	Mag. (p.u.)	Bus	Mag. (p.u.)
Max	1817	1.1420	1842	1.2583
Min	145 146	0.9546	145 146	0.9555

It shows that each scenario has different minimum and maximum values. However, the minimum values occur on the same buses 145 and 146. They have a slightly increase when raising the power capacities of EVCs. While the maximum values have significant change, which is $0.1163p.u.$.

In order to investigate slight result differences between each scenario, the numerical comparison is required. ERROR_1 is used to represent the result difference between scenario three and scenario four. If it is positive, it represents that the result of scenario four is larger than that of scenario three. When the absolute value of ERROR_1 is less than $0.01p.u.$, the results of two scenarios are considered as identical. Hence, the values of 84 buses are changed when increasing the power capacities of EVCs. The result differences between each scenario are illustrated in Figure 6.62 and Table 6.30 below.

Table 6.30: Summary of result differences between two different scenarios

No. of increasing: 76				No. of decreasing: 8			
Maximum		Minimum		Maximum		Minimum	
Bus	Mag. (p.u.)	Bus	Mag. (p.u.)	Bus	Mag. (p.u.)	Bus	Mag. (p.u.)
1842	0.1758	2119	0.0102	1817	-0.0452	2346	-0.0108

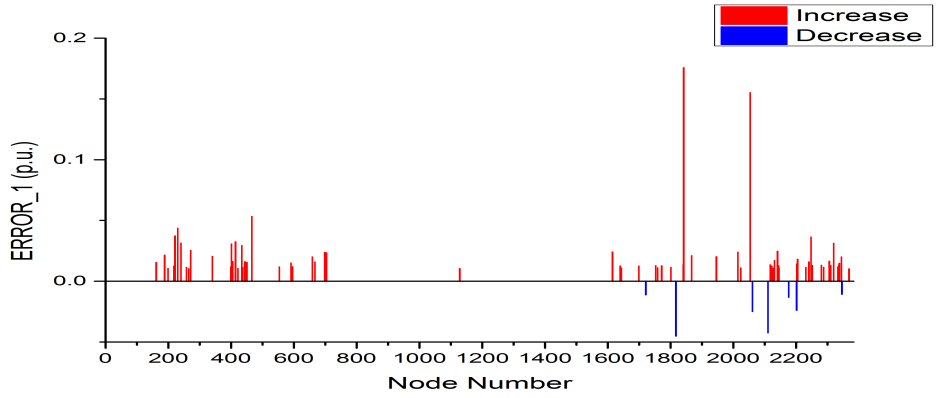

Figure 6.62: The result differences between two different scenarios

More buses (total 84 buses) are influenced with increasing of the power capacities of EVCs. Most of them are increased. The numbers of increased and decreased values are 76 and 8 respectively, as shown in Table 6.30. They are illustrated in red and blue rectangular bars respectively in Figure 6.62. The rms value of voltage magnitude on the bus 1842 changes significantly according to Table 6.30. It may be relative to its fundamental and harmonic bus voltage magnitudes. According to the calculating results, it has the same fundamental voltage magnitude in each different scenario. Therefore, the significant result difference of rms value on the bus 1842 should be influenced by its harmonic voltage magnitudes (excluding the fundamental frequency). Hence, the values of harmonic voltage magnitudes are compared in Figure 6.63 below.

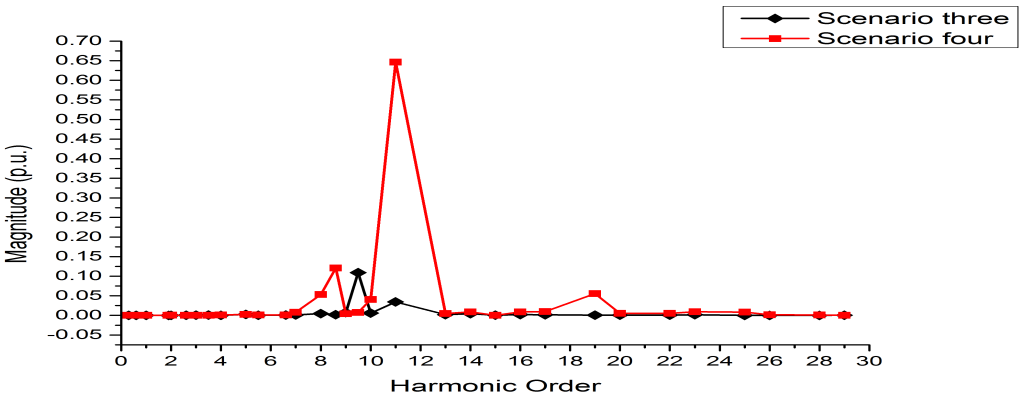

Figure 6.63: The result comparison of harmonic voltage magnitudes

The results of the harmonic bus voltage magnitudes (excluding the fundamental frequency) have thirty-one harmonic orders as well. The values of the fundamental voltage magnitudes (the 1^{st} harmonic order in the figure) in scenarios three and four are not considered and are assumed to be zero. Hence, the result shows that the values in the 8^{th}, 8.6^{th}, 10^{th}, 11^{th} and 19^{th} harmonic orders increase when raising the power capacities of EVCs. Though the value in the 9.5^{th} harmonic order decreases, the total amount of decrease, $-0.1956p.u.$, is much less than the total amount of increase, $1.6303p.u.$. Therefore, the change of harmonic voltage magnitudes leads to the maximum change of rms value of voltage magnitude on the bus 1842, and makes it increase.

A three levels of neighbourhood connection diagram of the bus 1842 is illustrated in Figure, in order to investigate whether it is influenced by any neighbourhood harmonic source (EVCs) connected bus. The first neighbourhood, second neighbourhood and third neighbourhood buses are marked in pink, yellow and green dashed box respectively. The bus 1842 is highlighted in blue. The other harmonic source connected buses are highlighted in red.

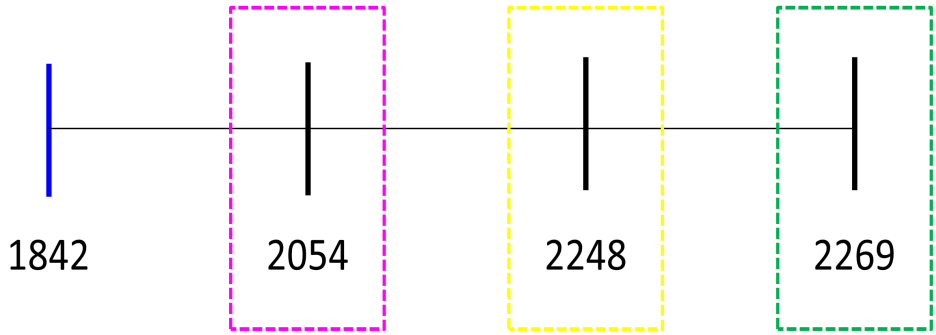

Figure 6.64: The neighbourhood connection diagram of the bus 1842

As shown in the above figure, the bus 1842 has only three neighbourhood buses.

They are not connected to the EVCs. Hence, the maximum change of rms value of voltage magnitude on the bus 1842 in not influenced by the change of power capacity on any neighbourhood bus.

Total Voltage Harmonic Distortion (THDv)

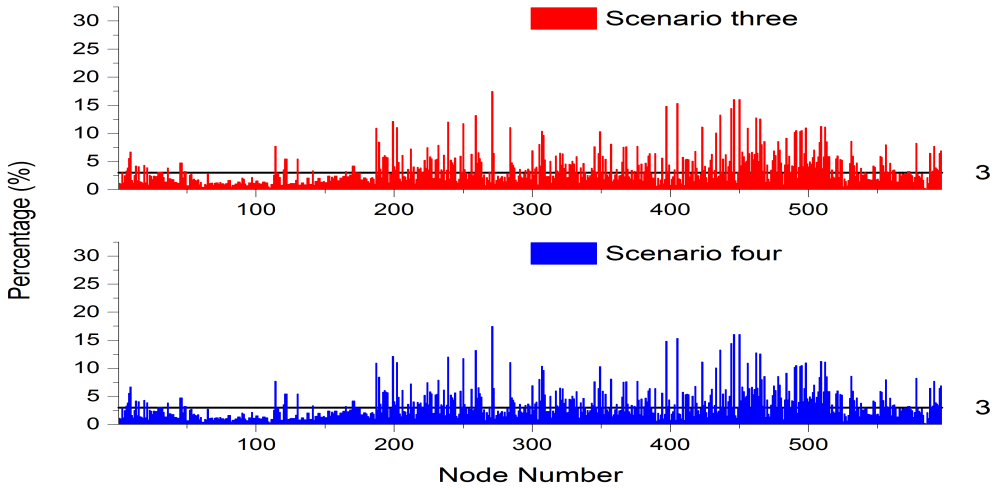

Figure 6.65: THDv of two different scenarios (part 1)

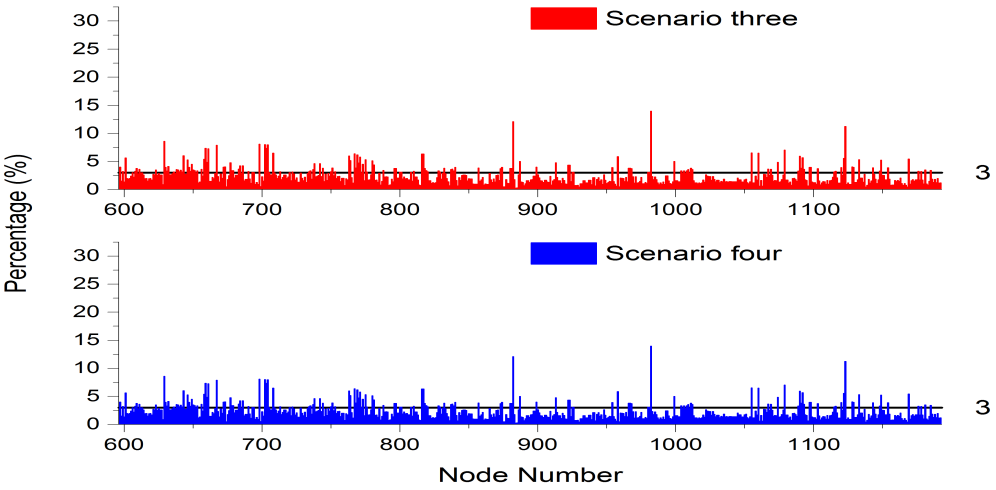

Figure 6.66: THDv of two different scenarios (part 2)

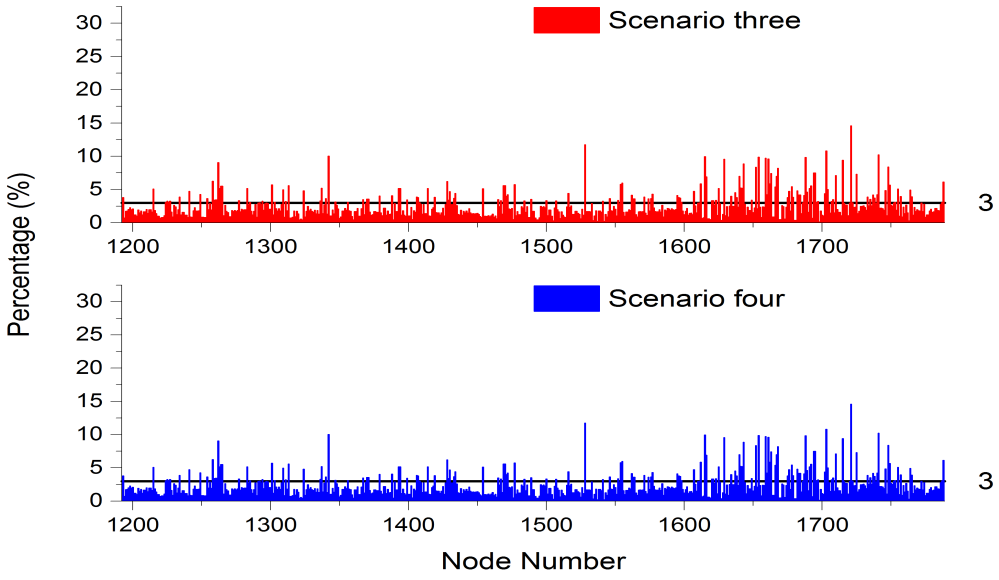

Figure 6.67: THDv of two different scenarios (part 3)

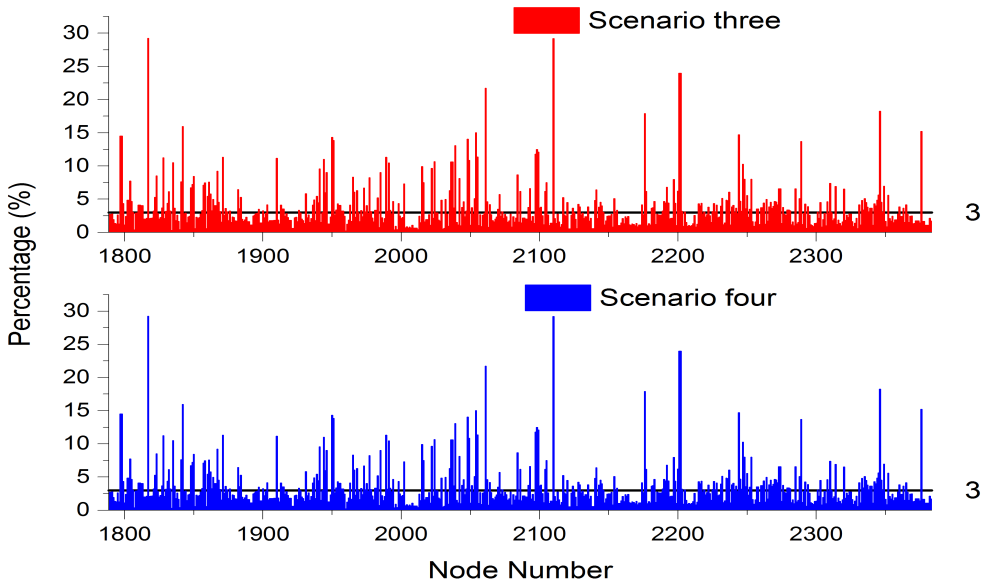

Figure 6.68: THDv of two different scenarios (part 4)

The results of the total harmonic voltage distortion (THDv) from two different scenarios are also illustrated in four parts, and they are shown in Figure 6.65, 6.66, 6.67 and 6.68 above. The black horizontal straight line in each panel represents the THDv limit level, 3%, in percentage [9]. The average and maximum values of the THDv of two scenarios are shown in Table 6.31.

Table 6.31: The maximum and average values of the THDv

Scenarios	Three	Four
Average (%)	1.80	2.37
Max. (%)	14.87	36.62

Two scenarios have the same vertical scope in each figure in order to compare the results and investigate the effects of increasing of the power capacities of EVCs. Most values on buses 1789 to 2383 of both scenarios are larger than those on other buses. The numbers of THDv values in different four penetration levels (i.e. 0 - 3 %, 3 - 6 %, 6 - 10 % and $>$ 10%) are summarized in Table 6.32 below.

Table 6.32: The summary of numbers of THDv values in different penetration levels

Categories	No. of Buses	
	Scenario three	Scenario four
0 - 3 %	1568	1407
3 - 6 %	607	637
6 - 10 %	138	224
$>$ 10%	70	115
$>$ 3%	815	976

Figures 6.65 to 6.68 denote that two scenarios have nearly the same result waveforms. It is difficult to find out any result differences between two scenarios according to the figures. However, the average and maximum values raise from 2.99 % to 3.53 % and from 14.87 % to 36.62 % respectively. According to Table 6.32, the numbers of THDv values in the first penetration level (0 - 3 %) decrease from 1568 to 1407 when increasing the power capacities and numbers of EVCs. While in other penetration levels, the number has a little bit increase respectively. Moreover, the total numbers of buses whose THDv values exceed the level of limit, 3 % [9], increase from 815 to 976. Hence, the THDv values of most buses are greatly influenced by changing the power capacities and numbers of harmonic sources (EVCs).

Buses 192, 2248 and 2376 are also selected to investigate the influence on their THDv values with increasing of the power capacities and numbers of EVCs. Their THDv values in different scenarios are shown in Table 6.33.

Table 6.33: THDv values of selected buses in two scenarios

Bus	Scenario three	Scenario four
192	5.77 %	2.32 %
2248	8.03 %	27.50 %
2376	15.23 %	7.73 %

As shown in Table 6.33, after increasing the power capacities of EVCs, the THDv values of the buses 192 and 2376 decrease and move to lower penetration level respectively. However, the value of the bus 2248 changes from 8.03 % to 27.50 %, which moves from the third penetration level to the fourth one. In order to investigate the influence on their neighbourhood buses, three levels of neighbourhood connection diagram of buses 192, 2248 and 2376 are illustrated in Figures 6.69 to 6.73.

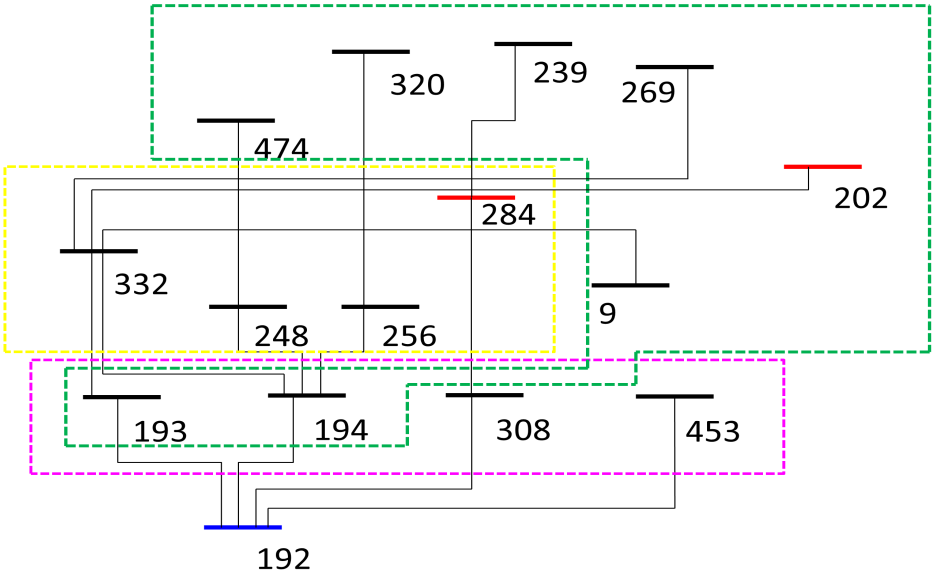

Figure 6.69: The neighbourhood connection diagram of the bus 192

The THDv values of neighbourhood buses of the bus 192 in two different scenarios

are shown in Table 6.34.

Table 6.34: THDv values of neighbourhood buses of the bus 192 in percentage

Bus	193	194	308	453	332	284	248
Scenario three	6.07	5.78	9.65	5.86	5.86	11.04	5.94
Scenario four	2.48	2.22	3.87	2.37	2.55	4.35	2.67
Bus	256	474	320	239	9	269	202
Scenario three	6.28	5.18	6.51	12.04	6.70	3.15	11.04
Scenario four	3.83	2.62	5.16	4.84	4.53	2.14	3.59

The maximum value in each scenario is highlighted in pink and yellow respectively. Hence, the maximum values occur on the buses 239 and 320 respectively, which are the third neighbourhood buses of the bus 192. In order to investigate the result variation of each neighbourhood bus with increasing the power capacities and numbers of EVCs, ERROR_1 is assumed to represent the result differences between two scenarios. Hence, the result differences are illustrated in Figure 6.70 below.

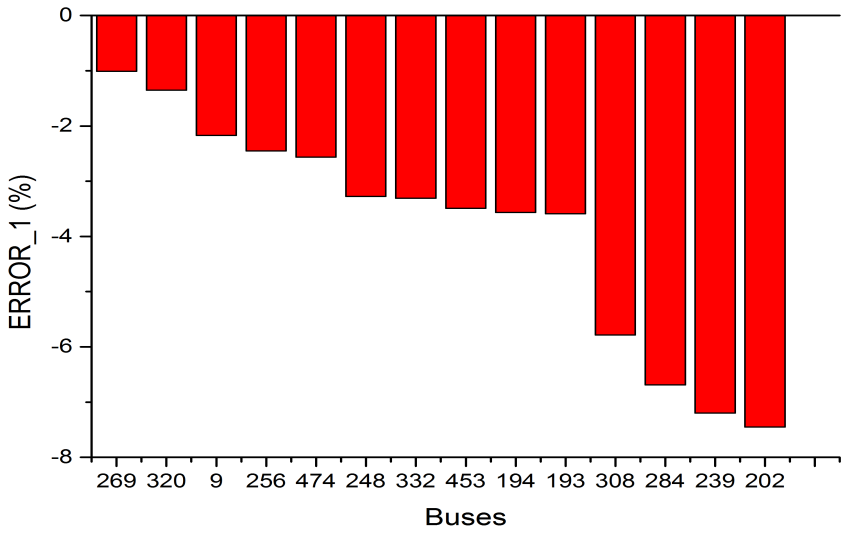

Figure 6.70: The result differences of neighbor buses of the bus 192

It indicates that all the results are negative, which is different to the results in previous two sections. It represents that the THDv values of all these buses decrease when

the power capacities and numbers of EVCs raise. It has a great influence on buses 308, 284, 202 and 239 as they generate larger result differences. Buses 202 and 284 are also connected to EVCs. Hence their THDv values change significantly with increasing the power capacities of EVCs. The bus 308 is in the first neighbourhood area of the bus 192. The great change of its THDv should be influenced by both bus 192 and bus 284. However, the bus 239 is in the third neighbourhood area. Its THDv value change may influenced by the bus 284 or other EVCs connected bus which are not shown in Figure 6.69. The other first neighbourhood buses of the bus 192 have nearly the same value change. In conclusion, without considering special cases (i.e. buses 284, 239 and 202), it generates more influence on the first neighbourhood buses than the buses in other two neighbourhood areas.

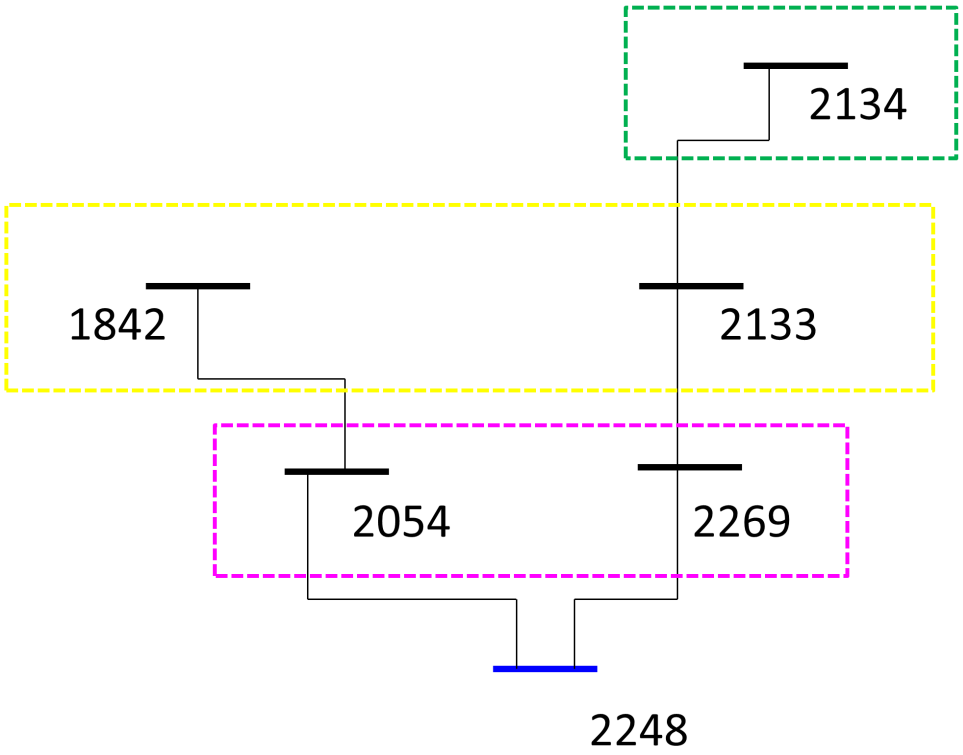

Figure 6.71: The neighbourhood connection diagram of the bus 2248

The THDv values of neighbourhood buses of the bus 2248 in two different scenarios are shown in Table 6.35. The result differences are illustrated in Figure 6.72.

Table 6.35: THDv values of neighbourhood buses of the bus 2248 in percentage

Bus	2054	2269	1842	2133	2134
Scenario three	15.02	3.91	15.97	2.37	2.37
Scenario four	58.09	10.70	62.09	9.87	9.88

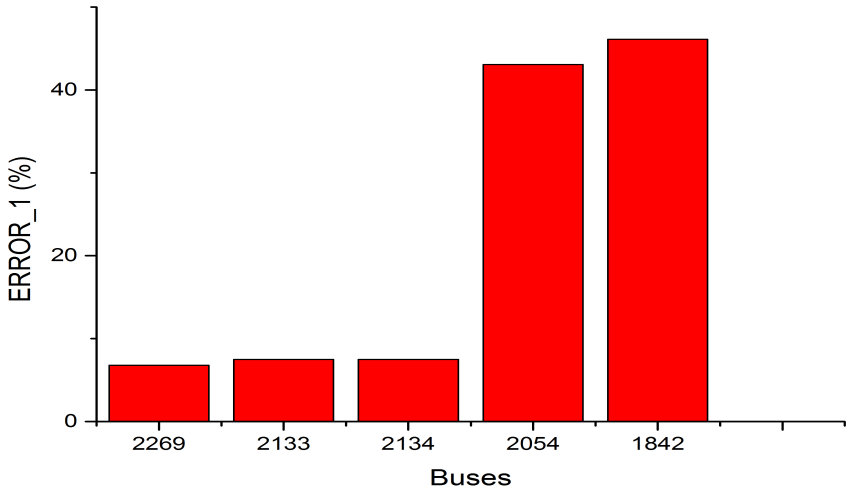

Figure 6.72: The result differences of neighbourhood buses of the bus 2248

The maximum value in each scenario is also highlighted in pink and yellow respectively as shown in Table 6.35. Therefore, the maximum values both occur on the bus 1842, which is in the second neighbourhood area. Another significant change of the THDv occurs on the bus 2054, which is the first neighbourhood bus of the bus 2248. Its value changes from 15.02 % to 58.09 %. According to Figure 6.72, all the results are positive. Hence, the THDv values of all neighbourhood buses of the bus 2248 increase when the power capacities of EVCs raise. It has an extreme influence on the values of buses 1842 and 2054 which are in the second and first neighbourhood area respectively. The result differences of their values are 46.12 % and 43.07 % respectively. Though the bus 2269 is also the first neighbourhood bus of the bus 2248, it has much less influence than the bus 2054. On both two branches of the bus 2248, the influence on the values of THDv to each neighbourhood bus increases with raising the distance to the bus 2248.

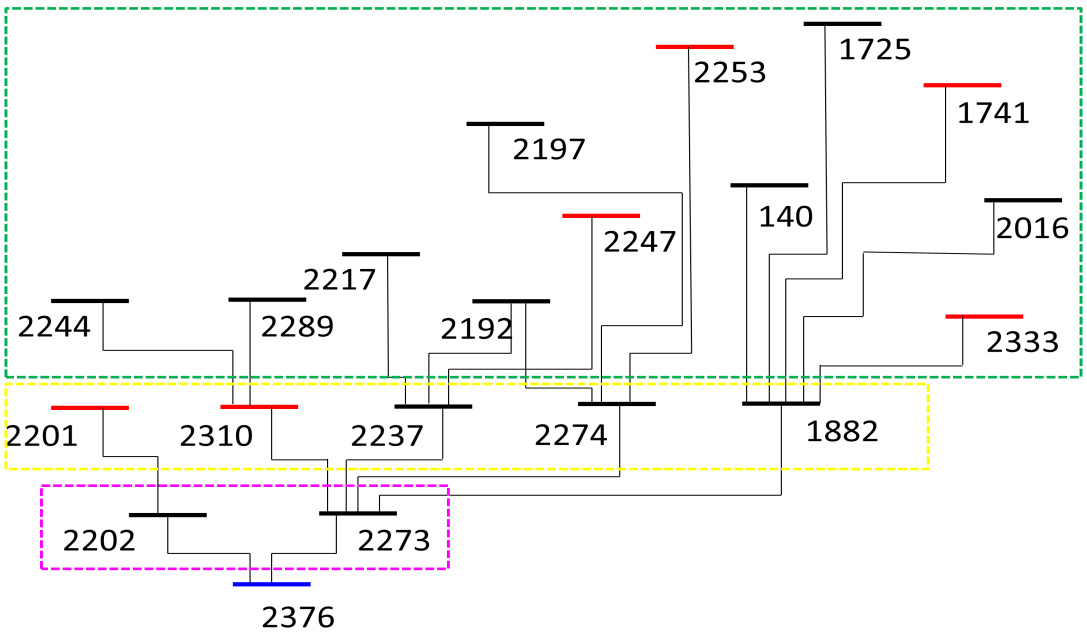

Figure 6.73: The neighbourhood connection diagram of the bus 2376

As shown in the above figure, six more buses are connected to the EVCs. They are buses 2201, 2301, 2247, 2253, 1741 and 2333. The THDv values of neighbourhood buses of the bus 2376 in two different scenarios are shown in Table 6.36 below. The maximum value in each scenario is highlighted in pink and yellow colour respectively.

Table 6.36: THDv values of neighbourhood buses of the bus 2376 in percentage

Bus	2273	2202	2201	1882	2274	2237	2310	2244	2289	2217
Scenario three	6.57	23.97	23.98	6.46	6.58	6.05	7.40	14.72	13.70	4.38
Scenario four	1.39	9.61	9.60	1.86	1.39	1.67	1.49	3.11	4.23	1.20
Bus	2192	2247	2197	2253	140	1725	1741	2016	2333	
Scenario three	6.82	10.29	7.98	8.00	0.94	7.30	10.24	7.52	4.83	
Scenario four	1.93	1.63	2.58	1.25	1.67	2.16	1.41	2.25	1.81	

The values of result differences between two scenarios are illustrated in Figure 6.74.

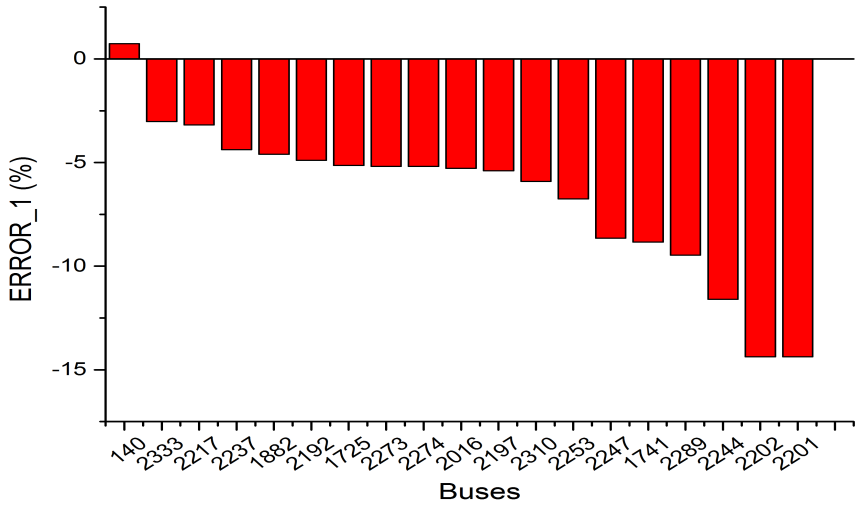

Figure 6.74: The result differences of neighbourhood buses of the bus 2376

Table 6.36 indicates that the maximum value of scenario three is on the bus 2201. However, the maximum value of scenario four is on the bus 2202. In addition, the THDv values of nearly 74 % neighbourhood buses decrease and reach to the first penetration level $(0-3\%)$ after increasing of the power capacities of EVCs. Figure 6.74 shows that all the values are negative except the bus 140. Hence, the THDv values of nearly all the buses decrease when increasing the power capacities of EVCs. The THDv values of buses 2202 and 2201 change significantly, whose result differences reach to -14.4%. The reason is that the bus 2201 is connected to EVCs itself, and the bus 2202 is also influenced by the harmonic source on the bus 2201. They are both along the first left-hand-side branch, but are separated in the first and second neighbourhood area of the bus 2376 respectively. The other harmonic source (EVCs) connected buses have more influence on their THDv values except the bus 2333. However, the other first and second neighbourhood buses have less influence than several fourth neighbourhood buses (i.e. buses 2289, 2244, 2197 and 2016). It may be because that those fourth neighbourhood buses were influenced by other connected harmonic source (EVCs) buses which were not shown in Figure 6.74. The bus 140 which is in the fourth neighbourhood area has smallest influence on the value of THDv.

Harmonic Powers

The total active and reactive powers at both sending and receiving ends (Ptotals, Ptotalr, Qtotals and Qtotalr) and the total power losses on each branch (Ptotalloss) are shown in Figures 6.75 to 6.79.

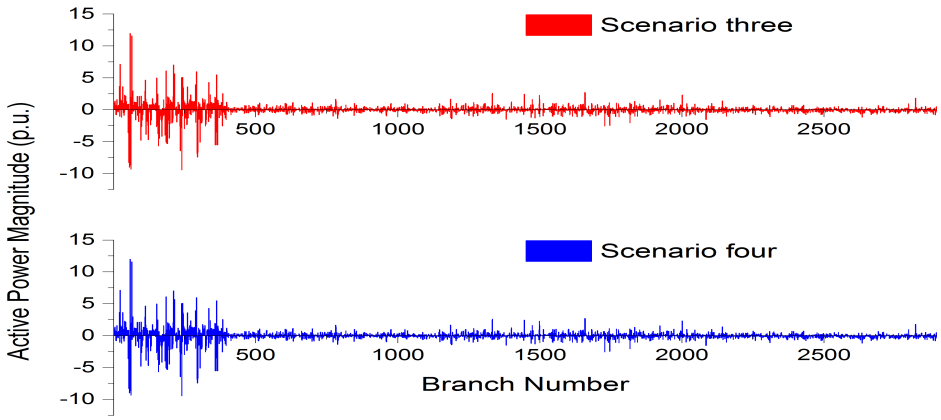

Figure 6.75: Total active powers at the sending end

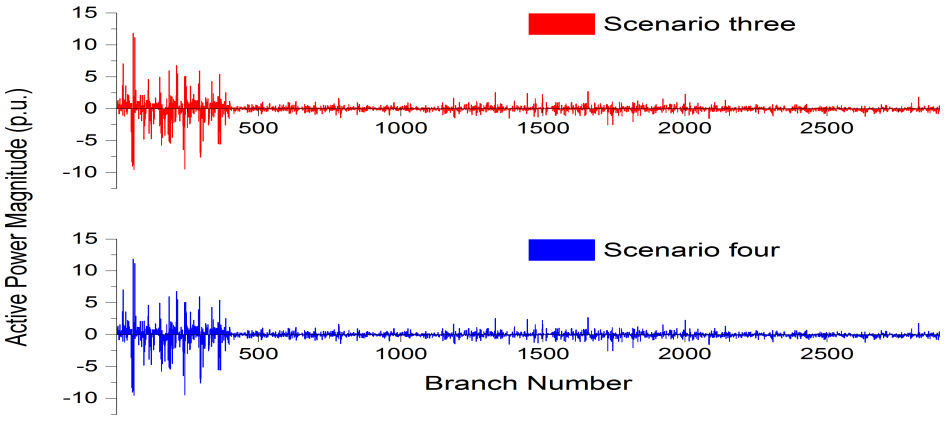

Figure 6.76: Total active powers at the receiving end

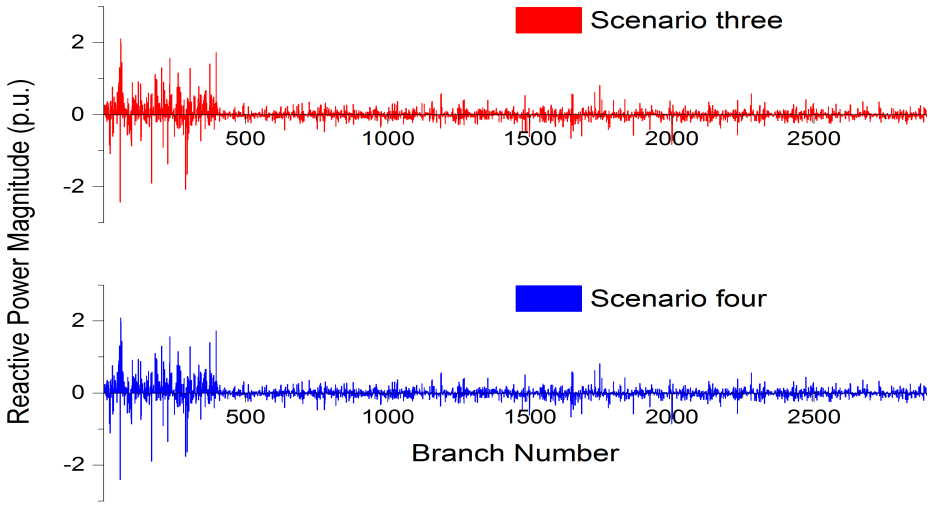

Figure 6.77: Total reactive powers at the sending end

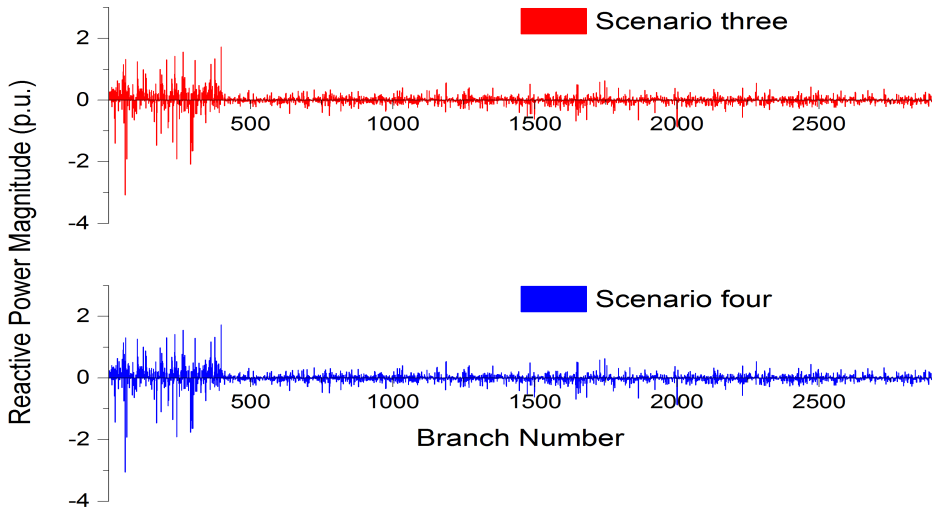

Figure 6.78: Total reactive powers at the receiving end

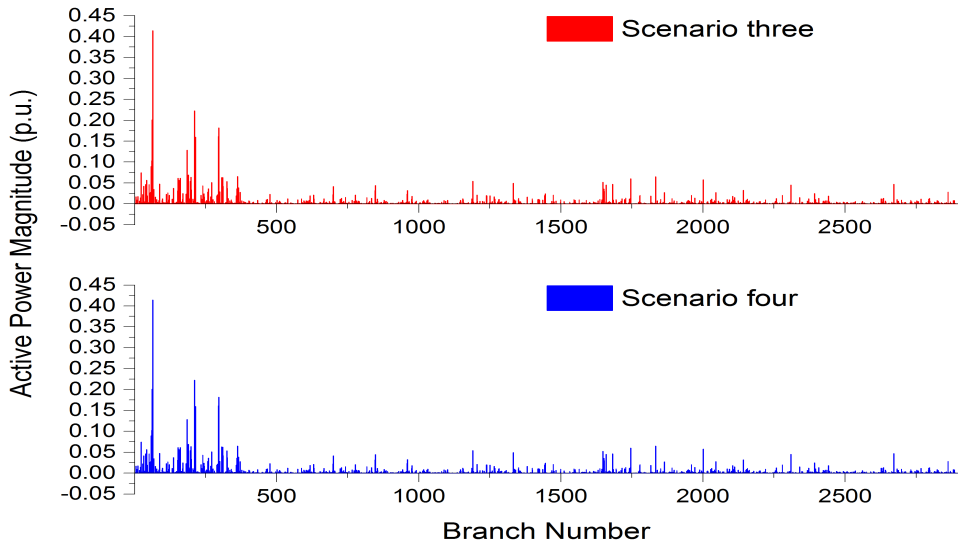

Figure 6.79: Total power losses on each branch

The results achieved from two different scenarios are illustrated in two layers with red and blue colour respectively in each diagram. Each scenario has the same vertical scope in each result category. The results of the Ptotals, Ptotalr, Qtotals and Qtotalr contain both positive and negative values. As mentioned, for the total active powers, if the values are positive, it denotes that the active powers flow from the sending ends to the receiving ends; otherwise, the active powers flow in the opposite way. For the total reacitve powers, if the results are positive, it means that the buses (sending and receiving ends) generate reactive powers; otherwise, they absorb reactive powers. The results show that the larger total active and reactive powers at both sending and receiving ends and power losses on each line are generated on the first 400 transmission lines, especially on the line 64 which generates the largest power loss, $0.4144 p.u.$ and $0.4142 p.u.$ respectively. It means more powers are transmitted on these lines during the harmonic penetration. The maximum values of these result categories are shown in Table 6.37 below.

Table 6.37: The maximum values of the Ptotals, Ptotalr, Qtotals, Qtotalr and Ptotalloss

Scenarios	Ptotals (p.u.)	Ptotalr (p.u.)	Qtotals (p.u.)	Qtotalr (p.u.)	Ptotalloss (p.u.)
Three	11.9709	11.8813	-2.4262	-3.0772	0.4144
Four	11.9772	11.8876	-2.4056	-3.0556	0.4142

The result waveforms that calculated from two different scenarios are nearly the same. It represents that increasing of the power capacities of EVCs may have no effects to the total active and reactive powers at both sending and receiving ends and the total power loss on each branch. In order to prove the this conclusion, the differences between each scenario are numerically illustrated in Figures 6.80 to 6.84, and the maximum values of them are shown in Table 6.38.

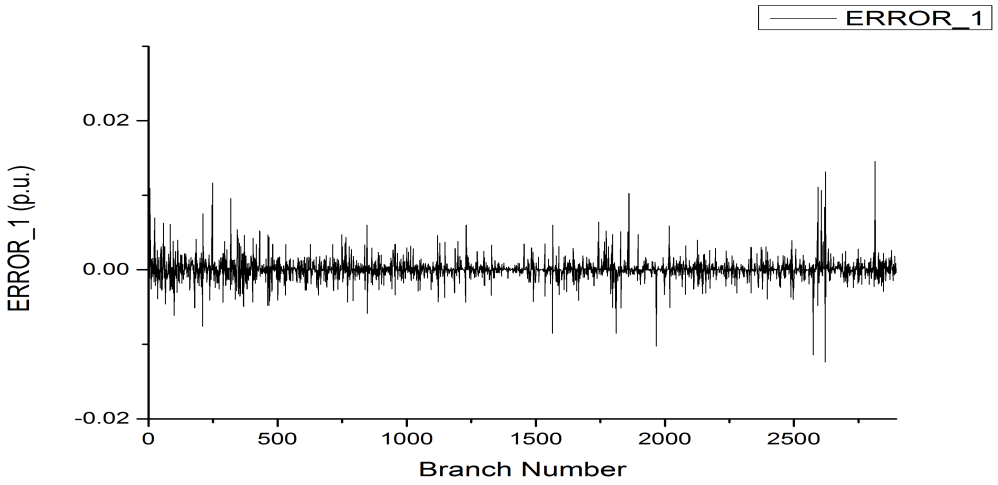

Figure 6.80: Total active powers at the sending end

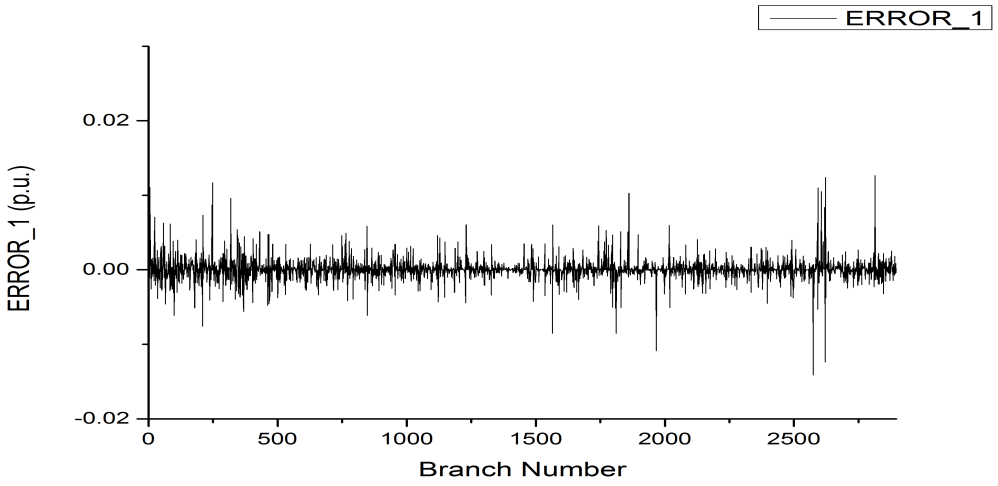

Figure 6.81: Total active powers at the receiving end

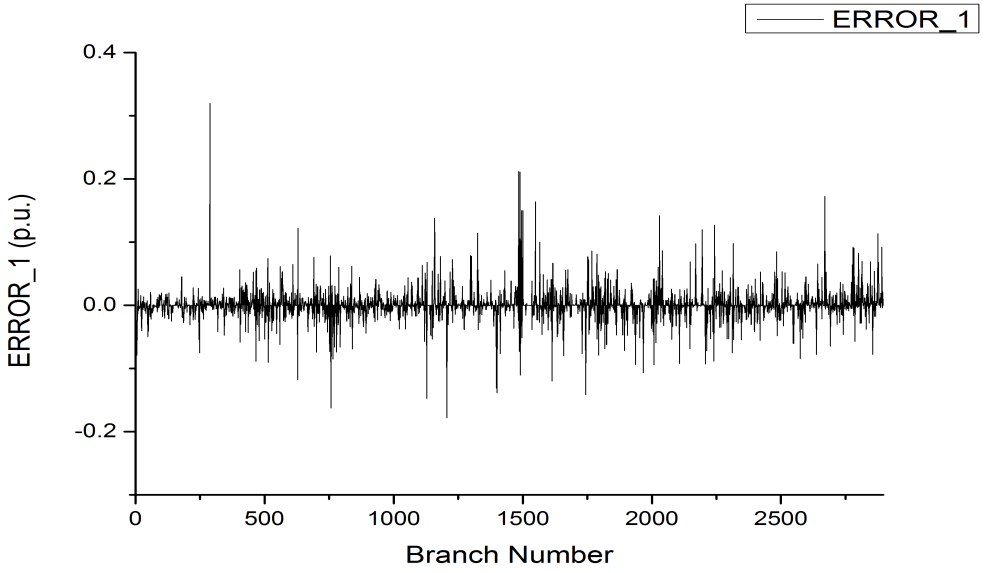

Figure 6.82: Total reactive powers at the sending end

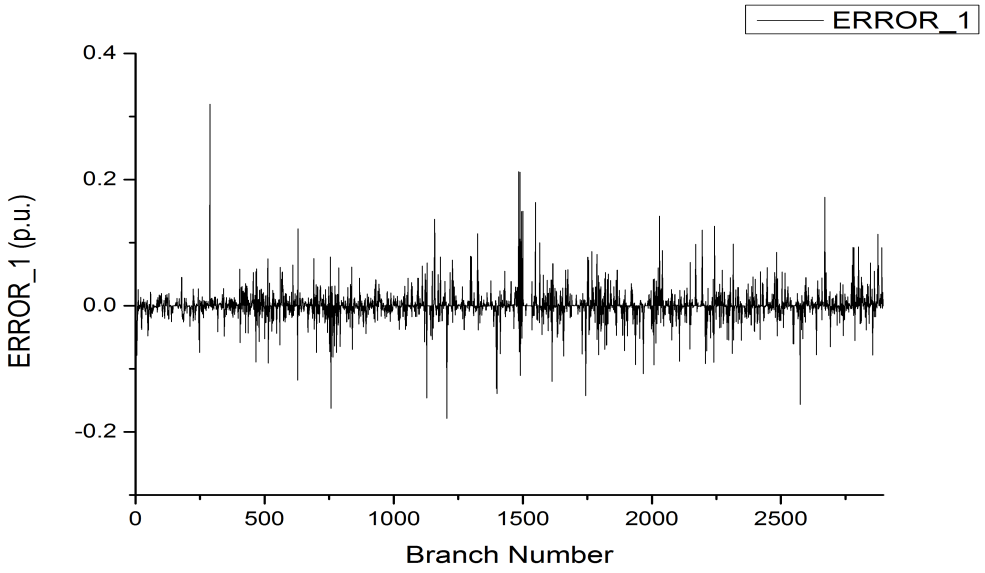

Figure 6.83: Total reactive powers at the receiving end

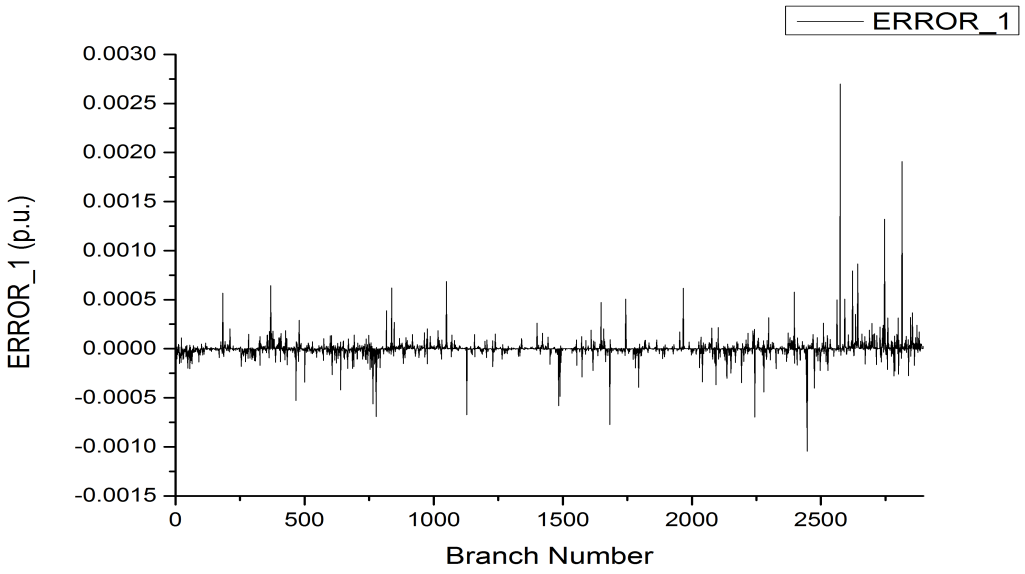

Figure 6.84: Total power losses on each branch

Table 6.38: The maximum difference values of the Ptotals, Ptotalr, Qtotals, Qtotalr and Ptotalloss

	Ptotals (p.u.)	Ptotalr (p.u.)	Qtotals (p.u.)	Qtotalr (p.u.)	Ptotalloss (p.u.)
ERROR_1	0.0146	-0.0141	0.3197	0.3198	0.0027

ERROR_1 in the figures above represent the result differences between scenario three and four. If the results are positive, it means the value achieved by scenario four is larger than that of scenario three. Both maximum values of the Ptotals and Ptotalr have a slight increase, $0.0063p.u.$. While other categories decrease with $0.0206p.u.$, $0.0216p.u.$ and $0.0002p.u.$ respectively, as shown in Table 6.37. When the absolute value of ERROR_1 is less than $0.01p.u.$, the results of two scenarios are considered as identical. Hence, raising of the power capacities of EVCs influences 11 lines of Ptotals, 11 lines of Ptotalr, 918 lines of Qtotals, 910 lines of Qtotalr and 0 lines of Ptotalloss. The greatest influence on Ptotals, Ptotalr, Qtotals and Qtotalr are on the line 2814, 2574, 288 and 288 with increasing of $0.0146p.u.$, $-0.0141p.u.$, $0.3197p.u.$ and $0.3198p.u.$ respectively, as shown in Table 6.38. Therefore, raising of the power capacities of EVCs by 15 % has more influence on total reactive powers at both sending and receiving ends with no regularity. However, it has nearly no influence on the total

power loss on each line as the number of assumed valid difference value is zero.

6.5 Result Summary

In this chapter, the proposed method was applied to a 2383-bus Polish power system connecting with multiple types of harmonic sources to calculate the harmonic power flow. The renewable generators such as wind turbines (WTs) and photovoltaic generators (PGs), the modern devices such as electric vehicle chargers (EVCs) and the traditional six-pulse line-commutated converters were regarded as harmonic sources in the calculation. Total 32 harmonic levels (including the fundamental frequency) were considered in the results, spanning sub-harmonics, inter-harmonics and integer-harmonics.

Furthermore, the effects of changing the power capacities of these harmonic sources to the harmonic penetration in this large power system, and the effects to the neighbourhood buses of these harmonic sources in different harmonic penetration levels were also investigated through three aspects:

- Combination one: changing of capacities of wind energy (scenarios one and two);
- Combination two: changing of capacities of multiple renewable energy (wind and solar) (scenarios one and three);
- Combination three: changing of power capacities of electric vehicle chargers (scenarios three and four).

The rms values of bus voltage magnitudes, the total harmonic voltage distortion (THDv), the total active and reactive powers at both sending and receiving ends (Ptotals, Ptotalr, Qtotals and Qtotalr) and the total power losses on each branch (Ptotalloss) were analysed.

6.5.1 Computing Time And Number Of Iterations

The computing time and the number of iterations are summarized in Table 6.39 below.

Table 6.39: Computing time and iterations

Scenarios	One	Two	Three	Four
Total power capacities	35 %	55 %	70 %	80 %
Computing time (s)	45.51	45.74	45.89	46.01
Iterations	5	5	5	5

The total power capacities represents the sum of power capacities of each kind of harmonic source. The result shows that the computing time of each scenario raises from 45.51 seconds to 46.01 seconds with increasing of the total harmonic capacities from 35 % to 80 %. However, the time differences between each scenario are only 0.23, 0.15 and 0.12 seconds respectively. They are very short. Hence, it has a little influence on the computing time with increasing of harmonic capacities. However, the number of iterations keeps in constant.

6.5.2 Voltage Magnitudes and THDv

All the result waveforms of rms values of voltage magnitudes achieved from two scenarios in each combination type were nearly the same. It was difficult to find out the difference only through the result diagrams. Therefore, the numerical comparisons between each scenario were required. The difference between the value of the two scenarios is considered as the error. When the absolute value of the error is less than $0.01 p.u.$, the error is considered as negligible and the results are considered as identical. The more numbers of errors were, the more buses were influenced, and the greater influence was. Hence, the numbers are summarized in Table 6.40.

Table 6.40: Summary of effects to the rms values of voltage magnitudes

	Combination one	**Combination two**	**Combination three**
No. of increasing	16	14	76
No. of decreasing	16	53	8
Total No.	32	67	84

The results of the scenario one, the scenario one and the scenario three in each combination type are regarded as the fundamental values respectively. If the error is positive, it represents that the results of the scenario two, the scenario three and the scenario four are increased respectively in each combination; if not, they are decreased respectively. Therefore, Table 6.40 shows that most buses are influenced when increas-

ing the power capacities of EVCs, which the total numbers of influenced buses are 84. It is because the numbers of harmonic source (EVCs) connected buses increase with raising the power capacities. In addition, the values of more buses decrease when increasing the power capacities of both WTs and PGs.

As the rms values of voltage magnitudes are relative to both fundamental voltage magnitudes and harmonic voltage magnitudes, the reason of changing of rms values could be fundamental voltage domain, harmonic voltage domain or fundamental-harmonic voltage domain. Hence, the value change on each bus would be irregular. Buses 1817, 1123 and 1842, that have greatest influence on the rms values of voltage magnitudes, were selected to achieve the investigation. As a result, the maximum changes of rms values of voltage magnitudes on buses 1817 and 1842 were mainly influenced by the harmonic voltage magnitudes. While the maximum change of rms value of voltage magnitude on the bus 1123 was influenced by the fundamental voltage magnitude. Moreover, these buses were not influenced by any neighbourhood harmonic source connected bus, according to their three levels of neighbourhood connection diagram.

The numerical comparison was also used to investigate the effects of changing power capacities of harmonic sources to the total voltage harmonic distortion (THDv). Hence, the total numbers of influenced buses are summarized in Table 6.41.

Table 6.41: Summary of effects to the THDv

	Combination one	**Combination two**	**Combination three**
Total No.	1158	1131	1205

It shows that the THDv values of nearly half buses of Polish 2383-bus power network are changed when raising the power capacities of WTs, multiple renewable generators and EVCs respectively. The THDv values in each different scenario (described in Tables 6.2 to 6.5) were categorized into four penetration levels. They were 0 - 3 %, 3 - 6 %, 6 - 10 % and $>$ 10% respectively. Therefore, the total numbers of THDv values in each penetration level in four scenarios is summarized in Table 6.42 below.

Table 6.42: The summary of numbers of THDv values in different penetration levels

Categories	No. of Buses			
	Scenario one	Scenario two	Scenario three	Scenario four
0 - 3 %	2198	1570	1568	1407
3 - 6 %	164	616	607	637
6 - 10 %	17	143	138	224
$>$ 10%	4	54	70	115
$>$ 3%	185	813	815	976
Total power capacities	35 %	55 %	70 %	80 %

The total power capacities represents the power capacities of harmonic sources. It indicates that the numbers of THDv values in both the first and fourth penetration levels increase with raising the total power capacities of harmonic sources from 35 % to 80 % (from Scenario one to Scenario four). Moreover, the numbers of THDv values that exceed the level of limit, 3 %, increased from 185 to 976.

Buses 192, 2248 and 2376 which were connected to WTs individually were chosen to investigate the harmonic penetration influence on their neighbourhood buses, based on the THDv values. They were selected from three different penetration levels in the basic scenario (i.e. Scenario one). The variation of their THDv values in different scenarios are summarized in Table 6.43 below.

Table 6.43: THDv values of selected buses in two scenarios

Bus	Scenario one	Scenario two	Scenario three	Scenario four
192	2.12 %	5.96 %	5.77 %	2.32 %
2248	4.18 %	8.19 %	8.03 %	27.50 %
2376	7.92 %	15.23 %	15.23 %	7.73 %

It shows that the THDv values of all these three buses increase when the power capacities of WTs and multiple renewable energy (WTs and PGs) increase respectively. However, their values decrease when increasing the power capacities of EVCs, except the bus 2248. It has an extreme increase to 27.50 %.

Three-level neighbourhood buses of these selected buses were illustrated in sections 6.4.1, 6.4.2 and 6.4.3 respectively. They are summarized in the following Table 6.44.

Table 6.44: Summary of neighbourhood buses

Bus	First neighbourhood	Second neighbourhood	Third neighbourhood
192	193, 194, 308, 453	332, 248, 256, 284, 239	9, 194, 269, 202, 474, 320
2248	2054, 2269	1842, 2133	2134
2376	2273, 2202	1882, 2274, 2237, 2310 2201	140, 1725, 1741, 2016, 2333 2192, 2197, 2253, 2217, 2247 2289

ERROR_1 was used to represent the result differences of THDv between each scenario in each combination type. It could denote the result variation on each neighbourhood bus directly. As mentioned before, the results of the scenario one, the scenario one and the scenario three in each combination type are regarded as the fundamental values respectively. If the value of ERROR_1 was positive, it represented that the results of the scenario two, the scenario three and the scenario four were increased respectively; otherwise, the they were decreased. As the third neighbourhood buses may be connected to other harmonic source (WTs, PGs and EVCs) buses which were not shown in the three levels of neighbourhood connection diagrams, two levels of neighbourhood buses were chosen to investigate the harmonic penetration influence. Therefore, the results are shown in Figures 6.85 to 6.87.

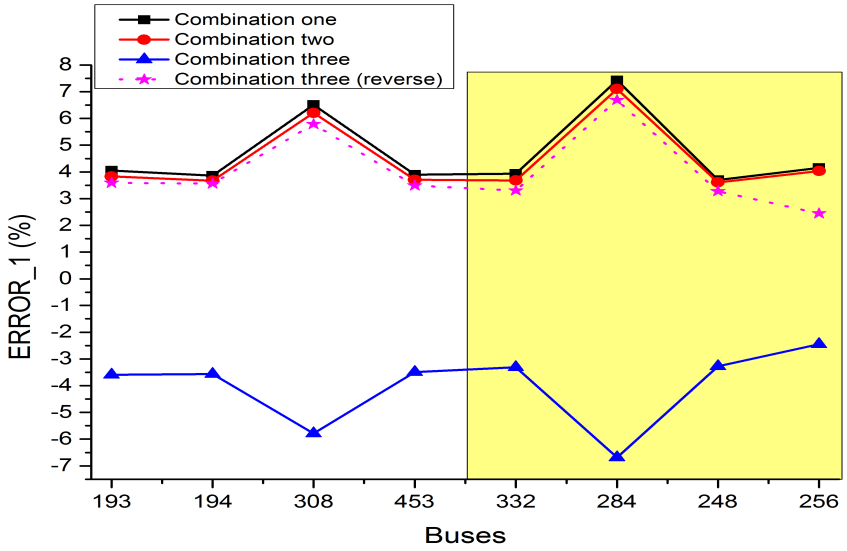

Figure 6.85: THDv values of neighbourhood buses of the bus 192

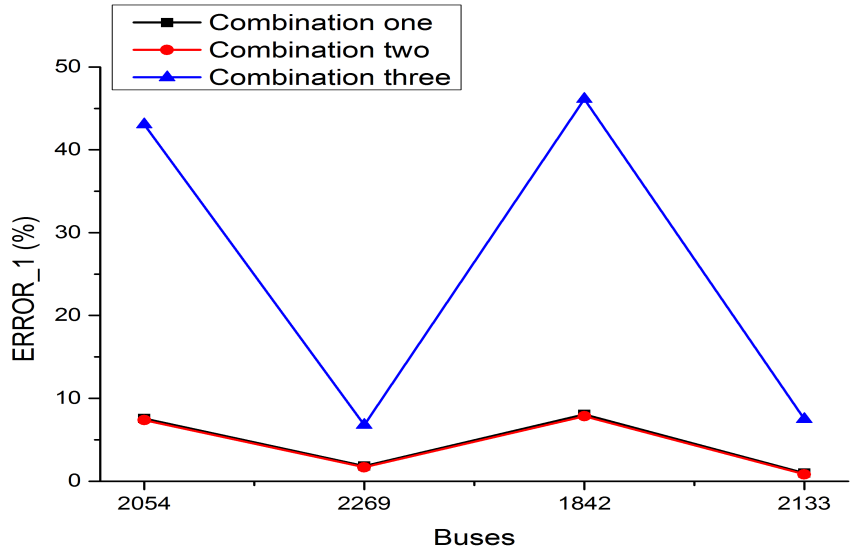

Figure 6.86: THDv values of neighbourhood buses of the bus 2248

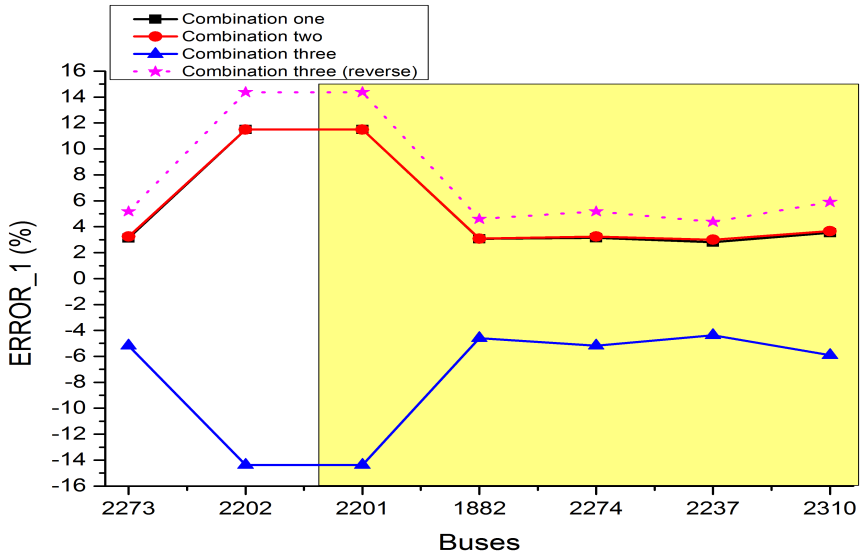

Figure 6.87: THDv values of neighbourhood buses of the bus 2376

All the second neighbourhood buses of the selected buses 192, 2248 and 2376 are illustrated in yellow area in each figure. Combination one, combination two and combination three represent increasing of power capacities of wind energy, multiple renewable energy and electric vehicle chargers respectively. As the result differences of neighbourhood buses of buses 192 and 2376 are negative in both combination one and three, they are reversed to positive and are illustrated in dot lines in Figures 6.85 and 6.87 respectively, in order to compare the variation. All the result differences are in percentage.

As shown in Figure 6.85, the neighbourhood buses of the bus 192 have more influence on their THDv values with increasing of the power capacities of WTs. Buses 193 and 332, buses 194 and 248, buses 194 and 256, and buses 308 and 284 are connected in four different branches respectively. These branches are assumed to be branch 1, branch 2, branch 3 and branch 4 respectively. Hence, according to the figure, the harmonic penetration influence decreases along the branch 1 in three combination aspects. However, the influence increases along both branch 3 and branch 4 in combination one and combination two.

Figure 6.86 indicates that the neighbourhood buses of the bus 2248 have more influence on their THDv values increasing the power capacities of EVCs. The influence in other two combination aspects are the same. Buses 2054 and 1842, and buses 2269 and 2133 are connected in different branches respectively. These two branches are assumed to be branch 1 and branch 2 respectively. The harmonic penetration influence on the first neighbourhood buses are more than that on the second neighbourhood buses in combination three. However, the influence decreases along the branch 2 in the combination one and combination two.

According to Figure 6.87, the neighbourhood buses of the bus 2376 have more influence on their THDv values when increasing the power capacities of EVCs. The influence in other two effect aspects are nearly the same. The harmonic penetration generates more influence on the first neighbourhood buses than the second neighbourhood buses in all three combination aspects.

6.5.3 Harmonic Powers

The results of numerical comparisons of total active and reactive powers at both sending and receiving ends (Ptotals, Ptotalr, Qtotals and Qtotalr) and total power loss on each line (Ptotalloss) are summarized in Table 6.45.

Table 6.45: Summary of effects ot the harmonic power flows

		Combination one	Combination two	Combination three
Ptotals	**No. of error**	2041	2125	11
	Max. error	9.2027 p.u.	16.6309 p.u.	0.0146 p.u.
Ptotalr	**No. of error**	2041	2122	11
	Max. error	9.2038 p.u.	16.5546 p.u.	-0.0141 p.u.
Qtotals	**No. of error**	1618	1873	918
	Max. error	-1.1234 p.u.	-3.1748 p.u.	0.3197 p.u.
Qtotalr	**No. of error**	1629	1865	910
	Max. error	-1.1113 p.u.	-4.0889 p.u.	0.3198 p.u.
Ptotalloss	**No. of error**	79	131	0
	Max. error	-0.1467 p.u.	0.3944 p.u.	0.0027 p.u.

The difference between the value of the two scenarios in each combination type was considered as the error. When the absolute value of the error was less than $0.01 p.u.$, the error was considered as negligible and the results were considered as identical. As shown in Table 6.45, the negative values represent the latter scenario (the scenario two, three and four) is larger than the former one (the scenario one and two) in each combination type. The more number and larger maximum value of errors were, the greater influence was. The Polish 2383-bus power system contains 2383 buses and 2896 branches. Therefore, the total active powers at both sending and receiving ends on most buses are influenced when increasing the power capacities of WTs and renewable generators respectively. While the reactive powers at both sending and receiving ends on half of buses were influenced. It had less influence on the total power loss in combination one and two. However, there was nearly no influence on the total active powers and total power loss with increasing of the power capacities of EVCs. The influence on each bus was irregular in each combination type.

References

[1] E. W. E. Association *et al.*, "Wind in power, 2013 european statistics," 2014, last data of access 13.06.2014. [Online]. Available: http://www.ewea.org/fileadmin/files/library/publications/statistics/EWEA_Annual_Statistics_2013.pdf xiii, 172, 173

[2] E. W. E. Association, "Statistics & targets," last date of access 13.06.2014. [Online]. Available: http://www.ewea.org/statistics/ 173

[3] ——, "2030: the next steps for eu climate and energy policy," 2013, last date of access 13.06.2014. [Online]. Available: http://www.ewea.org/fileadmin/files/library/publications/reports/2030.pdf

[4] E. W. E. T. Platform, "Strategic research agenda/ market deployment strategy (sra/mds)," 2014, last date of access 13.06.2014. [Online]. Available: http://www.windplatform.eu/fileadmin/ewetp_docs/Documents/reports/TPWind_SRA.pdf 173

[5] E. P. I. Association, "Solar photovoltaic electricity," last date of access 13.06.2014. [Online]. Available: http://www.epia.org/home/ 173

[6] R. Zimmerman, C. Murillo-Sanchez, and D. Gan, "Matpower: A matlab power system simulation package 2006," 2009, last date of access 12.06.2014. [Online]. Available: http://pserc.cornell.edu/matpower 174, 175

[7] P. S. E. S.A., "Annual report 2012," Tech. Rep., 2012, last date of access 17.06.2014. [Online]. Available: http://www.pse.pl/index.php?modul=10&gid=116 xiii, 175

[8] V. Pham and K. Wong, "Wavelet-transform-based algorithm for harmonic analysis of power system waveforms," in *Generation, Transmission and Distribution, IEE Proceedings-*, vol. 146, no. 3. IET, 1999, pp. 249–254. xxi, 176

[9] E. N. Association *et al.*, "Limits for harmonics in the uk electricity supply system," *Engineering Recommendation G5/4*, vol. 1, 2005. 188, 208, 210, 231

Chapter 7

Harmonic Power Flow Evaluation With Daily Generation And Load Tracking

7.1 Introduction

The previous chapter applied the proposed method to a large power system to calculate the harmonic power flow and investigate the effects of changing harmonic capacities with multiple types of harmonic sources, that consisting of wind turbines (WTs), photovoltaic generators (PGs), electric vehicle chargers (EVCs) and traditional converters. All the loads were constant in each scenario during the calculation, hence the harmonic power flows (including the fundamental frequency) generated using the proposed method were regarded as static harmonic load flow. It represents an instantaneous evaluation with discrete harmonic frequency. However, the output power capacities of generators (i.e. WTs and PGs) and the loads (i.e. EVCs, converters and linear-loads) capacities are changed in a time duration. For example, there more EVCs are used to charge the electrical vehicles in night-time than in day-time. The power generation of WTs and PGs varies with the wind speed and sunlight respectively. Consequently, the harmonic penetration will vary with tracking these changes of generators and loads. It may have a great influence on not only the power quality issue but also the electricity market (e.g. electricity pricing). Hence, the author is interested in in-

vestigating the harmonic penetration variation with tracking the generator and load capacities during a 24 hour period in this chapter.

The Polish 2383-bus power system is also used for the calculation. The WTs, PGs, EVCs and traditional six-pulse line-commutated converters, that including inter-harmonics, sub-harmonics and integer-harmonics, are regarded as harmonic sources, which is the same as chapter 6. The harmonic power flow variation during 24 hours is investigated through the results of the bus voltages, the total harmonic voltage distortion (THDv), the total active and reactive powers at both sending and receiving ends and the total power losses on each branch.

This chapter is arranged as follows: Section one is the introduction. Section two represents the proposed scenarios. The results and discussions are shown in the third section. The final section is the conclusion.

7.2 Scenarios

As mentioned before, the output powers of WTs and PGs vary with wind speed and sunlight respectively. Different seasons have different capacities of wind and solar sources. Moreover, the hourly demands on the consumer side (or the total load capacities) are also different in the four seasons [1, 2]. Hence, two scenarios are designed to investigate the daily harmonic penetration variation in this chapter. One is in summer and the other is in winter. It is assumed that 82 WTs, 86 PGs, 329 EVCs and 222 six-pulse converters are connected to the Polish 2383-bus power network. The time interval is defined as 15 minutes. However the time intervals of both hourly generation output data and hourly load demand data are one hour [1–6]. Therefore, one hour is separated into four equal time intervals with the same data. The output power capacities of generators are defined as the percentage of their total active powers to all generators. The power capacities of non-linear loads are defined as the percentage of their total active powers to all loads. The output power capacities of conventional generations are assumed to be constant. It is assumed that the harmonic injection currents (fundamental and higher harmonic frequencies) of harmonic sources are changed in the same ratio of their daily power generation model.

7.2.1 In Summer

It is assumed that the daily maximum output power capacity of PGs is 16 % of total generation output power. Its daily generation model is achieved from the weekday hourly data published by California ISO and Cambridge-Solar [3, 6]. It is shown in Table G.1 in Appendix G and Figure 7.1.

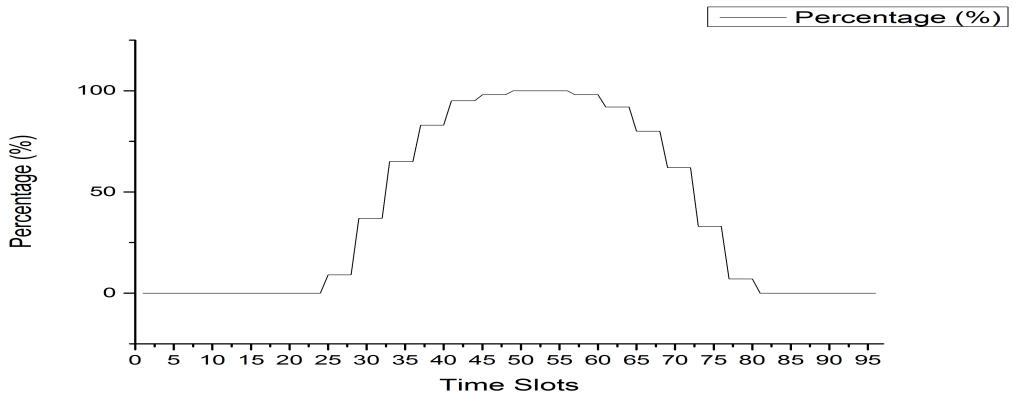

Figure 7.1: Diagram of hourly peak generation of PVs

The daily maximum output power capacity of WTs is assumed to be 20 % of total generation output power. In order to compensate output power of PGs, the daily generation model of WTs which obtained from California ISO [3] is used. The details are shown in Table G.2 in Appendix G and Figure 7.2 below.

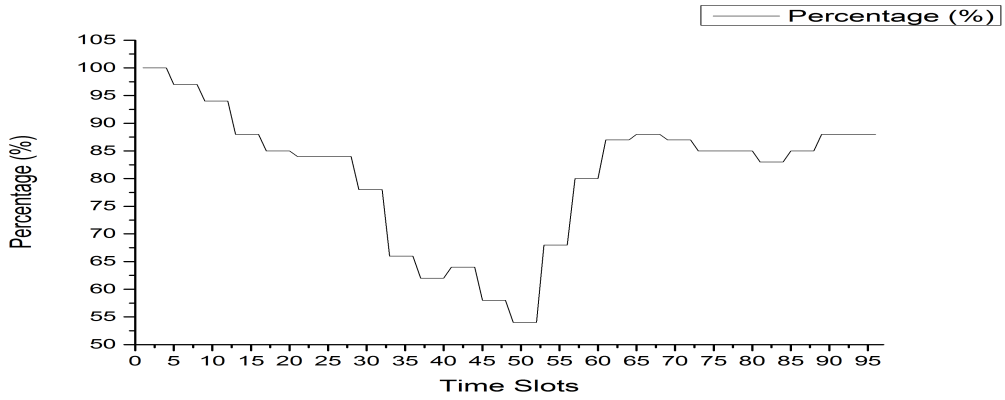

Figure 7.2: Diagram of hourly peak generation of WTs

The capacities of apparent powers of converters and linear loads are changed randomly per 15 minutes, following a weekday hourly load model in summer that is represented in reference [1, 2]. The data is illustrated in Table G.3 in Appendix G and the relative profile is shown in Figure 7.3 below.

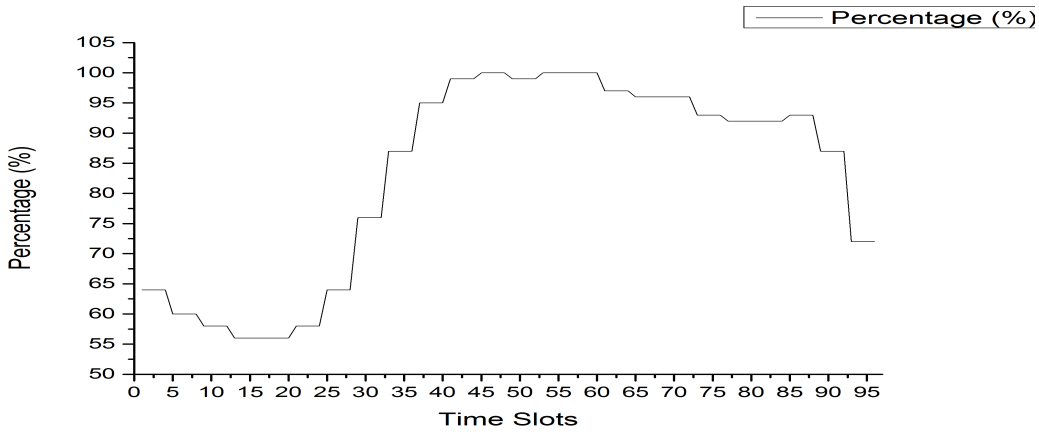

Figure 7.3: Diagram of hourly peak load of linear loads and converters

While the capacities of apparent powers of EVCs are changed per 15 minutes following the weekday hourly load model in reference [5]. The data and relative profile are shown in Table G.4 in Appendix G and Figure 7.4.

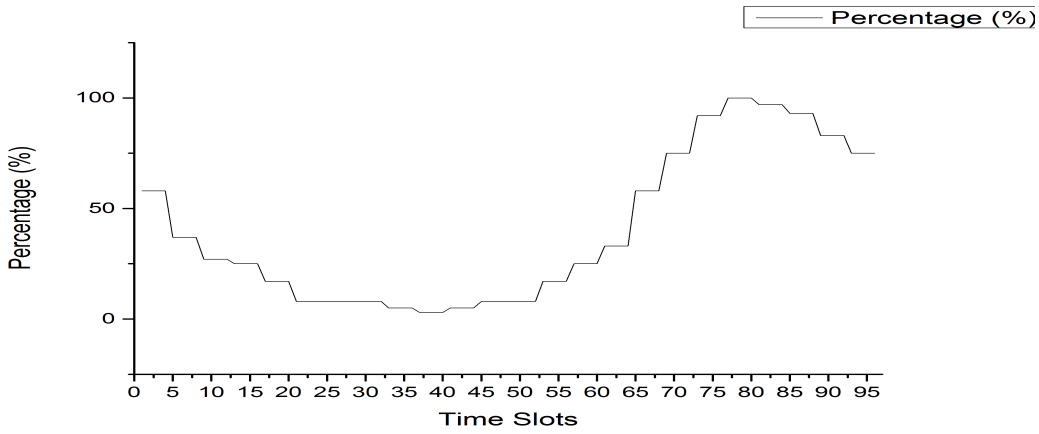

Figure 7.4: Diagram of hourly peak load of EVCs

7.2.2 In Winter

The number of hours of sunlight in winter are less than that in summer. Hence, the PGs generate less power. It is assumed the maximum output power capacity of PGs is also 16 % of total generation output power in summer. [4, 6]. Its daily generation model is achieved from the weekday hourly data in winter published by California ISO and Cambridge-Solar [4, 6]. It is shown in Table G.5 in Appendix G and Figure 7.5.

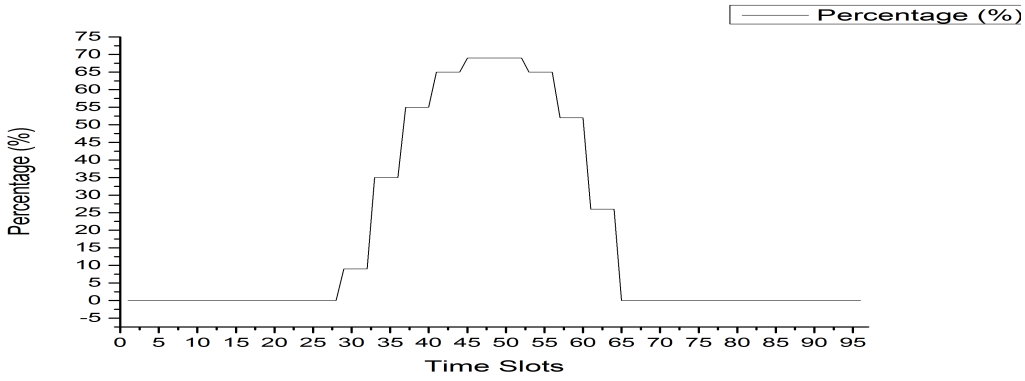

Figure 7.5: Diagram of hourly peak generation of PGs

While the capacities of apparent power of converters and linear loads are changed randomly per 15 minutes, following a weekday hourly load model in winter that is represented in reference [1, 2]. The data is illustrated in Table G.6 and the relative profile is shown in Figure 7.6 below.

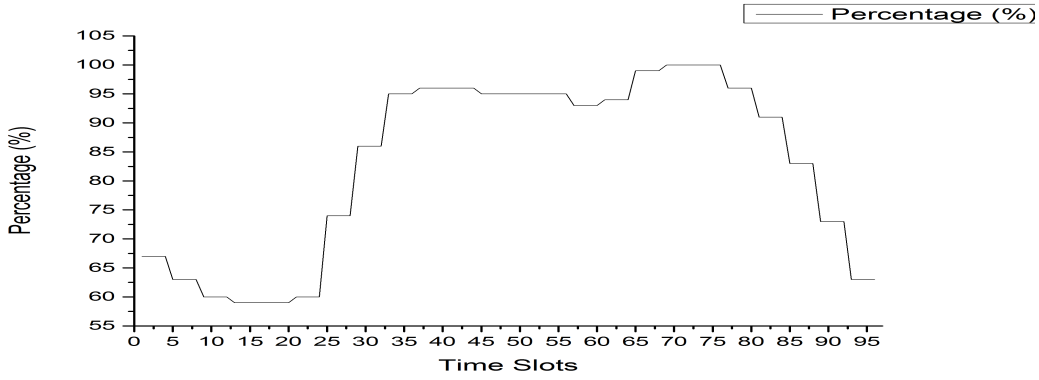

Figure 7.6: Diagram of hourly peak load of linear loads and converters

However, the daily generation and load model of WTs and EVCs in winter is assumed to be the same as the one in summer, respectively.

7.3 Results and Discussions

In this section, all the results are presented in two aspects: one is in summer and the other is in winter. In addition, the values of fundamental and higher order harmonic voltage magnitudes, total harmonic voltage distortion (THDv), total active and reactive powers at both sending and receiving ends and total power loss on each line are presented to investigate the harmonic penetration variation during 24 hours. The time interval is defined as 15 minutes. Therefore, 24 hours are divided into 96 time intervals.

7.3.1 Bus Voltage Magnitudes

Fundamental Voltage Magnitudes

In order to demonstrate the result precisely, buses 57, 84, 182, 202 and 225 are selected to present their values. They are connected to linear load, photovoltaic generator (PV), wind turbine (WT), electrical vehicle charger (EVC) and six-pulse converter respectively. Therefore, the results of fundamental voltage magnitudes on these buses during 24 hours in both summer and winter are shown in Figures 7.7 and 7.8 below.

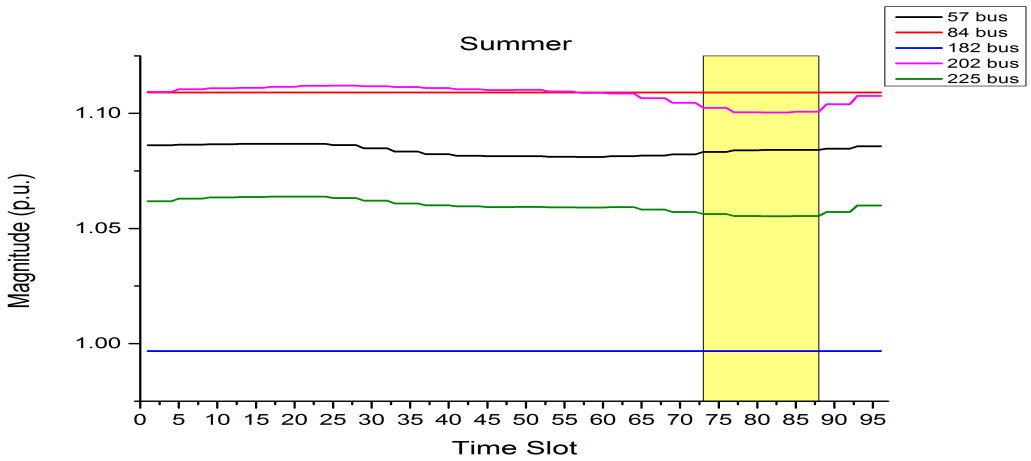

Figure 7.7: Fundamental voltage magnitudes during 24 hours in summer

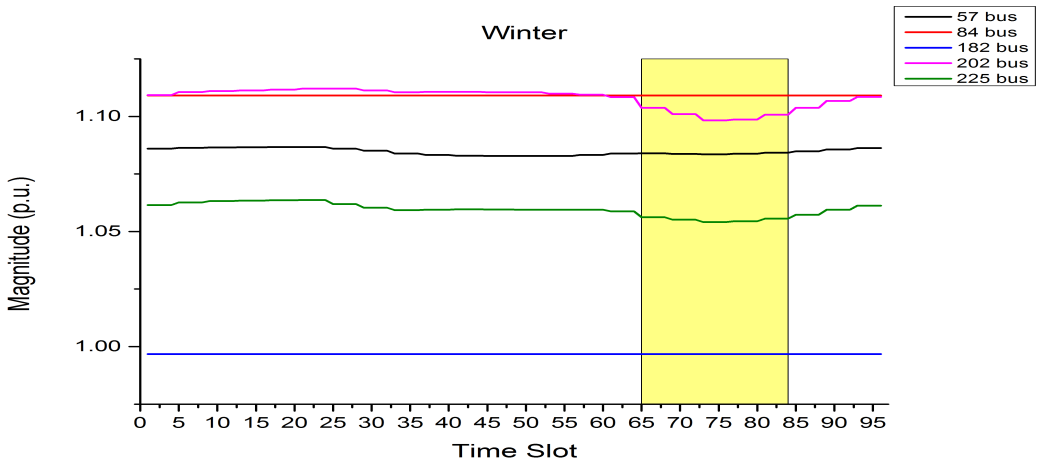

Figure 7.8: Fundamental voltage magnitudes during 24 hours in winter

The black, red, blue, pink and green curves in Figures 7.7 and 7.8 represent the fundamental voltage magnitude waveform of buses 57, 84, 182, 202 and 225 respectively. Each diagram has the same vertical scale. The waveforms of buses 84 and 182 in both diagrams are straight line respectively, which represents that the voltage magnitudes on these buses are constant during 24 hours. It is because that these two buses connected to PV and WT respectively are both voltage control buses. Their voltage magnitudes are assumed to be constant during the harmonic power flow calculation. The voltage curves of other buses have a little difference between summer and winter. Several results are highlighted in yellow area in each diagram. In summer, the area is from the 73^{rd} to 88^{th} time slot (from 6 pm to 10 pm). In winter, the area is from the 65^{th} to 84^{th} time slot (from 4 pm to 9 pm). In this yellow area there is a lack of output from renewable sources because of integrating wind turbines (WTs) and photovoltaic generators (PGs). The difference in generation is absorbed by the slack bus in order to obtain convergence. In real life situation a conventional generation allocation is needed. Hence, this yellow region needs to be considered carefully during the operational planning stage to maintain a balance between generation and demand.

The average and maximum values of fundamental voltage magnitudes on buses 57, 84, 182, 202 and 225 are summarized in Tables 7.1 and 7.2 respectively. The time interval is 15 minutes as mentioned before. However, four equal time slots in an hour

have same result value following the hourly peak generation and load models in section 7.2. Therefore, the time unit is defined as one hour in the table.

Table 7.1: Average values in both summer and winter

Buses	57	84	182	202	225
Ave. (p.u.) in summer	1.0839	1.1091	0.9967	1.1096	1.0608
Ave. (p.u.) in winter	1.0849	1.1091	0.9967	1.1099	1.0607

Table 7.2: Maximum values in both summer and winter

Buses	57	84	182	202	225
Time (hours)	4 - 5 am	24 hours	24 hours	6 - 7 am	4 - 5 am
Max. (p.u.) in summer	1.0868	1.1091	0.9967	1.1120	1.0639
Time (hours)	4 - 5 am	24 hours	24 hours	6 - 7 am	5 - 6 am
Max. (p.u.) in winter	1.0867	1.1091	0.9967	1.1121	1.0637

The average and maximum values in both summer and winter are calculated without the values that occur in the yellow area. The average values of buses 57, 84, 182, 202 and 225 in two different seasons are nearly the same. The maximum voltage magnitudes of buses 57 and 202 in two seasons occur in the same time slots, 4 - 5 am and 6 - 7 am, respectively. However, the maximum value of bus 225 in winter occurs one hour later than that in summer. The maximum values of buses 84 and 182 maintain constant during 24 hours in both summer and winter. Though the maximum values in two seasons of each bus are different, the differences are small enough to be ignored. Hence, it has nearly no influence on the fundamental voltage magnitudes of these selected buses when the season is changed from summer to winter.

Higher Harmonic Voltage Magnitudes

The harmonic emission currents contain thirty-one harmonic orders (excluding the fundamental frequency). Hence, the results of the harmonic bus voltage magnitudes also have thirty-one harmonic orders (excluding the fundamental frequency). It is not intended to show the results in all these harmonic orders in this section. Amongst all the results it is discovered that in most of the values the content of the 11^{th} harmonic is the most predominant. Hence, the values of the selected 11^{th} harmonic bus voltage magnitudes on buses 57, 84, 182, 202 and 225 in both summer and winter are illustrated in Figures 7.9 and 7.10 respectively. The yellow area in each diagram is also from the 73^{rd} to 88^{th} time slot (from 6 pm to 10 pm), and from the 65^{th} to 84^{th} time slot (from

4 pm to 9 pm), respectively. The lack of output from renewable sources in generation is absorbed by the slack bus in order to obtain convergence. Therefore, the values in this area are intended for illustration only and need to be considered carefully during the operational planning stage to maintain a balance between generation and demand.

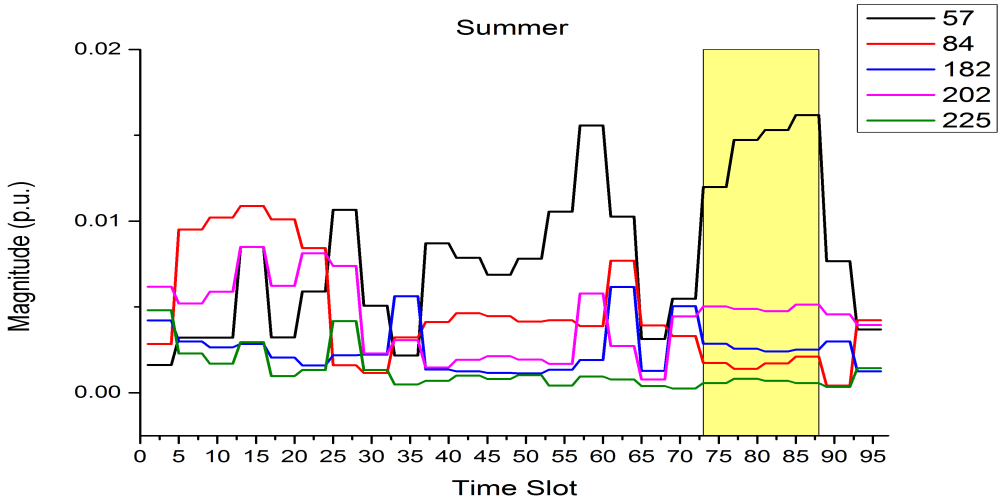

Figure 7.9: 11^{th} harmonic voltage magnitudes during 24 hours in summer

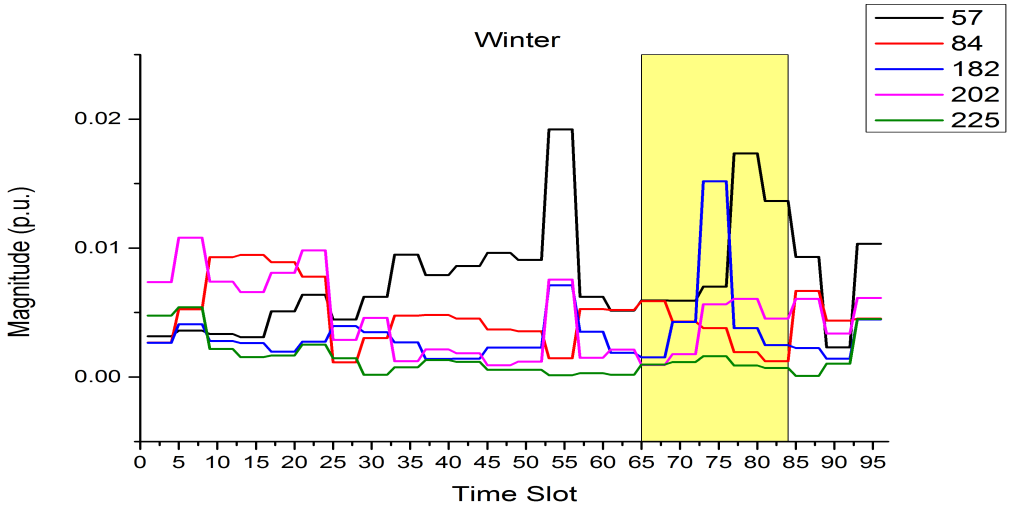

Figure 7.10: 11^{th} harmonic voltage magnitudes during 24 hours in winter

The results of the 11^{th} harmonic bus voltage magnitudes on buses 57, 84, 182, 202 and 225 are changed significantly during 24 hours in both summer and winter respectively. The result waveforms of these buses in winter are totally different to those in summer. The average and maximum values of the 11^{th} harmonic voltage magnitudes on these buses are summarized in Tables 7.3 and 7.4 respectively. The time unit is also defined as one hour. Moreover, the values in the yellow area are not considered.

Table 7.3: Average values in both summer and winter

Buses	57	84	182	202	225
Ave. (p.u.) in summer	0.0066	0.0052	0.0026	0.0042	0.0014
Ave. (p.u.) in winter	0.0070	0.0051	0.0029	0.0048	0.0016

Table 7.4: Maximum values in both summer and winter

Buses	57	84	182	202	225
Time (hours)	2 - 3 pm	3 - 4 am	3 - 4 pm	3 - 4 am	0 - 1 am
Max. (p.u.) in summer	0.0156	0.0109	0.0062	0.0085	0.0048
Time (hours)	1 - 2 pm	3 - 4 am	1 - 2 pm	1 - 2 am	1 - 2 am
Max. (p.u.) in winter	0.0192	0.0095	0.0071	0.0108	0.0054

The maximum values of the 11^{th} harmonic voltage magnitudes on each selected bus are different between summer and winter. In addition, they occur in different time slot, except bus 84. Therefore, it influences the 11^{th} harmonic voltage magnitudes a lot when the season is changed from summer to winter, according to Table 7.4 and the waveforms shown in Figures 7.9 and 7.10. However, their average values in summer and winter are nearly the same, as the differences are only in the order of 10^{-5}.

7.3.2 Total Harmonic Voltage Distortion (THDv)

In order to investigate the result clearly, buses 57, 84, 182, 202 and 225 are also selected to present their values of THDv. They are illustrated in black, red, blue, pink and green colour respectively in each result diagram. The same yellow area as defined in previous sub-section is also illustrated in each diagram to represent the imbalance area, where the total generation output powers cannot meet the total load consumption. However, the difference is absorbed by the slack bus in order to obtain convergence. Hence, the values in this area are achieved. A black straight line is illustrated in each

diagram. It represents the level of THDv limit, 3 %, described in the Engineering Recommendation G5/4 [7]. Hence, the results of THDv on buses 57, 84, 182, 202 and 225 in both summer and winter are illustrated in Figures 7.11 and 7.12 below.

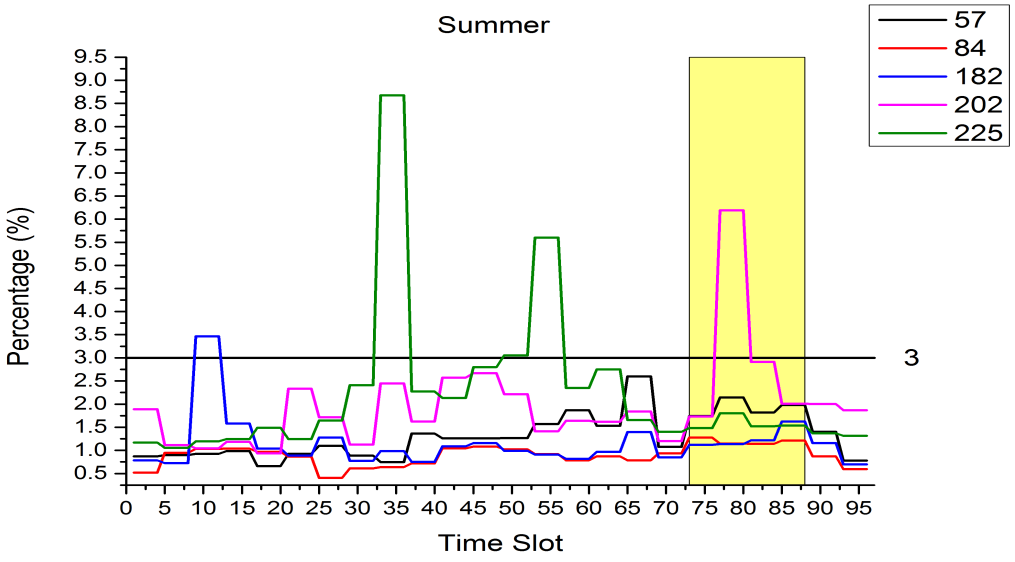

Figure 7.11: Results of THDv during 24 hours in summer

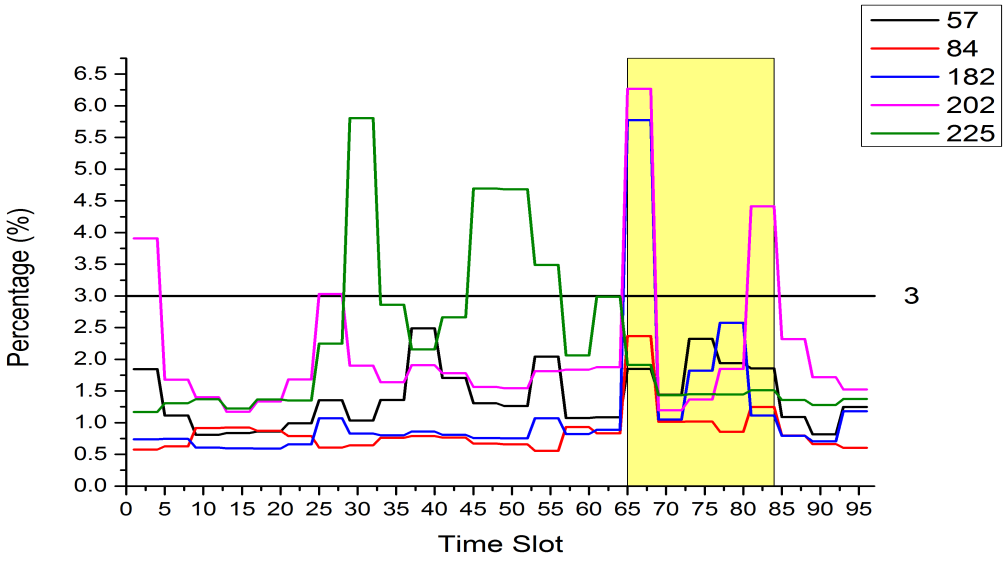

Figure 7.12: Results of THDv during 24 hours in winter

The results show that the waveform of each selected bus in summer is different to the one in winter. Hence, it had great influence on the THDv of each bus when the season is changed from summer to winter. The bus 225 generates the largest THDv value in both summer and winter without considering the values in the yellow area. In normal area, three values of THDv exceed the level of limit, 3 %, in summer. One is on bus 182, the other two are both on bus 225. While there are five values of THDv that exceed the limit. One is on bus 182, the other four are on bus 225. The maximum THDv values of selected buses are summarized in Table 7.5.

Table 7.5: Maximum THDv values in both summer and winter

Buses	57	84	182	202	225
Time (hours)	4 - 5 pm	11 - 12 am	2 - 3 am	11 - 12 am	8 - 9 am
Max. (p.u.) in summer	2.5986	1.0825	3.4630	2.6666	8.6738
Time (hours)	9 - 10 pm	2 - 3 pm	11 pm - 0 am	0 - 1 am	7 - 8 am
Max. (p.u.) in winter	2.4874	0.9332	1.1818	3.9068	5.8047

7.3.3 Power Flows

The lines 314 and 432 are selected to present the values of active and reactive powers at both sending and receiving ends and total power loss. The sending ends of these two lines are bus 239 and bus 182 respectively. While the receiving ends are bus 202 and bus 182 respectively. The power flow results of these two lines in both summer and winter are illustrated in Figures 7.13 to 7.18 below.

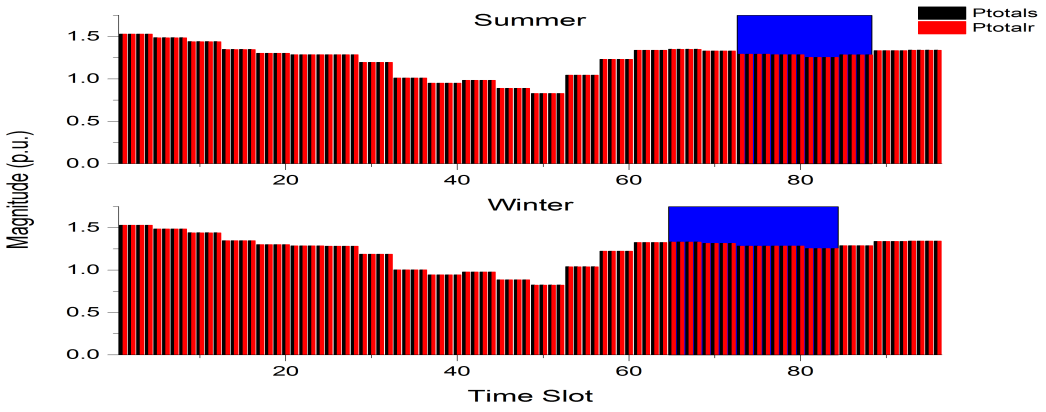

Figure 7.13: Active powers at both sending and receiving ends on line 314

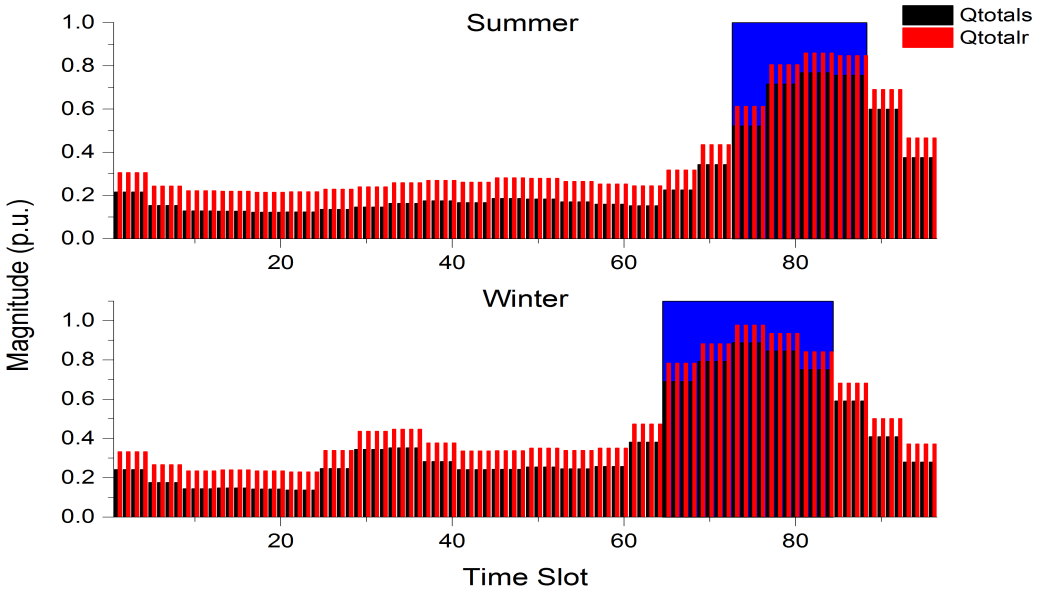

Figure 7.14: Reactive powers at both sending and receiving ends on line 314

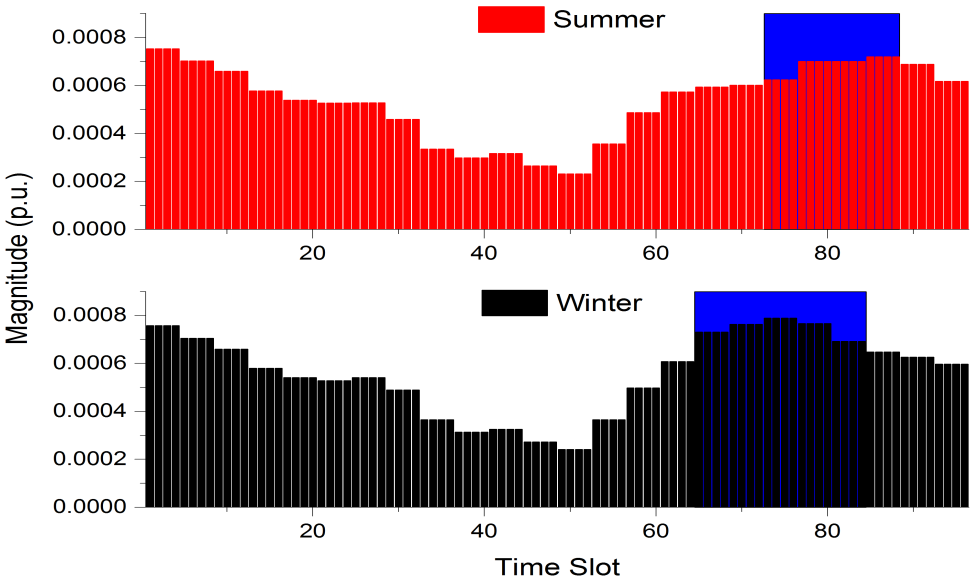

Figure 7.15: Total power loss on line 314

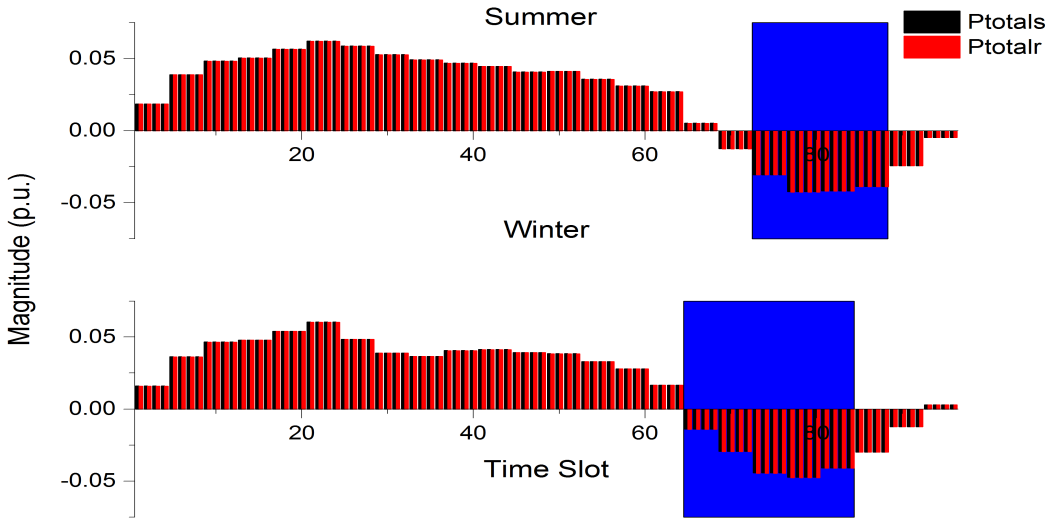

Figure 7.16: Active powers at both sending and receiving ends on line 432

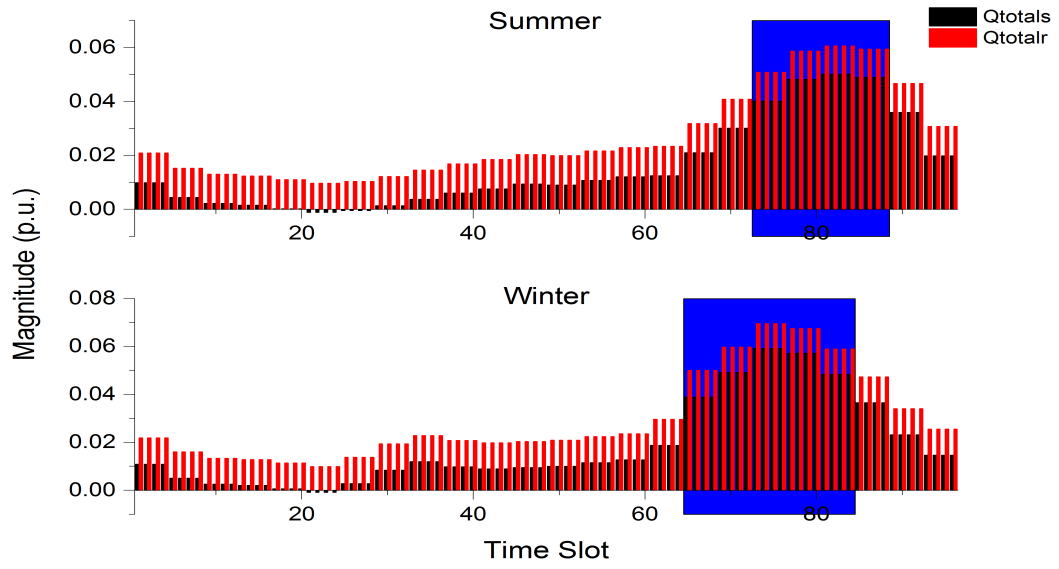

Figure 7.17: Reactive powers at both sending and receiving ends on line 432

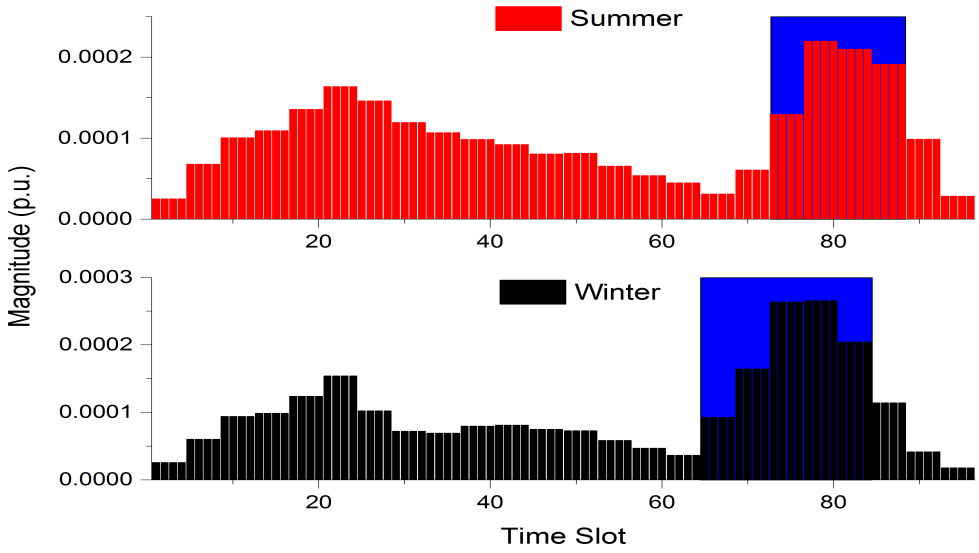

Figure 7.18: Total power loss on line 432

In Figures 7.13, 7.14, 7.16 and 7.17, the active or reactive power at sending and receiving ends are illustrated by black and red rectangular bar, respectively. However, the red and black rectangular bars represent the total power loss in summer and winter respectively, as shown in Figures 7.15 and 7.18. For active powers, if the values (both of two different columns) are positive, it denotes that the active powers flow from the sending ends to the receiving ends; otherwise, the active powers flow in the opposite way. For reactive powers, if the results are positive, it means that the buses (sending and receiving ends) generate reactive powers; otherwise, they absorb reactive powers. The blue area illustrated in each diagram represents the imbalance area, where the total generation output powers cannot meet the total load consumption. However, the difference is absorbed by the slack bus in order to obtain convergence. Hence, the values in this area are achieved. The border of this imbalance area is defined from the 73^{rd} to 88^{th} time slot (from 6 pm to 10 pm) in summer, and from the 65^{th} to 84^{th} time slot (from 4 pm to 9 pm) in winter.

The results show that the total active powers at both sending and receiving ends are nearly the same on both lines 314 and 432. Their result waveforms have a little difference between summer and winter. However, it has obvious differences of reactive

powers between sending and receiving ends in both summer and winter as shown in Figures 7.14 and 7.17. Moreover, their waveforms are also different between summer and winter. Hence, it generates more influences on the reactive power flows when the season is changed from summer to winter. In addition, the waveform of active powers and total power loss on the line 314 is similar to the WT daily peak generation model curve as shown in Figure 7.2. It is because that the bus 182 is one of two terminals on the line 314, which is connected to WT. The maximum values of total power loss on two selected lines in both summer and winter are only 1 kW. It is small comparing to the power base, 100 MW, and can be ignored.

7.4 Result Summary

The author applied the proposed method to a large Polish 2383-bus power system to calculate and investigate the harmonic power flow in 24 hours following the daily peak generation and load models. The wind turbines (WTs), photovoltaic generators (PGs), electric vehicle chargers (EVCs) and the traditional converters were connected to the power system as harmonic sources. The number and position of these harmonic sources were assumed to be constant.

Two scenarios were designed to achieve the investigation. One was in summer and the other was in winter. The output generation powers of conventional generators were assumed to be constant. However, the output generation powers of WTs and PGs varied with their daily peak generation models in both summer and winter. In addition, the load consumption curves of EVCs, converters and all linear loads were also changed following their daily peak load models in two seasons. The time interval was defined as 15 minutes. The time slot where total output generation powers could not meet the total load consumption was defined as imbalance area. However, the difference was absorbed by the slack bus in order to obtain convergence. Hence, the values in this area were achieved. But they were intended for illustration only. This shaded region needed to be considered carefully during the operational planning stage to maintain a balance between generation and demand.

Buses 57, 84, 182, 202 and 225 connected to linear load, PG, WT, EVC and six-

pulse converter respectively were selected to shown the results of voltages in both scenarios. The results indicated that the fundamental voltage magnitudes of buses 84 and 182 kept in constant during 24 hours, as they were voltage control buses. The values at other buses changed slightly. Moreover, the waveforms of these selected buses were nearly the same without considering the values in imbalance area. Hence, it had a little influence on the fundamental voltage magnitudes when the season was changed from summer to winter. Amongst all the results it was discovered that in most of the values the content of the 11^{th} harmonic was the most predominant. Hence, the 11^{th} harmonic voltage magnitude was selected to demonstrate the influence on the higher harmonic voltage magnitudes. Therefore, it indicated that it had great influence on the higher harmonic voltage magnitudes. The maximum root-mean-square (rms) values of bus voltages on all buses in summer and winter are summarized in Tables 7.6 and 7.7 respectively without considering the values in imbalance area. The time unit is defined as one hour, as the values of four equal time slots per hour are the same.

Table 7.6: The maximum rms values of bus voltages during 24 hours in summer

Time (hours)	12-1 am	1-2 am	2-3 am	3-4 am	4-5 am	5-6 am
Buses	301	301	2008	331	368	597
Max (p.u.)	1.1356	1.1359	1.2523	1.1444	1.1335	1.2676
Time (hours)	6-7 am	7-8 am	8-9 am	9-10 am	10-11 am	11 am-Noon
Buses	2355	368	466	368	368	368
Max (p.u.)	1.1371	1.1324	1.1874	1.1308	1.1307	1.1304
Time (hours)	Noon-1 pm	1-2 pm	2-3 pm	3-4 pm	4-5 pm	5-6 pm
Buses	368	368	368	368	368	368
Max (p.u.)	1.1304	1.1310	1.1316	1.1322	1.1322	1.1311
Time (hours)	10-11 pm	11 pm-12 am				
Buses	368	368				
Max (p.u.)	1.1295	1.1330				

Most of maximum rms values of voltages occur on bus 368 during 24 hours in both summer and winter. Table 7.6 shows that the highlighted value, $1.2676 p.u.$, is the maximum value between 5 - 6 am, which occurs on bus 597. Also it is the maximum rms value of voltage during 24 hours in summer. The value, $1.1883 p.u.$, highlighted in pink, is the maximum rms value between 2 - 3 am as shown in Table 7.7 in next page. It is also the maximum rms value of voltage during 24 hours in winter. It occurs on bus 1678.

Table 7.7: The maximum rms values of bus voltages during 24 hours in winter

Time (hours)	12-1 am	1-2 am	2-3 am	3-4 am	4-5 am	5-6 am
Buses	368	368	1678	368	368	368
Max (p.u.)	1.1342	1.1340	1.1883	1.1337	1.1334	1.1330
Time (hours)	6-7 am	7-8 am	8-9 am	9-10 am	10-11 am	11 am-Noon
Buses	1753	466	368	368	368	368
Max (p.u.)	1.1832	1.1316	1.1291	1.1296	1.1301	1.1301
Time (hours)	Noon-1 pm	1-2 pm	2-3 pm	3-4 pm	9-10 pm	10-11 pm
Buses	368	368	368	368	368	368
Max (p.u.)	1.1299	1.1305	1.1310	1.1301	1.1301	1.1328
Time (hours)	11 pm-12 am					
Buses	368					
Max (p.u.)	1.1345					

The results of THDv on buses 57, 84, 182, 202 and 225 changed significantly during 24 hours in both summer and winter. In addition, their result waveforms were respectively different between two seasons. Therefore, it also had a great influence on the values of THDv when the season was changed from summer to winter. It is very important to find out the numbers of buses that their THDv values exceed the limit, 3 %, presented in Engineering Recommendation G5/4 in each time slot. Hence, the results in both summer and winter are summarized in Table 7.8 below.

Table 7.8: Summary of number of THDv over 3 %

Hour	12-12.15 am	12.15-12.30 am	12.30-12.45 am	12.45-1 am
No. (summer)	187	187	187	187
No. (winter)	354	354	354	354
Hour	1-1.15 am	1.15-1.30 am	1.30-1.45 am	1.45-2 am
No. (summer)	143	143	143	143
No. (winter)	222	222	222	222
Hour	2-2.15 am	2.15-2.30 am	2.30-2.45 am	2.45-3 am
No. (summer)	345	345	345	345
No. (winter)	175	175	175	175

Continued on next page

Table 7.8- *Continued from previous page*

Hour	3-3.15 am	3.15-3.30 am	3.30-3.45 am	3.45-4 am
No. (summer)	282	282	282	282
No. (winter)	103	103	103	103
Hour	4-4.15 am	4.15-4.30 am	4.30-4.45 am	4.45-5 am
No. (summer)	119	119	119	119
No. (winter)	120	120	120	120
Hour	5-5.15 am	5.15-5.30 am	5.30-5.45 am	5.45-6 am
No. (summer)	309	309	309	309
No. (winter)	154	154	154	154
Hour	6-6.15 am	6.15-6.30 am	6.30-6.45 am	6.45-7 am
No. (summer)	276	276	276	276
No. (winter)	372	372	372	372
Hour	7-7.15 am	7.15-7.30 am	7.30-7.45 am	7.45-8 am
No. (summer)	123	123	123	123
No. (winter)	179	179	179	179
Hour	8-8.15 am	8.15-8.30 am	8.30-8.45 am	8.45-9 am
No. (summer)	143	143	143	143
No. (winter)	180	180	180	180
Hour	9-9.15 am	9.15-9.30 am	9.30-9.45 am	9.45-10 am
No. (summer)	167	167	167	167
No. (winter)	241	241	241	241
Hour	10-10.15 am	10.15-10.30 am	10.30-10.45 am	10.45-11 am
No. (summer)	287	287	287	287
No. (winter)	249	249	249	249
Hour	11-11.15 am	11.15-11.30 am	11.30-11.45 am	11.45-noon
No. (summer)	326	326	326	326
No. (winter)	152	152	152	152
Hour	noon-12.15 pm	12.15-12.30 pm	12.30-12.45 pm	12.45-1 pm
No. (summer)	277	277	277	277
No. (winter)	143	143	143	143

Continued on next page

Table 7.8- *Continued from previous page*

Hour	1-1.15 pm	1.15-1.30 pm	1.30-1.45 pm	1.45-2 pm
No. (summer)	241	241	241	241
No. (winter)	288	288	288	288
Hour	2-2.15 pm	2.15-2.30 pm	2.30-2.45 pm	2.45-3 pm
No. (summer)	248	248	248	248
No. (winter)	202	202	202	202
Hour	3-3.15 pm	3.15-3.30 pm	3.30-3.45 pm	3.45-4 pm
No. (summer)	354	354	354	354
No. (winter)	231	231	231	231
Hour	4-4.15 pm	4.15-4.30 pm	4.30-4.45 pm	4.45-5 pm
No. (summer)	359	359	359	359
No. (winter)	-	-	-	-
Hour	5-5.15 pm	5.15-5.30 pm	5.30-5.45 pm	5.45-6 pm
No. (summer)	355	355	355	355
No. (winter)	-	-	-	-
Hour	6-6.15 pm	6.15-6.30 pm	6.30-6.45 pm	6.45-7 pm
No. (summer)	-	-	-	-
No. (winter)	-	-	-	-
Hour	7-7.15 pm	7.15-7.30 pm	7.30-7.45 pm	7.45-8 pm
No. (summer)	-	-	-	-
No. (winter)	-	-	-	-
Hour	8-8.15 pm	8.15-8.30 pm	8.30-8.45 pm	8.45-9 pm
No. (summer)	-	-	-	-
No. (winter)	-	-	-	-
Hour	9-9.15 pm	9.15-9.30 pm	9.30-9.45 pm	9.45-10 pm
No. (summer)	-	-	-	-
No. (winter)	236	236	236	236
Hour	10-10.15 pm	10.15-10.30 pm	10.30-10.45 pm	10.45-11 pm
No. (summer)	274	274	274	274
No. (winter)	227	227	227	227

Continued on next page

Table 7.8- *Continued from previous page*

Hour	11-11.15 pm	11.15-11.30 pm	11.30-11.45 pm	11.45-12 am
No. (summer)	195	195	195	195
No. (winter)	328	328	328	328

'-' represents the value is in the imbalance area.

As shown in the above table, it has number of 359 buses that exceeds the limit, 3 %, between 4 - 5 pm in summer, and they are highlighted in yellow colour. While there are 372 buses that exceeds the limit between 6 - 7 am in winter, and they are highlighted in pink.

The lines 314 and 432 were selected to investigate the power flows in both summer and winter. The results indicated that it had more influence on the total reactive powers at both sending and receiving ends than the total active powers when the season was changed from summer to winter. The total power loss on each line in two seasons were both very small which were only in the order of 10^{-5}, comparing to the power base, 100 MW,.

References

[1] P. Subcommittee, "Ieee reliability test system," *Power Apparatus and Systems, IEEE Transactions on*, no. 6, pp. 2047–2054, 1979. 254, 256, 257

[2] C. Grigg, P. Wong, P. Albrecht, R. Allan, M. Bhavaraju, R. Billinton, Q. Chen, C. Fong, S. Haddad, S. Kuruganty *et al.*, "The ieee reliability test system-1996. a report prepared by the reliability test system task force of the application of probability methods subcommittee," *Power Systems, IEEE Transactions on*, vol. 14, no. 3, pp. 1010–1020, 1999. 254, 256, 257

[3] C. ISO, "Daily renewables output data," Tech. Rep., Jun. 2014, last date of access 25.06.2014. [Online]. Available: http://content.caiso.com/green/renewrpt/20140624_DailyRenewablesWatch.txt 255

[4] ——, "Daily renewables output data," Tech. Rep., Jan. 2014, last date of access 25.06.2014. [Online]. Available: http://content.caiso.com/green/renewrpt/20140101_DailyRenewablesWatch.txt 257

[5] K. Parks, P. Denholm, and A. J. Markel, *Costs and emissions associated with plug-in hybrid electric vehicle charging in the Xcel Energy Colorado service territory*. National Renewable Energy Laboratory Golden, CO, 2007. 256

[6] C. Solar, "Solar panels in cambridge," Tech. Rep., last date of access 25.06.2014. [Online]. Available: http://www.cambridge-solar.co.uk/solar-pv-cambridge/ 254, 255, 257

[7] E. N. Association *et al.*, "Limits for harmonics in the uk electricity supply system," *Engineering Recommendation G5/4*, vol. 1, 2005. 263

Chapter 8

Conclusions

8.1 Conclusions and Contributions

With increasing use of power electronic equipments, microprocessor controllers, renewable energy generations and modern electric devices for seeking higher system reliability and efficiency in the power systems, harmonics play a very important role in power quality issues. The harmonics have great influence on the power system equipment as well as on their operation. Harmonics can lead to operation failure of electrical and electronic components, overheating of neutral wires and transformer, failure of power factor correction capacitors, loss in power generation and transmission, and interference with protection, control and communication networks as well as customer loads. Hence, it is very important to design an accurate and efficient computer simulating method to evaluate the harmonic penetration in the power systems in order to analyse and eliminate the effects of harmonic injections. Therefore, the author devoted himself to develop a fast harmonic power flow calculation method and investigate the effects of harmonic penetration due to the integrating renewable energy generators and modern electronic devices.

The aim of this research had been achieved following two main parts: (a) developing a fast computer simulating methodology to evaluate the harmonic power flow in the power systems and (b) investigate the effects of harmonic penetration due to the integrating renewable energy generators and modern electronic devices with various

power capacities. The work results of these two parts are concluded in the following two sub-sections.

8.1.1 Development of Methodology

There are three steps when developing a fast computer simulating methodology to evaluate the harmonic power flow in the power systems: firstly the existing methods are reviewed and their disadvantages and problems are investigated, secondly a fast hybrid harmonic power flow calculation method is developed to solve the problems and improve the calculation and thirdly the proposed method is applied to several power systems to evaluate the harmonic penetration and the results are compared to those obtained by the Newton-Raphson based method (NRM) and the decoupled method (DM) to validate the proposed method.

In the first step, existing harmonic power flow methods are classified following four criteria: the modelling techniques of power system and non-linear loads simulations such as time domain, frequency domain and hybrid time-frequency domain, the system conditions such as single-phase and three-phase as well as balanced and unbalanced, the solution approaches such as coupled and decoupled and the modelling parameters of non-linear loads and power system components such as deterministic and stochastic, and are shown in Table 8.1 on next page.

Author is interested in development of fast harmonic power flow calculation method, that is implemented in frequency domain (static load flow) with discrete frequencies, in single-phase balanced power systems. The parameters of harmonic sources and power systems are deterministic. The NRM and the DM are mostly used to determine the harmonic penetration evaluation. However, they encounter two problems: firstly the iterative initial value should be close to the expected value, otherwise the calculation fail to converge; secondly the Jacobian matrix should be calculated in each iteration, which requires longer computing time and makes the calculation more complicated. In addition, the NRM may be difficult to converge when it is applied to a large power system with many non-linear loads and strong harmonic couplings.

Table 8.1: Classification and comparison of existing harmonic power flow methods

Methods	Modelling techniques				Modelling parameters	
	For systems	For non-linear loads	Solution approaches	System conditions	For systems	For non-linear loads
Newton HPF [a]	Frequency	Frequency	Coupled	Balanced	Deterministic	Deterministic
Decoupled HPF	Frequency	Frequency	Decoupled	Balanced	Deterministic	Deterministic
Fast Decoupled HPF	Frequency	Frequency	Decoupled	Balanced	Deterministic	Deterministic
Fast HPF	Frequency	Frequency	Decoupled	Balanced Unbalanced	Deterministic	Deterministic
Fuzzy HPF	Frequency	Time Frequency Hybrid	Coupled	Balanced	Deterministic	Stochastic
Probabilistic HPF	Frequency	Time Frequency Hybrid	Coupled	Balanced	Stochastic Deterministic	Stochastic
Modular HPF	Time Frequency Hybrid	Time Frequency Hybrid	Coupled	Balanced Unbalanced	Deterministic	Deterministic

[a] Harmonic power flow

A fast hybrid harmonic power flow calculation method (FHM) was proposed to solve the above problems. It uses the secant method to calculate the iterative initial value rather than random selection. Hence, it solves the convergence problem caused by poor initial values. Moreover, it integrates the Newton-Downhill method in the DM to calculate the harmonic power flow in order to simplify the iterative calculation of the Jacobian matrix, reduce the computing time and make the calculation converge successfully.

The proposed FHM was applied to 14-bus, 39-bus, 57-bus and 118-bus power systems with two six-pulse line-commutated converters that were regarded as harmonic sources to calculate the harmonic power flow in the third step. Moreover, the results were compared to those obtained by the NRM and the DM, in order to investigate the accuracy of the FHM and whether it could solve the convergence problem with poor initial values. According to the result comparison of computing time, iterations and convergence conditions, the NRM and the DM were limited in the initial value, i.e. they failed to converge when the initial values were $0.5p.u.$ and $0.6p.u.$ (generally, the region of initial value spans from $0.5p.u.$ to $1.5p.u.$ according to published simulation experiences). However, the FHM was not effected by the initial value setting. Despite, sometimes, the DM accomplished the calculation more quickly than the FHM especially in small power system, the difference in computing time was under 0.1 seconds. Larger the power system is FHM performs better. In addition, the result errors between each method are in the order of 10^{-5}, 10^{-6} and $10^{-7}p.u.$ and are sufficiently small to be neglected. Therefore, the proposed FHM succeeds in solving the convergence problem and accomplishes the harmonic power flow calculation with accurate results in a shorter computing time.

8.1.2 Effects of Integrating Renewable Energy Generators and Modern Devices

In this thesis, the effects of integrating renewable energy generators and modern electronic devices are investigated by applying the proposed FHM to a Polish 2383-bus single-phase power system with wind turbines (WTs), photovoltaic generators (PGs), electric vehicle chargers (EVCs) and traditional six-pulse converters in both momen-

tary and long time durations.

Four scenarios are designed to investigate the effects by changing the power capacities of harmonic sources in chapter 6. It is achieved through three aspects: effects of changing the wind power capacities (combination of scenario one and two); effects of changing the multiple renewable energy capacities (wind and solar) (combination of scenario one and three) and effects of changing the power capacities of EVCs (combination of scenario three and four). It was assumed that 186 converters, 252 WTs and 76 PGs were connected to the power network. Their quantity and connecting location remained constant. However, the output generation power capacities of WTs and PGs increased by 20 % and 15 % (from 20 % to 40 % and from 5 % to 20 %) respectively. The connecting location and quantity of EVCs were changed randomly, when increasing their power capacities from 5 % to 15 %. The results indicate that the computing time has a slightly increase with the increasing of the total power capacities of WTs, PGs and EVCs from 35 % to 80 %. Under these increases it is difficult to spot the difference directly from the diagrams in chapter 6, it has a little influence on the fundamental voltage magnitudes in each effect type according to the numerical comparison. However, it has more influence on the higher harmonic voltage magnitudes. It greatly influences the total harmonic voltage distortion (THDv) when increasing the power capacities of harmonic sources with the values of nearly half buses are changed. In addition, the number of THDv values that exceed the level of the limit, 3 %, also increase, which are 185, 813, 815 and 976 respectively. Nearly all the total active powers and half of the reactive powers at both sending and receiving ends are influenced when increasing the power capacities of WTs and multiple renewable generators respectively. However, there is nearly no influence on the total active powers and total power loss with increasing of the power capacities of EVCs, when comparing to other result categories. The influence of each result category is not uniform in each combination type.

In addition, the effects to the neighbourhood buses of harmonic sources in different harmonic penetration level are investigated based on THDv. Buses 192, 2248 and 2376 which are connected to WTs individually are selected for investigation. It indicates that the neighbourhood buses of bus 192 have more influence on their THDv values when

increasing power capacities of all the WTs. Moreover, the harmonic penetration influence decreases along the branch that consists of buses 194 and 248 in three different combination type. The neighbourhood buses of bus 2248 have more influence on their THDv values when increasing power capacities of all the EVCs. The harmonic penetration effect to the first neighbourhood buses are in general more than that to the second neighbourhood buses. Also it has more influence on the THDv values of the neighbourhood buses of bus 2376 when increasing power capacities of all the EVCs.

The effects due to the harmonic penetration in the Polish 2383-bus power system by integrating WTs, PGs and EVCs during 24 hours are demonstrated in chapter 7. The following two scenarios are studied: one is in summer and the other is in winter. The generation power outputs of conventional generators are assumed to be constant. However, the generation power outputs of WTs and PGs vary with their daily peak generation models in both summer and winter. In addition, the load consumption curves of EVCs, converters and all linear loads are also changed following their daily peak load models in two seasons. The time interval is defined as 15 minutes. The time slot where total generation power outputs could not meet the total load consumption is defined as imbalance area. In this region, there is insufficient output from renewable sources by integrating WTs and PGs. The difference in generation is absorbed by the slack bus in order to obtain convergence. In real life situation a re-allocation of conventional generation is needed. It needs to be considered carefully during the operational planning stage to maintain a balance between generation and demand. The results indicates that the higher order harmonic voltage magnitudes (excluding the fundamental frequency), THDv, active and reactive powers at both ends and total power loss on each transmission line have changed significantly during 24 hours in both summer and winter. In addition, it has a great influence on the higher order harmonic voltage magnitudes , THDv and total reactive powers at both sending and receiving ends when the season changes from summer to winter. A total of 359 and 372 buses exceed the level of 3 % limit in summer and winter respectively. The total power loss on each transmission line during 24 hours in two seasons are both very small when compared to the power base, 100 MW, as they are in the order of 10^{-5} (i.e. 1 kW).

8.2 Suggestions for Future Work

This thesis contributes to develop a fast computer simulation method to evaluate the harmonic penetration in power networks. It then investigates the effects of integrating the renewable energy generations (i.e. WTs and PGs) and modern electronic device (i.e. EVCs) with changing their power capacities in both instantaneous time and over a 24 hours period. However, it still has several possible expansion and improvements that can be considered for the methods. They are presented in the following aspects:

- The results of bus voltage magnitudes at harmonic frequencies and the total harmonic voltage distortion are mainly concerned in the study. Because the harmonic distortion limit in Engineering Recommendation G5/4 is generally based on the harmonic voltage. However, it usually uses equipment to measure the harmonic current at each bus to analyse the harmonic penetration in industry. The total harmonic current distortion (THD_i) and the harmonic currents at each bus will be evaluated and analysed in the future.

- In chapter 7, each type of harmonic source follows the same daily generation or load demand curve. However, it is different in practice. Because the difference of climate and demand situation. For example, two area of a power system have different climate situation: one is sunny, the other is raining. Therefore the photovoltaic generators in these two area may have different daily generation curves. If one load is industry, another load is commercial building in the power system. They may also have different daily demand curves. Hence each type of harmonic source with variable daily generation or load demand curves may be considered in future study.

- The proposed method is designed for harmonic penetration evaluation in single-phase balanced power system. However, three-phase power system gives better insight in the harmonic issue especially when it encounters unbalanced situation. Hence, the three-phase unbalanced power system can be considered in the future work.

- Harmonic penetration evaluation in power networks plays an important role in electricity market. The industries try to reduce the electricity price achieved by

renewable generations in order to motivate more people to use green energy. However, the more renewable energy is generated, the more harmonics it produces. Hence, the result of harmonic penetration evaluation is very important for investigating the effects of increasing use of renewable energy to electricity pricing.

Appendix A

Derivations of Jacobian Sub-matrix

The fundamental active and reactive powers at each linear bus i is represented as:

$$P_i^{(1)} = V_i^{(1)} \sum_{j=1}^{n} V_j^{(1)} (G_{(i,j)}^{(1)} \cos\theta_{(i,j)}^{(1)} + B_{(i,j)}^{(1)} \sin\theta_{(i,j)}^{(1)}) \tag{A.1}$$

$$Q_i^{(1)} = V_i^{(1)} \sum_{j=1}^{n} V_j^{(1)} (G_{(i,j)}^{(1)} \sin\theta_{(i,j)}^{(1)} - B_{(i,j)}^{(1)} \cos\theta_{(i,j)}^{(1)}) \tag{A.2}$$

where $G_{(i,j)}^{(1)}$ and $B_{(i,j)}^{(1)}$ are the real and imaginary parts of fundamental power system admittance $\tilde{Y}_{(i,j)}^{(1)}$.

Then we get:

$$P_i^{(1)} = (V_i^{(1)})^2 G_{(i,i)}^{(1)} + V_i^{(1)} \sum_{j=1\&j\neq i}^{n} V_j^{(1)} (G_{(i,j)}^{(1)} \cos\theta_{(i,j)}^{(1)} + B_{(i,j)}^{(1)} \sin\theta_{(i,j)}^{(1)}) \tag{A.3}$$

$$Q_i^{(1)} = -(V_i^{(1)})^2 B_{(i,i)}^{(1)} + V_i^{(1)} \sum_{j=1\&j\neq i}^{n} V_j^{(1)} (G_{(i,j)}^{(1)} \sin\theta_{(i,j)}^{(1)} - B_{(i,j)}^{(1)} \cos\theta_{(i,j)}^{(1)}) \tag{A.4}$$

The real and imaginary power mismatches at linear bus i are given as:

$$\begin{aligned} \Delta P_i^{(1)} &= P_i^{sp} - P_i^{(1)} \\ &= P_i^{sp} - V_i^{(1)} \sum_{j=1}^{n} V_j^{(1)} (G_{(i,j)}^{(1)} \cos\theta_{(i,j)}^{(1)} + B_{(i,j)}^{(1)} \sin\theta_{(i,j)}^{(1)}) \end{aligned} \tag{A.5}$$

$$\begin{aligned}\Delta Q_i^{(1)} &= Q_i^{sp} - Q_i^{(1)} \\ &= Q_i^{sp} - V_i^{(1)} \sum_{j=1}^{n} V_j^{(1)} (G_{(i,j)}^{(1)} \sin\theta_{(i,j)}^{(1)} - B_{(i,j)}^{(1)} \cos\theta_{(i,j)}^{(1)})\end{aligned} \tag{A.6}$$

Differentiating equation A.5 and A.6 with respect to fundamental bus voltage phase angle and magnitude, we obtain:

$$\frac{\partial \Delta P_i^{(1)}}{\partial \theta_j^{(1)}} = \begin{cases} \text{For} \quad i \neq j & -V_i^{(1)} V_j^{(1)} (G_{(i,j)}^{(1)} \sin\theta_{(i,j)}^{(1)} - B_{(i,j)}^{(1)} \cos\theta_{(i,j)}^{(1)}) \\ \text{For} \quad i = j & V_i^{(1)} \sum_{j=1 \& j \neq i}^{n} V_j^{(1)} (G_{(i,j)}^{(1)} \sin\theta_{(i,j)}^{(1)} - B_{(i,j)}^{(1)} \cos\theta_{(i,j)}^{(1)}) \\ & = Q_i^{(1)} + (V_i^{(1)})^2 B_{(i,i)}^{(1)} \end{cases} \tag{A.7}$$

$$\frac{\partial \Delta Q_i^{(1)}}{\partial \theta_j^{(1)}} = \begin{cases} \text{For} \quad i \neq j & V_i^{(1)} V_j^{(1)} (G_{(i,j)}^{(1)} \cos\theta_{(i,j)}^{(1)} + B_{(i,j)}^{(1)} \sin\theta_{(i,j)}^{(1)}) \\ \text{For} \quad i = j & -V_i^{(1)} \sum_{j=1 \& j \neq i}^{n} V_j^{(1)} (G_{(i,j)}^{(1)} \cos\theta_{(i,j)}^{(1)} + B_{(i,j)}^{(1)} \sin\theta_{(i,j)}^{(1)}) \\ & = -P_i^{(1)} + (V_i^{(1)})^2 G_{(i,i)}^{(1)} \end{cases} \tag{A.8}$$

$$\frac{\partial \Delta P_i^{(1)}}{\partial V_j^{(1)}} = \begin{cases} \text{For} \quad i \neq j & -V_i^{(1)} (G_{(i,j)}^{(1)} \cos\theta_{(i,j)}^{(1)} + B_{(i,j)}^{(1)} \sin\theta_{(i,j)}^{(1)}) \\ \text{For} \quad i = j & -\sum_{j=1 \& j \neq i}^{n} V_j^{(1)} (G_{(i,j)}^{(1)} \cos\theta_{(i,j)}^{(1)} + B_{(i,j)}^{(1)} \sin\theta_{(i,j)}^{(1)}) \\ & = -P_i^{(1)} + (V_i^{(1)})^2 G_{(i,i)}^{(1)} \end{cases} \tag{A.9}$$

$$\frac{\partial \Delta Q_i^{(1)}}{\partial V_j^{(1)}} = \begin{cases} \text{For} \quad i \neq j & -V_i^{(1)} (G_{(i,j)}^{(1)} \sin\theta_{(i,j)}^{(1)} - B_{(i,j)}^{(1)} \cos\theta_{(i,j)}^{(1)}) \\ \text{For} \quad i = j & -\sum_{j=1 \& j \neq i}^{n} V_j^{(1)} (G_{(i,j)}^{(1)} \sin\theta_{(i,j)}^{(1)} - B_{(i,j)}^{(1)} \cos\theta_{(i,j)}^{(1)}) \\ & = -Q_i^{(1)} + (V_i^{(1)})^2 B_{(i,i)}^{(1)} \end{cases} \tag{A.10}$$

For non-linear load, the derivatives of each element in $\overline{J}^{(h)}$ are similar to those in $\overline{J}^{(1)}$. But the values of active and reactive powers, real and imaginary power system ad-

mittance, bus voltage magnitude and phase angle are at harmonic frequencies. Hence, the elements of harmonic Jacobian sub-matrix, $\overline{J}^{(h)}$, are defined below:

$$\frac{\partial \Delta P_i^{(h)}}{\partial \theta_j^{(h)}} = \begin{cases} \text{For} \quad i \neq j & -V_i^{(h)} V_j^{(h)} (G_{(i,j)}^{(h)} \sin\theta_{(i,j)}^{(h)} - B_{(i,j)}^{(h)} \cos\theta_{(i,j)}^{(h)}) \\ \text{For} \quad i = j & V_i^{(h)} \sum_{j=1\&j\neq i}^{n} V_j^{(h)} (G_{(i,j)}^{(h)} \sin\theta_{(i,j)}^{(h)} - B_{(i,j)}^{(h)} \cos\theta_{(i,j)}^{(h)}) \\ & = Q_i^{(h)} + (V_i^{(h)})^2 B_{(i,i)}^{(h)} \end{cases} \tag{A.11}$$

$$\frac{\partial \Delta Q_i^{(h)}}{\partial \theta_j^{(h)}} = \begin{cases} \text{For} \quad i \neq j & V_i^{(h)} V_j^{(h)} (G_{(i,j)}^{(h)} \cos\theta_{(i,j)}^{(h)} + B_{(i,j)}^{(h)} \sin\theta_{(i,j)}^{(h)}) \\ \text{For} \quad i = j & -V_i^{(h)} \sum_{j=1\&j\neq i}^{n} V_j^{(h)} (G_{(i,j)}^{(h)} \cos\theta_{(i,j)}^{(h)} + B_{(i,j)}^{(h)} \sin\theta_{(i,j)}^{(h)}) \\ & = -P_i^{(h)} + (V_i^{(h)})^2 G_{(i,i)}^{(h)} \end{cases} \tag{A.12}$$

$$\frac{\partial \Delta P_i^{(h)}}{\partial V_j^{(h)}} = \begin{cases} \text{For} \quad i \neq j & -V_i^{(h)} (G_{(i,j)}^{(h)} \cos\theta_{(i,j)}^{(h)} + B_{(i,j)}^{(h)} \sin\theta_{(i,j)}^{(h)}) \\ \text{For} \quad i = j & -\sum_{j=1\&j\neq i}^{n} V_j^{(h)} (G_{(i,j)}^{(h)} \cos\theta_{(i,j)}^{(h)} + B_{(i,j)}^{(h)} \sin\theta_{(i,j)}^{(h)}) \\ & = -P_i^{(h)} + (V_i^{(h)})^2 G_{(i,i)}^{(h)} \end{cases} \tag{A.13}$$

$$\frac{\partial \Delta Q_i^{(h)}}{\partial V_j^{(h)}} = \begin{cases} \text{For} \quad i \neq j & -V_i^{(h)} (G_{(i,j)}^{(h)} \sin\theta_{(i,j)}^{(h)} - B_{(i,j)}^{(h)} \cos\theta_{(i,j)}^{(h)}) \\ \text{For} \quad i = j & -\sum_{j=1\&j\neq i}^{n} V_j^{(h)} (G_{(i,j)}^{(h)} \sin\theta_{(i,j)}^{(h)} - B_{(i,j)}^{(h)} \cos\theta_{(i,j)}^{(h)}) \\ & = -Q_i^{(h)} + (V_i^{(h)})^2 B_{(i,i)}^{(h)} \end{cases} \tag{A.14}$$

Appendix B

Derivatives of The C Matrix

The h^{th} harmonic line current at bus p is written as the p^{th} row of h^{th} harmonic power system admittance multiplied by the bus harmonic voltage vector:

$$\begin{aligned} I_p^{\tilde{(h)}} &= \sum_{q=1}^{n} \overline{Y}_{(p,q)}^{(h)} \overline{V}_q^{(h)} \\ &= I_{r,p}^{(h)} + jI_{i,p}^{(h)} \end{aligned} \tag{B.1}$$

where $I_{r,p}^{(h)}$ is the real part of h^{th} harmonic line current at bus p. $I_{i,p}^{(h)}$ represents the imaginary part of h^{th} harmonic line current at bus p.

Writing the h^{th} harmonic voltage of bus p, $\tilde{V}_p^{(h)}$, and the h^{th} harmonic power system admittance, $\tilde{Y}_{p,q}^{(h)}$, in phasor notation, we get:

$$\tilde{V}_p^{(h)} = \mid V_p^{(h)} \mid e^{j\theta_p^{(h)}} \tag{B.2}$$

$$\tilde{Y}_{p,q}^{(h)} = \mid Y_{p,q}^{(h)} \mid e^{j\delta_{p,q}^{(h)}} \tag{B.3}$$

where $\theta_p^{(h)}$ and $\delta_{p,q}^{(h)}$ denote the h^{th} harmonic bus voltage phase angle and power system admittance angle, respectively.

Then, the real and imaginary components of the h^{th} harmonic line current at bus p

are:

$$\frac{\partial I_{r,p}^{(h)}}{\partial \theta_q^{(h)}} = - \mid Y_{p,q}^{(h)} \mid\mid V_p^{(h)} \mid \sin(\delta_{p,q}^{(h)} + \theta_p^{(h)}) \tag{B.4}$$

$$\frac{\partial I_{r,p}^{(h)}}{\partial V_q^{(h)}} = \mid Y_{p,q}^{(h)} \mid \cos(\delta_{p,q}^{(h)} + \theta_p^{(h)}) \tag{B.5}$$

$$\frac{\partial I_{i,p}^{(h)}}{\partial \theta_q^{(h)}} = \mid Y_{p,q}^{(h)} \mid\mid V_p^{(h)} \mid \cos(\delta_{p,q}^{(h)} + \theta_p^{(h)}) \tag{B.6}$$

$$\frac{\partial I_{i,p}^{(h)}}{\partial V_q^{(h)}} = \mid Y_{p,q}^{(h)} \mid \sin(\delta_{p,q}^{(h)} + \theta_p^{(h)}) \tag{B.7}$$

Appendix C

Hth Harmonic Line Current And Power Flow

No transformer between the sending end p and the receiving end q

The π equivalent diagram of a transmission line without transformer is shown in Figure C.1.

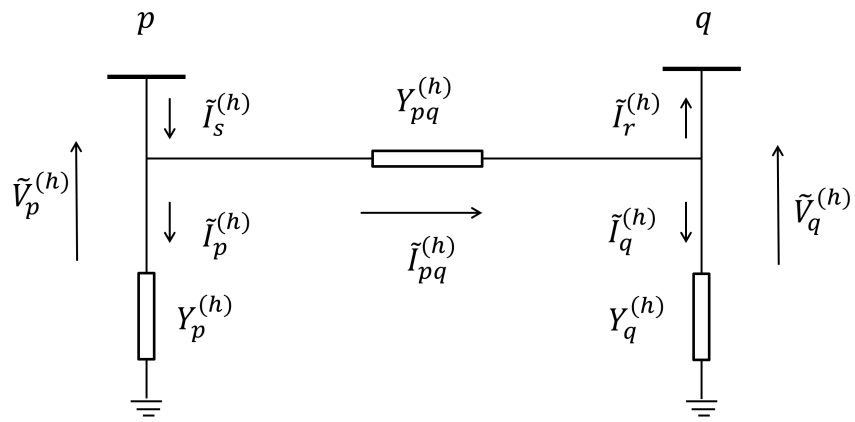

Figure C.1: π equivalent diagram of a transmission line without transformer

According to the figure, it gives:

$$\begin{aligned}\tilde{I}_p^{(h)} = \tilde{V}_p^{(h)} Y_p^{(h)} &= \mid V_p \mid^{(h)} \angle\theta_p^{(h)} Y_p^{(h)} \\ &= \mid V_p \mid^{(h)} \left(\cos\theta_p^{(h)} + j\sin\theta_p^{(h)}\right) Y_p^{(h)} \\ &= \mid V_p \mid^{(h)} \left(\cos\theta_p^{(h)} + j\sin\theta_p^{(h)}\right) (j\frac{hB}{2}) \\ &= \mid V_p \mid^{(h)} \left(j(\frac{hB}{2})\cos\theta_p^{(h)} - (\frac{hB}{2})\sin\theta_p^{(h)}\right) \\ &= -\frac{\mid V_p \mid^{(h)} hB}{2}\left(\sin\theta_p^{(h)} - j\cos\theta_p^{(h)}\right)\end{aligned} \tag{C.1}$$

$$\begin{aligned}\tilde{I}_q^{(h)} = \tilde{V}_q^{(h)} Y_q^{(h)} &= \mid V_q \mid^{(h)} \angle\theta_q^{(h)} Y_q^{(h)} \\ &= \mid V_q \mid^{(h)} \left(\cos\theta_q^{(h)} + j\sin\theta_q^{(h)}\right) (j\frac{hB}{2}) \\ &= -\frac{\mid V_q \mid^{(h)} hB}{2}\left(\sin\theta_q^{(h)} - j\cos\theta_q^{(h)}\right)\end{aligned} \tag{C.2}$$

and

$$\tilde{I}_{pq}^{(h)} = \left(\tilde{V}_p^{(h)} - \tilde{V}_q^{(h)}\right) Y_{pq}^{(h)} \tag{C.3}$$

Then the currents at the sending end and the receiving end are achieved as follows:

$$\tilde{I}_s^{(h)} = \tilde{I}_p^{(h)} + \tilde{I}_{pq}^{(h)} \tag{C.4}$$

$$\tilde{I}_r^{(h)} = \tilde{I}_{pq}^{(h)} - \tilde{I}_q^{(h)} \tag{C.5}$$

The active and reactive powers at the sending end and the receiving end are expressed by:

$$\tilde{S}_s^{(h)} = \tilde{V}_p^{(h)} (\tilde{I}_s^{(h)})^* = P_s^{(h)} + jQ_s^{(h)} \tag{C.6}$$

$$\tilde{S}_r^{(h)} = \tilde{V}_q^{(h)} (\tilde{I}_r^{(h)})^* = P_r^{(h)} + jQ_r^{(h)} \tag{C.7}$$

where $\tilde{S}_s^{(h)}$ and $\tilde{S}_r^{(h)}$ represent the voltamperes at the sending end and the receiving end respectively. $P_s^{(h)}$ and $P_r^{(h)}$ denote the active powers at the sending end and the receiving end. $Q_s^{(h)}$ and $Q_r^{(h)}$ are the reactive powers at the sending end and the receiving end.

The power loss on each line at h^{th} harmonic order equals the active power at sending end minus the one at receiving end, for the active powers at both ends are in the same direction. This can be expressed mathematically as follow:

$$P_{loss}^{(h)} = P_s^{(h)} - P_r^{(h)} \tag{C.8}$$

A transformer between the sending end p and the receiving end q

The π equivalent diagram of a transmission line with a transformer is shown in Figure C.2.

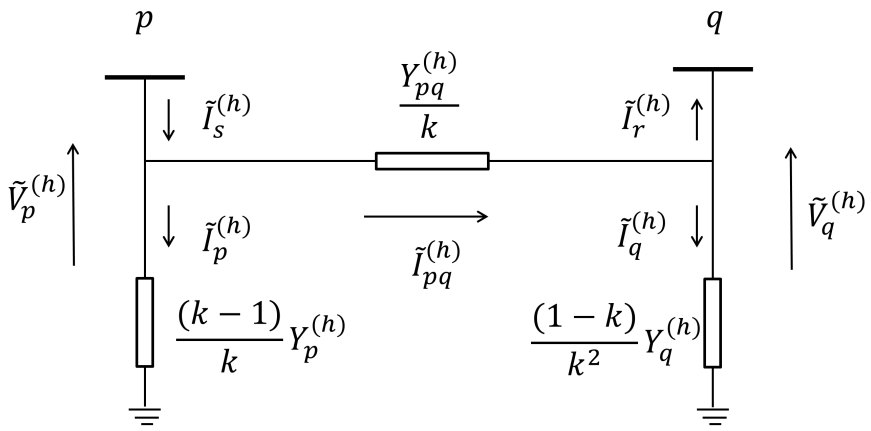

Figure C.2: π equivalent diagram of a transmission line with a transformer

According to the figure, it gives:

$$\begin{aligned} \tilde{I}_p^{(h)} &= \tilde{V}_p^{(h)} \left(\frac{(k-1)Y_{pq}^{(h)}}{k} \right) \\ &= \tilde{V}_p^{(h)} \left(\frac{(k-1)(G_{pq}^{(h)} + jhB_{pq}^{(h)})}{k} \right) \end{aligned} \tag{C.9}$$

$$\begin{aligned} \tilde{I}_q^{(h)} &= \tilde{V}_q^{(h)} \left(\frac{(1-k)Y_{pq}^{(h)}}{k^2} \right) \\ &= \tilde{V}_q^{(h)} \left(\frac{(1-k)(G_{pq}^{(h)} + jhB_{pq}^{(h)})}{k^2} \right) \end{aligned} \tag{C.10}$$

and

$$\tilde{I}_{pq}^{(h)} = \left(\tilde{V}_p^{(h)} - \tilde{V}_q^{(h)}\right)\left(\frac{Y_{pq}^{(h)}}{k}\right) \tag{C.11}$$

Then, use equation C.4 and C.5 to calculate the currents at the sending end and the receiving end. Equations C.6, C.7 and C.8 are applied to establish the active and reactive powers at the sending and receiving ends and the power losses on each line.

Appendix D

Power System Data

D.1 IEEE 14-bus Power System

Table D.1: The bus data of an IEEE 14-bus power system

Bus	Type	Voltage (p.u.)	Load			Generator	
			MW	MVar	MVA	MW	MVar
1	Slack	1.06	0	0	-	-	-
2	PV	1.045	21.7	12.7	-	40	-
3	PV	1.01	94.2	19	-	0	-
4	PQ	-	47.8	-3.9	-	0	0
5	PQ	-	7.6	1.6	-	0	0
6	PV	1.07	11.2	7.5	-	0	-
7	PQ	-	0	0	-	0	0
8	PV	1.09	0	0	-	0	-
9	PQ	-	29.5	16.6	-	0	0
10	PQ	-	9	5.8	-	0	0
11	PQ	-	3.5	1.8	-	0	0
12	PQ	-	6.1	1.6	-	0	0
13	PQ	-	13.5	5.8	-	0	0
14	PQ	-	14.9	5	-	0	0
“-” means the value needs to be calculated.							

Table D.2: The line and transformer data of an IEEE 14-bus power system

Line No.	Line data					Transformer Tap	
	From	To	R (p.u.)	X (p.u.)	B (p.u.)	Magnitude	Angle
1	5	6	0	0.252	0	0.932	0
2	4	7	0	0.2091	0	0.978	0
3	4	9	0	0.5562	0	0.969	0
4	1	2	0.0194	0.0592	0.0528	1	0
5	2	3	0.047	0.198	0.0438	1	0
6	2	4	0.0581	0.1763	0.0374	1	0
7	1	5	0.054	0.223	0.0492	1	0
8	2	5	0.057	0.1739	0.034	1	0
9	3	4	0.067	0.171	0.0346	1	0
10	4	5	0.0134	0.0421	0.0128	1	0
11	7	8	0	0.1762	0	1	0
12	7	9	0	0.11	0	1	0
13	9	10	0.0318	0.0845	0	1	0
14	6	11	0.095	0.1989	0	1	0
15	6	12	0.1229	0.2558	0	1	0
16	6	13	0.0662	0.1303	0	1	0
17	9	14	0.1271	0.2704	0	1	0
18	10	11	0.0821	0.1921	0	1	0
19	12	13	0.2209	0.1999	0	1	0
20	13	14	0.1709	0.348	0	1	0

D.2 New England 39-bus Power System

Table D.3: The bus data of the New England 39-bus power system

Bus	Type	Voltage (p.u.)	Load			Generator	
			MW	MVar	MVA	MW	MVar
1	PQ	-	0	0	-	0	0
2	PQ	-	0	0	-	0	0
3	PQ	-	322	2.4	-	0	0
4	PQ	-	500	184	-	0	0
5	PQ	-	0	0	-	0	0
6	PQ	-	0	0	-	0	0
7	PQ	-	233.8	84	-	0	0
8	PQ	-	522	176	-	0	0
9	PQ	-	0	0	-	0	0
10	PQ	-	0	0	-	0	0
11	PQ	-	0	0	-	0	0
12	PQ	-	7.5	88	-	0	0
13	PQ	-	0	0	-	0	0
14	PQ	-	0	0	-	0	0
15	PQ	-	320	153	-	0	0
16	PQ	-	329	32.3	-	0	0
17	PQ	-	0	0	-	0	0
18	PQ	-	158	30	-	0	0
19	PQ	-	0	0	-	0	0
20	PQ	-	628	103	-	0	0
21	PQ	-	274	115	-	0	0
22	PQ	-	0	0	-	0	0
23	PQ	-	247.5	84.6	-	0	0
24	PQ	-	308.6	-92	-	0	0

Continued on next page

Table D.3- *Continued from previous page*

Bus	Type	Voltage (p.u.)	Load			Generator	
			MW	MVar	MVA	MW	MVar
25	PQ	-	224	47.2	-	0	0
26	PQ	-	139	17	-	0	0
27	PQ	-	281	75.5	-	0	0
28	PQ	-	206	27.6	-	0	0
29	PQ	-	283.5	26.9	-	0	0
30	PV	1.0475	0	0	-	250	-
31	Slack	0.982	9.2	4.6	-	-	-
32	PV	0.9831	0	0	-	650	-
33	PV	0.9972	0	0	-	632	-
34	PV	1.0123	0	0	-	508	-
35	PV	1.0493	0	0	-	650	-
36	PV	1.0635	0	0	-	560	-
37	PV	1.0278	0	0	-	540	-
38	PV	1.0265	0	0	-	830	-
39	PV	1.03	1104	250	-	1000	-
"-" means the value needs to be calculated.							

Table D.4: The line and transformer data of the New England 39-bus power system

Line No.	Line data					Transformer Tap	
	From	To	R (p.u.)	X (p.u.)	B (p.u.)	Magnitude	Angle
1	1	2	0.0035	0.0411	0.6987	1	0
2	1	39	0.001	0.025	0.75	1	0
3	2	3	0.0013	0.0151	0.2572	1	0

Continued on next page

Table D.4- *Continued from previous page*

Line No.	Line data					Transformer Tap	
	From	To	R (p.u.)	X (p.u.)	B (p.u.)	Magnitude	Angle
4	2	25	0.007	0.0086	0.146	1	0
5	2	30	0	0.0181	0	1.025	0
6	3	4	0.0013	0.0213	0.2214	1	0
7	3	18	0.0011	0.0133	0.2138	1	0
8	4	5	0.0008	0.0128	0.1342	1	0
9	4	14	0.0008	0.0129	0.1382	1	0
10	5	6	0.0002	0.0026	0.0434	1	0
11	5	8	0.0008	0.0112	0.1476	1	0
12	6	7	0.0006	0.0092	0.113	1	0
13	6	11	0.0007	0.0082	0.1389	1	0
14	6	31	0	0.025	0	1.07	0
15	7	8	0.0004	0.0046	0.078	1	0
16	8	9	0.0023	0.0363	0.3804	1	0
17	9	39	0.001	0.025	1.2	1	0
18	10	11	0.0004	0.0043	0.0729	1	0
19	10	13	0.0004	0.0043	0.0729	1	0
20	10	32	0	0.02	0	1.07	0
21	11	12	0.0016	0.0435	0	1.006	0
22	12	13	0.0016	0.0435	0	1.006	0
23	13	14	0.0009	0.0101	0.1723	1	0
24	14	15	0.0018	0.0217	0.366	1	0
25	15	16	0.0009	0.0094	0.171	1	0

Continued on next page

Table D.4- *Continued from previous page*

Line No.	Line data					Transformer Tap	
	From	To	R (p.u.)	X (p.u.)	B (p.u.)	Magnitude	Angle
26	16	17	0.0007	0.0089	0.1342	1	0
27	16	19	0.0016	0.0195	0.304	1	0
28	16	21	0.0008	0.0135	0.2548	1	0
29	16	24	0.0003	0.0059	0.068	1	0
30	17	18	0.0007	0.0082	0.1319	1	0
31	17	27	0.0013	0.0173	0.3216	1	0
32	19	20	0.0007	0.0138	0	1.06	0
33	19	33	0.0007	0.0142	0	1.07	0
34	20	34	0.0009	0.018	0	1.009	0
35	21	22	0.0008	0.014	0.2565	1	0
36	22	23	0.0006	0.0096	0.1846	1	0
37	22	35	0	0.0143	0	1.025	0
38	23	24	0.0022	0.035	0.361	1	0
39	23	36	0.0005	0.0272	0	1	0
40	25	26	0.0032	0.0323	0.513	1	0
41	25	37	0.0006	0.0232	0	1.025	0
42	26	27	0.0014	0.0147	0.2396	1	0
43	26	28	0.0043	0.0474	0.7802	1	0
44	26	29	0.0057	0.0625	1.029	1	0
45	28	29	0.0014	0.0151	0.249	1	0
46	29	38	0.0008	0.0156	0	1.025	0

D.3 IEEE 57-bus Power System

Table D.5: The bus data of an IEEE 57-bus power system

Bus	Type	Voltage	Generator		Load		
		(p.u.)	MVA	MW	MVar	MW	MVar
1	SLACK	1.04	-	-	55	17	-
2	PV	1.01	0	-	3	88	-
3	PV	0.985	40	-	41	21	-
4	PQ	-	0	0	0	0	-
5	PQ	-	0	0	13	4	-
6	PV	0.98	0	-	75	2	-
7	PQ	-	0	0	0	0	-
8	PV	1.005	450	-	150	22	-
9	PV	0.98	0	-	121	26	-
10	PQ	-	0	0	5	2	-
11	PQ	-	0	0	0	0	-
12	PV	1.015	310	-	377	24	-
13	PQ	-	0	0	18	2.3	-
14	PQ	-	0	0	10.5	5.3	-
15	PQ	-	0	0	22	5	-
16	PQ	-	0	0	43	3	-
17	PQ	-	0	0	42	8	-
18	PQ	-	0	0	27.2	9.8	-
19	PQ	-	0	0	3.3	0.6	-
20	PQ	-	0	0	2.3	1	-

Continued on next page

Table D.5- *Continued from previous page*

Bus	Type	Voltage (p.u.)	Generator		Load		
			MVA	MW	MVar	MW	MVar
21	PQ	-	0	0	0	0	-
22	PQ	-	0	0	0	0	-
23	PQ	-	0	0	6.3	2.1	-
24	PQ	-	0	0	0	0	-
25	PQ	-	0	0	6.3	3.2	-
26	PQ	-	0	0	0	0	-
27	PQ	-	0	0	9.3	0.5	-
28	PQ	-	0	0	4.6	2.3	-
29	PS	-	0	0	17	2.6	-
30	PQ	-	0	0	3.6	1.8	-
31	PQ	-	0	0	5.8	2.9	-
32	PQ	-	0	0	1.6	0.8	-
33	PQ	-	0	0	3.8	1.9	-
34	PQ	-	0	0	0	0	-
35	PQ	-	0	0	6	3	-
36	PQ	-	0	0	0	0	-
37	PQ	-	0	0	0	0	-
38	PQ	-	0	0	14	7	-
39	PQ	-	0	0	0	0	-
40	PQ	-	0	0	0	0	-
41	PQ	-	0	0	6.3	3	-
42	PQ	-	0	0	7.1	4.4	-
43	PQ	-	0	0	2	1	-

Continued on next page

Table D.5- *Continued from previous page*

Bus	Type	Voltage (p.u.)	Generator		Load		
			MVA	MW	MVar	MW	MVar
44	PQ	-	0	0	12	1.8	-
45	PQ	-	0	0	0	0	-
46	PQ	-	0	0	0	0	-
47	PQ	-	0	0	29.7	11.6	-
48	PQ	-	0	0	0	0	-
49	PQ	-	0	0	18	8.5	-
50	PQ	-	0	0	21	10.5	-
51	PQ	-	0	0	18	5.3	-
52	PQ	-	0	0	4.9	2.2	-
53	PQ	-	0	0	20	10	-
54	PQ	-	0	0	4.1	1.4	-
55	PQ	-	0	0	6.8	3.4	-
56	PQ	-	0	0	7.6	2.2	-
57	PQ	-	0	0	6.7	2	-
“-” means the value needs to be calculated.							

Table D.6: The line and transformer data of an IEEE 57-bus power system

Line No.	Line data					Transformer Tap	
	From	To	R (p.u.)	X (p.u.)	B (p.u.)	Magnitude	Angle
1	1	2	0.0083	0.028	0.129	1	0
2	2	3	0.0298	0.085	0.0818	1	0
3	3	4	0.0112	0.0366	0.038	1	0
4	4	5	0.0625	0.132	0.0258	1	0
5	4	6	0.043	0.148	0.0348	1	0
6	6	7	0.02	0.102	0.0276	1	0
7	6	8	0.0339	0.173	0.047	1	0
8	8	9	0.0099	0.0505	0.0548	1	0
9	9	10	0.0369	0.1679	0.044	1	0
10	9	11	0.0258	0.0848	0.0218	1	0
11	9	12	0.0648	0.295	0.0772	1	0
12	9	13	0.0481	0.158	0.0406	1	0
13	13	14	0.0132	0.0434	0.011	1	0
14	13	15	0.0269	0.0869	0.023	1	0
15	1	15	0.0178	0.091	0.0988	1	0
16	1	16	0.0454	0.206	0.0546	1	0
17	1	17	0.0238	0.108	0.0286	1	0
18	3	15	0.0162	0.053	0.0544	1	0
19	4	18	0	0.555	0	0.97	0
20	4	18	0	0.43	0	0.978	0

Continued on next page

Table D.6- *Continued from previous page*

Line No.	Line data					Transformer Tap	
	From	To	R (p.u.)	X (p.u.)	B (p.u.)	Magnitude	Angle
21	5	6	0.0302	0.0641	0.0124	1	0
22	7	8	0.0139	0.0712	0.0194	1	0
23	10	12	0.0277	0.1262	0.0328	1	0
24	11	13	0.0223	0.0732	0.0188	1	0
25	12	13	0.0178	0.058	0.0604	1	0
26	12	16	0.018	0.0813	0.0216	1	0
27	12	17	0.0397	0.179	0.0476	1	0
28	14	15	0.0171	0.0547	0.0148	1	0
29	18	19	0.461	0.685	0	1	0
30	19	20	0.283	0.434	0	1	0
31	21	20	0	0.7767	0	1.043	0
32	21	22	0.0736	0.117	0	1	0
33	22	23	0.0099	0.0152	0	1	0
34	23	24	0.166	0.256	0.0084	1	0
35	24	25	0	1.182	0	1	0
36	24	25	0	1.23	0	1	0
37	24	26	0	0.0473	0	1.043	0
38	26	27	0.165	0.254	0	1	0
39	27	28	0.0618	0.0954	0	1	0
40	28	29	0.0418	0.0587	0	1	0
41	7	29	0	0.0648	0	0.967	0
42	25	30	0.135	0.202	0	1	0

Continued on next page

Table D.6- *Continued from previous page*

Line No.	Line data					Transformer Tap	
	From	To	R (p.u.)	X (p.u.)	B (p.u.)	Magnitude	Angle
43	30	31	0.326	0.497	0	1	0
44	31	32	0.507	0.755	0	1	0
45	32	33	0.0392	0.036	0	1	0
46	34	32	0	0.953	0	0.975	0
47	34	35	0.052	0.078	0.0032	1	0
48	35	36	0.043	0.0537	0.0016	1	0
49	36	37	0.029	0.0366	0	1	0
50	37	38	0.0651	0.1009	0.002	1	0
51	37	39	0.0239	0.0379	0	1	0
52	36	40	0.03	0.0466	0	1	0
53	22	38	0.0192	0.0295	0	1	0
54	11	41	0	0.749	0	0.955	0
55	41	42	0.207	0.352	0	1	0
56	41	43	0	0.412	0	1	0
57	38	44	0.0289	0.0585	0.002	1	0
58	15	45	0	0.1042	0	0.955	0
59	14	46	0	0.0735	0	0.9	0
60	46	47	0.023	0.068	0.0032	1	0
61	47	48	0.0182	0.0233	0	1	0
62	48	49	0.0834	0.129	0.0048	1	0
63	49	50	0.0801	0.128	0	1	0
64	50	51	0.1386	0.22	0	1	0

Continued on next page

Table D.6- *Continued from previous page*

Line No.	Line data					Transformer Tap	
	From	To	R (p.u.)	X (p.u.)	B (p.u.)	Magnitude	Angle
65	10	51	0	0.0712	0	0.93	0
66	13	49	0	0.191	0	0.895	0
67	29	52	0.1442	0.187	0	1	0
68	52	53	0.0762	0.0984	0	1	0
69	53	54	0.1878	0.232	0	1	0
70	54	55	0.1732	0.2265	0	1	0
71	11	43	0	0.153	0	0.958	0
72	44	45	0.0624	0.1242	0.004	1	0
73	40	56	0	1.195	0	0.958	0
74	56	41	0.553	0.549	0	1	0
75	56	42	0.2125	0.354	0	1	0
76	39	57	0	1.355	0	0.98	0
77	57	56	0.174	0.26	0	1	0
78	38	49	0.115	0.177	0.003	1	0
79	38	48	0.0312	0.0482	0	1	0
80	9	55	0	0.1205	0	0.94	0

D.4 IEEE 118-bus Power System

Table D.7: The bus data of an IEEE 118-bus power system

Bus	Type	Voltage	Load			Generator	
		(p.u.)	MW	MVar	MVA	MW	MVar
1	PV	0.955	51	27	-	0	-
2	PQ	-	20	9	-	0	0
3	PQ	-	39	10	-	0	0
4	PV	0.998	30	12	-	-9	-
5	PQ	-	0	0	-	0	0
6	PV	0.99	52	22	-	0	-
7	PQ	-	19	2	-	0	0
8	PV	1.015	0	0	-	-28	-
9	PQ	-	0	0	-	0	0
10	PV	1.05	0	0	-	450	-
11	PQ	-	70	23	-	0	0
12	PV	0.99	47	10	-	85	-
13	PQ	-	34	16	-	0	0
14	PQ	-	14	1	-	0	0
15	PV	0.97	90	30	-	0	-
16	PQ	-	25	10	-	0	0
17	PQ	-	11	3	-	0	0
18	PV	0.973	60	34	-	0	-
19	PV	0.962	45	25	-	0	-
20	PQ	-	18	3	-	0	0

Continued on next page

Table D.7- *Continued from previous page*

Bus	Type	Voltage	Load			Generator	
		(p.u.)	MW	MVar	MVA	MW	MVar
21	PQ	-	14	8	-	0	0
22	PS	-	10	-	20	0	0
23	PQ	-	7	3	-	0	0
24	PV	0.992	0	0	-	-13	-
25	PV	1.05	0	0	-	220	-
26	PV	1.015	0	0	-	314	-
27	PV	0.968	62	13	-	-9	-
28	PQ	-	17	7	-	0	0
29	PQ	-	24	4	-	0	0
30	PQ	-	0	0	-	0	0
31	PV	0.967	43	27	-	7	-
32	PV	0.963	59	23	-	0	-
33	PQ	-	23	9	-	0	0
34	PV	0.984	59	26	-	0	-
35	PQ	-	33	9	-	0	0
36	PV	0.98	31	17	-	0	-
37	PQ	-	0	0	-	0	0
38	PQ	-	0	0	-	0	0
39	PQ	-	27	11	-	0	0
40	PV	0.97	20	23	-	-46	-
41	PQ	-	37	10	-	0	0
42	PV	0.985	37	23	-	-59	-
43	PQ	-	18	7	-	0	0

Continued on next page

Table D.7- *Continued from previous page*

Bus	Type	Voltage	Load			Generator	
		(p.u.)	MW	MVar	MVA	MW	MVar
44	PQ	-	16	8	-	0	0
45	PQ	-	53	22	-	0	0
46	PV	1.005	28	10	-	19	-
47	PQ	-	34	0	-	0	0
48	PQ	-	20	11	-	0	0
49	PV	1.025	87	30	-	204	-
50	PQ	-	17	4	-	0	0
51	PQ	-	17	8	-	0	0
52	PQ	-	18	5	-	0	0
53	PQ	-	23	11	-	0	0
54	PV	0.955	113	32	-	48	-
55	PV	0.952	63	22	-	0	-
56	PV	0.954	84	18	-	0	-
57	PQ	-	12	3	-	0	0
58	PQ	-	12	3	-	0	0
59	PV	0.985	277	113	-	155	-
60	PQ	-	78	3	-	0	0
61	PV	0.995	0	0	-	160	-
62	PV	0.998	77	14	-	0	-
63	PQ	-	0	0	-	0	0
64	PQ	-	0	0	-	0	0
65	PV	1.005	0	0	-	391	-
66	PV	1.05	39	18	-	392	-

Continued on next page

Table D.7- *Continued from previous page*

Bus	Type	Voltage	Load			Generator	
		(p.u.)	MW	MVar	MVA	MW	MVar
67	PQ	-	28	7	-	0	0
68	PQ	-	0	0	-	0	0
69	Slack	1.035	0	0	-	-	-
70	PV	0.984	66	20	-	0	-
71	PQ	-	0	0	-	0	0
72	PV	0.98	0	0	-	-12	-
73	PV	0.991	0	0	-	-6	-
74	PV	0.958	68	27	-	0	-
75	PQ	-	47	11	-	0	0
76	PV	0.943	68	36	-	0	-
77	PV	1.006	61	28	-	0	-
78	PQ	-	71	26	-	0	0
79	PQ	-	39	32	-	0	0
80	PV	1.04	130	26	-	477	-
81	PQ	-	0	0	-	0	0
82	PQ	-	54	27	-	0	0
83	PQ	-	20	10	-	0	0
84	PQ	-	11	7	-	0	0
85	PV	0.985	24	15	-	0	-
86	PQ	-	21	10	-	0	0
87	PV	1.015	0	0	-	4	-
88	PQ	-	48	10	-	0	0
89	PV	1.005	0	0	-	607	-

Continued on next page

Table D.7- *Continued from previous page*

Bus	Type	Voltage	Load			Generator	
		(p.u.)	MW	MVar	MVA	MW	MVar
90	PV	0.985	78	42	-	-85	-
91	PV	0.98	0	0	-	-10	-
92	PV	0.99	65	10	-	0	-
93	PQ	-	12	7	-	0	0
94	PQ	-	30	16	-	0	0
95	PS	-	42	-	60	0	0
96	PQ	-	38	15	-	0	0
97	PQ	-	15	9	-	0	0
98	PQ	-	34	8	-	0	0
99	PV	1.01	0	0	-	-42	-
100	PV	1.017	37	18	-	252	-
101	PQ	-	22	15	-	0	0
102	PQ	-	5	3	-	0	0
103	PV	1.01	23	16	-	40	-
104	PV	0.971	38	25	-	0	-
105	PV	0.965	31	26	-	0	-
106	PQ	-	43	16	-	0	0
107	PV	0.952	28	12	-	-22	-
108	PQ	-	2	1	-	0	0
109	PQ	-	8	3	-	0	0
110	PV	0.973	39	30	-	0	-
111	PV	0.98	0	0	-	36	-
112	PV	0.975	25	13	-	-43	-

Continued on next page

Table D.7- *Continued from previous page*

Bus	Type	Voltage (p.u.)	Load			Generator	
			MW	MVar	MVA	MW	MVar
113	PV	0.993	0	0	-	-6	-
114	PQ	-	8	3	-	0	0
115	PQ	-	22	7	-	0	0
116	PV	1.005	0	0	-	-184	-
117	PQ	-	20	8	-	0	0
118	PQ	-	33	15	-	0	0
"-" means the value needs to be calculated.							

Table D.8: The line and transformer data of an IEEE 118-bus power system

Line No.	Line data					Transformer Tap	
	From	To	R (p.u.)	X (p.u.)	B (p.u.)	Magnitude	Angle
1	1	2	0.0303	0.0999	0.0254	1	0
2	1	3	0.0129	0.0424	0.0108	1	0
3	2	12	0.0187	0.0616	0.0157	1	0
4	3	5	0.0241	0.108	0.0284	1	0
5	3	12	0.0484	0.16	0.0406	1	0
6	4	5	0.0018	0.008	0.0021	1	0
7	11	4	0.0209	0.0688	0.0175	1	0
8	5	6	0.0119	0.054	0.0143	1	0
9	8	5	0	0.0267	0	0.985	0

Continued on next page

Table D.8- *Continued from previous page*

Line No.	Line data					Transformer Tap	
	From	To	R (p.u.)	X (p.u.)	B (p.u.)	Magnitude	Angle
10	11	5	0.0203	0.0682	0.0174	1	0
11	6	7	0.0046	0.0208	0.0055	1	0
12	7	12	0.0086	0.034	0.0087	1	0
13	8	9	0.0024	0.0305	1.162	1	0
14	30	8	0.0043	0.0504	0.514	1	0
15	9	10	0.0026	0.0322	1.23	1	0
16	11	12	0.006	0.0196	0.005	1	0
17	11	13	0.0222	0.0731	0.0188	1	0
18	12	14	0.0215	0.0707	0.0182	1	0
19	12	16	0.0212	0.0834	0.0214	1	0
20	12	117	0.0329	0.14	0.0358	1	0
21	13	15	0.0744	0.2444	0.0627	1	0
22	14	15	0.0595	0.195	0.0502	1	0
23	15	17	0.0132	0.0437	0.0444	1	0
24	15	19	0.012	0.0394	0.0101	1	0
25	15	33	0.038	0.1244	0.0319	1	0
26	16	17	0.0454	0.1801	0.0466	1	0
27	17	18	0.0123	0.0505	0.013	1	0
28	30	17	0	0.0388	0	0.96	0
29	17	31	0.0474	0.1563	0.0399	1	0
30	17	113	0.0091	0.0301	0.0077	1	0
31	18	19	0.0112	0.0493	0.0114	1	0

Continued on next page

Table D.8- *Continued from previous page*

Line No.	Line data					Transformer Tap	
	From	To	R (p.u.)	X (p.u.)	B (p.u.)	Magnitude	Angle
32	19	20	0.0252	0.117	0.0298	1	0
33	34	19	0.0752	0.247	0.0632	1	0
34	20	21	0.0183	0.0849	0.0216	1	0
35	21	22	0.0209	0.097	0.0246	1	0
36	22	23	0.0342	0.159	0.0404	1	0
37	23	24	0.0135	0.0492	0.0498	1	0
38	23	25	0.0156	0.08	0.0864	1	0
39	32	23	0.0317	0.1153	0.1173	1	0
40	70	24	0.1022	0.4115	0.102	1	0
41	24	72	0.0488	0.196	0.0488	1	0
42	26	25	0	0.0382	0	0.96	0
43	25	27	0.0318	0.163	0.1764	1	0
44	30	26	0.008	0.086	0.908	1	0
45	28	27	0.0191	0.0855	0.0216	1	0
46	32	27	0.0229	0.0755	0.0193	1	0
47	27	115	0.0164	0.0741	0.0197	1	0
48	29	28	0.0237	0.0943	0.0238	1	0
49	31	29	0.0108	0.0331	0.0083	1	0
50	30	38	0.0046	0.054	0.422	1	0
51	31	32	0.0298	0.0985	0.0251	1	0
52	31	113	0	0.1	0	1	0
53	113	32	0.0615	0.203	0.0518	1	0

Continued on next page

Table D.8- *Continued from previous page*

Line No.	Line data					Transformer Tap	
	From	To	R (p.u.)	X (p.u.)	B (p.u.)	Magnitude	Angle
54	32	114	0.0135	0.0612	0.0163	1	0
55	33	37	0.0415	0.142	0.0366	1	0
56	34	36	0.0087	0.0268	0.0057	1	0
57	37	34	0.0026	0.0094	0.0098	1	0
58	34	43	0.0413	0.1681	0.0423	1	0
59	36	35	0.0022	0.0102	0.0027	1	0
60	37	35	0.011	0.0497	0.0132	1	0
61	38	37	0	0.0375	0	0.935	0
62	39	37	0.0321	0.106	0.027	1	0
63	37	40	0.0593	0.168	0.042	1	0
64	38	65	0.009	0.0986	1.046	1	0
65	39	40	0.0184	0.0605	0.0155	1	0
66	40	41	0.0145	0.0487	0.0122	1	0
67	40	42	0.0555	0.183	0.0466	1	0
68	41	42	0.041	0.135	0.0344	1	0
69	42	49	0.0238	0.1077	0.258	1	0
70	43	44	0.0608	0.2454	0.0607	1	0
71	44	45	0.0224	0.0901	0.0224	1	0
72	45	46	0.04	0.1356	0.0332	1	0
73	45	49	0.0684	0.186	0.0444	1	0
74	46	47	0.038	0.127	0.0316	1	0
75	46	48	0.0601	0.189	0.0472	1	0

Continued on next page

Table D.8- *Continued from previous page*

Line No.	Line data					Transformer Tap	
	From	To	R (p.u.)	X (p.u.)	B (p.u.)	Magnitude	Angle
76	47	49	0.0191	0.0625	0.016	1	0
77	47	69	0.0844	0.2778	0.0709	1	0
78	48	49	0.0179	0.0505	0.0126	1	0
79	49	50	0.0267	0.0752	0.0187	1	0
80	49	51	0.0486	0.137	0.0342	1	0
81	54	49	0.0257	0.0966	0.2206	1	0
82	49	66	0.006	0.0306	0.0744	1	0
83	49	69	0.0985	0.324	0.0828	1	0
84	50	57	0.0474	0.134	0.0332	1	0
85	51	52	0.0203	0.0588	0.014	1	0
86	58	51	0.0255	0.0719	0.0179	1	0
87	52	53	0.0405	0.1635	0.0406	1	0
88	53	54	0.0263	0.122	0.031	1	0
89	54	55	0.0169	0.0707	0.0202	1	0
90	54	56	0.0028	0.0096	0.0073	1	0
91	54	59	0.0503	0.2293	0.0598	1	0
92	56	55	0.0049	0.0151	0.0037	1	0
93	55	59	0.0474	0.2158	0.0565	1	0
94	57	56	0.0343	0.0966	0.0242	1	0
95	58	56	0.0343	0.0966	0.0242	1	0
96	56	59	0.0273	0.0823	0.1672	1	0
97	59	60	0.0317	0.145	0.0376	1	0

Continued on next page

Table D.8- *Continued from previous page*

Line No.	Line data					Transformer Tap	
	From	To	R (p.u.)	X (p.u.)	B (p.u.)	Magnitude	Angle
98	61	59	0.0328	0.15	0.0388	1	0
99	63	59	0	0.0386	0	0.96	0
100	60	61	0.0026	0.0135	0.0146	1	0
101	60	62	0.0123	0.0561	0.0147	1	0
102	61	62	0.0082	0.0376	0.0098	1	0
103	64	61	0	0.0268	0	0.985	0
104	66	62	0.0482	0.218	0.0578	1	0
105	62	67	0.0258	0.117	0.031	1	0
106	63	64	0.0017	0.02	0.216	1	0
107	64	65	0.0027	0.0302	0.38	1	0
108	65	66	0	0.037	0	0.935	0
109	68	65	0.0014	0.016	0.638	1	0
110	66	67	0.0224	0.1015	0.0268	1	0
111	68	69	0	0.037	0	0.935	0
112	68	81	0.0018	0.0202	0.808	1	0
113	68	116	0.003	0.004	0.164	1	0
114	70	69	0.03	0.127	0.122	1	0
115	75	69	0.0405	0.122	0.124	1	0
116	69	77	0.0309	0.101	0.1038	1	0
117	70	71	0.0088	0.0355	0.0088	1	0
118	70	74	0.0401	0.1323	0.0337	1	0
119	70	75	0.0428	0.141	0.036	1	0

Continued on next page

Table D.8- *Continued from previous page*

Line No.	Line data					Transformer Tap	
	From	To	R (p.u.)	X (p.u.)	B (p.u.)	Magnitude	Angle
120	72	71	0.0446	0.18	0.0444	1	0
121	71	73	0.0087	0.0454	0.0118	1	0
122	74	75	0.0123	0.0406	0.0103	1	0
123	75	77	0.0601	0.1999	0.0498	1	0
124	75	118	0.0145	0.0481	0.012	1	0
125	77	76	0.0444	0.148	0.0368	1	0
126	118	76	0.0164	0.0544	0.0136	1	0
127	77	78	0.0038	0.0124	0.0126	1	0
128	77	80	0.0066	0.0197	0.1172	1	0
129	77	82	0.0298	0.0853	0.0817	1	0
130	78	79	0.0055	0.0244	0.0065	1	0
131	79	80	0.0156	0.0704	0.0187	1	0
132	81	80	0	0.037	0	0.935	0
133	96	80	0.0356	0.182	0.0494	1	0
134	97	80	0.0183	0.0934	0.0254	1	0
135	80	98	0.0238	0.108	0.0286	1	0
136	80	99	0.0454	0.206	0.0546	1	0
137	83	82	0.0112	0.0366	0.038	1	0
138	82	96	0.0162	0.053	0.0544	1	0
139	83	84	0.0625	0.132	0.0258	1	0
140	85	83	0.043	0.148	0.0348	1	0
141	84	85	0.0302	0.0641	0.0123	1	0

Continued on next page

Table D.8- *Continued from previous page*

Line No.	Line data					Transformer Tap	
	From	To	R (p.u.)	X (p.u.)	B (p.u.)	Magnitude	Angle
142	85	86	0.035	0.123	0.0276	1	0
143	85	88	0.02	0.102	0.0276	1	0
144	85	89	0.0239	0.173	0.047	1	0
145	86	87	0.0283	0.2074	0.0445	1	0
146	88	89	0.0139	0.0712	0.0193	1	0
147	90	89	0.0124	0.0484	0.2116	1	0
148	89	92	0.0044	0.0218	0.151	1	0
149	90	91	0.0254	0.0836	0.0214	1	0
150	91	92	0.0387	0.1272	0.0327	1	0
151	92	93	0.0258	0.0848	0.0218	1	0
152	92	94	0.0481	0.158	0.0406	1	0
153	92	100	0.0648	0.295	0.0472	1	0
154	92	102	0.0123	0.0559	0.0146	1	0
155	93	94	0.0223	0.0732	0.0188	1	0
156	95	94	0.0132	0.0434	0.0111	1	0
157	96	94	0.0269	0.0869	0.023	1	0
158	94	100	0.0178	0.058	0.0604	1	0
159	96	95	0.0171	0.0547	0.0147	1	0
160	96	97	0.0173	0.0885	0.024	1	0
161	98	100	0.0397	0.179	0.0476	1	0
162	99	100	0.018	0.0813	0.0216	1	0
163	101	100	0.0277	0.1262	0.0328	1	0

Continued on next page

Table D.8- *Continued from previous page*

Line No.	Line data					Transformer Tap	
	From	To	R (p.u.)	X (p.u.)	B (p.u.)	Magnitude	Angle
164	100	103	0.016	0.0525	0.0536	1	0
165	100	104	0.0451	0.204	0.0541	1	0
166	100	106	0.0605	0.229	0.062	1	0
167	102	101	0.0246	0.112	0.0294	1	0
168	104	103	0.0466	0.1584	0.0407	1	0
169	103	105	0.0535	0.1625	0.0408	1	0
170	103	110	0.0391	0.1813	0.0461	1	0
171	104	105	0.0099	0.0378	0.0099	1	0
172	105	106	0.014	0.0547	0.0143	1	0
173	105	107	0.053	0.183	0.0472	1	0
174	105	108	0.0261	0.0703	0.0184	1	0
175	107	106	0.053	0.183	0.0472	1	0
176	108	109	0.0105	0.0288	0.0076	1	0
177	109	110	0.0278	0.0762	0.0202	1	0
178	110	111	0.022	0.0755	0.02	1	0
179	110	112	0.0247	0.064	0.062	1	0
180	114	115	0.0023	0.0104	0.0028	1	0

Appendix E

Principle of Newton-Raphson Iterative Approach

The Newton-Raphson method is an iterative approach to calculate the non-linear equation. It has one variable shown as:

$$f(x) = 0 \tag{E.1}$$

An approximate solution $x^{(0)}$ is assumed, and the error between this approximate solution and the real solution is $\Delta x^{(0)}$. Then,

$$f(x^{(0)} + \Delta x^{(0)}) = 0 \tag{E.2}$$

Expanding equation E.2 using the Taylor series:

$$\begin{aligned} f(x^{(0)} + \Delta x^{(0)}) = & f(x^{(0)}) + f'(x^{(0)})\Delta x^{(0)} + f''(x^{(0)})\frac{(\Delta x^{(0)})^2}{2!} \\ & + \ldots + f^{(n)}(x^{(0)})\frac{(\Delta x^{(0)})^n}{n!} \end{aligned} \tag{E.3}$$

where $f'(x^{(0)}), \ldots, f^{(n)}(x^{(0)})$ are the first, $\ldots$, n^{th} order derivative of function $f(x)$ at point $x^{(0)}$, respectively.

Equation E.3 is simplified by eliminating the higher order (bigger than one) deriva-

tives, as $\Delta x^{(0)}$ is very small. Then:

$$f(x^{(0)} + \Delta x^{(0)}) = f(x^{(0)}) + f'(x^{(0)})\Delta x^{(0)} = 0 \tag{E.4}$$

This is the linear equation for correction $\Delta x^{(0)}$. It is called the correction equation. The expression for correction $\Delta x^{(0)}$ is achieved by solving this equation:

$$\Delta x^{(0)} = -\frac{f(x^{(0)})}{f'(x^{(0)})} \tag{E.5}$$

If this correction $\Delta x^{(0)}$ is used to modify the approximate solution x, then:

$$x^{(1)} = x^{(0)} + \Delta x^{(0)} = x^{(0)} - \frac{f(x^{(0)})}{f'(x^{(0)})} \tag{E.6}$$

This calculation is iterated in order to achieve an accurate result. The iterative expression is defined as:

$$x^{(k+1)} = x^{(k)} - \frac{f(x^{(k)})}{f'(x^{(k)})} \tag{E.7}$$

where k is the number of iterations.

And the convergence criterion is

$$| f(x^{(k)}) | < \varepsilon_1 \tag{E.8}$$

$$\text{or} \quad | \Delta x^{(k)} | < \varepsilon_2 \tag{E.9}$$

where ε_1 and ε_2 are specified.

The principle of the Newton-Raphson iterative approach can be explained by Figure E.1 also.

The curve in the figure represents the function $y = f(x)$. The junction between the curve and the x-axis is the solution for $y = f(x)$. It is assumed $x^{(k)}$ is the solution achieved in the k^{th} iteration. Then, a tangent is drawn at the point $[x^{(k)}, y^{(k)} = f(x^{(k)})]$, the junction between this tangent and the x-axis is the solution obtained in the next iteration, $x^{(k+1)}$. Then a tangent is drawn at the point $[x^{(k+1)}, y^{(k+1)} = f(x^{(k+1)})]$, and a better solution $x^{(k+2)}$ is achieved, and so on. Finally, an accurate solution can be

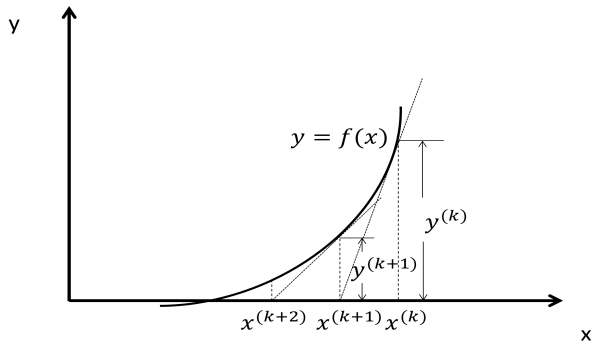

Figure E.1: Newton-Raphson method explained in geometry

obtained using the convergence criterion.

For non-linear equations with n variables:

$$\begin{cases} f_1(x_1, x_2, \ldots, x_n) = 0 \\ f_2(x_1, x_2, \ldots, x_n) = 0 \\ \quad \vdots \\ f_n(x_1, x_2, \ldots, x_n) = 0 \end{cases} \tag{E.10}$$

Assume the initial values in the $(k+1)^{th}$ iteration are $x_1^{(k)}, x_2^{(k)}, \ldots, x_n^{(k)}$, and the correction of each initial value is $\Delta x_1^{(k)}, \Delta x_2^{(k)}, \ldots, \Delta x_n^{(k)}$ respectively. Then:

$$\begin{cases} f_1(x_1^{(k)} + \Delta x_1^{(k)}, x_2^{(k)} + \Delta x_2^{(k)}, \ldots, x_n^{(k)} + \Delta x_n^{(k)}) = 0 \\ f_2(x_1^{(k)} + \Delta x_1^{(k)}, x_2^{(k)} + \Delta x_2^{(k)}, \ldots, x_n^{(k)} + \Delta x_n^{(k)}) = 0 \\ \quad \vdots \\ f_n(x_1^{(k)} + \Delta x_1^{(k)}, x_2^{(k)} + \Delta x_2^{(k)}, \ldots, x_n^{(k)} + \Delta x_n^{(k)}) = 0 \end{cases} \tag{E.11}$$

Expanding equation E.11 using the Taylor series and eliminating the higher order

(bigger than one) derivatives:

$$\begin{cases} f_1(x_1^{(k)},x_2^{(k)},\ldots,x_n^{(k)}) + \left.\frac{\partial f_1}{\partial x_1}\right|_k \Delta x_1^{(k)} + \left.\frac{\partial f_1}{\partial x_2}\right|_k \Delta x_2^{(k)} + \ldots + \left.\frac{\partial f_1}{\partial x_n}\right|_k \Delta x_n^{(k)} = 0 \\ f_2(x_1^{(k)},x_2^{(k)},\ldots,x_n^{(k)}) + \left.\frac{\partial f_2}{\partial x_1}\right|_k \Delta x_1^{(k)} + \left.\frac{\partial f_2}{\partial x_2}\right|_k \Delta x_2^{(k)} + \ldots + \left.\frac{\partial f_2}{\partial x_n}\right|_k \Delta x_n^{(k)} = 0 \\ \vdots \\ f_n(x_1^{(k)},x_2^{(k)},\ldots,x_n^{(k)}) + \left.\frac{\partial f_n}{\partial x_1}\right|_k \Delta x_1^{(k)} + \left.\frac{\partial f_n}{\partial x_2}\right|_k \Delta x_2^{(k)} + \ldots + \left.\frac{\partial f_n}{\partial x_n}\right|_k \Delta x_n^{(k)} = 0 \end{cases} \tag{E.12}$$

The equation E.12 can be transformed into a matrix:

$$\begin{bmatrix} f_1(x_1^{(k)},x_2^{(k)},\ldots,x_n^{(k)}) \\ f_2(x_1^{(k)},x_2^{(k)},\ldots,x_n^{(k)}) \\ \vdots \\ f_n(x_1^{(k)},x_2^{(k)},\ldots,x_n^{(k)}) \end{bmatrix} = - \begin{bmatrix} \left.\frac{\partial f_1}{\partial x_1}\right|_k & \left.\frac{\partial f_1}{\partial x_2}\right|_k \cdots \left.\frac{\partial f_1}{\partial x_n}\right|_k \\ \left.\frac{\partial f_2}{\partial x_1}\right|_k & \left.\frac{\partial f_2}{\partial x_2}\right|_k \cdots \left.\frac{\partial f_2}{\partial x_n}\right|_k \\ \vdots \\ \left.\frac{\partial f_n}{\partial x_1}\right|_k & \left.\frac{\partial f_n}{\partial x_2}\right|_k \cdots \left.\frac{\partial f_n}{\partial x_n}\right|_k \end{bmatrix} \begin{bmatrix} \Delta x_1^k \\ \Delta x_2^k \\ \vdots \\ \Delta x_n^k \end{bmatrix} \tag{E.13}$$

By solving equation E.13, the corrections $\Delta x_1^{(k)}$, $\Delta x_2^{(k)}$, …, $\Delta x_n^{(k)}$ can be achieved. Then, the initial values $x_1^{(k)}$, $x_2^{(k)}$, …, $x_n^{(k)}$ can be modified by:

$$x_i^{(k+1)} = x_i^{(k)} + \Delta x_i^{(k)} \qquad (i = 1,2,\ldots,n) \tag{E.14}$$

The equation E.13 and E.14 can be abbreviated as below:

$$F(X^{(k)}) = -J^{(k)}\Delta X^{(k)} \tag{E.15}$$

$$\text{and} \quad X^{(k+1)} = X^{(k)} + \Delta X^{(k)} \tag{E.16}$$

where J is the $n \times n$ Jacobian matrix and $F(X)$, X and ΔX are the $n \times 1$ matrix, respectively.

The convergence criterion is:

$$\max(|\, f_i(x_1^{(k)},x_2^{(k)},\ldots,x_n^{(k)}) \,|) < \varepsilon_1 \tag{E.17}$$

$$\text{or} \qquad \max(|\, \Delta x_i^{(k)} \,|) < \varepsilon_2 \tag{E.18}$$

where ε_1 and ε_2 are specified.

Appendix F

Diagrams Of Result Comparison In Chapter 5

F.1 Case One: In A 14-bus Power System

The result differences of the total harmonic voltage distortion, the total active and reactive powers at both sending and receiving ends and the total power losses on each branch between three different methods are illustrated in Figures F.1 to F.4 below.

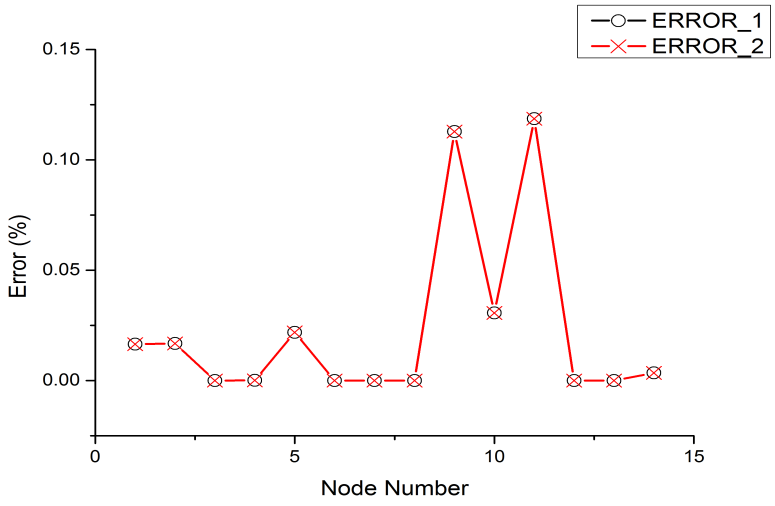

Figure F.1: The result differences of the total voltage harmonic distortion

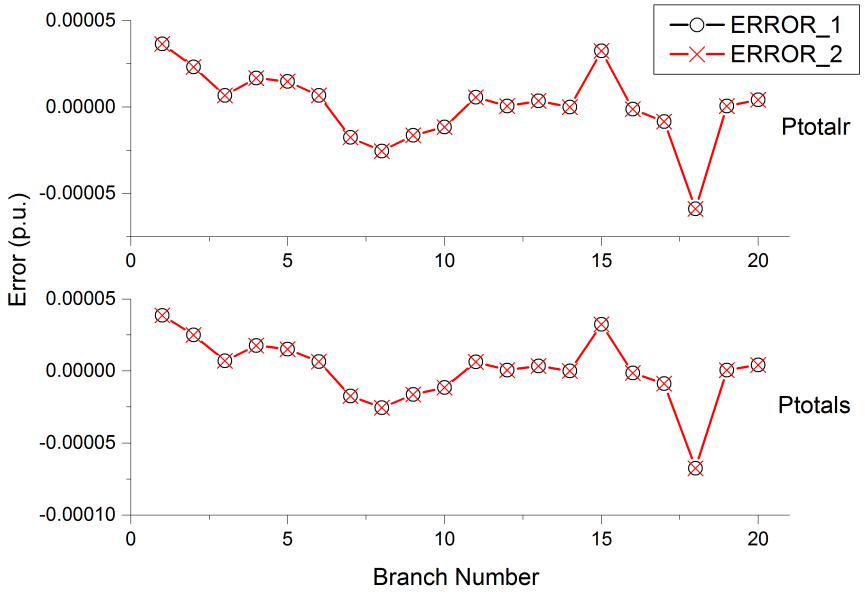

Figure F.2: The result differences of the total active powers at both sending and receiving ends

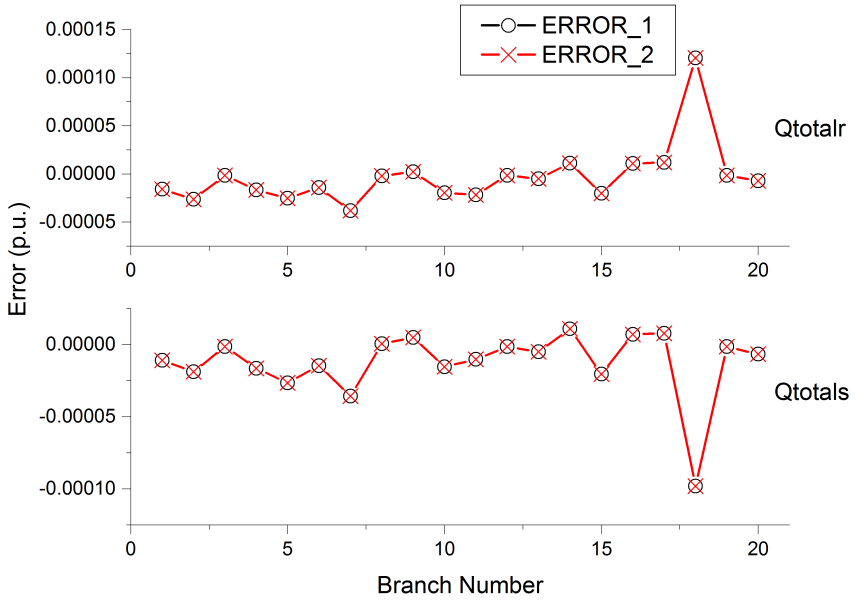

Figure F.3: The result differences of the total reactive powers at both sending and receiving ends

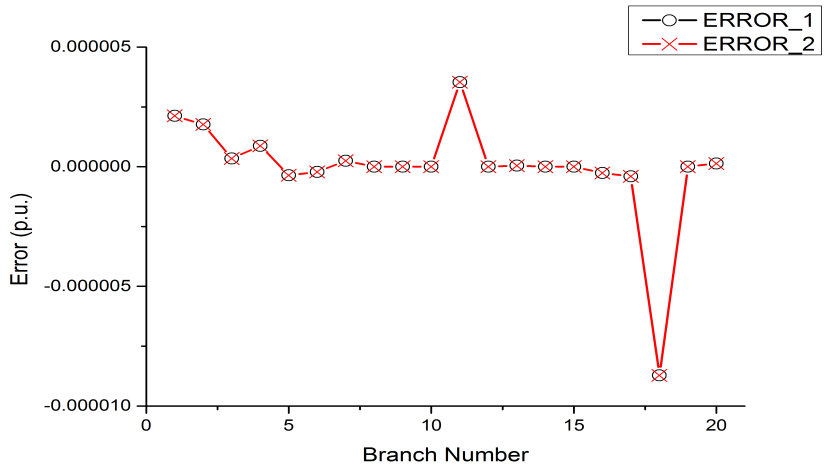

Figure F.4: The result differences of the total power losses on each branch

F.2 Case Two: In A 39-bus Power System

The result differences of the fundamental bus voltage magnitudes, the total harmonic voltage distortion, the total active and reactive powers at both sending and receiving ends and the total power losses on each branch between three different methods are illustrated in Figures F.5 to F.9 below.

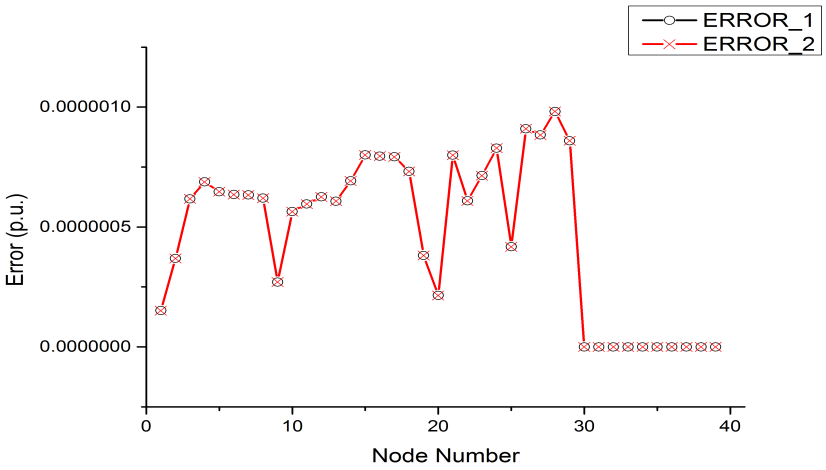

Figure F.5: The result differences of the fundamental bus voltage magnitude

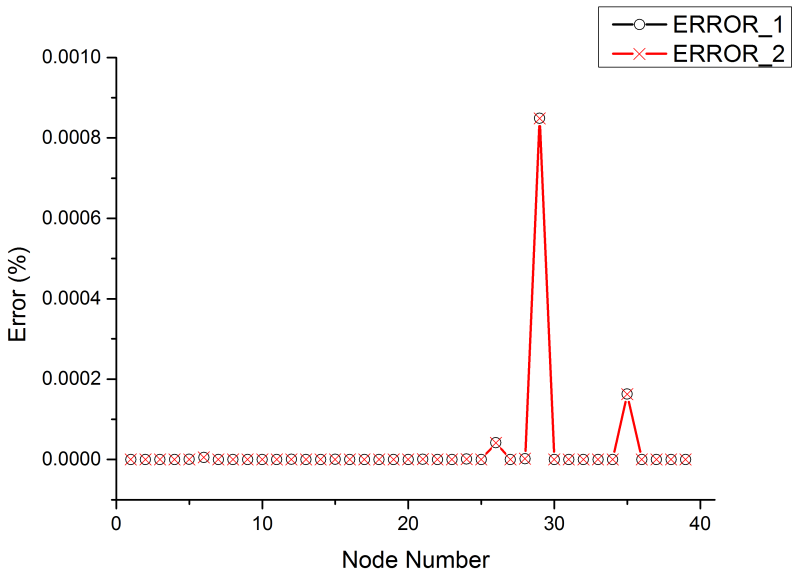

Figure F.6: The result differences of the total voltage harmonic distortion

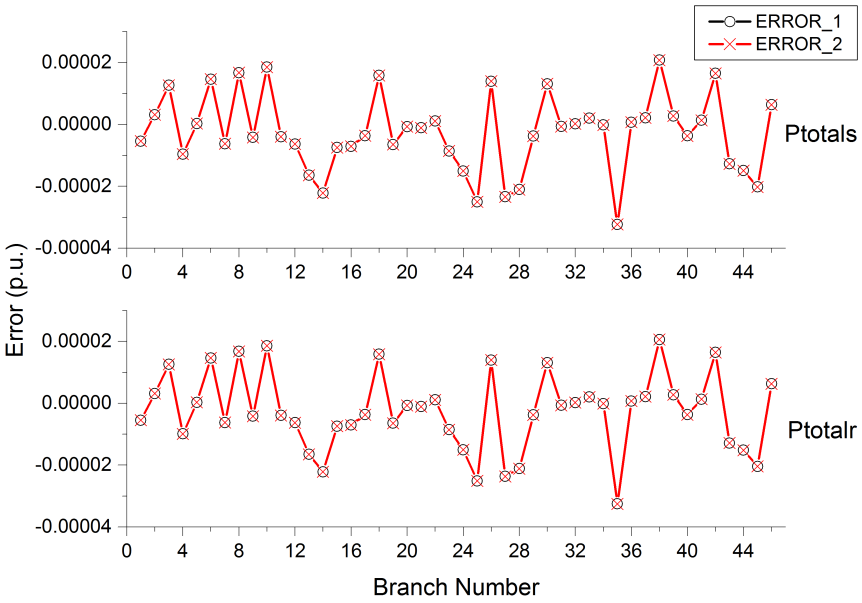

Figure F.7: The result differences of the total active powers at both sending and receiving ends

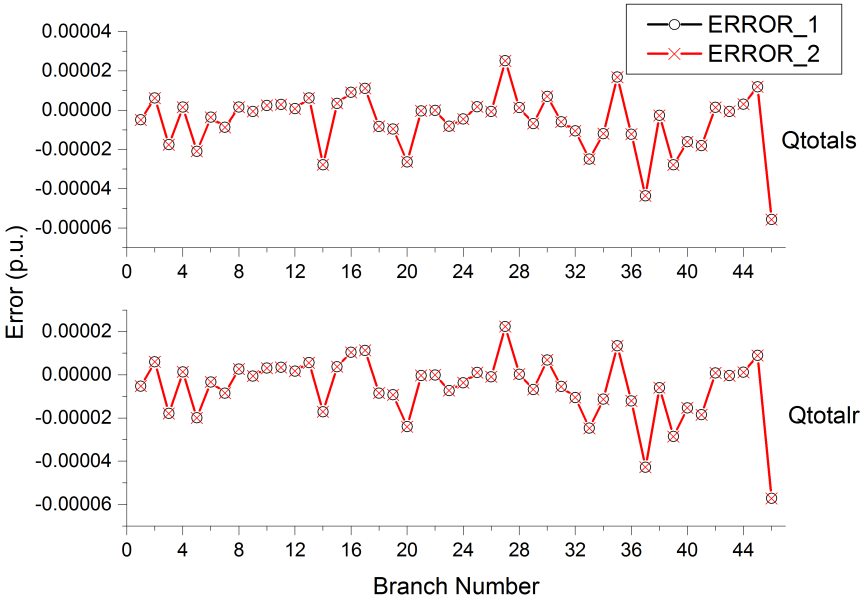

Figure F.8: The result differences of the total reactive powers at both sending and receiving ends

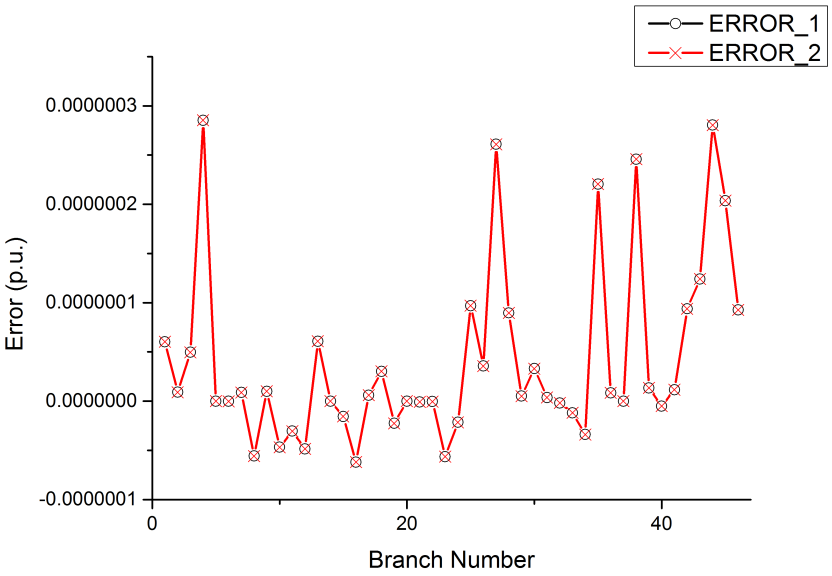

Figure F.9: The result differences of the total power losses on each branch

F.3 Case Three: In A 57-bus Power System

The result differences of the fundamental bus voltage magnitudes, the total harmonic voltage distortion, the total active and reactive powers at both sending and receiving ends and the total power losses on each branch between three different methods are illustrated in Figures F.10 to F.14 below.

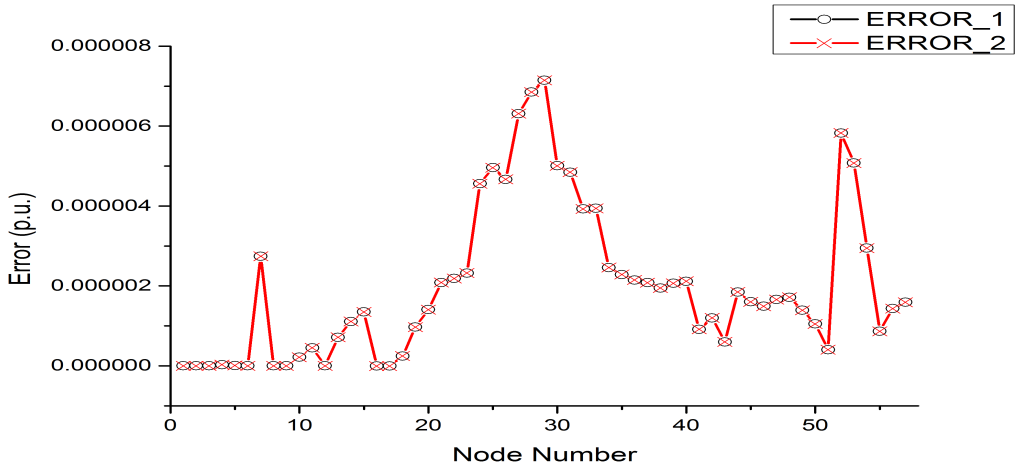

Figure F.10: The result differences of the fundamental bus voltage magnitude

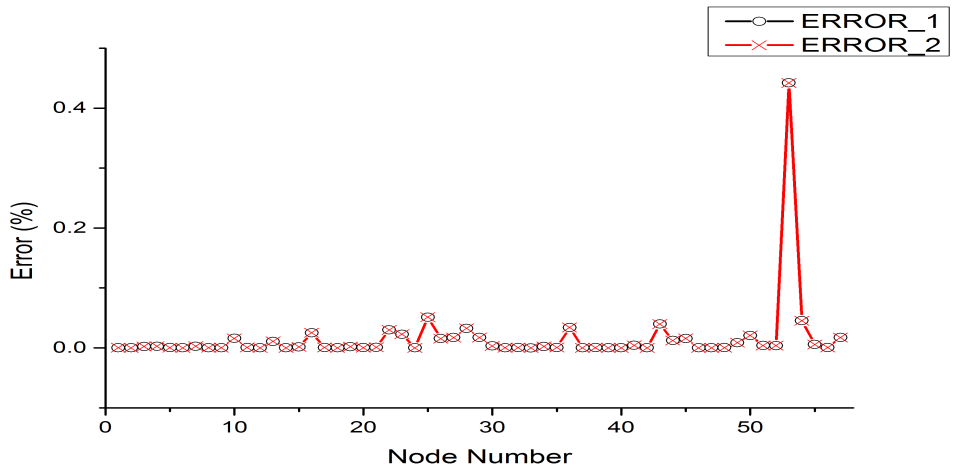

Figure F.11: The result differences of the total voltage harmonic distortion

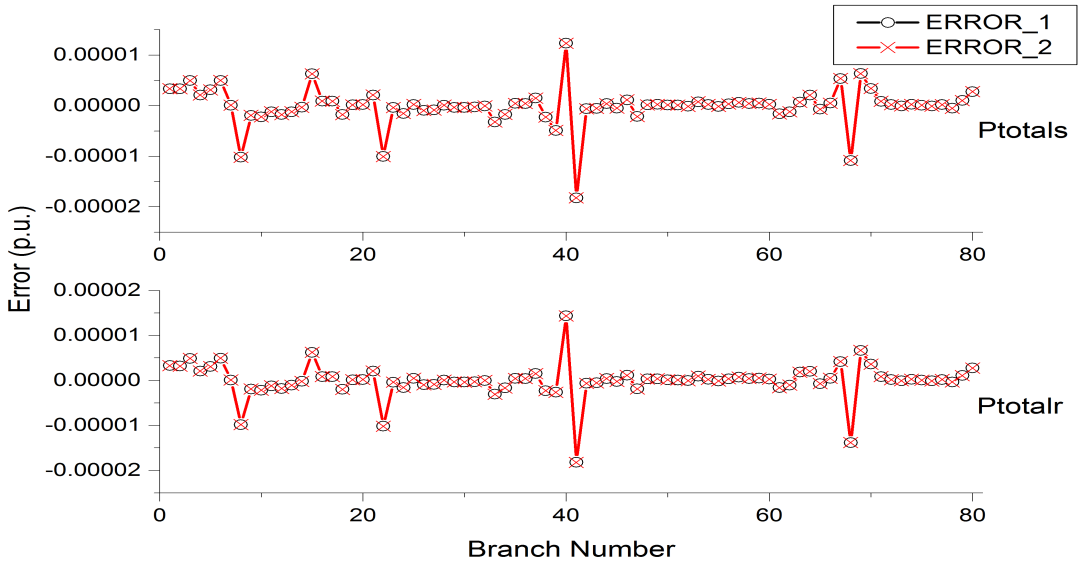

Figure F.12: The result differences of the total active powers at both sending and receiving ends

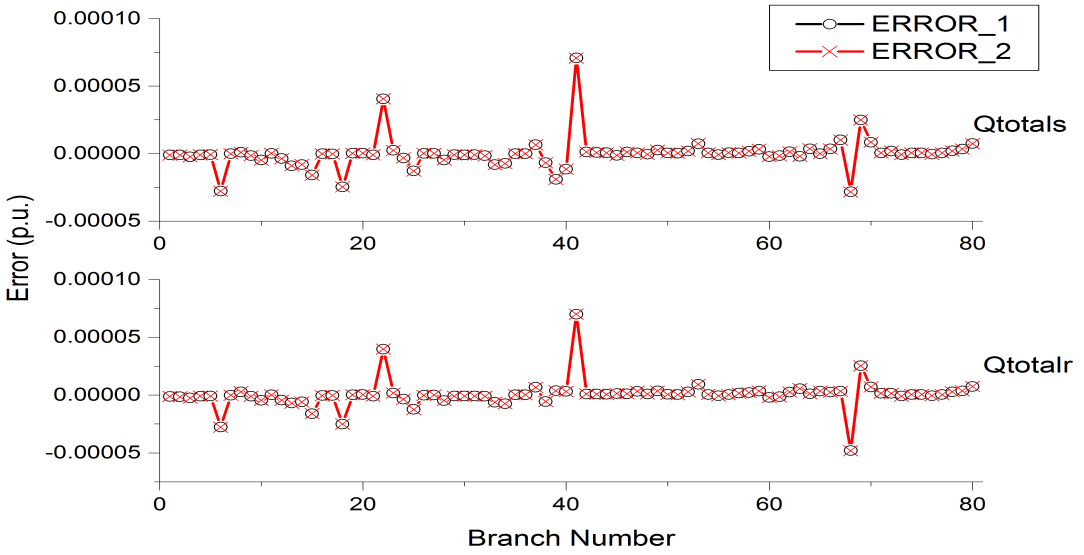

Figure F.13: The result differences of the total reactive powers at both sending and receiving ends

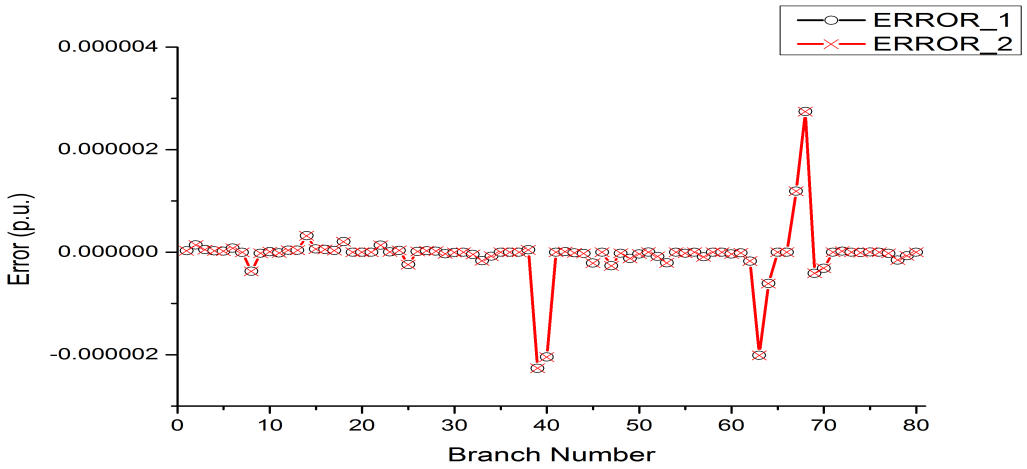

Figure F.14: The result differences of the total power losses on each branch

F.4 Case Three: In A 118-bus Power System

The result differences of the fundamental bus voltage magnitudes, the total harmonic voltage distortion, the total active and reactive powers at both sending and receiving ends and the total power losses on each branch between three different methods are illustrated in Figures F.15 to F.21 below.

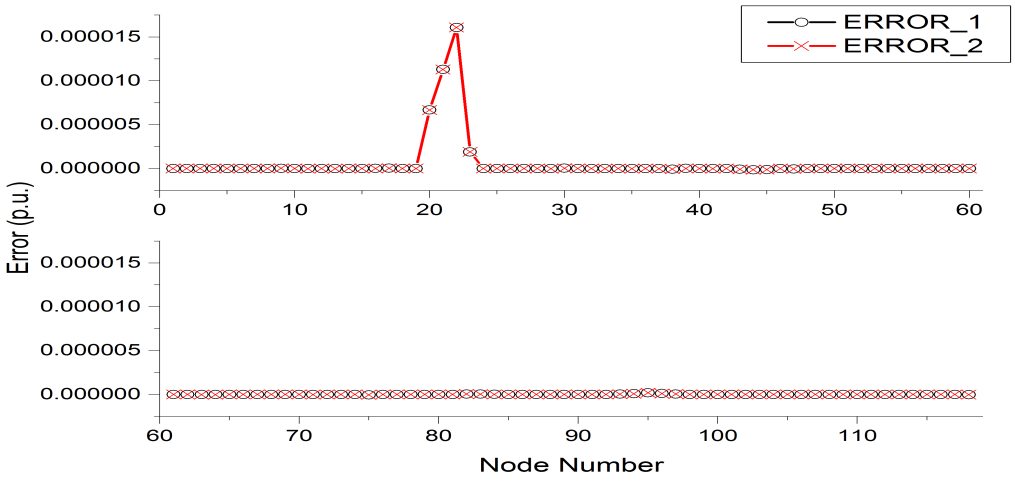

Figure F.15: The result differences of the fundamental bus voltage magnitude

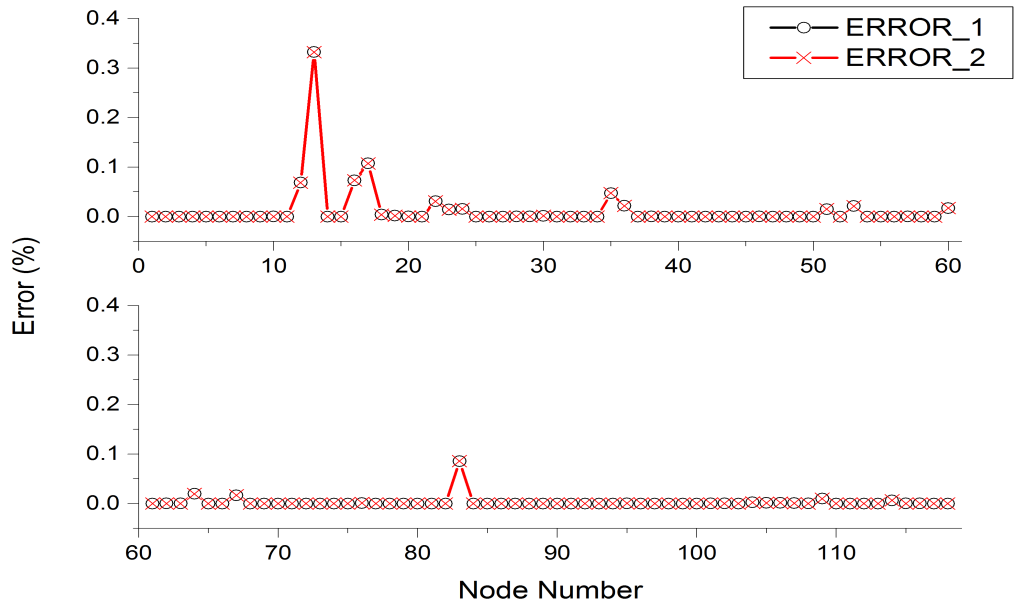

Figure F.16: The result differences of the total voltage harmonic distortion

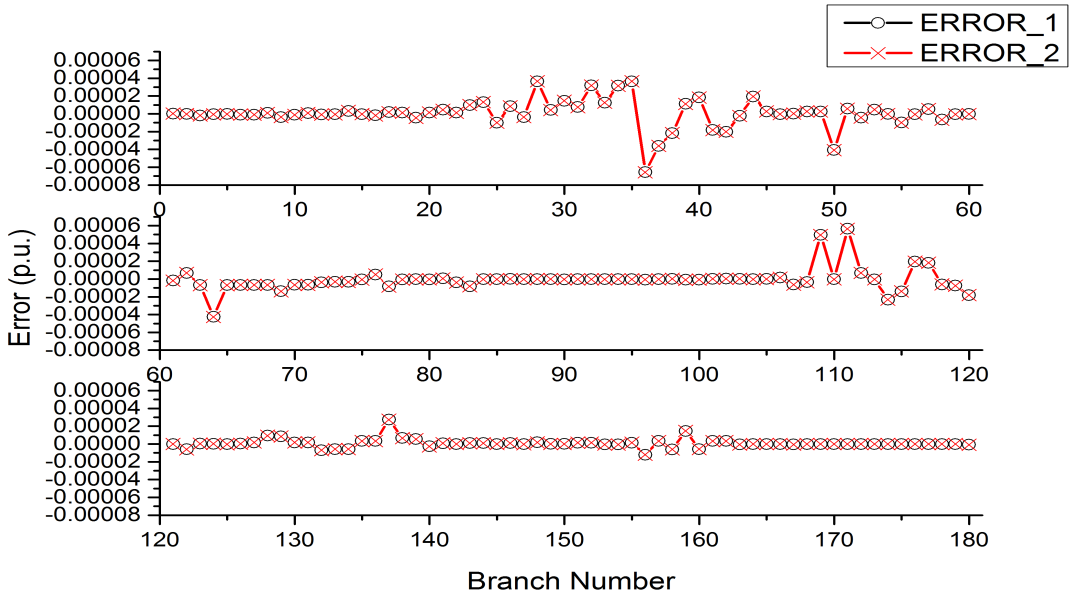

Figure F.17: The result differences of the total active powers at sending end

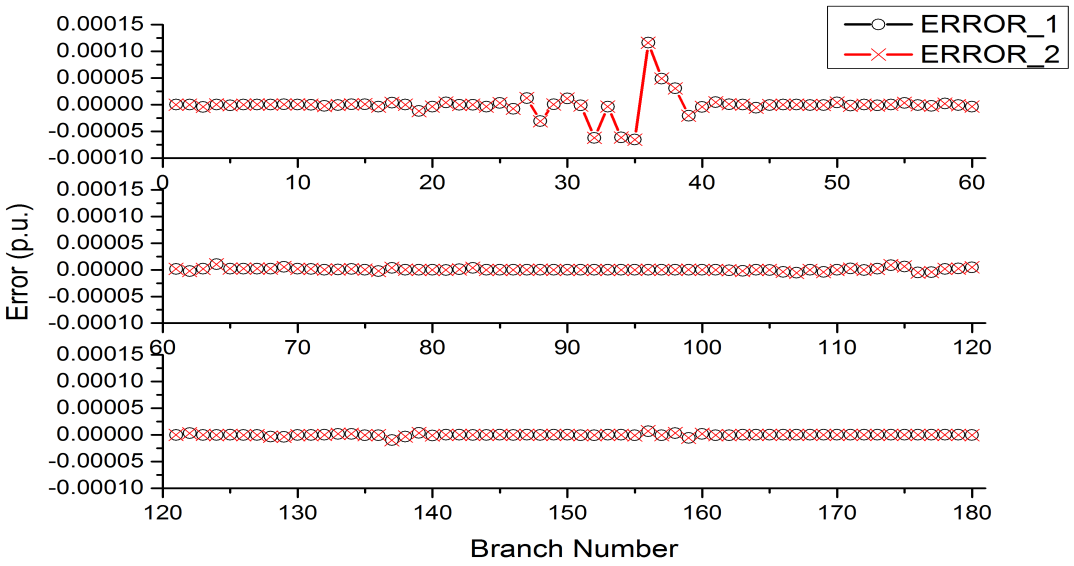

Figure F.18: The result differences of the total reactive powers at sending end

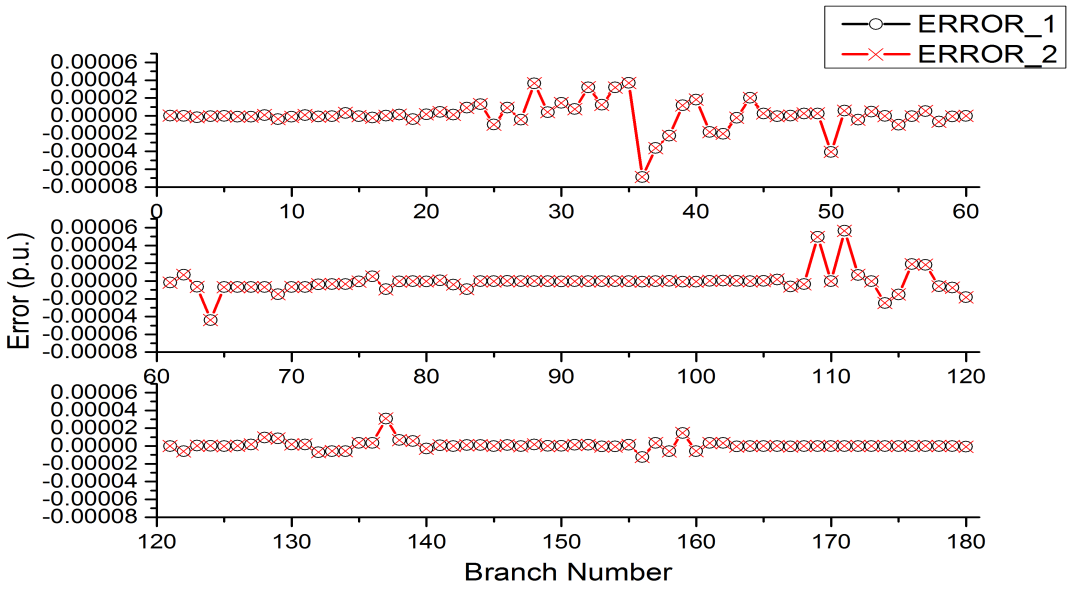

Figure F.19: The result differences of the total active powers at receiving end

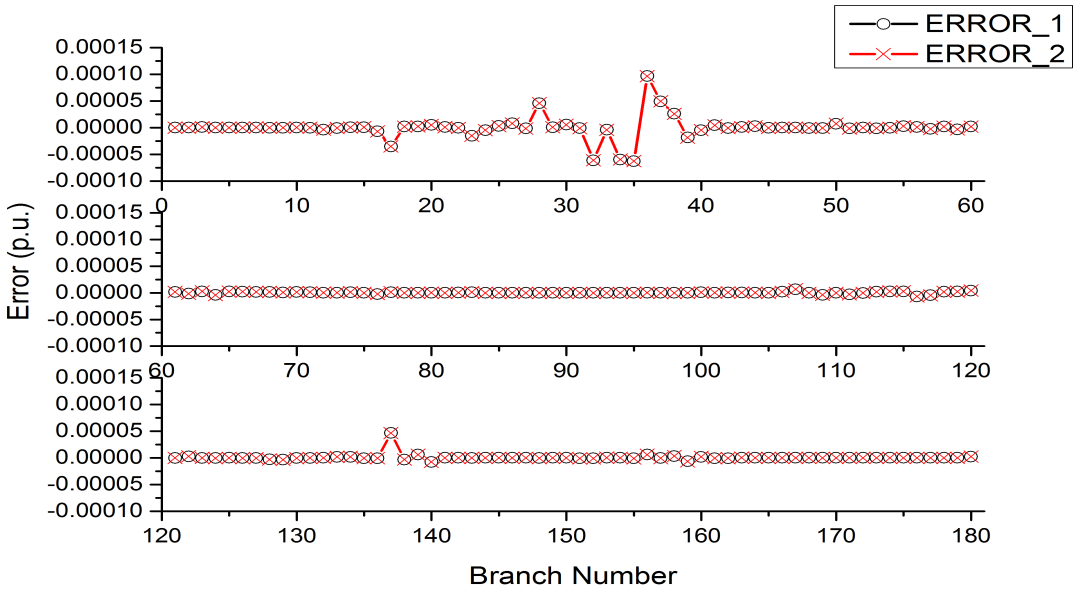

Figure F.20: The result differences of the total reactive powers at receiving end

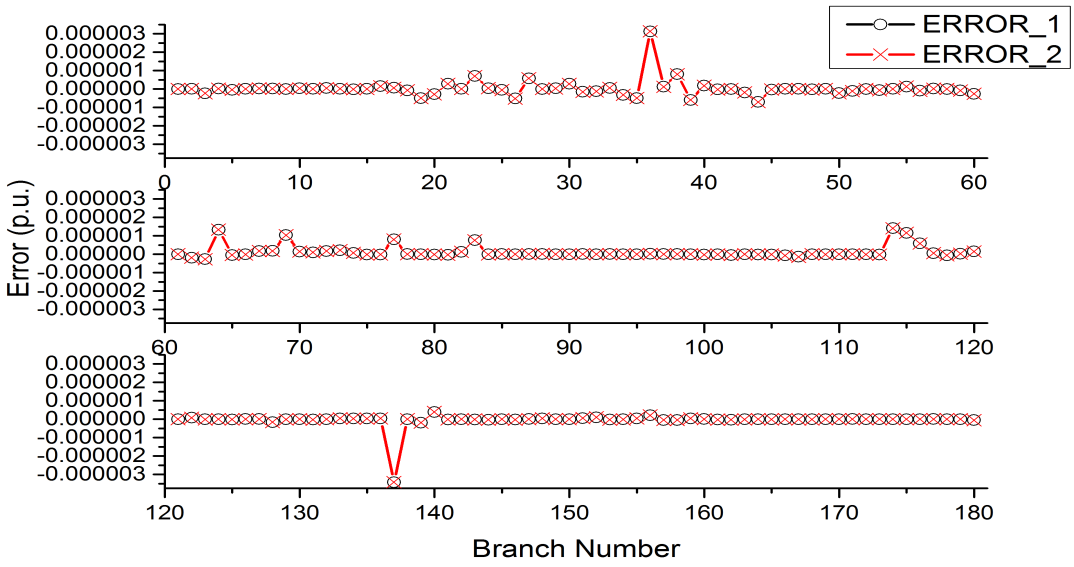

Figure F.21: The result differences of the total power loss on each branch

Appendix G

Weekday Hourly Generation And Load Model

G.1 In Summer

G.1.1 Daily Generation Model Of PVs

The data of weekday hourly peak generation in percent of daily peak of PVs is shown in Table G.1.

Table G.1: Hourly peak generation of PVs

Hour	12-12.15 am	12.15-12.30 am	12.30-12.45 am	12.45-1 am
Percentage (%)	0	0	0	0
Hour	1-1.15 am	1.15-1.30 am	1.30-1.45 am	1.45-2 am
Percentage (%)	0	0	0	0
Hour	2-2.15 am	2.15-2.30 am	2.30-2.45 am	2.45-3 am
Percentage (%)	0	0	0	0
Hour	3-3.15 am	3.15-3.30 am	3.30-3.45 am	3.45-4 am
Percentage (%)	0	0	0	0
Hour	4-4.15 am	4.15-4.30 am	4.30-4.45 am	4.45-5 am
Percentage (%)	0	0	0	0
Hour	5-5.15 am	5.15-5.30 am	5.30-5.45 am	5.45-6 am
Percentage (%)	0	0	0	0
Hour	6-6.15 am	6.15-6.30 am	6.30-6.45 am	6.45-7 am
Percentage (%)	9	9	9	9
Hour	7-7.15 am	7.15-7.30 am	7.30-7.45 am	7.45-8 am
Percentage (%)	37	37	37	37
Hour	8-8.15 am	8.15-8.30 am	8.30-8.45 am	8.45-9 am
Percentage (%)	65	65	65	65
Hour	9-9.15 am	9.15-9.30 am	9.30-9.45 am	9.45-10 am
Percentage (%)	83	83	83	83
Hour	10-10.15 am	10.15-10.30 am	10.30-10.45 am	10.45-11 am
Percentage (%)	95	95	95	95
Hour	11-11.15 am	11.15-11.30 am	11.30-11.45 am	11.45-noon

Continued on next page

Table G.1- *Continued from previous page*

Percentage (%)	98	98	98	98
Hour	noon-12.15 pm	12.15-12.30 pm	12.30-12.45 pm	12.45-1 pm
Percentage (%)	100	100	100	100
Hour	1-1.15 pm	1.15-1.30 pm	1.30-1.45 pm	1.45-2 pm
Percentage (%)	100	100	100	100
Hour	2-2.15 pm	2.15-2.30 pm	2.30-2.45 pm	2.45-3 pm
Percentage (%)	98	98	98	98
Hour	3-3.15 pm	3.15-3.30 pm	3.30-3.45 pm	3.45-4 pm
Percentage (%)	92	92	92	92
Hour	4-4.15 pm	4.15-4.30 pm	4.30-4.45 pm	4.45-5 pm
Percentage (%)	80	80	80	80
Hour	5-5.15 pm	5.15-5.30 pm	5.30-5.45 pm	5.45-6 pm
Percentage (%)	62	62	62	62
Hour	6-6.15 pm	6.15-6.30 pm	6.30-6.45 pm	6.45-7 pm
Percentage (%)	33	33	33	33
Hour	7-7.15 pm	7.15-7.30 pm	7.30-7.45 pm	7.45-8 pm
Percentage (%)	7	7	7	7
Hour	8-8.15 pm	8.15-8.30 pm	8.30-8.45 pm	8.45-9 pm
Percentage (%)	0	0	0	0
Hour	9-9.15 pm	9.15-9.30 pm	9.30-9.45 pm	9.45-10 pm
Percentage (%)	0	0	0	0
Hour	10-10.15 pm	10.15-10.30 pm	10.30-10.45 pm	10.45-11 pm
Percentage (%)	0	0	0	0
Hour	11-11.15 pm	11.15-11.30 pm	11.30-11.45 pm	11.45-12 am
Percentage (%)	0	0	0	0

G.1.2 Daily Generation Model Of WTs

The data of weekday hourly peak generation in percent of daily peak of PVs is shown in Table G.2.

Table G.2: Hourly peak generation of WTs

Hour	12-12.15 am	12.15-12.30 am	12.30-12.45 am	12.45-1 am
Percentage (%)	100	100	100	100
Hour	1-1.15 am	1.15-1.30 am	1.30-1.45 am	1.45-2 am
Percentage (%)	97	97	97	97
Hour	2-2.15 am	2.15-2.30 am	2.30-2.45 am	2.45-3 am
Percentage (%)	94	94	94	94
Hour	3-3.15 am	3.15-3.30 am	3.30-3.45 am	3.45-4 am
Percentage (%)	88	88	88	88
Hour	4-4.15 am	4.15-4.30 am	4.30-4.45 am	4.45-5 am
Percentage (%)	85	85	85	85
Hour	5-5.15 am	5.15-5.30 am	5.30-5.45 am	5.45-6 am
Percentage (%)	84	84	84	84
Hour	6-6.15 am	6.15-6.30 am	6.30-6.45 am	6.45-7 am
Percentage (%)	84	84	84	84
Hour	7-7.15 am	7.15-7.30 am	7.30-7.45 am	7.45-8 am
Percentage (%)	78	78	78	78
Hour	8-8.15 am	8.15-8.30 am	8.30-8.45 am	8.45-9 am
Percentage (%)	66	66	66	66
Hour	9-9.15 am	9.15-9.30 am	9.30-9.45 am	9.45-10 am
Percentage (%)	62	62	62	62
Hour	10-10.15 am	10.15-10.30 am	10.30-10.45 am	10.45-11 am
Percentage (%)	64	64	64	64
Hour	11-11.15 am	11.15-11.30 am	11.30-11.45 am	11.45-noon
Percentage (%)	58	58	58	58
Hour	noon-12.15 pm	12.15-12.30 pm	12.30-12.45 pm	12.45-1 pm

Continued on next page

Table G.2- *Continued from previous page*

Percentage (%)	54	54	54	54
Hour	1-1.15 pm	1.15-1.30 pm	1.30-1.45 pm	1.45-2 pm
Percentage (%)	68	68	68	68
Hour	2-2.15 pm	2.15-2.30 pm	2.30-2.45 pm	2.45-3 pm
Percentage (%)	80	80	80	80
Hour	3-3.15 pm	3.15-3.30 pm	3.30-3.45 pm	3.45-4 pm
Percentage (%)	87	87	87	87
Hour	4-4.15 pm	4.15-4.30 pm	4.30-4.45 pm	4.45-5 pm
Percentage (%)	88	88	88	88
Hour	5-5.15 pm	5.15-5.30 pm	5.30-5.45 pm	5.45-6 pm
Percentage (%)	87	87	87	87
Hour	6-6.15 pm	6.15-6.30 pm	6.30-6.45 pm	6.45-7 pm
Percentage (%)	85	85	85	85
Hour	7-7.15 pm	7.15-7.30 pm	7.30-7.45 pm	7.45-8 pm
Percentage (%)	85	85	85	85
Hour	8-8.15 pm	8.15-8.30 pm	8.30-8.45 pm	8.45-9 pm
Percentage (%)	83	83	83	83
Hour	9-9.15 pm	9.15-9.30 pm	9.30-9.45 pm	9.45-10 pm
Percentage (%)	85	85	85	85
Hour	10-10.15 pm	10.15-10.30 pm	10.30-10.45 pm	10.45-11 pm
Percentage (%)	88	88	88	88
Hour	11-11.15 pm	11.15-11.30 pm	11.30-11.45 pm	11.45-12 am
Percentage (%)	88	88	88	88

G.1.3 Daily Load Model Of Linear Loads And Converters

The data of weekday hourly peak generation in percent of daily peak of PVs is shown in Table G.3.

Table G.3: Hourly peak generation of linear loads and converters

Hour	12-12.15 am	12.15-12.30 am	12.30-12.45 am	12.45-1 am
Percentage (%)	64	64	64	64
Hour	1-1.15 am	1.15-1.30 am	1.30-1.45 am	1.45-2 am
Percentage (%)	60	60	60	60
Hour	2-2.15 am	2.15-2.30 am	2.30-2.45 am	2.45-3 am
Percentage (%)	58	58	58	58
Hour	3-3.15 am	3.15-3.30 am	3.30-3.45 am	3.45-4 am
Percentage (%)	56	56	56	56
Hour	4-4.15 am	4.15-4.30 am	4.30-4.45 am	4.45-5 am
Percentage (%)	56	56	56	56
Hour	5-5.15 am	5.15-5.30 am	5.30-5.45 am	5.45-6 am
Percentage (%)	58	58	58	58
Hour	6-6.15 am	6.15-6.30 am	6.30-6.45 am	6.45-7 am
Percentage (%)	64	64	64	64
Hour	7-7.15 am	7.15-7.30 am	7.30-7.45 am	7.45-8 am
Percentage (%)	76	76	76	76
Hour	8-8.15 am	8.15-8.30 am	8.30-8.45 am	8.45-9 am
Percentage (%)	87	87	87	87
Hour	9-9.15 am	9.15-9.30 am	9.30-9.45 am	9.45-10 am
Percentage (%)	95	95	95	95
Hour	10-10.15 am	10.15-10.30 am	10.30-10.45 am	10.45-11 am
Percentage (%)	99	99	99	99
Hour	11-11.15 am	11.15-11.30 am	11.30-11.45 am	11.45-noon
Percentage (%)	100	100	100	100

Continued on next page

Table G.3- *Continued from previous page*

Hour	noon-12.15 pm	12.15-12.30 pm	12.30-12.45 pm	12.45-1 pm
Percentage (%)	99	99	99	99
Hour	1-1.15 pm	1.15-1.30 pm	1.30-1.45 pm	1.45-2 pm
Percentage (%)	100	100	100	100
Hour	2-2.15 pm	2.15-2.30 pm	2.30-2.45 pm	2.45-3 pm
Percentage (%)	100	100	100	100
Hour	3-3.15 pm	3.15-3.30 pm	3.30-3.45 pm	3.45-4 pm
Percentage (%)	97	97	97	97
Hour	4-4.15 pm	4.15-4.30 pm	4.30-4.45 pm	4.45-5 pm
Percentage (%)	96	96	96	96
Hour	5-5.15 pm	5.15-5.30 pm	5.30-5.45 pm	5.45-6 pm
Percentage (%)	96	96	96	96
Hour	6-6.15 pm	6.15-6.30 pm	6.30-6.45 pm	6.45-7 pm
Percentage (%)	93	93	93	93
Hour	7-7.15 pm	7.15-7.30 pm	7.30-7.45 pm	7.45-8 pm
Percentage (%)	92	92	92	92
Hour	8-8.15 pm	8.15-8.30 pm	8.30-8.45 pm	8.45-9 pm
Percentage (%)	92	92	92	92
Hour	9-9.15 pm	9.15-9.30 pm	9.30-9.45 pm	9.45-10 pm
Percentage (%)	93	93	93	93
Hour	10-10.15 pm	10.15-10.30 pm	10.30-10.45 pm	10.45-11 pm
Percentage (%)	87	87	87	87
Hour	11-11.15 pm	11.15-11.30 pm	11.30-11.45 pm	11.45-12 am
Percentage (%)	72	72	72	72

G.1.4 Daily Load Model Of EVCs

The data of weekday hourly peak generation in percent of daily peak of EVCs is shown in Table G.4.

Table G.4: Hourly peak generation of EVCs

Hour	12-12.15 am	12.15-12.30 am	12.30-12.45 am	12.45-1 am
Percentage (%)	58	58	58	58
Hour	1-1.15 am	1.15-1.30 am	1.30-1.45 am	1.45-2 am
Percentage (%)	37	37	37	37
Hour	2-2.15 am	2.15-2.30 am	2.30-2.45 am	2.45-3 am
Percentage (%)	27	27	27	27
Hour	3-3.15 am	3.15-3.30 am	3.30-3.45 am	3.45-4 am
Percentage (%)	25	25	25	25
Hour	4-4.15 am	4.15-4.30 am	4.30-4.45 am	4.45-5 am
Percentage (%)	17	17	17	17
Hour	5-5.15 am	5.15-5.30 am	5.30-5.45 am	5.45-6 am
Percentage (%)	8	8	8	8
Hour	6-6.15 am	6.15-6.30 am	6.30-6.45 am	6.45-7 am
Percentage (%)	8	8	8	8
Hour	7-7.15 am	7.15-7.30 am	7.30-7.45 am	7.45-8 am
Percentage (%)	8	8	8	8
Hour	8-8.15 am	8.15-8.30 am	8.30-8.45 am	8.45-9 am
Percentage (%)	5	5	5	5
Hour	9-9.15 am	9.15-9.30 am	9.30-9.45 am	9.45-10 am
Percentage (%)	3	3	3	3
Hour	10-10.15 am	10.15-10.30 am	10.30-10.45 am	10.45-11 am
Percentage (%)	5	5	5	5
Hour	11-11.15 am	11.15-11.30 am	11.30-11.45 am	11.45-noon
Percentage (%)	8	8	8	8
Hour	noon-12.15 pm	12.15-12.30 pm	12.30-12.45 pm	12.45-1 pm

Continued on next page

Table G.4- *Continued from previous page*

Percentage (%)	8	8	8	8
Hour	1-1.15 pm	1.15-1.30 pm	1.30-1.45 pm	1.45-2 pm
Percentage (%)	17	17	17	17
Hour	2-2.15 pm	2.15-2.30 pm	2.30-2.45 pm	2.45-3 pm
Percentage (%)	25	25	25	25
Hour	3-3.15 pm	3.15-3.30 pm	3.30-3.45 pm	3.45-4 pm
Percentage (%)	33	33	33	33
Hour	4-4.15 pm	4.15-4.30 pm	4.30-4.45 pm	4.45-5 pm
Percentage (%)	58	58	58	58
Hour	5-5.15 pm	5.15-5.30 pm	5.30-5.45 pm	5.45-6 pm
Percentage (%)	75	75	75	75
Hour	6-6.15 pm	6.15-6.30 pm	6.30-6.45 pm	6.45-7 pm
Percentage (%)	92	92	92	92
Hour	7-7.15 pm	7.15-7.30 pm	7.30-7.45 pm	7.45-8 pm
Percentage (%)	100	100	100	100
Hour	8-8.15 pm	8.15-8.30 pm	8.30-8.45 pm	8.45-9 pm
Percentage (%)	97	97	97	97
Hour	9-9.15 pm	9.15-9.30 pm	9.30-9.45 pm	9.45-10 pm
Percentage (%)	93	93	93	93
Hour	10-10.15 pm	10.15-10.30 pm	10.30-10.45 pm	10.45-11 pm
Percentage (%)	83	83	83	83
Hour	11-11.15 pm	11.15-11.30 pm	11.30-11.45 pm	11.45-12 am
Percentage (%)	75	75	75	75

G.2 In Winter

G.2.1 Daily Generation Model Of PVs

The data of weekday hourly peak generation in percent of daily peak of PVs in winter is shown in Table G.5.

Table G.5: Hourly peak generation of PVs

Hour	12-12.15 am	12.15-12.30 am	12.30-12.45 am	12.45-1 am
Percentage (%)	0	0	0	0
Hour	1-1.15 am	1.15-1.30 am	1.30-1.45 am	1.45-2 am
Percentage (%)	0	0	0	0
Hour	2-2.15 am	2.15-2.30 am	2.30-2.45 am	2.45-3 am
Percentage (%)	0	0	0	0
Hour	3-3.15 am	3.15-3.30 am	3.30-3.45 am	3.45-4 am
Percentage (%)	0	0	0	0
Hour	4-4.15 am	4.15-4.30 am	4.30-4.45 am	4.45-5 am
Percentage (%)	0	0	0	0
Hour	5-5.15 am	5.15-5.30 am	5.30-5.45 am	5.45-6 am
Percentage (%)	0	0	0	0
Hour	6-6.15 am	6.15-6.30 am	6.30-6.45 am	6.45-7 am
Percentage (%)	0	0	0	0
Hour	7-7.15 am	7.15-7.30 am	7.30-7.45 am	7.45-8 am
Percentage (%)	9	9	9	9
Hour	8-8.15 am	8.15-8.30 am	8.30-8.45 am	8.45-9 am
Percentage (%)	35	35	35	35
Hour	9-9.15 am	9.15-9.30 am	9.30-9.45 am	9.45-10 am
Percentage (%)	55	55	55	55
Hour	10-10.15 am	10.15-10.30 am	10.30-10.45 am	10.45-11 am
Percentage (%)	65	65	65	65
Hour	11-11.15 am	11.15-11.30 am	11.30-11.45 am	11.45-noon

Continued on next page

Table G.5- *Continued from previous page*

Percentage (%)	69	69	69	69
Hour	noon-12.15 pm	12.15-12.30 pm	12.30-12.45 pm	12.45-1 pm
Percentage (%)	69	69	69	69
Hour	1-1.15 pm	1.15-1.30 pm	1.30-1.45 pm	1.45-2 pm
Percentage (%)	65	65	65	65
Hour	2-2.15 pm	2.15-2.30 pm	2.30-2.45 pm	2.45-3 pm
Percentage (%)	52	52	52	52
Hour	3-3.15 pm	3.15-3.30 pm	3.30-3.45 pm	3.45-4 pm
Percentage (%)	26	26	26	26
Hour	4-4.15 pm	4.15-4.30 pm	4.30-4.45 pm	4.45-5 pm
Percentage (%)	0	0	0	0
Hour	5-5.15 pm	5.15-5.30 pm	5.30-5.45 pm	5.45-6 pm
Percentage (%)	0	0	0	0
Hour	6-6.15 pm	6.15-6.30 pm	6.30-6.45 pm	6.45-7 pm
Percentage (%)	0	0	0	0
Hour	7-7.15 pm	7.15-7.30 pm	7.30-7.45 pm	7.45-8 pm
Percentage (%)	0	0	0	0
Hour	8-8.15 pm	8.15-8.30 pm	8.30-8.45 pm	8.45-9 pm
Percentage (%)	0	0	0	0
Hour	9-9.15 pm	9.15-9.30 pm	9.30-9.45 pm	9.45-10 pm
Percentage (%)	0	0	0	0
Hour	10-10.15 pm	10.15-10.30 pm	10.30-10.45 pm	10.45-11 pm
Percentage (%)	0	0	0	0
Hour	11-11.15 pm	11.15-11.30 pm	11.30-11.45 pm	11.45-12 am
Percentage (%)	0	0	0	0

G.2.2 Daily Load Model Of Linear Loads And Converters

The data of weekday hourly peak generation in percent of daily peak of PVs in winter is shown in Table G.6.

Table G.6: Hourly peak generation of linear loads and converters

Hour	12-12.15 am	12.15-12.30 am	12.30-12.45 am	12.45-1 am
Percentage (%)	67	67	67	67
Hour	1-1.15 am	1.15-1.30 am	1.30-1.45 am	1.45-2 am
Percentage (%)	63	63	63	63
Hour	2-2.15 am	2.15-2.30 am	2.30-2.45 am	2.45-3 am
Percentage (%)	60	60	60	60
Hour	3-3.15 am	3.15-3.30 am	3.30-3.45 am	3.45-4 am
Percentage (%)	59	59	59	59
Hour	4-4.15 am	4.15-4.30 am	4.30-4.45 am	4.45-5 am
Percentage (%)	59	59	59	59
Hour	5-5.15 am	5.15-5.30 am	5.30-5.45 am	5.45-6 am
Percentage (%)	60	60	60	60
Hour	6-6.15 am	6.15-6.30 am	6.30-6.45 am	6.45-7 am
Percentage (%)	74	74	74	74
Hour	7-7.15 am	7.15-7.30 am	7.30-7.45 am	7.45-8 am
Percentage (%)	86	86	86	86
Hour	8-8.15 am	8.15-8.30 am	8.30-8.45 am	8.45-9 am
Percentage (%)	95	95	95	95
Hour	9-9.15 am	9.15-9.30 am	9.30-9.45 am	9.45-10 am
Percentage (%)	96	96	96	96
Hour	10-10.15 am	10.15-10.30 am	10.30-10.45 am	10.45-11 am
Percentage (%)	96	96	96	96
Hour	11-11.15 am	11.15-11.30 am	11.30-11.45 am	11.45-noon
Percentage (%)	95	95	95	95

Continued on next page

Table G.6- *Continued from previous page*

Hour	noon-12.15 pm	12.15-12.30 pm	12.30-12.45 pm	12.45-1 pm
Percentage (%)	95	95	95	95
Hour	1-1.15 pm	1.15-1.30 pm	1.30-1.45 pm	1.45-2 pm
Percentage (%)	95	95	95	95
Hour	2-2.15 pm	2.15-2.30 pm	2.30-2.45 pm	2.45-3 pm
Percentage (%)	93	93	93	93
Hour	3-3.15 pm	3.15-3.30 pm	3.30-3.45 pm	3.45-4 pm
Percentage (%)	94	94	94	94
Hour	4-4.15 pm	4.15-4.30 pm	4.30-4.45 pm	4.45-5 pm
Percentage (%)	99	99	99	99
Hour	5-5.15 pm	5.15-5.30 pm	5.30-5.45 pm	5.45-6 pm
Percentage (%)	100	100	100	100
Hour	6-6.15 pm	6.15-6.30 pm	6.30-6.45 pm	6.45-7 pm
Percentage (%)	100	100	100	100
Hour	7-7.15 pm	7.15-7.30 pm	7.30-7.45 pm	7.45-8 pm
Percentage (%)	96	96	96	96
Hour	8-8.15 pm	8.15-8.30 pm	8.30-8.45 pm	8.45-9 pm
Percentage (%)	91	91	91	91
Hour	9-9.15 pm	9.15-9.30 pm	9.30-9.45 pm	9.45-10 pm
Percentage (%)	83	83	83	83
Hour	10-10.15 pm	10.15-10.30 pm	10.30-10.45 pm	10.45-11 pm
Percentage (%)	73	73	73	73
Hour	11-11.15 pm	11.15-11.30 pm	11.30-11.45 pm	11.45-12 am
Percentage (%)	63	63	63	63